

**Novel insights into the functioning and
regulation of FER-LIKE IRON DEFICIENCY-
INDUCED TRANSCRIPTION FACTOR (FIT) on
post-translational and subcellular level**

Inaugural-Dissertation

zur Erlangung des Doktorgrades
der Mathematisch-Naturwissenschaftlichen Fakultät
der Heinrich-Heine-Universität Düsseldorf

vorgelegt von

Ksenia Trofimov
aus Toljatti, Russland

Düsseldorf, November 2022

aus dem Institut für Botanik
der Heinrich-Heine-Universität Düsseldorf

Gedruckt mit der Genehmigung der
Mathematisch-Naturwissenschaftlichen Fakultät der
Heinrich-Heine-Universität Düsseldorf

Berichtersteller:

1. Prof. Dr. Petra Bauer
2. apl. Prof. Dr. Yvonne Stahl

Tag der mündlichen Prüfung: 21.12.2022

Eidesstattliche Erklärung

Ich versichere an Eides Statt, dass die Dissertation von mir selbstständig und ohne unzulässige fremde Hilfe unter Beachtung der „Grundsätze zur Sicherung guter wissenschaftlicher Praxis an der Heinrich-Heine-Universität Düsseldorf“ erstellt worden ist.

Ich habe die Dissertation in dieser oder ähnlicher Form bisher keiner anderen Fakultät vorgelegt.

Ich habe bisher keine erfolglosen Promotionsversuche unternommen.

Ksenia Trofimov

Düsseldorf, 03.11.2022

Acknowledgements

I would like to thank Prof. Dr. Petra Bauer for the past years, starting with my Master work and continuing into my doctorate time. Thank you for the possibility to work on a project that I could choose and develop myself. Thank you for cherishing my work and the support.

I also would like to thank apl. Prof. Dr. Yvonne Stahl, who has also supported me since my Master work until now. Thank you for your advice and help in my work.

These years flew by very quickly, even though I have been part of the Botany lab since 2016. Tzvetina and Rumen 'found' me in a Master course and put me onboard. I joined the lab as an intern, then later as a Master student, and then [please mind the gap] as a doctoral researcher. Ever since Tzvetina and Rumen have supported me personally and my work at all times. I am very grateful for that.

I would also like to thank all former and current members of the lab, who have been along the way. Regina, Birte, Dani, Anna, Inga, Moni, Jannik, Elke, Ginte, Hansi, Sieglinde, numerous students and many more people who have been part of the lab. There are too many people to name. We enjoyed many breaks, cakes, celebrations - we always had a good time. I have found friends in many of you, and I thank you for that. Especially, big hugs to Dani for your honest opinion and support, Inga for our brainstorming coffee sessions and help at any time, Moni for always seeing the positive side and being a haven of peace, and Jannik for always making me laugh and your creative solutions.

I am thankful to my parents and my sister, who do not exactly know what I am doing here but are always proud of me.

Thank you to my two furry companions, Kiwi and Pino. You are very fine cats.

My deepest gratitude goes to Marius, for the excellent off-time and vacation organization, finest cuisine, and future planning. I wish everyone could have a partner like you.

This too shall pass.

- Persian adage

Table of contents

1	Preface	3
2	Summary	5
3	Zusammenfassung	6
4	Introduction	8
4.1	Importance of iron for humans and plants	8
4.1.1	Iron uptake in plants	9
4.1.1.1	Strategy I – reduction-based iron uptake strategy	9
4.1.2	Transcriptional regulation of iron uptake	10
4.1.2.1	Transcriptional regulation of <i>FIT</i>	11
4.1.3	Post-translational regulation of iron uptake	12
4.1.3.1	Post-translational regulation of FIT	13
4.1.4	Long distance signaling in iron uptake	15
4.2	Subcellular protein partitioning	16
4.2.1	Condensation	17
4.2.2	Condensation in plants	18
4.2.2.1	Cytoplasmic condensates	19
4.2.2.2	Nuclear condensates	19
5	Thesis objectives	22
6	Paper I	33
7	Paper II	75
8	Paper III	111
9	Manuscript I	129
10	Concluding remarks	173

1 Preface

This dissertation addresses novel regulatory aspects of the iron uptake regulating transcription factor (TF) FER-LIKE IRON DEFICIENCY-INDUCED TRANSCRIPTION FACTOR (FIT) with focus on post-translational modification and subcellular organization in plants. The overarching open questions and aims are addressed in an introductory part and concluded in a final concluding remarks part. The main body of this thesis consists of three publications and a submitted manuscript:

1. CIPK11-Dependent Phosphorylation Modulates FIT Activity to Promote Arabidopsis Iron Acquisition in Response to Calcium Signaling

Regina Gratz*, Prabha Manishankar*, Rumen Ivanov, Philipp Köster, Inga Mohr, **Ksenia Trofimov**, Leonie Steinhorst, Johannes Meiser, Hans-Jörg Mai, Maria Drerup, Sibylle Arendt, Michael Holtkamp, Uwe Karst, Jörg Kudla, Petra Bauer, and Tzvetina Brumbarova

* Authors contributed equally

published in Developmental Cell (2019), Volume 48, Issue 5, Pages 726-740

DOI: <https://doi.org/10.1016/j.devcel.2019.01.006>

In this publication, we identified a calcium-dependent protein kinase, that phosphorylated FIT at Ser271/272. This phospho-site was found relevant for complementation of *fit* mutant plants, localization and mobility of FIT within the cell, and homo- and heterodimerization with an interacting partner of FIT, TF BASIC HELIX-LOOP-HELIX039 (bHLH039). This work suggests that phosphorylation at Ser271/272 is of high importance for FIT activity. I contributed to this work with my expertise in microscopy and conducted interaction studies showing differences in the interaction strength of phospho-mutated FIT.

2. Phospho-mutant activity assays provide evidence for alternative phospho-regulation pathways of the transcription factor FER-LIKE IRON DEFICIENCY-INDUCED TRANSCRIPTION FACTOR

Regina Gratz, Tzvetina Brumbarova, Rumen Ivanov, **Ksenia Trofimov**, Laura Tünnermann, Rocio Ochoa-Fernandez, Tim Blomeier, Johannes Meiser, Stefanie Weidtkamp-Peters, Matias D. Zurbriggen, and Petra Bauer

published in New Phytologist (2020), Volume 225, Issue 1, Pages 250-267

DOI: <https://doi.org/10.1111/nph.16168>

In this publication, we extended the knowledge on predicted phosphorylation sites for FIT regulation and found that FIT was inactivated by phosphorylation at Tyr residues. We observed differential interaction and cellular localization of FIT, depending on mutations at different phosphorylation sites. FIT protein was rendered less active with phospho-mimicking mutations at two Tyr residues. These mutant forms complemented insufficiently *fit* mutant

plants, and turnover of FIT was promoted in one of the Tyr mutant form. Altogether, this work shows that FIT activity is differentially regulated via phosphorylation. My contribution to this work was my expertise in imaging and conduction of interaction studies, showing differentiating FIT interaction upon phospho-mutation.

3. Mobility and localization of the iron deficiency-induced transcription factor bHLH039 change in the presence of FIT

Ksenia Trofimov*, Rumen Ivanov*, Monique Eutebach, Büsra Acaroglu, Inga Mohr, Petra Bauer, and Tzvetina Brumbarova

* Authors contributed equally

published in Plant Direct (2019), Volume 3, Issue 12, Pages 1-11

DOI: <https://doi.org/10.1002/pld3.190>

In this publication, we examined the subcellular localization of bHLH039 in presence and absence of FIT. We could show that subcellular localization of bHLH039 was dependent on FIT. Without FIT, bHLH039 was retained in immobile cytoplasmic foci close to the plasma membrane. In presence of FIT, bHLH039 and FIT both were localized in the nucleus. Further, we could show that the subcellular localization was also iron- and organ-dependent. This work suggests that dynamic protein localization and subcellular partitioning are important for iron uptake regulation. I contributed to this work by initially identifying this phenomenon and conducting localization and biochemical studies to characterize the subcellular partitioning.

4. FER-LIKE IRON DEFICIENCY-INDUCED TRANSCRIPTION FACTOR (FIT) accumulates in homo- and heterodimeric complexes in dynamic and inducible nuclear condensates associated with speckle components

Ksenia Trofimov, Regina Gratz, Rumen Ivanov, Yvonne Stahl, Petra Bauer, and Tzvetina Brumbarova

submitted

In this submitted manuscript we investigated the subcellular localization of FIT and found that FIT formed condensates in the nucleus. We characterized the condensate formation and function. We could show that FIT engaged in these nuclear bodies (NBs) in an inducible and dynamic manner, most likely by liquid-liquid phase separation. Furthermore, FIT NBs were homo- and heterodimerization sites and colocalized with splicing components, indicating a possible transcriptional or post-transcriptional modification function of FIT NBs. This work elucidated an unknown property of FIT and opened the possibility for iron uptake finetuning on subnuclear scale. This work was mainly conducted by me, starting with the identification of FIT condensation and subsequent detailed analysis of condensate formation and characteristics by extensive application of microscopic techniques.

2 Summary

Iron is an essential micronutrient for animals and plants. Within iron uptake in plants, an important protein is the basic helix-loop-helix (bHLH) transcription factor (TF) FER-LIKE IRON DEFICIENCY-INDUCED TRANSCRIPTION FACTOR (FIT). Together with an interaction partner, such as bHLH039, FIT is upregulating gene transcription of the iron uptake machinery upon iron deficiency. Iron uptake has to be tightly regulated to avoid deficiency or excess. Thus, regulation of FIT activity is an important step in balancing the uptake. It was proposed that FIT exists in two pools within the cell, an active and an inactive pool, but FIT regulation was mainly described in the context of protein turnover. Therefore, an important question to answer is how FIT is activated and deactivated to regulate iron uptake. Identification of a protein kinase interacting with FIT opened the possibility of FIT being phosphorylated. Therefore, one aim of this work was to investigate the influence of phosphorylation on FIT activity. Apart from this, the subcellular localization of FIT and other TFs involved in iron uptake was barely in focus of research, missing out on valuable information on an additional regulatory level. Another aim was therefore to investigate the subcellular localization of TFs involved in iron uptake regulation in more detail.

In my dissertation, I contributed to show that FIT activity was dually regulated via phosphorylation. Ser271/272 was identified as an important phosphorylation site for FIT activation, and I could show that upon mutation to a phospho-dead FIT form, this mutant FIT showed reduced homo- and heterodimerization with bHLH039 compared to wild-type FIT. The phospho-dead FIT form was not able to complement *fit* mutant plants and showed altered localization and protein mobility. In further work, we predicted other phosphorylation sites and showed that phosphorylation of Tyr residues deactivated FIT and subjected it to proteasomal degradation. Phospho-mimicking tyrosine mutants showed altered localization, protein mobility, and promoter transactivation activity. Also here, I could show that FIT mutants had altered homo- and heterodimerization capacity with bHLH039 compared to wild-type FIT.

Iron uptake regulation could be further refined on subcellular level. As a result of an extensive microscopy study, I identified that bHLH039 was nucleocytoplasmically partitioned depending on FIT. In absence of FIT, bHLH039 was retained in cytoplasmic foci. With FIT, bHLH039 localized in the nucleus. Furthermore, I found that FIT underwent condensation within the nucleus upon a light stimulus. The formation of these nuclear bodies (NBs) functioned as a hub for FIT homo- and heterodimerization with bHLH039. Additionally, colocalization studies pointed at a possible transcriptional or post-transcriptional function of these FIT NBs.

This work provides detailed insight into finetuning of FIT activity via a dual post-translational regulation in form of phosphorylation and uncovers the dynamic subcellular localization of FIT and its interaction partner bHLH039.

3 Zusammenfassung

Eisen ist ein essenzieller Mikronährstoff für Tiere und Pflanzen. Ein wichtiges Protein bei der Eisenaufnahme in Pflanzen ist der basic helix-loop-helix (bHLH) Transkriptionsfaktor (TF) FER-LIKE IRON DEFICIENCY-INDUCED TRANSCRIPTION FACTOR (FIT). Zusammen mit einem Interaktionspartner wie bHLH039 reguliert FIT die Gentranskription der Eisenaufnahmemaschinerie bei Eisenmangel hoch. Die Eisenaufnahme muss streng reguliert werden, um einen Mangel oder Überschuss zu vermeiden. Daher ist die Regulierung der FIT-Aktivität ein wichtiger Schritt, um die Aufnahme auszugleichen. Es wurde vorgeschlagen, dass FIT in zwei Pools innerhalb der Zelle existiert, einem aktiven und einem inaktiven Pool, aber die FIT-Regulierung wurde hauptsächlich im Zusammenhang mit Proteinumsatz beschrieben. Daher ist eine wichtige zu beantwortende Frage, wie FIT aktiviert und deaktiviert wird, um die Eisenaufnahme zu regulieren. Die Identifizierung einer Proteinkinase, die mit FIT interagiert, eröffnete die Möglichkeit, dass FIT phosphoryliert wird. Daher war ein Ziel dieser Arbeit, den Einfluss der Phosphorylierung auf die FIT-Aktivität zu untersuchen. Abgesehen davon stand die subzelluläre Lokalisierung von FIT und anderen an der Eisenaufnahme beteiligten TF kaum im Fokus der Forschung, wodurch wertvolle Informationen auf einer zusätzlichen regulatorischen Ebene ausgelassen wurden. Ein weiteres Ziel war es daher, die subzelluläre Lokalisation von TF, die an der Regulation der Eisenaufnahme beteiligt sind, genauer zu untersuchen.

In meiner Dissertation habe ich dazu beigetragen zu zeigen, dass die FIT-Aktivität dual über Phosphorylierung reguliert wird. Ser271/272 wurde als wichtige Phosphorylierungsstelle für die FIT-Aktivierung identifiziert, und ich konnte zeigen, dass nach Mutation zu einer nicht phosphorylierbaren FIT-Form, das mutierte FIT im Vergleich zu Wildtyp-FIT eine reduzierte Homo- und Heterodimerisierung mit bHLH039 zeigte. Die nicht phosphorylierbare FIT-Form war nicht in der Lage, mutante *fit*-Pflanzen zu komplementieren und zeigte eine veränderte Lokalisierung und Proteinmobilität. Des Weiteren sagten wir andere Phosphorylierungsstellen voraus und zeigten, dass die Phosphorylierung von Tyrosinresten FIT deaktiviert und zu einem proteasomalen Abbau führte. Phosphorylierungsnachahmende Tyrosin-Mutanten zeigten eine veränderte Lokalisierung, Proteinmobilität und Promotor-Transaktivierungsaktivität. Auch hier konnte ich zeigen, dass FIT Mutanten eine veränderte Homo- und Heterodimerisierungsfähigkeit mit bHLH039 im Vergleich zu Wildtyp-FIT aufwiesen.

Die Regulierung der Eisenaufnahme könnte auf subzellulärer Ebene weiter verfeinert werden. Als Ergebnis einer umfangreichen Mikroskopiestudie identifizierte ich, dass bHLH039 in Abhängigkeit von FIT nukleozytoplasmatisch partitioniert war. In Abwesenheit von FIT wurde bHLH039 in zytoplasmatischen Foci zurückgehalten. Mit FIT lokalisierte bHLH039 im Zellkern. Außerdem fand ich heraus, dass FIT bei einem Lichtreiz im Zellkern kondensierte. Die Bildung dieser Kernkörperchen fungierte als Zentrum für die FIT Homo- und

Heterodimerisierung mit bHLH039. Zusätzlich wiesen Koloalierungsstudien auf eine mögliche transkriptionelle oder post-transkriptionelle Funktion dieser FIT-Kernkörperchen hin.

Diese Arbeit bietet detaillierte Einblicke in die Feinjustierung der FIT-Aktivität über eine duale post-translationale Regulation in Form von Phosphorylierung und deckt die dynamische subzelluläre Lokalisierung von FIT und seinem Interaktionspartner bHLH039 auf.

4 Introduction

4.1 Importance of iron for humans and plants

The micronutrient iron (Fe) is of high importance for human and plant health. In humans, iron deficiency is the most common nutritional disorder worldwide (<http://www.who.int/nutrition/topics/ida/en/>; Stoltzfus, 2001; McLean et al., 2008; Abbaspour et al., 2014). Especially women and children are in high need of iron for proper development and body function but also a geographical prevalence for higher risk of suffering from iron deficiency is observed (McLean et al., 2008). Symptoms of iron deficiency are e.g., fatigue, paleness, brittle nails, hair loss, irritability, and most prominently anemia (Al-Fartusie and Mohssan, 2017; DeLoughery, 2017). Most iron is incorporated in hemoglobin as part of erythrocytes (Hentze et al., 2004; Al-Fartusie and Mohssan, 2017). Speaking of the worldwide population, the main source of iron is a plant-based diet. In countries with a low diet diversity, iron malnutrition is hard to overcome (Naranjo Arcos and Bauer, 2016). Therefore, understanding iron uptake, distribution, and storage in plants is crucial for future biofortification to battle iron deficiency (Bouis et al., 2011; Briat et al., 2015; Connorton and Balk, 2019).

Iron deficiency has equally severe consequences on plant vitality as on human health. Plants lacking iron have reduced biomass and are chlorotic, since iron is abundantly present in chloroplasts, with about 80% of total cellular content (Hänsch and Mendel, 2009; Nouet et al., 2011; Briat et al., 2015; López-Millán et al., 2016). Besides, iron is important for the respiratory chain in mitochondria (Nouet et al., 2011), where also co-factors for enzymatic reactions are synthesized, such as heme and iron-sulfur clusters (Balk and Pilon, 2011; Jain and Connolly, 2013; Balk and Schaedler, 2014; Briat et al., 2015). Iron deficiency triggers changes in gene expression (Mai et al., 2016; Schwarz and Bauer, 2020) and morphological changes of the root (Marschner et al., 1989; Schmidt, 1999; Giehl et al., 2013; Li et al., 2016a). Still, as harmful as iron deficiency is for a plant, excess iron affects the plant as well. Bronzing of the leaves and cell damage is the consequence of iron overaccumulation because iron participates in the Fenton reaction generating reactive oxygen species (Hell and Stephan, 2003; Sperotto et al., 2010; Balk and Pilon, 2011; Distéfano et al., 2021). To avoid that, iron is present in chelates, such as citrate chelates (xylem) or nicotianamine chelates (phloem) (Durrett et al., 2007; Schuler et al., 2012), and is quickly stored in the vacuole or the apoplast (Kobayashi et al., 2019a). Therefore, iron uptake must be tightly controlled.

Even though iron is a highly abundant element in the earth's crust (Wedepohl, 1995), its uptake is a challenge for plants because of its low soluble state in the soil. At neutral pH, iron is mainly present in its oxidized, ferric form (Fe^{3+}) and trapped in complexes not available to the plant, and even more so in calcareous and alkaline soil (Römheld and Marschner, 1986b; Guerinot and Yi, 1994). In the light of global warming and the progressive calcification of the soil, it is a major challenge to develop crops that can overcome these unfavorable soil conditions and take up iron efficiently.

4.1.1 Iron uptake in plants

Plants have evolved two iron uptake strategies that aim to make iron bioavailable for uptake (Marschner et al., 1986; Guerinot and Yi, 1994). Strategy I is a reduction-based uptake strategy employed by non-grasses, e.g., *Arabidopsis thaliana* (*Arabidopsis*) and *Solanum lycopersicum* (tomato). Strategy II is a chelation-based strategy and utilized by the Poacea family (grasses), e.g., *Zea mays* (maize), *Oryza sativa* (rice), and *Hordeum vulgare* (barley) (Römheld and Marschner, 1986b; Römheld, 1987; Marschner and Römheld, 1994; Kobayashi and Nishizawa, 2012; Martín-Barranco et al., 2021). Despite their differences, a strict separation of the two strategies cannot be made since Strategy I plants utilize chelation of iron as well (Rodriguez-Celma et al., 2013; Fourcroy et al., 2014; Schmid et al., 2014), and Strategy II plants express orthologues of Strategy I uptake genes (Eide et al., 1996; Bughio et al., 2002; Ishimaru et al., 2006; Lee and An, 2009; Sun et al., 2013; Li et al., 2015). Especially for rice a combination of both strategies due to its special growth under flooding conditions is proposed (Ishimaru et al., 2006; Wairich et al., 2019; Martín-Barranco et al., 2021).

4.1.1.1 Strategy I – reduction-based iron uptake strategy

Strategy I underlies a three step-based reduction process of iron (Figure 1). As a first step, the plasma membrane-localized proton extrusion pump ARABIDOPSIS H⁺-ATPASE2 (AHA2) acidifies the soil by pumping H⁺ into the rhizosphere. The acidification releases iron from insoluble complexes and solubilizes it (Santi and Schmidt, 2009). An additional step of iron chelation by phenolic compounds of the coumarin class (scopoletin, esculetin, sideretin, and fraxetin), traps iron and facilitates the solubilization (Römheld and Marschner, 1983; Rodriguez-Celma et al., 2013; Fourcroy et al., 2014; Schmid et al., 2014; Clemens and Weber, 2016; Sisó-Terraza et al., 2016; Tsai and Schmidt, 2017; Rajniak et al., 2018; Tsai et al., 2018). This is mediated by the transporter PLEIOTROPIC DRUG RESISTANCE9 (PDR9, or ATP-BINDING CASSETTE G37 (ABCG37)). Secondly, the plasma membrane bound FERRIC REDUCTASE-OXIDASE2 (FRO2) enzyme reduces Fe³⁺ to ferrous iron (Fe²⁺; Yi and Guerinot, 1996; Robinson et al., 1999). In a final step, the plasma membrane localized divalent cation transporter and transceptor IRON REGULATED TRANSPORTER1 (IRT1) takes up Fe²⁺ into root epidermal cells (Eide et al., 1996; Guerinot, 2000; Varotto et al., 2002; Vert et al., 2002; Dubeaux et al., 2018; Cointry and Vert, 2019). IRT1 transports also other divalent metals like cadmium (Cd), cobalt (Co), manganese (Mn), and zinc (Zn) (Korshunova et al., 1999; Henriques et al., 2002; Lee and An, 2009). AHA2, FRO2, and IRT1 form a complex at the plasma membrane (Martín-Barranco et al., 2020), most likely for an efficient iron uptake.

4.1.1.2 Strategy II – chelation-based iron uptake strategy

The main difference between Strategy I and Strategy II is the utilization of phytosiderophores as chelators for trapping iron. The efflux transporter TRANSPORTER OF MUGINEIC ACID1 (TOM1) releases phytosiderophores, such as mugineic acid (Takagi et al.,

1984; Römheld and Marschner, 1986a; Nozoye et al., 2011). Chelated Fe^{3+} is taken up into the epidermal root cell via a proton-coupled transporter YELLOW STRIPE1 (ZmYS1), e.g., in maize (Curie et al., 2001; Schaaf et al., 2004), and homologues of YS1, YELLOW STRIPE1-LIKEs (OsYSLs) in rice (Inoue et al., 2009), and (HvYSLs) in barley (Murata et al., 2006; Araki et al., 2011).

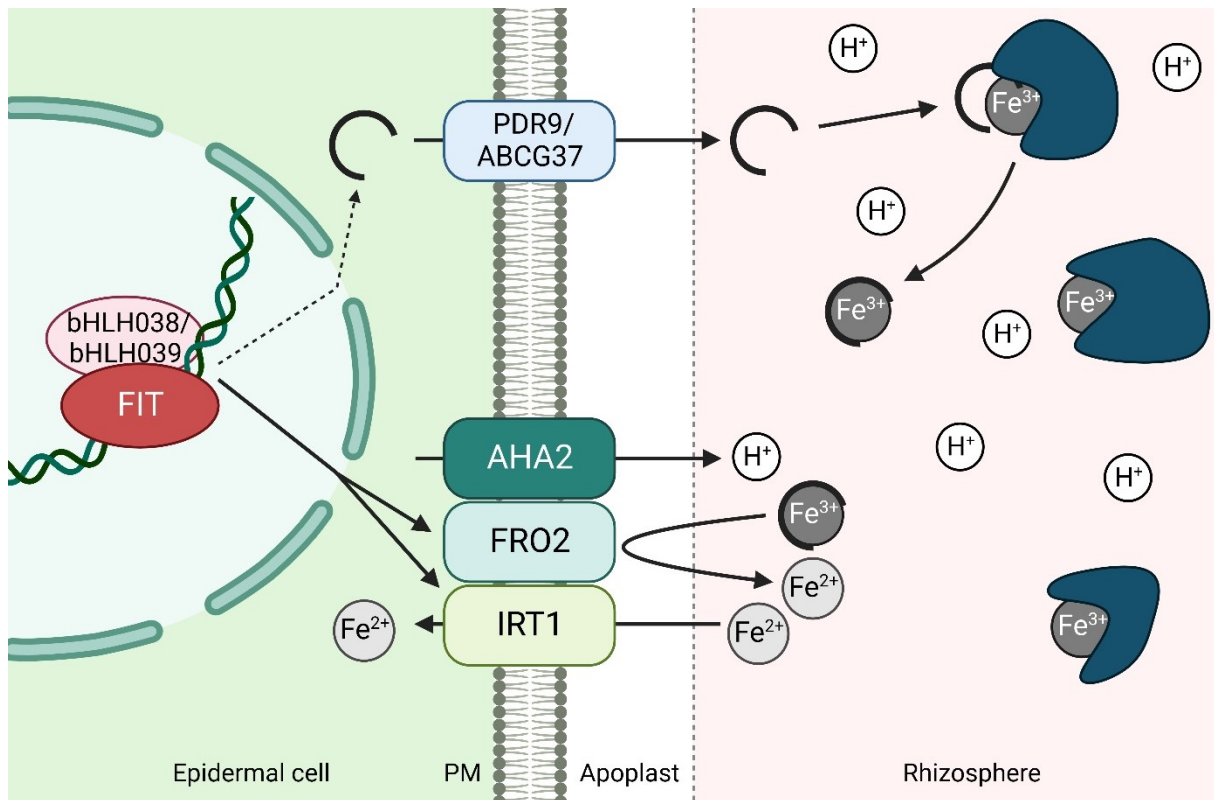


Figure 1. Strategy I – reduction-based iron uptake strategy.

Iron uptake strategy of *Arabidopsis thaliana*. The uptake takes place in epidermal root cells following several individual steps. Iron is trapped in insoluble complexes within the soil. Excretion of protons via ARABIDOPSIS H⁺-ATPASE2 (AHA2) acidifies the rhizosphere and solubilizes ferric iron (Fe^{3+}). Additionally, PLEIOTROPIC DRUG RESISTANCE9 (PDR9, or ATP-BINDING CASSETTE G37 (ABCG37)) secretes coumarins to chelate Fe^{3+} and further solubilizes it. FERRIC REDUCTASE-OXIDASE2 (FRO2) reduces Fe^{3+} to ferrous iron (Fe^{2+}). Fe^{2+} is finally taken up via IRON REGULATED TRANSPORTER1 (IRT1). The upregulation of *FRO2*, *IRT1*, and necessary proteins for coumarin biosynthesis occurs upon iron deficiency and is regulated via a heterodimer of basic helix-loop-helix (bHLH) transcription factors (TFs) FER-LIKE IRON DEFICIENCY-INDUCED TRANSCRIPTION FACTOR (FIT) and bHLH038/bHLH039, described in the following in 4.1.2. Figure created with BioRender.com.

4.1.2 Transcriptional regulation of iron uptake

To regulate iron uptake, an extensive signaling cascade of basic helix-loop-helix (bHLH) transcription factors (TFs) is active (Figure 2; Heim et al., 2003; Gao et al., 2019). BHLH TFs are conserved TFs present in animals and plants (Murre et al., 1989; Heim et al., 2003; Pires and Dolan, 2010), and the third largest group of TFs behind MYB and APETALA2/ethylene responsive element binding protein (AP2/EREBP) TFs in *Arabidopsis* (Riechmann et al., 2000). They consist of a basic N-terminal DNA-binding domain and a helix-

loop-helix (HLH) domain for interaction with other bHLH TFs and usually function as dimers in order to bind to DNA (Ferré-D'Amaré et al., 1993; Ma et al., 1994; Shimizu et al., 1997; Heim et al., 2003; Toledo-Ortiz et al., 2003). In Arabidopsis, bHLH TFs are organized in groups and subgroups according to structural similarities (Heim et al., 2003).

Starting at the most upstream position in the Arabidopsis signaling cascade, UPSTREAM REGULATOR OF IRT1 (URI, or bHLH121, subgroup IVb) interacts under iron deficiency with the members of subgroup IVc, namely bHLH034, bHLH104, bHLH105 (or IAA-LEUCINE RESISTANT3 (ILR3)), and bHLH115 (Kim et al., 2019; Gao et al., 2020; Lei et al., 2020). Subgroup IVc is functionally redundant and regulates the transcription of *subgroup Ib* and *POPEYE* (*PYE*, subgroup IVb; Zhang et al., 2015; Li et al., 2016b; Liang et al., 2017; Kim et al., 2019; Gao et al., 2020). *PYE* is a TF involved in control of iron homeostasis and translocation (Long et al., 2010). The homo- and heterodimerization of members of subgroup IVc and *PYE* is an important part of the regulatory cascade (Long et al., 2010; Selote et al., 2015; Zhang et al., 2015; Li et al., 2016b; Liang et al., 2017; Samira et al., 2018; Tissot et al., 2019). With bHLH11 (subgroup IVb), transcription of *subgroup Ib* via subgroup IVc can be repressed (Li et al., 2022). Subgroup Ib consist of bHLH038, bHLH039, bHLH100, and bHLH101 (Wang et al., 2007). Even though these TFs show redundancy (Wang et al., 2007, 2013), they are not entirely redundant. bHLH038 and bHLH039 are involved in the upregulation of the iron uptake machinery, specifically *FRO2* and *IRT1* (Yuan et al., 2008; Wang et al., 2013), while bHLH100 and bHLH101 are involved in the distribution of iron and do not regulate *FRO2* or *IRT1* (Sivitz et al., 2012). Function of bHLH038 and bHLH039 within the upregulation of the iron uptake machinery is only possible in dimerization with the essential TF FER-LIKE IRON DEFICIENCY-INDUCED TRANSCRIPTION FACTOR (*FIT*, subgroup IIIa; Colangelo and Gueriot, 2004; Jakoby et al., 2004; Yuan et al., 2005; Bauer et al., 2007; Yuan et al., 2008; Wang et al., 2013) as an iron uptake module, supporting once more the importance of dimerization of bHLH TFs for their functionality.

Between Arabidopsis and the Strategy II plant rice this extensive iron uptake regulating network is largely conserved (Kobayashi, 2019). Among the bHLH TFs in Arabidopsis, many orthologues in rice were identified, e.g., OsbHLH057, OsbHLH058, OsbHLH059, and OsbHLH060 (or POSITIVE REGULATOR OF IRON HOMEOSTASIS1 (OsPRI1)) as orthologues of subgroup IVc (Zhang et al., 2017; Kobayashi et al., 2019b), IRON-RELATED BHLH TRANSCRIPTION FACTOR3 (OsIRO3) as orthologue of *PYE* (Zheng et al., 2010), OsIRO2 as orthologue of subgroup Ib (Ogo et al., 2007), and OsbHLH156 as orthologue of *FIT* (Wang et al., 2020).

4.1.2.1 Transcriptional regulation of *FIT*

Work on the TF FER in tomato (Ling et al., 2002; Brumbarova and Bauer, 2005) led to the identification of the homologue *FIT* in Arabidopsis. *FER* is upregulated under iron-deficient conditions (Brumbarova and Bauer, 2005) and *fer* loss-of-function mutants show chlorosis and

die without additional iron supply (Ling et al., 2002). Similarly, *fit* loss-of-function mutants are chlorotic and FIT is upregulated under iron deficiency (Jakoby et al., 2004; Colangelo and Guerinot, 2004). FIT is mainly expressed in the root and *FIT* promoter is active in epidermal cells of the differentiation and elongation root zone, central cylinder and also in lateral roots (Colangelo and Guerinot, 2004; Jakoby et al., 2004). Many genes involved in iron uptake are regulated in a FIT-dependent manner, especially *FRO2* and *IRT1* (Figure 2; Colangelo and Guerinot, 2004; Jakoby et al., 2004; Ivanov et al., 2012; Sivitz et al., 2012; Schmid et al., 2014; Mai et al., 2015, 2016; Schwarz and Bauer, 2020). FIT, and subgroup Ib TFs, are upregulated in an iron-deficient manner (Colangelo and Guerinot, 2004; Jakoby et al., 2004; Wang et al., 2007; Naranjo-Arcos et al., 2017). *FIT* itself is regulated transcriptionally by itself and the FIT-bHLH039 heterodimer (Wang et al., 2007; Naranjo-Arcos et al., 2017). Apart from repressing transcription of *subgroup Ib*, bHLH11 also represses *FIT* expression (Tanabe et al., 2019; Li et al., 2022). *FIT* transcription levels are also reduced in Mediator complex subunit mutants under iron deficiency (Yang et al., 2014).

Transcriptional regulation of *FIT* is also influenced by other regulatory cascades (Figure 2). Briefly, auxin, nitric oxide, and ethylene application under iron deficiency are a positive regulator of *FIT* expression (Lucena et al., 2006; Chen et al., 2010; García et al., 2010; Yang et al., 2013), while jasmonic acid, cytokinin, and H₂O₂ have a negative effect on *FIT* expression (Séguéla et al., 2008; Le et al., 2016; Cui et al., 2018). Despite transcriptional control of *FIT*, *FIT* regulation mainly occurs on post-translational level and will be elucidated in section 4.1.3.1.

4.1.3 Post-translational regulation of iron uptake

Post-translational modifications are a versatile tool to finetune signaling cascades (Friso and Van Wijk, 2015; Millar et al., 2019; Yin et al., 2019; Han et al., 2022). This is also true for the regulation of iron uptake. Post-translational regulation can be found at different positions of the iron uptake signaling cascade (Figure 2), most prominently among them are ubiquitination and phosphorylation.

The E3 ligase BRUTUS (BTS) targets URI/bHLH121 and members of the subgroup IVc for proteasomal degradation (Long et al., 2010; Selote et al., 2015; Kim et al., 2019). BTS homologue BRUTUS-LIKE1 (BTSL1; Hindt et al., 2017) is proposed to mediate subgroup IVc and PYE degradation (Lichtblau et al., 2022). In absence of subgroup IVc, *subgroup Ib* genes are not transcribed, hence iron uptake is negatively regulated. Two orthologues of BTS, HAEMERYTHRIN MOTIF-CONTAINING REALLY INTERESTING NEW GENE - AND ZINC-FINGER PROTEIN1 and 2 (OsHRZ1/OsHRZ2), exist also in rice (Kobayashi et al., 2013). Depending on the concentration of different non-iron metals, IRT1 is monoubiquitinated by a RING E3 ubiquitin ligase IRT1 DEGRADATION FACTOR1 (IDF1) and degraded (Barberon et al., 2011; Shin et al., 2013). This mechanism avoids overaccumulation of iron and other non-essential metals due to the poor selectivity of IRT1. Phosphorylation of IRT1 by CBL-

INTERACTING PROTEIN KINASE23 (CIPK23) facilitates the degradation process by IDF1 (Dubeaux et al., 2018), and is additionally shown to reduce FRO2 activity (Tian et al., 2016). Phosphorylation is also observed for URI/bHLH121. Phosphorylated URI/bHLH121 is accumulated under iron-deficient conditions and proposed to be the form of URI/bHLH121 that interacts with subgroup IVc. In turn, under iron-sufficient conditions, phosphorylated URI/bHLH121 is targeted for degradation by BTS (Kim et al., 2019). A combination of both activation and deactivation via phosphorylation by the calcium-dependent protein kinase CIPK11 is observed for AHA2 (Fuglsang et al., 2007, 2014).

4.1.3.1 Post-translational regulation of FIT

FIT protein stability is widely subject to regulation, by either stabilizing or destabilizing the protein (Figure 2). Ethylene is produced under iron deficiency and the TFs ETHYLENE INSENSITIVE3 (EIN3) and ETHYLENE INSENSITIVE3-LIKE1 (EIL1) acting in the ethylene signaling pathway are proposed to stabilize FIT protein by direct interaction (Romera et al., 1999; Lingam et al., 2011). By this, FIT is less prone to undergo proteasomal degradation, which has a positive effect on iron uptake regulation. Ethylene synthesis inhibitors as well as *ein3 eil1* mutants have the opposite effect (Lingam et al., 2011). Additionally, EIN3/EIL1 interact with a subunit of the Mediator complex, MED25, which in turn associates with MED16 (Yang et al., 2014). MED16 interacts with FIT and can recruit the FIT-subgroup Ib heterodimer to the promoters of *FRO2* and *IRT1* under iron deficiency (Zhang et al., 2014b). Similar to ethylene, nitric oxide has also a stabilizing effect on FIT protein. In presence of nitric oxide, FIT does not undergo proteasomal degradation. Inhibitors of nitric oxide reduce FIT protein abundance and also FIT activity (Meiser et al., 2011).

As suspected in Lingam et al. (2011) and Meiser et al. (2011), FIT undergoes proteasomal turnover. Under iron deficiency, FIT protein is accumulated but is also rapidly degraded. This is most likely the consequence of FIT target gene promoter binding and the 'used' protein being removed, allowing a new FIT protein to bind (Sivitz et al., 2011). Recently, it was shown that FIT degradation is promoted by BTSL2 (Hindt et al., 2017) by polyubiquitination under iron-deficient conditions (Rodríguez-Celma et al., 2019), but the reported interaction of BTSL1 and BTSL2 with FIT in Rodríguez-Celma et al. (2019) could not be verified in the work of Lichtblau et al. (2022). bHLH TFs of the subgroup IVa, namely bHLH18, bHLH19, bHLH20, and bHLH25, interact with FIT and redundantly lead to FIT degradation in presence of jasmonic acid (Cui et al., 2018). Inhibition of the iron uptake machinery via protein interaction is also shown in the gibberellin context. Gibberellin-regulated DELLA proteins interact with bHLH038, bHLH039, and FIT, preventing the proteins from associating with the target gene promoters (Wild et al., 2016). Similarly, ZINC FINGER OF ARABIDOPSIS THALIANA12 (ZAT12) is also trapping FIT in an interaction preventing it from action (Le et al., 2016).

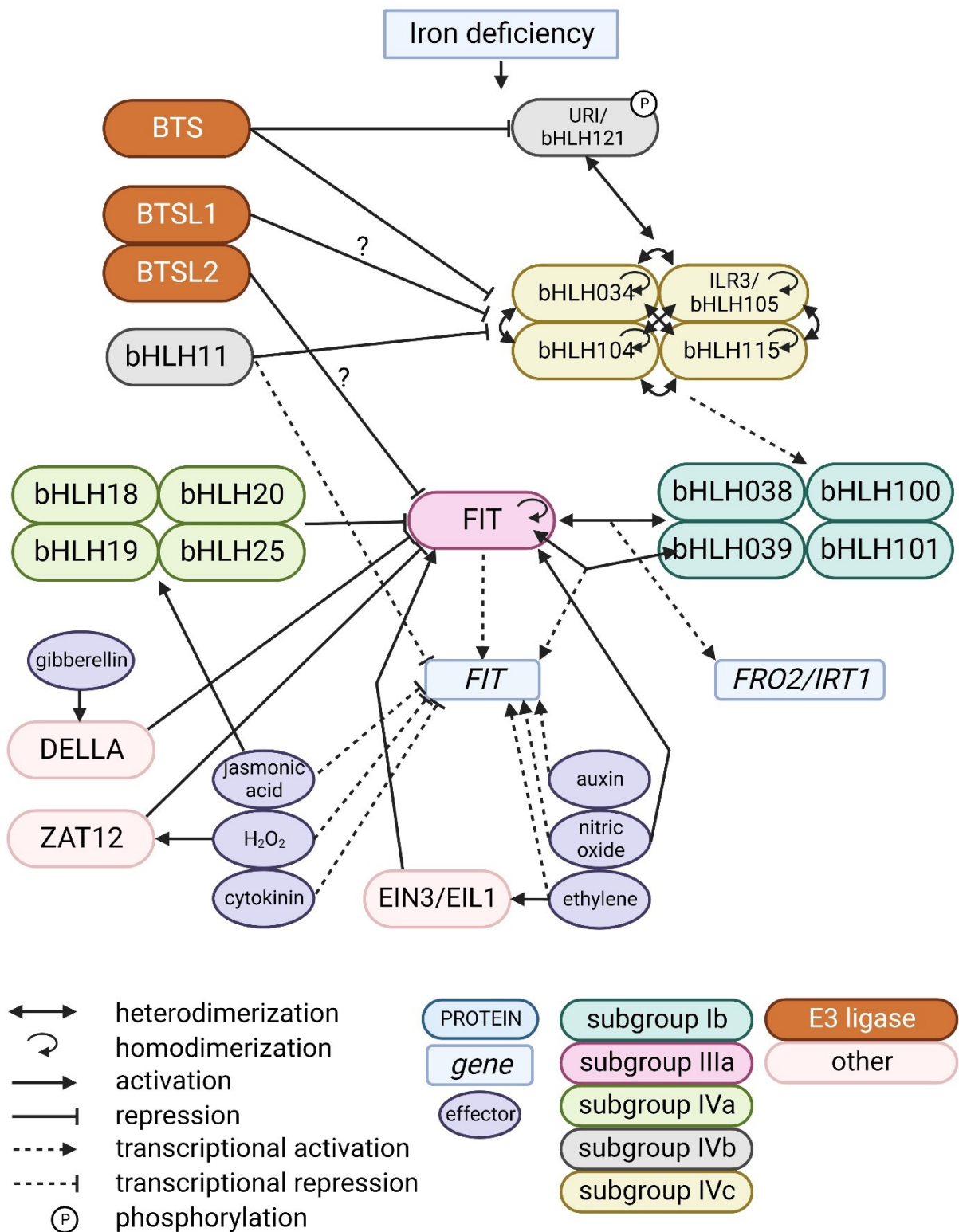


Figure 2. Transcriptional and post-translational regulation of the iron signaling cascade with focus on FIT.

Iron uptake is regulated through an extensive signaling cascade of basic helix-loop-helix (bHLH) transcription factors (TFs), which are divided into subgroups. Phosphorylated UPSTREAM REGULATOR OF IRT1 (URI, or bHLH121, subgroup IVb) interacts with the members of subgroup IVc (bHLH034, bHLH104, bHLH105 (or IAA-LEUCINE RESISTANT3 (ILR3)), bHLH115) to transcriptionally upregulate *subgroup Ib* (bHLH038, bHLH039, bHLH100, bHLH101). bHLH11 (subgroup IVb) can repress *subgroup Ib* expression by repressing subgroup IVc activity. bHLH038/bHLH039 together with FER-LIKE IRON DEFICIENCY-INDUCED TRANSCRIPTION FACTOR (FIT, subgroup IIIa) upregulate the expression of *FERRIC REDUCTASE-OXIDASE2* (*FRO2*) and *IRON REGULATED TRANSPORTER1* (*IRT1*). FIT alone and together with bHLH039 can upregulate its own transcription.

FIT transcription is promoted by auxin, nitric oxide, and ethylene, and repressed by bHLH11, jasmonic acid, H₂O₂, and cytokinin. FIT protein stability is promoted by nitric oxide, and ethylene via ETHYLENE INSENSITIVE3 (EIN3) and ETHYLENE INSENSITIVE3-LIKE1 (EIL1), and destabilized by H₂O₂ via ZINC FINGER OF ARABIDOPSIS THALIANA12 (ZAT12), gibberellin via DELLA proteins, and jasmonic acid via subgroup IVa (bHLH18, bHLH19, bHLH20, bHLH25). E3 ligase BRUTUS (BTS) targets URI/bHLH121 and subgroup IVc for proteasomal degradation, while BTS homologues BRUTUS-LIKE1 and BRUTUS-LIKE2 (BTSL1/BTSL2) might negatively regulate subgroup IVc and FIT, respectively. Figure created with BioRender.com.

FIT is regulated differently from its target genes. While e.g., *FRO2* and *IRT1* are transcribed during the light period, *FIT* is transcribed during the night (Vert et al., 2003; Santi and Schmidt, 2009). This suggests that FIT protein is available during the light period and therefore the regulation of FIT should rather occur on the post-translational level. This perfectly makes sense considering that fast adjustment of iron uptake is needed either to upregulate iron uptake and ensure iron nutrition, but also to downregulate iron uptake to avoid overaccumulation. Hence, *de novo* synthesis of FIT protein may be too time consuming to keep up with the rapid environmental changes. Protein turnover is a way to regulate FIT protein abundance, but it is not clear how FIT activity is regulated before degradation. Thus, finetuning of FIT regulation still remains unclear.

4.1.4 Long distance signaling in iron uptake

As sink and source tissue are physiologically distinct, plants must have a way to signal iron demand in the shoot and upregulate iron uptake in the root. Split-root assays and grafting experiments already showed that such a signal exists, but it remains unclear what kind of signaling is coupling demand and acquisition. Local and systemic signals promote a response by the iron uptake machinery (Vert et al., 2003; Kumar et al., 2017; Nguyen et al., 2022), but the actual long distance signal is not known. Proposed candidates are oxygen/redox status, heme, iron sulfur cluster, phloem mobile iron and nicotianamine (Kobayashi and Nishizawa, 2014). In fact, phloem levels of iron seem to be important for a proper communication of shoot and root iron status. When phloem is loaded with iron, no iron uptake takes place. In this, OLIGOPEPTIDE TRANSPORTER3 (OPT3) is important for proper shoot-to-root signaling and translocation of iron (Stacey et al., 2008; García et al., 2013, 2018; Zhai et al., 2014; Khan et al., 2018). Recently, evidence of involvement of small effector proteins in shoot-to-root iron signaling is rising (Grillet et al., 2018; Hirayama et al., 2018; Li et al., 2021; Kobayashi et al., 2021; Lichtblau et al., 2022).

Since light is one the most fundamental environmental cues, it is not surprising that it is the input for many molecular mechanisms. To adjust the uptake of nutrients according to changes in light and thereby to plant need is a way to avoid deficiency or toxicity of the respective nutrient. Calcium (Ca), copper (Cu), and magnesium (Mg) homeostasis are influenced by light and also the circadian clock (Dalchau et al., 2010; Hermans et al., 2010; Zhang et al., 2014a; Perea-García et al., 2016; de Melo et al., 2021; Rivière et al., 2021; Xu et

al., 2022). In case of iron, several studies previously showed that expression or transcript abundancies of *BHLH039*, *FRO2*, *IRT1*, and *AHA2* are under diurnal or circadian clock regulation or altered by a shoot-borne signal (Vert et al., 2003; Santi and Schmidt, 2009; Hong et al., 2013; Xu et al., 2019). Also, the circadian period of clock components is lengthened under iron deficiency, in dependency with iron concentration, or in iron uptake-deficient mutants (Chen et al., 2013; Hong et al., 2013; Salomé et al., 2013). In turn, promoter activity of *BHLH039* and *IRT1* cycles in continuous light, similar to clock components (Hong et al., 2013). Chloroplasts, as major iron sinks, must have a way communicate their iron need. Therefore, they are thought to be responsible for the lengthening of the circadian period under iron deficiency to ensure iron uptake (Chen et al., 2013). Another study suggested that photoactivated phytochromes (phy) act as direct input on the circadian clock and through the induced photomorphogenesis, the chloroplast development creates an iron sink, but the exact signals to coordinate this remain unknown (Salomé et al., 2013; Tissot et al., 2014). In tomato, red light-activated phyB is responsible for accumulation of the basic leucine zipper (bZIP) TF ELONGATED HYPOCOTYL5 (HY5) and its movement to the root, where it induces the transcription of *FER*, by binding to the ACE motif of *FER* promoter (Guo et al., 2021). Interestingly, also *FIT* promoter has an ACE motif. Similarly, light mediated HY5 also acts as a long-distance signal for nitrate and phosphorus uptake (Chen et al., 2016; Sakuraba et al., 2018). HY5 is also important for mediation of blue light regulated phosphate deficiency-induced primary root growth inhibition, and also here HY5 acts as a shoot-derived signal (Gao et al., 2021). The same study also showed that iron accumulation is high under blue light in the apical meristem and decreases up to the elongation zone in Col-0 but is lowest in the *cry1 cry2* and *hy5* mutant. This makes the blue light photoreceptors cryptochrome1 and 2 (*cry1/cry2*) as well as HY5 possible candidates for signal mediation of light regulated iron uptake. Nevertheless, only little work was conducted in recent years to understand the connection between light and iron acquisition.

4.2 Subcellular protein partitioning

Post-translational modification is an important tool to regulate activation and deactivation of a protein. Nevertheless, the localization of a protein is also crucial for a functioning signal transduction (Meier and Somers, 2011; Allen and Strader, 2021). Finetuning of protein activity can be achieved by a changing localization between two cell compartments. Such an example is nucleocytoplasmic partitioning. Three possible ways to achieve this partitioning are described (combinations are possible): (i) protein modification or conformational change unmasking a nuclear localization signal (NLS) or nuclear export signal, (ii) heterocomplex formation that allows a protein to follow the interactors' relocation or remain in cytoplasm or nucleus via interaction, and (iii) retention in cytoplasm via membrane association and release by proteolysis (Meier and Somers, 2011; Allen and Strader, 2021). An example for conformational change is the relocation of photoreceptor phyB from the cytoplasm

into the nucleus. phyB is abundantly present in the cytoplasm in darkness. Light illumination leads to the release of the N- and C-terminal interaction within the protein, exposing the NLS and shuttling phyB into the nucleus (Chen et al., 2005). PhyA, on the other hand, requires an interaction partner. The small proteins FAR-RED ELONGATED HYPOCOTYL1 (FHY1) and FAR-RED ELONGATED HYPOCOTYL-LIKE (FHL) possess a phyA-binding domain and an NLS. Also here depending on light illumination, FHY1 and phyA interact and are translocated together into the nucleus due to the NLS of FHY1 (Hiltbrunner et al., 2005, 2006; Rösler et al., 2007; Genoud et al., 2008). An example for retention at a membrane with proteolysis is ETHYLENE INSENSITIVE2 (EIN2). EIN2 is located at the endoplasmic reticulum membrane. Ethylene-triggered dephosphorylation of EIN2 leads to C-terminal cleavage and EIN2 can enter the nucleus and positively act on target gene transcription (Ju et al., 2012; Qiao et al., 2012; Wen et al., 2012). More examples for nucleocytoplasmic partitioning exist in hormone, temperature, and pathogen signaling.

A lot of effort was put in understanding of iron uptake regulation in plants but subcellular distribution of the key players within iron uptake was barely in focus up to now, even though finetuning of subcellular localization could be an additional form of regulation. Therefore, an open question remains how the precise localization of TFs involved in iron uptake could be dictating TF function (Gao et al., 2019). Slowly, evidence of nucleocytoplasmic partitioning within iron uptake regulation is rising. Two studies demonstrated that subgroup IVc proteins alter the localization of two other bHLH TFs. URI/bHLH121 has a dual localization in cytoplasm and nucleus but changes to a nuclear localization when subgroup IVc proteins are present. It is also observed that URI/bHLH121 has a dual localization under iron-sufficient conditions and localizes to nucleus, only, under iron-deficient conditions. This nuclear localization could be facilitated by the interaction with subgroup IVc proteins, as subgroup IVc proteins are upregulated under iron deficiency (Lei et al., 2020). Also bHLH11, the closest homologue of URI/bHLH121, has a dual localization in cytoplasm and nucleus and shows a nuclear-only localization upon interaction with the subgroup IVc proteins. This allows the inhibition of subgroup IVc proteins and the downregulation of *subgroup Ib* genes and consequently iron uptake (Li et al., 2022). Interestingly, in parallel to this thesis, change of subcellular localization of bHLH039 orthologue OsIRO2 in rice was observed. The orthologue of FIT, OsbHLH156, has a nuclear localization (Wang et al., 2020), and the presence of OsbHLH156 changes the cytoplasmic localization of IRO2 to a nuclear localization (Liang et al., 2020; Wang et al., 2020).

4.2.1 Condensation

Cellular organization is a fundamental and highly sophisticated part of cell function. Enclosed regions within the cell enable separated biochemical reaction and are essential for cell functioning. Transcription in the nucleus, translation in the cytosol, degradation, and subsequent recycling in the endosomal compartments display a functioning eukaryotic cell. For a long time, membrane-separated organelles were in focus in terms of cellular

organization. With the advancement of microscopy, further compartments were identified, namely (biomolecular) condensates. These condensates are widely diversified membraneless subcompartments. Their occurrence in mammalian and plant field underlines their suggested ancient nature of further compartmentalization of the cell, creating microenvironments for interaction and signaling, and displaying another level of regulatory mechanism (Emenecker et al., 2020). Examples of combined nucleocytoplasmic partitioning and condensation only begin to show the possibilities of how these two cellular organizations can act hand in hand (Powers et al., 2019; Allen and Strader, 2021; Jing et al., 2022).

Condensates can be of dynamic or stable nature. Their formation can occur as phase separation, meaning a solution separating into two or more phases (Emenecker et al., 2020). This can happen as liquid-liquid phase separation (LLPS). LLPS is a rather dynamic condensate formation with dynamic protein exchange. The liquid state can further undergo a phase transition into a gel-like state, an intermediate state, that can lead to a final solid-like state. Solid-like condensates occur as stable compartments, rather associated with terminated reactions, degradation, or diseases (Shin et al., 2017). Experimentally, these properties can be assessed by testing the dynamics of protein exchange and morphology of the condensates (Shin et al., 2017; Weber, 2017).

A prerequisite for proteins to localize in condensates is multivalency, the ability to form numerous interactions. Proteins that have many interaction partners also often have intrinsically disordered regions (IDRs) or are intrinsically disordered proteins, which favor a flexible protein structure and by this enable multiple interactions (Tarczewska and Greb-Markiewicz, 2019; Emenecker et al., 2020). To note, an intrinsically disordered protein or a protein with IDRs does not necessarily have to localize in condensates. Within IDRs, the amino acid composition is an important feature that has influence on the morphology and dynamics of condensates (Powers et al., 2019; Emenecker et al., 2021; Huang et al., 2022). The regulation of condensate formation can occur within these IDRs, e.g., via post-translational modifications such as phosphorylation (Owen and Shewmaker, 2019). In the formation of condensates, some proteins can act as scaffolds, meaning these proteins are driving the formation of condensates. Other proteins may act as clients, meaning that these proteins are not essential for the formation but are localizing in condensates (Banani et al., 2017).

4.2.2 Condensation in plants

In general, condensation in plants is less well studied compared to the mammalian field. Still, this topic has advanced a lot in the past years and evidence is provided that many plant proteins undergo condensation. As plants are exposed to constant environmental changes, condensates could provide a way to spatially concentrate cell components by creating a hub for action when needed (Meyer, 2020). One can distinguish between several condensate types that have a particular function in the cell. Animals and plants share condensate types, but also possess animal- or plant-specific condensates. Partly, proteins that

undergo condensation are identified, but the condensate type is not specified. These condensates are often named after the protein itself. Condensates are mainly found in cytoplasm and nucleus. The following sections will briefly introduce selected condensates found in plants (Figure 3).

4.2.2.1 Cytoplasmic condensates

Processing bodies (P-bodies, also found in animals), repress translation and are responsible for mRNA decay (Parker and Sheth, 2007). They are ribonucleoprotein (RNP, RNA-protein complexes) granules. Their composition is mRNA, proteins repressing translation, proteins involved in 5'-to-3' mRNA decay, decapping, RNA modifying enzymes, and RNA binding proteins (Maldonado-Bonilla, 2014; Luo et al., 2018). In animals, P-bodies are described as dynamic condensates and their formation is shown to occur via LLPS (Kedersha et al., 2005; Kroschwald et al., 2015; Riback et al., 2020). Post-translational modifications, such as phosphorylation and ubiquitination, are a possible way to regulate P-body formation (Chiang et al., 2013; Tenekeci et al., 2016).

Stress granules (SGs, also found in animals), appear upon a stress stimulus (e.g., heat and salt stress) and are of transient nature. During stress, they arrest translation, but unlike P-bodies, their reinstall translation after overcoming stressful conditions. Components of SGs therefore are mRNA, RNA-binding proteins, non-RNA-binding proteins, and factors for translation initiation (Protter and Parker, 2016). Because of their overlapping functions, SGs share some components with P-bodies (Kedersha et al., 2005). Also for SGs, LLPS is a suggested formation process in animals (Kedersha et al., 2005; Riback et al., 2020), and post-translational modification a suggested assembly and disassembly control (Cao et al., 2020).

4.2.2.2 Nuclear condensates

The most prominent and essential component of the nucleus and condensate is the nucleolus (also found in animals). It harbors ribosomal DNA and RNA and is mainly site of ribosomal DNA transcription, ribosomal RNA processing, and ribosome biogenesis (Kalinina et al., 2018; Lafontaine et al., 2021). Additional proteins involved in splicing and RNA modification (e.g., small nucleolar and small nuclear RNPs) are also found in the nucleolus, indicating also possible other functions (Shaw and Brown, 2004; Pendle et al., 2005; Shaw and Brown, 2012; Ohtani, 2018). The nucleolus is further divided into subcompartments, that are not well studied (Shaw and Brown, 2004, 2012), but are liquid phases with different properties, making the nucleolus a multiphase condensate that underlies LLPS (Brangwynne et al., 2011; Feric et al., 2016; Riback et al., 2020). In animals, dephosphorylation processes are important for proper nucleolus assembly (Lyon et al., 1997).

One of the oldest known nuclear condensates are Cajal bodies (also found in animals). Cajal bodies are connected with the nucleolus and therefore share some of their components, like small nucleolar and small nuclear RNPs (Boudonck et al., 1999; Love et al., 2017; Trinkle-

Mulcahy and Sleeman, 2017; Ohtani, 2018). The biogenesis of these components takes place in Cajal bodies and since these components are precursor forms of the slicing machinery, they are passed on the nucleolus and speckles (Sleeman and Lamond, 1999). An important protein for Cajal body formation, but not essential in plants, is coilin (Collier et al., 2006; Makarov et al., 2013). Phosphorylation of coilin influences Cajal body formation (Hearst et al., 2009). Since Cajal bodies are dynamic condensates, it is suggested, but not shown, that they form via LLPS (Neugebauer, 2017; Riback et al., 2020). Cajal bodies vary in number depending on cell type, cell cycle, and developmental stage (Boudonck et al., 1998, 1999).

Another, and very diverse, type of condensates are speckles (also found in animals). Here, the splicing machinery is located (Reddy et al., 2012; Galganski et al., 2017). Parts of the splicing machinery are small nuclear RNPs and splicing factors, like the serine-arginine proteins (Lorković et al., 2004; Shaw and Brown, 2004). The high diversification of speckles most likely bears different tasks for the respective subtype (Lorković et al., 2008). Phosphorylation of serine-arginine proteins has an influence on both the protein dynamics and proper speckle formation (Ali et al., 2003; Reddy et al., 2012; Greig et al., 2020), which is shown in animals in form of LLPS (Xue et al., 2019; Greig et al., 2020). Speckles are also responsive to changes in temperature and transcription activity (Ali et al., 2003; Reddy et al., 2012).

Photobodies (PBs) are plant-specific condensates that are sites for photomorphogenic regulation via photoreceptors and involved proteins (Ronald and Davis, 2019; Pardi and Nusinow, 2021). The most prominent PBs contain the red/far-red light phytochrome photoreceptors and the bHLH TFs PHYTOCHROME INTERACTING FACTORS (PIFs). Photoactivated phytochromes are relocated from the cytoplasm into the nucleus and form PBs (Kircher et al., 2002; Chen et al., 2005; Hiltbrunner et al., 2005, 2006; Rösler et al., 2007; Genoud et al., 2008; Van Buskirk et al., 2012, 2014). Phytochromes form two types of PBs, a transient and a stable type (Kevei et al., 2007; Chen, 2008). One important task of PBs is PIF degradation that promotes photomorphogenic responses. This occurs upon interaction with phytochromes which in turn leads to PIF phosphorylation and ubiquitination (Bauer et al., 2004; Monte et al., 2004; Park et al., 2004; Shen et al., 2005, 2007; Al-Sady et al., 2006; Lorrain et al., 2008; Ni et al., 2013, 2017; Van Buskirk et al., 2014; Dong et al., 2017). Besides, also the blue light cryptochrome photoreceptors form PBs. Cryptochrome PBs are sites for proteasomal degradation of cryptochromes after photoactivation (Yu et al., 2009; Zuo et al., 2012) and for interaction with other proteins (Lian et al., 2011; Zuo et al., 2011, 2012; Wang et al., 2021). Recently, formation of cry2 PBs via LLPS was shown (Wang et al., 2021). Because of their direct responsiveness to external stimuli like light and temperature (and circadian clock), PBs are considered to translate this information into a developmental readout in form of gene regulation (Kaiserli et al., 2015; Meyer, 2020; Pardi and Nusinow, 2021).

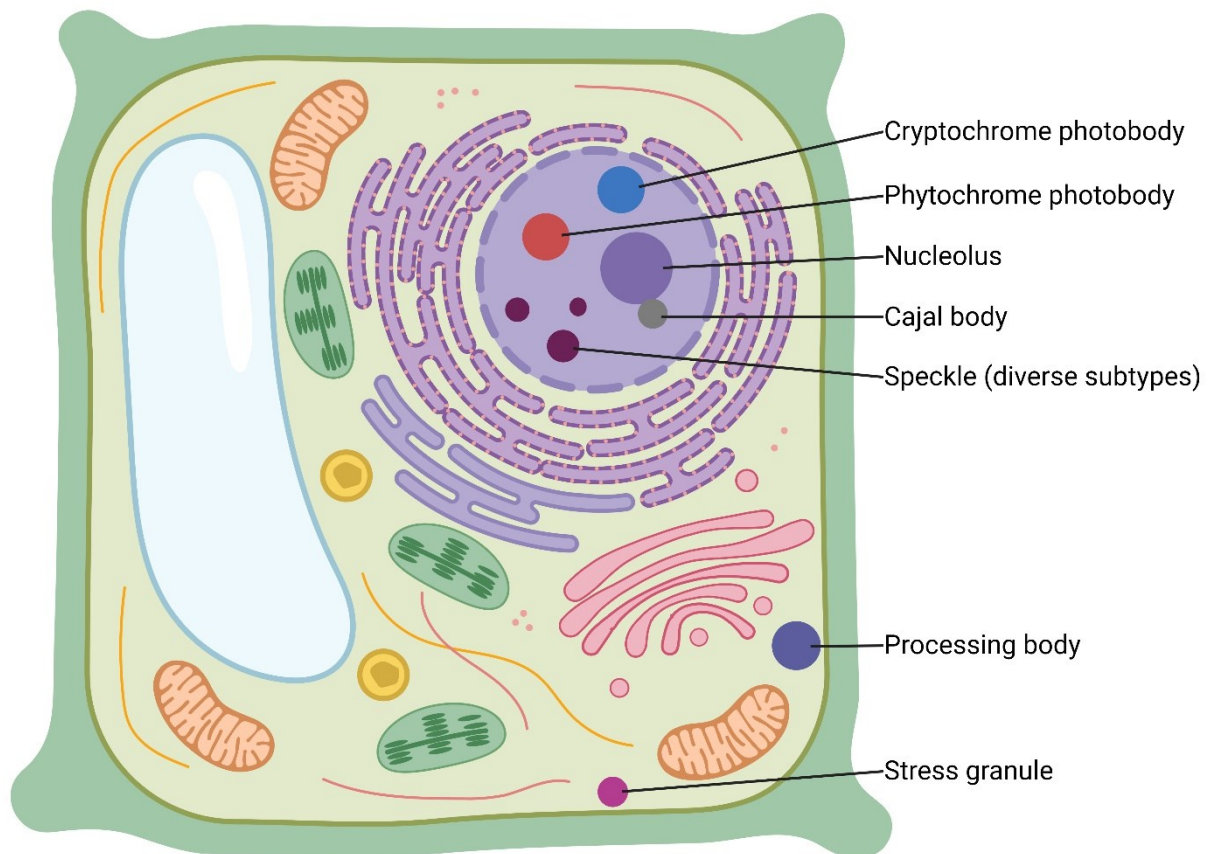


Figure 3. Overview over selected condensates within a plant cell.

Apart from cell organelles that are separated from other cellular compartments by a membrane (in the figure shown: nucleus, rough and smooth endoplasmic reticulum, Golgi apparatus, Golgi vesicles, mitochondria, peroxisomes, chloroplast, and vacuole), condensates without membranes coexist with organelles. These structures are microenvironments with particular tasks and can be found mainly in cytoplasm and nucleus. Cytoplasmic condensates are e.g., processing bodies (P-bodies) for repression of translation, and stress granules (SGs) for translation initiation after stressful conditions. Nuclear condensates are e.g., cryptochrome or phytochrome photobodies (PBs) for photomorphogenesis and gene regulation, nucleoli for ribosome biogenesis, Cajal bodies for biogenesis of precursor forms of the splicing machinery, and speckles for splicing. Figure created with BioRender.com.

Creating microenvironments for a fast regulation of molecular mechanisms could display an adaptation of plants to an ever-changing environment. In total 6% of all *Arabidopsis* proteins are TFs (Riechmann et al., 2000). Interestingly, they are enriched in IDRs (Salladini et al., 2020; Strader et al., 2022). Vertebrate, invertebrate, and plant bHLH TFs all possess IDRs as well, so a flexible protein sequence is a conserved feature of bHLH TFs (Tarczewska and Greb-Markiewicz, 2019; Salladini et al., 2020). Although transcriptional regulation within plant condensates is a proposed and also shown function (Kaiserli et al., 2015; Pardi and Nusinow, 2021; Huang et al., 2022), condensation of TFs is a relatively poorly examined but slowly rising topic (Khan et al., 2014; Perez et al., 2019; Burkart et al., 2022; Huang et al., 2022; Shuai et al., 2022). Especially in the context of nutrition, information on TF condensation is lacking.

5 Thesis objectives

Even though it must display a crucial step in the iron uptake regulation, it is not clear how FIT activity is modulated apart from protein turn-over. A pool of active and inactive FIT is proposed (Lingam et al., 2011; Meiser et al., 2011; Sivitz et al., 2011), but how is the finetuning of FIT activation or deactivation occurring in detail? Our group identified the calcium-dependent protein kinase CIPK11 as an interacting partner of FIT. This indicates a potential involvement of post-translational modification in form of phosphorylation on FIT. Despite the extensive work on molecular and physiological aspects of iron uptake, only little to no information exists on the subcellular localization of the involved TFs. Since subcellular localization dynamics can be a way of finetuning molecular regulation, what are the subcellular localization and dynamics of TFs involved in iron uptake? Therefore, two main objectives guided my work:

1. Examine the influence of phosphorylation on the iron uptake module FIT-bHLH039

The FIT-bHLH039 heterodimer is an important regulatory module for iron uptake. A possible activation and deactivation of FIT will most likely influence the action of this module and thereby alter iron uptake. It was therefore of interest to investigate how the possibility of FIT phosphorylation could influence FIT interaction. For this, phospho-mutant forms of FIT were tested for their capacity to homo- and heterodimerize with bHLH039. This question was assessed with fluorescence resonance energy transfer-after photobleaching (FRET-APB) measurements and partly by bimolecular fluorescence complementation (BiFC) microscopy.

2. Decipher the subcellular localization of the iron uptake module FIT-bHLH039

Subcellular localization, and especially changes in subcellular localization, can alter the regulation of molecular processes. As no information on FIT and bHLH039 was available, it was of interest to investigate their subcellular localization in detail and to close this gap of knowledge. To examine this, an initial extensive microscopy study on the subcellular localization of FIT and bHLH039 was conducted. The observations made in this initial work revealed that (i) bHLH039 showed nucleocytoplasmic partitioning depending on FIT, and that (ii) FIT formed condensates in the nucleus, short nuclear bodies (NBs). Firstly, nucleocytoplasmic partitioning of bHLH039 was examined. To understand the importance of FIT on bHLH039 localization, bHLH039 localization was examined in different expression systems, alone or in combination with FIT, and quantification of microscopy and biochemical data was performed to verify the observations. Secondly, characterization and assignment of a function to FIT NBs was performed. FIT NBs were examined in different expression systems. To characterize FIT NBs, quantification of protein dynamics via fluorescence recovery after photobleaching (FRAP), formation, number, size, and morphology was conducted. To assign a function to FIT NBs, homo- and heterodimerization differences between NBs and cytoplasm were quantified via anisotropy (homo-FRET) and FRET-fluorescence lifetime imaging microscopy (FLIM) measurements, and co-expression with marker proteins was performed.

References

- Abbaspour, N., Hurrell, R., and Kelishadi, R.** (2014). Review on iron and its importance for human health. *J. Res. Med. Sci.* **19**: 164–174.
- Al-Fartusie, F.S. and Mohssan, S.N.** (2017). Essential Trace Elements and Their Vital Roles in Human Body. *Indian J. Adv. Chem. Sci.* **5**: 127–136.
- Al-Sady, B., Ni, W., Kircher, S., Schäfer, E., and Quail, P.H.** (2006). Photoactivated Phytochrome Induces Rapid PIF3 Phosphorylation Prior to Proteasome-Mediated Degradation. *Mol. Cell* **23**: 439–446.
- Ali, G.S., Golovkin, M., and Reddy, A.S.N.** (2003). Nuclear localization and in vivo dynamics of a plant-specific serine/arginine-rich protein. *Plant J.* **36**: 883–893.
- Allen, J.R. and Strader, L.C.** (2021). Nucleocytoplasmic partitioning as a mechanism to regulate Arabidopsis signaling events. *Curr. Opin. Cell Biol.* **69**: 136–141.
- Araki, R., Murata, J., and Murata, Y.** (2011). A Novel Barley Yellow Stripe 1-Like Transporter (HvYSL2) Localized to the Root Endodermis Transports Metal–Phytosiderophore Complexes. *Plant Cell Physiol.* **52**: 1931–1940.
- Balk, J. and Pilon, M.** (2011). Ancient and essential: the assembly of iron-sulfur clusters in plants. *Trends Plant Sci.* **16**: 218–226.
- Balk, J. and Schaedler, T.A.** (2014). Iron Cofactor Assembly in Plants. *Annu. Rev. Plant Biol.* **65**: 125–153.
- Banani, S.F., Lee, H.O., Hyman, A.A., and Rosen, M.K.** (2017). Biomolecular condensates: organizers of cellular biochemistry. *Nat. Rev. Mol. Cell Biol.* **18**: 285–298.
- Barberon, M., Zelazny, E., Robert, S., Conéjéro, G., Curie, C., Friml, J., and Vert, G.** (2011). Monoubiquitin-dependent endocytosis of the IRON-REGULATED TRANSPORTER 1 (IRT1) transporter controls iron uptake in plants. *Proc. Natl. Acad. Sci.* **108**: E450–E458.
- Bauer, D., Viczian, A., Kircher, S., Nobis, T., Nitschke, R., Kunkel, T., Panigrahi, K.C.S., Ádám, É., Fejes, E., Schäfer, E., and Nagy, F.** (2004). Constitutive Photomorphogenesis 1 and Multiple Photoreceptors Control Degradation of Phytochrome Interacting Factor 3, a Transcription Factor Required for Light Signaling in Arabidopsis. *Plant Cell* **16**: 1433–1445.
- Bauer, P., Ling, H.Q., and Guerinot, M. Lou** (2007). FIT, the FER-LIKE IRON DEFICIENCY INDUCED TRANSCRIPTION FACTOR in Arabidopsis. *Plant Physiol. Biochem.* **45**: 260–261.
- Boudonck, K., Dolan, L., and Shaw, P.J.** (1998). Coiled body numbers in the Arabidopsis root epidermis are regulated by cell type, developmental stage and cell cycle parameters. *J. Cell Sci.* **111**: 3687–3694.
- Boudonck, K., Dolan, L., and Shaw, P.J.** (1999). The Movement of Coiled Bodies Visualized in Living Plant Cells by the Green Fluorescent Protein. *Mol. Biol. Cell* **10**: 2297–2307.
- Bouis, H.E., Hotz, C., McClafferty, B., Meenakshi, J. V., and Pfeiffer, W.H.** (2011). Biofortification: A new tool to reduce micronutrient malnutrition. *Food Nutr. Bull.* **32**: 31–40.
- Brangwynne, C.P., Mitchison, T.J., and Hyman, A.A.** (2011). Active liquid-like behavior of nucleoli determines their size and shape in *Xenopus laevis* oocytes. *Proc. Natl. Acad. Sci. U. S. A.* **108**: 4334–4339.
- Briat, J.F., Dubos, C., and Gaymard, F.** (2015). Iron nutrition, biomass production, and plant product quality. *Trends Plant Sci.* **20**: 33–40.
- Brumbarova, T. and Bauer, P.** (2005). Iron-Mediated Control of the Basic Helix-Loop-Helix Protein FER, a Regulator of Iron Uptake in Tomato. *Plant Physiol.* **137**: 1018–1026.
- Bughio, N., Yamaguchi, H., Nishizawa, N.K., Nakanishi, H., and Mori, S.** (2002). Cloning an iron-regulated metal transporter from rice. *J. Exp. Bot.* **53**: 1677–1682.
- Burkart, R.C., Strotmann, V.I., Kirschner, G.K., Akinci, A., Czempik, L., Dolata, A., Maizel, A., Weidtkamp-Peters, S., and Stahl, Y.** (2022). PLETHORA-WOX5 interaction and subnuclear localization control Arabidopsis root stem cell maintenance. *EMBO Rep.* **23**: 1–18.
- Van Buskirk, E.K., Decker, P. V., and Chen, M.** (2012). Photobodies in Light Signaling. *Plant Physiol.* **158**: 52–60.
- Van Buskirk, E.K., Reddy, A.K., Nagatani, A., and Chen, M.** (2014). Photobody Localization of Phytochrome B Is Tightly Correlated with Prolonged and Light-Dependent Inhibition of Hypocotyl Elongation in the Dark. *Plant Physiol.* **165**: 595–607.
- Cao, X., Jin, X., and Liu, B.** (2020). The involvement of stress granules in aging and aging-associated diseases. *Aging Cell* **19**: 1–20.
- Chen, M.** (2008). Phytochrome nuclear body: an emerging model to study interphase nuclear dynamics and signaling. *Curr. Opin. Plant Biol.* **11**: 503–508.
- Chen, M., Tao, Y., Lim, J., Shaw, A., and Chory, J.** (2005). Regulation of Phytochrome B Nuclear Localization through Light-Dependent Unmasking of Nuclear-Localization Signals. *Curr. Biol.* **15**: 637–642.
- Chen, W.W., Yang, J.L., Qin, C., Jin, C.W., Mo, J.H., Ye, T., and Zheng, S.J.** (2010). Nitric Oxide Acts Downstream of Auxin to Trigger Root Ferric-Chelate Reductase Activity in Response to Iron Deficiency in Arabidopsis. *Plant Physiol.* **154**: 810–819.
- Chen, X., Yao, Q., Gao, X., Jiang, C., Harberd, N.P., and Fu, X.** (2016). Shoot-to-Root Mobile Transcription Factor HY5 Coordinates Plant Carbon and Nitrogen Acquisition. *Curr. Biol.* **26**: 640–646.

- Chen, Y.-Y., Wang, Y., Shin, L.-J., Wu, J.-F., Shanmugam, V., Tsednee, M., Lo, J.-C., Chen, C.-C., Wu, S.-H., and Yeh, K.-C. (2013). Iron Is Involved in the Maintenance of Circadian Period Length in Arabidopsis. *Plant Physiol.* **161**: 1409–1420.
- Chiang, P.-Y., Shen, Y.-F., Su, Y.-L., Kao, C.-H., Lin, N.-Y., Hsu, P.-H., Tsai, M.-D., Wang, S.-C., Chang, G.-D., Lee, S.-C., and Chang, C.-J. (2013). Phosphorylation of mRNA Decapping Protein Dcp1a by the ERK Signaling Pathway during Early Differentiation of 3T3-L1 Preadipocytes. *PLoS One* **8**: 1–12.
- Clemens, S. and Weber, M. (2016). The essential role of coumarin secretion for Fe acquisition from alkaline soil. *Plant Signal. Behav.* **11**: 1–6.
- Cointry, V. and Vert, G. (2019). The bifunctional transporter-receptor IRT1 at the heart of metal sensing and signalling. *New Phytol.* **223**: 1173–1178.
- Colangelo, E.P. and Gueriot, M. Lou (2004). The Essential Basic Helix-Loop-Helix Protein FIT1 Is Required for the Iron Deficiency Response. *Plant Cell* **16**: 3400–3412.
- Collier, S., Pendle, A., Boudonck, K., van Rij, T., Dolan, L., and Shaw, P. (2006). A Distant Coilin Homologue Is Required for the Formation of Cajal Bodies in Arabidopsis. *Mol. Biol. Cell* **17**: 2942–2951.
- Connorton, J.M. and Balk, J. (2019). Iron Biofortification of Staple Crops: Lessons and Challenges in Plant Genetics. *Plant Cell Physiol.* **60**: 1447–1456.
- Cui, Y., Chen, C.L., Cui, M., Zhou, W.J., Wu, H.L., and Ling, H.Q. (2018). Four IVa bHLH Transcription Factors Are Novel Interactors of FIT and Mediate JA Inhibition of Iron Uptake in Arabidopsis. *Mol. Plant* **11**: 1166–1183.
- Curie, C., Panaviene, Z., Loulergue, C., Dellaporta, S.L., Briat, J.F., and Walker, E.L. (2001). Maize yellow stripe1 encodes a membrane protein directly involved in Fe(III) uptake. *Nature* **409**: 346–349.
- Dalchau, N., Hubbard, K.E., Robertson, F.C., Hotta, C.T., Briggs, H.M., Stan, G.-B., Gonçalves, J.M., and Webb, A.A.R. (2010). Correct biological timing in Arabidopsis requires multiple light-signaling pathways. *Proc. Natl. Acad. Sci.* **107**: 13171–13176.
- DeLoughery, T.G. (2017). Iron Deficiency Anemia. *Med. Clin. North Am.* **101**: 319–332.
- Distéfano, A.M., López, G.A., Setzes, N., Marchetti, F., Cainzos, M., Cascallares, M., Zabaleta, E., and Pagnussat, G.C. (2021). Ferroptosis in plants: Triggers, proposed mechanisms, and the role of iron in modulating cell death. *J. Exp. Bot.* **72**: 2125–2135.
- Dong, J., Ni, W., Yu, R., Deng, X.W., Chen, H., and Wei, N. (2017). Light-Dependent Degradation of PIF3 by SCF(EBF1/2) Promotes a Photomorphogenic Response in Arabidopsis. *Curr. Biol.* **27**: 2420–2430.
- Dubeaux, G., Neveu, J., Zelazny, E., and Vert, G. (2018). Metal Sensing by the IRT1 Transporter-Receptor Orchestrates Its Own Degradation and Plant Metal Nutrition. *Mol. Cell* **69**: 953–964.
- Durrett, T.P., Gassmann, W., and Rogers, E.E. (2007). The FRD3-Mediated Efflux of Citrate into the Root Vasculature Is Necessary for Efficient Iron Translocation. *Plant Physiol.* **144**: 197–205.
- Eide, D., Broderius, M., Fett, J., and Gueriot, M. Lou (1996). A novel iron-regulated metal transporter from plants identified by functional expression in yeast. *Proc. Natl. Acad. Sci.* **93**: 5624–5628.
- Emenecker, R.J., Holehouse, A.S., and Strader, L.C. (2020). Emerging Roles for Phase Separation in Plants. *Dev. Cell* **55**: 69–83.
- Emenecker, R.J., Holehouse, A.S., and Strader, L.C. (2021). Sequence determinants of in cell condensate morphology, dynamics, and oligomerization as measured by number and brightness analysis. *Cell Commun. Signal.* **19**: 1–15.
- Feric, M., Vaidya, N., Harmon, T.S., Mitrea, D.M., Zhu, L., Richardson, T.M., Kriwacki, R.W., Pappu, R. V., and Brangwynne, C.P. (2016). Coexisting Liquid Phases Underlie Nucleolar Subcompartments. *Cell* **165**: 1686–1697.
- Ferré-D'Amaré, A.R., Prendergast, G.C., Ziff, E.B., and Burley, S.K. (1993). Recognition by Max of its cognate DNA through a dimeric b/HLH/Z domain. *Nature* **363**: 38–45.
- Fourcroy, P., Sisó-Terraza, P., Sudre, D., Savirón, M., Rey, G., Gaymard, F., Abadía, A., Abadía, J., Álvarez-Fernández, A., and Briat, J.F. (2014). Involvement of the ABCG37 transporter in secretion of scopoletin and derivatives by Arabidopsis roots in response to iron deficiency. *New Phytol.* **201**: 155–167.
- Friso, G. and Van Wijk, K.J. (2015). Posttranslational Protein Modifications in Plant Metabolism. *Plant Physiol.* **169**: 1469–1487.
- Fuglsang, A.T., Guo, Y., Cuin, T.A., Qiu, Q., Song, C., Kristiansen, K.A., Bych, K., Schulz, A., Shabala, S., Schumaker, K.S., Palmgren, M.G., and Zhu, J.-K. (2007). Arabidopsis Protein Kinase PKS5 Inhibits the Plasma Membrane H⁺-ATPase by Preventing Interaction with 14-3-3 Protein. *Plant Cell* **19**: 1617–1634.
- Fuglsang, A.T., Kristensen, A., Cuin, T.A., Schulze, W.X., Persson, J., Thuesen, K.H., Ytting, C.K., Oehlenschläger, C.B., Mahmood, K., Sondergaard, T.E., Shabala, S., and Palmgren, M.G. (2014). Receptor kinase-mediated control of primary active proton pumping at the plasma membrane. *Plant J.* **80**: 951–964.
- Galganski, L., Urbanek, M.O., and Krzyzosiak, W.J. (2017). Nuclear speckles: Molecular organization, biological function and role in disease. *Nucleic Acids Res.* **45**: 10350–10368.
- Gao, F., Robe, K., Bettembourg, M., Navarro, N., Rofidal, V., Santoni, V., Gaymard, F., Vignols, F.,

- Roschzttardtz, H., Izquierdo, E., and Dubos, C.** (2020). The Transcription Factor bHLH121 Interacts with bHLH105 (ILR3) and Its Closest Homologs to Regulate Iron Homeostasis in Arabidopsis. *Plant Cell* **32**: 508–524.
- Gao, F., Robe, K., Gaymard, F., Izquierdo, E., and Dubos, C.** (2019). The Transcriptional Control of Iron Homeostasis in Plants: A Tale of bHLH Transcription Factors? *Front. Plant Sci.* **10**: 1–8.
- Gao, Y.Q., Bu, L.H., Han, M.L., Wang, Y.L., Li, Z.Y., Liu, H.T., and Chao, D.Y.** (2021). Long-distance blue light signalling regulates phosphate deficiency-induced primary root growth inhibition. *Mol. Plant* **14**: 1539–1553.
- García, M.J., Corpas, F.J., Lucena, C., Alcántara, E., Pérez-Vicente, R., Zamarreño, Á.M., Bacaicoa, E., García-Mina, J.M., Bauer, P., and Romera, F.J.** (2018). A Shoot Fe Signaling Pathway Requiring the OPT3 Transporter Controls GSNO Reductase and Ethylene in Arabidopsis thaliana Roots. *Front. Plant Sci.* **9**: 1–17.
- García, M.J., Lucena, C., Romera, F.J., Alcántara, E., and Pérez-Vicente, R.** (2010). Ethylene and nitric oxide involvement in the up-regulation of key genes related to iron acquisition and homeostasis in Arabidopsis. *J. Exp. Bot.* **61**: 3885–3899.
- García, M.J., Romera, F.J., Stacey, M.G., Stacey, G., Villar, E., Alcántara, E., and Pérez-Vicente, R.** (2013). Shoot to root communication is necessary to control the expression of iron-acquisition genes in Strategy I plants. *Planta* **237**: 65–75.
- Genoud, T., Schweizer, F., Tscheuschler, A., Debrieux, D., Casal, J.J., Schäfer, E., Hiltbrunner, A., and Fankhauser, C.** (2008). FHY1 Mediates Nuclear Import of the Light-Activated Phytochrome A Photoreceptor. *PLoS Genet.* **4**: 1–12.
- Giehl, R.F.H., Gruber, B.D., and Von Wirén, N.** (2013). It's time to make changes: modulation of root system architecture by nutrient signals. *J. Exp. Bot.* **65**: 769–778.
- Greig, J.A., Nguyen, T.A., Lee, M., Holehouse, A.S., Posey, A.E., Pappu, R. V., and Jedd, G.** (2020). Arginine-Enriched Mixed-Charge Domains Provide Cohesion for Nuclear Speckle Condensation. *Mol. Cell* **77**: 1237–1250.
- Grillet, L., Lan, P., Li, W., Mokkapati, G., and Schmidt, W.** (2018). IRON MAN is a ubiquitous family of peptides that control iron transport in plants. *Nat. Plants* **4**: 953–963.
- Guerinot, M. Lou** (2000). The ZIP family of metal transporters. *Biochim. Biophys. Acta* **1465**: 190–198.
- Guerinot, M. Lou and Yi, Y.** (1994). Iron: Nutritious, Noxious, and Not Readily Available. *Plant Physiol.* **104**: 815–820.
- Guo, Z., Xu, J., Wang, Y., Hu, C., Shi, K., Zhou, J., Xia, X., Zhou, Y., Foyer, C.H., and Yu, J.** (2021). The phyB-dependent induction of HY5 promotes iron uptake by systemically activating FER expression. *EMBO Rep.* **22**: 1–15.
- Han, D., Yu, Z., Lai, J., and Yang, C.** (2022). Post-translational modification: a strategic response to high temperature in plants. *aBIOTECH* **3**: 49–64.
- Hänsch, R. and Mendel, R.R.** (2009). Physiological functions of mineral micronutrients (Cu, Zn, Mn, Fe, Ni, Mo, B, Cl). *Curr. Opin. Plant Biol.* **12**: 259–266.
- Hearst, S.M., Gilder, A.S., Negi, S.S., Davis, M.D., George, E.M., Whittom, A.A., Toyota, C.G., Husedzinovic, A., Gruss, O.J., and Hebert, M.D.** (2009). Cajal-body formation correlates with differential coilin phosphorylation in primary and transformed cell lines. *J. Cell Sci.* **122**: 1872–1881.
- Heim, M.A., Jakoby, M., Werber, M., Martin, C., Weisshaar, B., and Bailey, P.C.** (2003). The Basic Helix-Loop-Helix Transcription Factor Family in Plants: A Genome-Wide Study of Protein Structure and Functional Diversity. *Mol. Biol. Evol.* **20**: 735–747.
- Hell, R. and Stephan, U.W.** (2003). Iron uptake, trafficking and homeostasis in plants. *Planta* **216**: 541–551.
- Henriques, R., Jásik, J., Klein, M., Martinoia, E., Feller, U., Schell, J., Pais, M.S., and Koncz, C.** (2002). Knock-out of Arabidopsis metal transporter gene IRT1 results in iron deficiency accompanied by cell differentiation defects. *Plant Mol. Biol.* **50**: 587–597.
- Hentze, M.W., Muckenthaler, M.U., and Andrews, N.C.** (2004). Balancing Acts: Molecular Control of Mammalian Iron Metabolism. *Trends Biochem. Sci.* **117**: 285–297.
- Hermans, C., Vuylsteke, M., Coppens, F., Craciun, A., Inzé, D., and Verbruggen, N.** (2010). Early transcriptomic changes induced by magnesium deficiency in Arabidopsis thaliana reveal the alteration of circadian clock gene expression in roots and the triggering of abscisic acid-responsive genes. *New Phytol.* **187**: 119–131.
- Hiltbrunner, A., Tscheuschler, A., Viczián, A., Kunkel, T., Kircher, S., and Schäfer, E.** (2006). FHY1 and FHL Act Together to Mediate Nuclear Accumulation of the Phytochrome A Photoreceptor. *Plant Cell Physiol.* **47**: 1023–1034.
- Hiltbrunner, A., Viczián, A., Bury, E., Tscheuschler, A., Kircher, S., Tóth, R., Honsberger, A., Nagy, F., Fankhauser, C., and Schäfer, E.** (2005). Nuclear Accumulation of the Phytochrome A Photoreceptor Requires FHY1. *Curr. Biol.* **15**: 2125–2130.
- Hindt, M.N., Akmakjian, G.Z., Pivarski, K.L., Punshon, T., Baxter, I., Salt, D.E., and Guerinot, M. Lou** (2017). BRUTUS and its paralogs, BTS LIKE1 and BTS LIKE2, encode important negative regulators of the iron deficiency response in Arabidopsis thaliana. *Metallomics* **9**: 876–890.

- Hirayama, T., Lei, G.J., Yamaji, N., Nakagawa, N., and Ma, J.F. (2018). The Putative Peptide Gene FEP1 Regulates Iron Deficiency Response in Arabidopsis. *Plant Cell Physiol.* **59**: 1739–1752.
- Hong, S., Kim, S.A., Guerinot, M. Lou, and McClung, C.R. (2013). Reciprocal Interaction of the Circadian Clock with the Iron Homeostasis Network in Arabidopsis. *Plant Physiol.* **161**: 893–903.
- Huang, X., Xiao, N., Zou, Y., Xie, Y., Tang, L., Zhang, Y., Yu, Y., Li, Y., and Xu, C. (2022). Heterotypic transcriptional condensates formed by prion-like paralogous proteins canalize flowering transition in tomato. *Genome Biol.* **23**: 1–21.
- Inoue, H., Kobayashi, T., Nozoye, T., Takahashi, M., Kakei, Y., Suzuki, K., Nakazono, M., Nakanishi, H., Mori, S., and Nishizawa, N.K. (2009). Rice OsYSL15 Is an Iron-regulated Iron (III)-Deoxymugineic Acid Transporter Expressed in the Roots and Is Essential for Iron Uptake in Early Growth of the Seedlings. *J. Biol. Chem.* **284**: 3470–3479.
- Ishimaru, Y. et al. (2006). Rice plants take up iron as an Fe³⁺-phytosiderophore and as Fe²⁺. *Plant J.* **45**: 335–346.
- Ivanov, R., Brumbarova, T., and Bauer, P. (2012). Fitting into the Harsh Reality: Regulation of Iron-deficiency Responses in Dicotyledonous Plants. *Mol. Plant* **5**: 27–42.
- Jain, A. and Connolly, E.L. (2013). Mitochondrial iron transport and homeostasis in plants. *Front. Plant Sci.* **4**: 1–6.
- Jakoby, M., Wang, H.Y., Reidt, W., Weisshaar, B., and Bauer, P. (2004). FRU (BHLH029) is required for induction of iron mobilization genes in Arabidopsis thaliana. *FEBS Lett.* **577**: 528–534.
- Jing, H., Korasick, D.A., Emenecker, R.J., Morffy, N., Wilkinson, E.G., Powers, S.K., and Strader, L.C. (2022). Regulation of AUXIN RESPONSE FACTOR condensation and nucleo-cytoplasmic partitioning. *Nat. Commun.* **13**: 1–11.
- Ju, C. et al. (2012). CTR1 phosphorylates the central regulator EIN2 to control ethylene hormone signaling from the ER membrane to the nucleus in Arabidopsis. *Proc. Natl. Acad. Sci. U. S. A.* **109**: 19486–19491.
- Kaiserli, E., Páldi, K., O'Donnell, L., Batalov, O., Pedmale, U. V., Nusinow, D.A., Kay, S.A., and Chory, J. (2015). Integration of Light and Photoperiodic Signaling in Transcriptional Nuclear Foci. *Dev. Cell* **35**: 311–321.
- Kalinina, N.O., Makarova, S., Makhotenko, A., Love, A.J., and Taliansky, M. (2018). The Multiple Functions of the Nucleolus in Plant Development, Disease and Stress Responses. *Front. Plant Sci.* **9**: 1–19.
- Kedersha, N., Stoecklin, G., Ayodele, M., Yacono, P., Lykke-Andersen, J., Fritzler, M.J., Scheuner, D., Kaufman, R.J., Golan, D.E., and Anderson, P. (2005). Stress granules and processing bodies are dynamically linked sites of mRNP remodeling. *J. Cell Biol.* **169**: 871–884.
- Kevei, E., Schafer, E., and Nagy, F. (2007). Light-regulated nucleo-cytoplasmic partitioning of phytochromes. *J. Exp. Bot.* **58**: 3113–3124.
- Khan, M., Rozhon, W., Unterholzner, S.J., Chen, T., Eremina, M., Wurzinger, B., Bachmair, A., Teige, M., Sieberer, T., Isono, E., and Poppenberger, B. (2014). Interplay between phosphorylation and SUMOylation events determines CESTA protein fate in brassinosteroid signalling. *Nat. Commun.* **5**: 1–10.
- Khan, M.A., Castro-Guerrero, N.A., McInturf, S.A., Nguyen, N.T., Dame, A.N., Wang, J., Bindbeutel, R.K., Joshi, T., Jurisson, S.S., Nusinow, D.A., and Mendoza-Cozatl, D.G. (2018). Changes in iron availability in Arabidopsis are rapidly sensed in the leaf vasculature and impaired sensing leads to opposite transcriptional programs in leaves and roots. *Plant Cell Environ.* **41**: 2263–2276.
- Kim, S.A., Lacroix, I.S., Gerber, S.A., and Guerinot, M. Lou (2019). The iron deficiency response in Arabidopsis thaliana requires the phosphorylated transcription factor URI. *Proc. Natl. Acad. Sci.* **116**: 24933–24942.
- Kircher, S., Gil, P., Kozma-Bognár, L., Fejes, E., Speth, V., Husselstein-Muller, T., Bauer, D., Ádám, É., Schäfer, E., and Nagy, F. (2002). Nucleocytoplasmic Partitioning of the Plant Photoreceptors Phytochrome A, B, C, D, and E Is Regulated Differentially by Light and Exhibits a Diurnal Rhythm. *Plant Cell* **14**: 1541–1555.
- Kobayashi, T. (2019). Understanding the Complexity of Iron Sensing and Signaling Cascades in Plants. *Plant Cell Physiol.* **60**: 1440–1446.
- Kobayashi, T., Nagano, A.J., and Nishizawa, N.K. (2021). Iron deficiency-inducible peptide-coding genes OsIMA1 and OsIMA2 positively regulate a major pathway of iron uptake and translocation in rice. *J. Exp. Bot.* **72**: 2196–2211.
- Kobayashi, T., Nagasaka, S., Senoura, T., Itai, R.N., Nakanishi, H., and Nishizawa, N.K. (2013). Iron-binding haemerythrin RING ubiquitin ligases regulate plant iron responses and accumulation. *Nat. Commun.* **4**: 1–12.
- Kobayashi, T. and Nishizawa, N.K. (2014). Iron sensors and signals in response to iron deficiency. *Plant Sci.* **224**: 36–43.
- Kobayashi, T. and Nishizawa, N.K. (2012). Iron Uptake, Translocation, and Regulation in Higher Plants. *Annu. Rev. Plant Biol.* **63**: 131–152.
- Kobayashi, T., Nozoye, T., and Nishizawa, N.K. (2019a). Iron transport and its regulation in plants. *Free Radic. Biol. Med.* **133**: 11–20.

- Kobayashi, T., Ozu, A., Kobayashi, S., An, G., Jeon, J.S., and Nishizawa, N.K.** (2019b). OsbHLH058 and OsbHLH059 transcription factors positively regulate iron deficiency responses in rice. *Plant Mol. Biol.* **101**: 471–486.
- Korshunova, Y.O., Eide, D., Clark, W.G., Guerinot, M. Lou, and Himadri, B.** (1999). The IRT1 protein from *Arabidopsis thaliana* is a metal transporter with a broad substrate range. *Plant Mol. Biol.* **40**: 37–44.
- Kroschwald, S., Maharana, S., Mateju, D., Malinowska, L., Nüske, E., Poser, I., Richter, D., and Alberti, S.** (2015). Promiscuous interactions and protein disaggregases determine the material state of stress-inducible RNP granules. *Elife* **4**: 1–32.
- Kumar, R.K., Chu, H.H., Abundis, C., Vasques, K., Rodriguez, D.C., Chia, J.C., Huang, R., Vatamaniuk, O.K., and Walker, E.L.** (2017). Iron-Nicotianamine Transporters are Required for Proper Long Distance Iron Signaling. *Plant Physiol.* **175**: 1254–1268.
- Lafontaine, D.L.J., Riback, J.A., Bascetin, R., and Brangwynne, C.P.** (2021). The nucleolus as a multiphase liquid condensate. *Nat. Rev. Mol. Cell Biol.* **22**: 165–182.
- Le, C.T.T., Brumbarova, T., Ivanov, R., Stoof, C., Weber, E., Mohrbacher, J., Fink-Straube, C., and Bauer, P.** (2016). ZINC FINGER OF ARABIDOPSIS THALIANA12 (ZAT12) Interacts with FER-LIKE IRON DEFICIENCY-INDUCED TRANSCRIPTION FACTOR (FIT) Linking Iron Deficiency and Oxidative Stress Responses. *Plant Physiol.* **170**: 540–557.
- Lee, S. and An, G.** (2009). Over-expression of OsIRT1 leads to increased iron and zinc accumulations in rice. *Plant, Cell Environ.* **32**: 408–416.
- Lei, R., Li, Y., Cai, Y., Li, C., Pu, M., Lu, C., Yang, Y., and Liang, G.** (2020). bHLH121 Functions as a Direct Link that Facilitates the Activation of FIT by bHLH IVc Transcription Factors for Maintaining Fe Homeostasis in *Arabidopsis*. *Mol. Plant* **13**: 634–649.
- Li, G., Kronzucker, H.J., and Shi, W.** (2016a). The Response of the Root Apex in Plant Adaptation to Iron Heterogeneity in Soil. *Front. Plant Sci.* **7**: 1–7.
- Li, S., Zhou, X., Li, H., Liu, Y., Zhu, L., Guo, J., Liu, X., Fan, Y., Chen, J., and Chen, R.** (2015). Overexpression of ZmIRT1 and ZmZIP3 Enhances Iron and Zinc Accumulation in Transgenic *Arabidopsis*. *PLoS One* **10**: 1–21.
- Li, X., Zhang, H., Ai, Q., Liang, G., and Yu, D.** (2016b). Two bHLH Transcription Factors, bHLH34 and bHLH104, Regulate Iron Homeostasis in *Arabidopsis thaliana*. *Plant Physiol.* **170**: 2478–2493.
- Li, Y., Lei, R., Pu, M., Cai, Y., Lu, C., Li, Z., and Liang, G.** (2022). bHLH11 inhibits bHLH IVc proteins by recruiting the TOPLESS/TOPLESS-RELATED corepressors. *Plant Physiol.* **188**: 1335–1349.
- Li, Y., Lu, C.K., Li, C.Y., Lei, R.H., Pu, M.N., Zhao, J.H., Peng, F., Ping, H.Q., Wang, D., and Liang, G.** (2021). IRON MAN interacts with BRUTUS to maintain iron homeostasis in *Arabidopsis*. *Proc. Natl. Acad. Sci.* **118**: 1–10.
- Lian, H.-L., He, S.-B., Zhang, Y.-C., Zhu, D.-M., Zhang, J.-Y., Jia, K.-P., Sun, S.-X., Li, L., and Yang, H.-Q.** (2011). Blue-light-dependent interaction of cryptochrome 1 with SPA1 defines a dynamic signaling mechanism. *Genes Dev.* **25**: 1023–1028.
- Liang, G., Zhang, H., Li, X., Ai, Q., and Yu, D.** (2017). bHLH transcription factor bHLH115 regulates iron homeostasis in *Arabidopsis thaliana*. *J. Exp. Bot.* **68**: 1743–1755.
- Liang, G., Zhang, H., Li, Y., Pu, M., Yang, Y., Li, C., Lu, C., Xu, P., and Yu, D.** (2020). *Oryza sativa* FER-LIKE FE DEFICIENCY-INDUCED TRANSCRIPTION FACTOR (OsFIT/OsbHLH156) interacts with OsIRO2 to regulate iron homeostasis. *J. Integr. Plant Biol.* **62**: 668–689.
- Lichtblau, D.M., Schwarz, B., Baby, D., Endres, C., and Bauer, P.** (2022). The Iron Deficiency-Regulated Small Protein Effector FEP3/IRON MAN1 Modulates Interaction of BRUTUS-LIKE1 With bHLH Subgroup IVc and POPEYE Transcription Factors. *Front. Plant Sci.* **13**: 1–22.
- Ling, H.-Q., Bauer, P., Berczky, Z., Keller, B., and Ganai, M.** (2002). The tomato fer gene encoding a bHLH protein controls iron-uptake responses in roots. *Proc. Natl. Acad. Sci.* **99**: 13938–13943.
- Lingam, S., Mohrbacher, J., Brumbarova, T., Potuschak, T., Fink-Straube, C., Blondet, E., Genschik, P., and Bauer, P.** (2011). Interaction between the bHLH Transcription Factor FIT and ETHYLENE INSENSITIVE3/ETHYLENE INSENSITIVE3-LIKE1 Reveals Molecular Linkage between the Regulation of Iron Acquisition and Ethylene Signaling in *Arabidopsis*. *Plant Cell* **23**: 1815–1829.
- Long, T.A., Tsukagoshi, H., Busch, W., Lahner, B., Salt, D.E., and Benfey, P.N.** (2010). The bHLH Transcription Factor POPEYE Regulates Response to Iron Deficiency in *Arabidopsis* Roots. *Plant Cell* **22**: 2219–2236.
- López-Millán, A.F., Duy, D., and Philippar, K.** (2016). Chloroplast Iron Transport Proteins – Function and Impact on Plant Physiology. *Front. Plant Sci.* **7**: 1–12.
- Lorković, Z.J., Hilscher, J., and Barta, A.** (2008). Co-localisation studies of *Arabidopsis* SR splicing factors reveal different types of speckles in plant cell nuclei. *Exp. Cell Res.* **314**: 3175–3186.
- Lorković, Z.J., Hilscher, J., and Barta, A.** (2004). Use of Fluorescent Protein Tags to Study Nuclear Organization of the Spliceosomal Machinery in Transiently Transformed Living Plant Cells. *Mol. Biol. Cell* **15**: 3233–3243.
- Lorrain, S., Allen, T., Duek, P.D., Whitelam, G.C., and Fankhauser, C.** (2008). Phytochrome-mediated inhibition of shade avoidance involves degradation of growth-promoting bHLH transcription factors. *Plant J.* **53**: 312–

- 323.
- Love, A.J., Yu, C., Petukhova, N. V., Kalinina, N.O., Chen, J., and Taliansky, M.E.** (2017). Cajal bodies and their role in plant stress and disease responses. *RNA Biol.* **14**: 779–790.
- Lucena, C., Waters, B.M., Romera, F.J., José García, M., Morales, M., Alcántara, E., and Pérez-Vicente, R.** (2006). Ethylene could influence ferric reductase, iron transporter, and H⁺-ATPase gene expression by affecting FER (or FER-like) gene activity. *J. Exp. Bot.* **57**: 4145–4154.
- Luo, Y., Na, Z., and Slavoff, S.A.** (2018). P-Bodies: Composition, Properties, and Functions. *Biochemistry* **57**: 2424–2431.
- Lyon, C.E., Bohmann, K., Sleeman, J., and Lamond, A.I.** (1997). Inhibition of Protein Dephosphorylation Results in the Accumulation of Splicing snRNPs and Coiled Bodies within the Nucleolus. *Exp. Cell Res.* **230**: 84–93.
- Ma, P.C.M., Rould, M.A., Weintraub, H., and Pabo, C.O.** (1994). Crystal Structure of MyoD bHLH Domain-DNA Complex: Perspectives on DNA Recognition and Implications for Transcriptional Activation. *Cell* **77**: 451–459.
- Mai, H.-J., Pateyron, S., and Bauer, P.** (2016). Iron homeostasis in *Arabidopsis thaliana*: Transcriptomic analyses reveal novel FIT-regulated genes, iron deficiency marker genes and functional gene networks. *BMC Plant Biol.* **16**: 1–22.
- Mai, H.J., Lindermayr, C., von Toerne, C., Fink-Straube, C., Durner, J., and Bauer, P.** (2015). Iron and FER-LIKE IRON DEFICIENCY-INDUCED TRANSCRIPTION FACTOR-dependent regulation of proteins and genes in *Arabidopsis thaliana* roots. *Proteomics* **15**: 3030–3047.
- Makarov, V., Rakitina, D., Protopopova, A., Yaminsky, I., Arutiunian, A., Love, A.J., Taliansky, M., and Kalinina, N.** (2013). Plant Coilin: Structural Characteristics and RNA-Binding Properties. *PLoS One* **8**: 1–13.
- Maldonado-Bonilla, L.D.** (2014). Composition and function of P bodies in *Arabidopsis thaliana*. *Front. Plant Sci.* **5**: 1–11.
- Marschner, H. and Römheld, V.** (1994). Strategies of plants for acquisition of iron. *Plant Soil* **165**: 261–274.
- Marschner, H., Römheld, V., and Kissel, M.** (1986). Different strategies in higher plants in mobilization and uptake of iron. *J. Plant Nutr.* **9**: 695–713.
- Marschner, H., Treeby, M., and Römheld, V.** (1989). Role of root-induced changes in the rhizosphere for iron acquisition in higher plants. *Zeitschrift für Pflanzenernährung und Bodenkd.* **152**: 197–204.
- Martín-Barranco, A., Spielmann, J., Dubeaux, G., Vert, G., and Zelazny, E.** (2020). Dynamic Control of the High-Affinity Iron Uptake Complex in Root Epidermal Cells. *Plant Physiol.* **184**: 1236–1250.
- Martín-Barranco, A., Thomine, S., Vert, G., and Zelazny, E.** (2021). A quick journey into the diversity of iron uptake strategies in photosynthetic organisms. *Plant Signal. Behav.* **16**: 1–9.
- McLean, E., Cogswell, M., Egli, I., Wojdyla, D., and De Benoist, B.** (2008). Worldwide prevalence of anaemia, WHO Vitamin and Mineral Nutrition Information System, 1993-2005. *Public Health Nutr.* **12**: 444–454.
- Meier, I. and Somers, D.E.** (2011). Regulation of nucleocytoplasmic trafficking in plants. *Curr. Opin. Plant Biol.* **14**: 538–546.
- Meiser, J., Lingam, S., and Bauer, P.** (2011). Posttranslational Regulation of the Iron Deficiency Basic Helix-Loop-Helix Transcription Factor FIT Is Affected by Iron and Nitric Oxide. *Plant Physiol.* **157**: 2154–2166.
- de Melo, J.R.F., Gutsch, A., De Caluwé, T., Leloup, J.C., Gonze, D., Hermans, C., Webb, A.A.R., and Verbruggen, N.** (2021). Magnesium maintains the length of the circadian period in *Arabidopsis*. *Plant Physiol.* **185**: 519–532.
- Meyer, H.M.** (2020). In search of function: nuclear bodies and their possible roles as plant environmental sensors. *Curr. Opin. Plant Biol.* **58**: 33–40.
- Millar, A.H., Heazlewood, J.L., Giglione, C., Holdsworth, M.J., Bachmair, A., and Schulze, W.X.** (2019). The Scope, Functions, and Dynamics of Posttranslational Protein Modifications. *Annu. Rev. Plant Biol.* **70**: 119–151.
- Monte, E., Tepperman, J.M., Al-Sady, B., Kaczorowski, K.A., Alonso, J.M., Ecker, J.R., Li, X., Zhang, Y., and Quail, P.H.** (2004). The phytochrome-interacting transcription factor, PIF3, acts early, selectively, and positively in light-induced chloroplast development. *Proc. Natl. Acad. Sci.* **101**: 16091–16098.
- Murata, Y., Ma, J.F., Yamaji, N., Ueno, D., Nomoto, K., and Iwashita, T.** (2006). A specific transporter for iron (III)-phytosiderophore in barley roots. *Plant J.* **46**: 563–572.
- Murre, C., Schonleber McCaw, P., and Baltimore, D.** (1989). A New DNA Binding and Dimerization Motif in Immunoglobulin Enhancer Binding, daughterless, MyoD, and myc Proteins. *Cell* **56**: 777–783.
- Naranjo-Arcos, M.A., Maurer, F., Meiser, J., Pateyron, S., Fink-Straube, C., and Bauer, P.** (2017). Dissection of iron signaling and iron accumulation by overexpression of subgroup Ib bHLH039 protein. *Sci. Rep.* **7**: 1–12.
- Naranjo Arcos, M.A. and Bauer, P.** (2016). Iron Nutrition, Oxidative Stress, and Pathogen Defense. In *Intech*, pp. 63–98.
- Neugebauer, K.M.** (2017). Special focus on the Cajal Body. *RNA Biol.* **14**: 669–670.
- Nguyen, N.T., Khan, M.A., Castro-Guerrero, N.A., Chia, J.-C., Vatamaniuk, O.K., Mari, S., Jurisson, S.S., and Mendoza-Cozatl, D.G.** (2022). Iron Availability within the Leaf Vasculature Determines the Magnitude of Iron Deficiency Responses in Source and Sink Tissues in *Arabidopsis*. *Plant Cell Physiol.* **63**: 829–841.

- Ni, W., Xu, S.-L., Chalkley, R.J., Pham, T.N.D., Guan, S., Maltby, D.A., Burlingame, A.L., Wang, Z.-Y., and Quail, P.H. (2013). Multisite Light-Induced Phosphorylation of the Transcription Factor PIF3 Is Necessary for Both Its Rapid Degradation and Concomitant Negative Feedback Modulation of Photoreceptor phyB Levels in Arabidopsis. *Plant Cell* **25**: 2679–2698.
- Ni, W., Xu, S.-L., González-Grandío, E., Chalkley, R.J., Huhmer, A.F.R., Burlingame, A.L., Wang, Z.-Y., and Quail, P.H. (2017). PPKs mediate direct signal transfer from phytochrome photoreceptors to transcription factor PIF3. *Nat. Commun.* **8**: 1–11.
- Nouet, C., Motte, P., and Hanikenne, M. (2011). Chloroplastic and mitochondrial metal homeostasis. *Trends Plant Sci.* **16**: 395–404.
- Nozoye, T., Nagasaka, S., Kobayashi, T., Takahashi, M., Sato, Y., Sato, Y., Uozumi, N., Nakanishi, H., and Nishizawa, N.K. (2011). Phytosiderophore Efflux Transporters Are Crucial for Iron Acquisition in Gramineous Plants. *J. Biol. Chem.* **286**: 5446–5454.
- Ogo, Y., Itai, R.N., Nakanishi, H., Kobayashi, T., Takahashi, M., Mori, S., and Nishizawa, N.K. (2007). The rice bHLH protein OsIRO2 is an essential regulator of the genes involved in Fe uptake under Fe-deficient conditions. *Plant J.* **51**: 366–377.
- Ohtani, M. (2018). Plant snRNP Biogenesis: A Perspective from the Nucleolus and Cajal Bodies. *Front. Plant Sci.* **8**: 1–9.
- Owen, I. and Shewmaker, F. (2019). The Role of Post-Translational Modifications in the Phase Transitions of Intrinsically Disordered Proteins. *Int. J. Mol. Sci.* **20**: 1–14.
- Pardi, S.A. and Nusinow, D.A. (2021). Out of the Dark and Into the Light: A New View of Phytochrome Photobodies. *Front. Plant Sci.* **12**: 1–15.
- Park, E., Kim, J., Lee, Y., Shin, J., Oh, E., Chung, W.-I., Liu, J.R., and Choi, G. (2004). Degradation of Phytochrome Interacting Factor 3 in Phytochrome-Mediated Light Signaling. *Plant Cell Physiol.* **45**: 968–975.
- Parker, R. and Sheth, U. (2007). P bodies and the control of mRNA translation and degradation. *Mol. Cell* **25**: 635–646.
- Pendle, A.F., Cark, G.P., Boon, R., Lewandowska, D., Lam, Y.W., Andersen, J., Mann, M., Lamond, A.I., Brown, J.W.S., and Shaw, P.J. (2005). Proteomic Analysis of the Arabidopsis Nucleolus Suggests Novel Nucleolar Functions. *Mol. Biol. Cell* **16**: 260–269.
- Perea-García, A., Andrés-Bordería, A., Mayo De Andrés, S., Sanz, A., Davis, A.M., Davis, S.J., Huijser, P., and Peñarrubia, L. (2016). Modulation of copper deficiency responses by diurnal and circadian rhythms in Arabidopsis thaliana. *J. Exp. Bot.* **67**: 391–403.
- Perez, M., Guerringue, Y., Ranty, B., Pouzet, C., Jauneau, A., Robe, E., Mazars, C., Galaud, J.P., and Aldon, D. (2019). Specific TCP transcription factors interact with and stabilize PRR2 within different nuclear sub-domains. *Plant Sci.* **287**: 110197.
- Pires, N. and Dolan, L. (2010). Origin and Diversification of Basic-Helix-Loop-Helix Proteins in Plants. *Mol. Biol. Evol.* **27**: 862–874.
- Powers, S.K. et al. (2019). Nucleo-cytoplasmic Partitioning of ARF Proteins Controls Auxin Responses in Arabidopsis thaliana. *Mol. Cell* **76**: 177–190.
- Protter, D.S.W. and Parker, R. (2016). Principles and Properties of Stress Granules. *Trends Cell Biol.* **26**: 668–679.
- Qiao, H., Shen, Z., Huang, S.-S.C., Schmitz, R.J., Urich, M.A., Briggs, S.P., and Ecker, J.R. (2012). Processing and Subcellular Trafficking of ER-Tethered EIN2 Control Response to Ethylene Gas. *Science* (80-.). **338**: 390–393.
- Rajniak, J., Giehl, R.F.H., Chang, E., Murgia, I., Von Wirén, N., and Sattely, E.S. (2018). Biosynthesis of redox-active metabolites in response to iron deficiency in plants. *Nat. Chem. Biol.* **14**: 442–450.
- Reddy, A.S.N., Day, I.S., Gohring, J., and Barta, A. (2012). Localization and Dynamics of Nuclear Speckles in Plants. *Plant Physiol.* **158**: 67–77.
- Riback, J.A., Zhu, L., Ferrolino, M.C., Tolbert, M., Mitrea, D.M., Sanders, D.W., Wei, M.-T., Kriwacki, R.W., and Brangwynne, C.P. (2020). Composition-dependent thermodynamics of intracellular phase separation. *Nature* **581**: 209–214.
- Riechmann, J.L. et al. (2000). Arabidopsis Transcription Factors: Genome-Wide Comparative Analysis Among Eukaryotes. *Science* (80-.). **290**: 2105–2111.
- Rivière, Q., Xiao, Q., Gutsch, A., Defrance, M., Webb, A.A.R., and Verbruggen, N. (2021). Mg deficiency interacts with the circadian clock and phytochromes pathways in Arabidopsis. *Ann. Appl. Biol.* **178**: 387–399.
- Robinson, N.J., Procter, C.M., Connolly, E.L., and Guerinot, M. Lou (1999). A ferric-chelate reductase for iron uptake from soils. *Nature* **397**: 694–697.
- Rodríguez-Celma, J., Connorton, J.M., Kruse, I., Green, R.T., Franceschetti, M., Chen, Y.-T., Cui, Y., Ling, H.-Q., Yeh, K.-C., and Balk, J. (2019). Arabidopsis BRUTUS-LIKE E3 ligases negatively regulate iron uptake by targeting transcription factor FIT for recycling. *Proc. Natl. Acad. Sci.* **116**: 17584–17591.
- Rodríguez-Celma, J., Lin, W.-D., Fu, G.-M., Abadía, J., López-Millán, A.-F., and Schmidt, W. (2013). Mutually Exclusive Alterations in Secondary Metabolism Are Critical for the Uptake of Insoluble Iron Compounds by

- Arabidopsis and *Medicago truncatula*. *Plant Physiol.* **162**: 1473–1485.
- Romera, F.J., Alcántara, E., and de la Guardia, M.D.** (1999). Ethylene Production by Fe-deficient Roots and its Involvement in the Regulation of Fe-deficiency Stress Responses by Strategy I Plants. *Ann. Bot.* **83**: 51–55.
- Römheld, V.** (1987). Different strategies for iron acquisition in higher plants. *Physiol. Plant.* **70**: 231–234.
- Römheld, V. and Marschner, H.** (1986a). Evidence for a Specific Uptake System for Iron Phytosiderophores in Roots of Grasses. *Plant Physiol.* **80**: 175–180.
- Römheld, V. and Marschner, H.** (1983). Mechanism of Iron Uptake by Peanut Plants. *Plant Physiol.* **71**: 949–954.
- Römheld, V. and Marschner, H.** (1986b). Mobilization of iron in the rhizosphere of different plant species. *Adv. Plant Nutr.* **2**: 155–204.
- Ronald, J. and Davis, S.J.** (2019). Focusing on the nuclear and subnuclear dynamics of light and circadian signalling. *Plant Cell Environ.* **42**: 2871–2884.
- Rösler, J., Klein, I., and Zeidler, M.** (2007). Arabidopsis *fhl/fhy1* double mutant reveals a distinct cytoplasmic action of phytochrome A. *Proc. Natl. Acad. Sci. U. S. A.* **104**: 10737–10742.
- Sakuraba, Y., Kanno, S., Mabuchi, A., Monda, K., Iba, K., and Yanagisawa, S.** (2018). A phytochrome-B-mediated regulatory mechanism of phosphorus acquisition. *Nat. Plants* **4**: 1089–1101.
- Salladini, E., Jørgensen, M.L.M., Theisen, F.F., and Skriver, K.** (2020). Intrinsic Disorder in Plant Transcription Factor Systems: Functional Implications. *Int. J. Mol. Sci.* **21**: 1–35.
- Salomé, P.A., Oliva, M., Weigel, D., and Krämer, U.** (2013). Circadian clock adjustment to plant iron status depends on chloroplast and phytochrome function. *EMBO J.* **32**: 511–523.
- Samira, R., Li, B., Kliebenstein, D., Li, C., Davis, E., Gillikin, J.W., and Long, T.A.** (2018). The bHLH transcription factor ILR3 modulates multiple stress responses in Arabidopsis. *Plant Mol. Biol.* **97**: 297–309.
- Santi, S. and Schmidt, W.** (2009). Dissecting iron deficiency-induced proton extrusion in Arabidopsis roots. *New Phytol.* **183**: 1072–1084.
- Schaaf, G., Ludewig, U., Erenoglu, E.B., Mori, S., Kitahara, T., and Wirén, N. von** (2004). ZmYS1 Functions as a Proton-coupled Symporter for Phytosiderophore- and Nicotianamine-chelated Metals. *J. Biol. Chem.* **279**: 9091–9096.
- Schmid, N.B., Giehl, R.F.H., Doll, S., Mock, H.-P., Strehmel, N., Scheel, D., Kong, X., Hider, R.C., and von Wirén, N.** (2014). Feruloyl-CoA 6'-Hydroxylase1-Dependent Coumarins Mediate Iron Acquisition from Alkaline Substrates in Arabidopsis. *Plant Physiol.* **164**: 160–172.
- Schmidt, W.** (1999). Mechanisms and regulation of reduction-based iron uptake in plants. *New Phytol.* **141**: 1–26.
- Schuler, M., Rellán-Álvarez, R., Fink-Straube, C., Abadía, J., and Bauer, P.** (2012). Nicotianamine Functions in the Phloem-Based Transport of Iron to Sink Organs, in Pollen Development and Pollen Tube Growth in Arabidopsis. *Plant Cell* **24**: 2380–2400.
- Schwarz, B. and Bauer, P.** (2020). FIT, a regulatory hub for iron deficiency and stress signaling in roots, and FIT-dependent and -independent gene signatures. *J. Exp. Bot.* **71**: 1694–1705.
- Séguéla, M., Briat, J.-F., Vert, G., and Curie, C.** (2008). Cytokinins negatively regulate the root iron uptake machinery in Arabidopsis through a growth-dependent pathway. *Plant J.* **55**: 289–300.
- Selote, D., Samira, R., Matthiadis, A., Gillikin, J.W., and Long, T.A.** (2015). Iron-Binding E3 Ligase Mediates Iron Response in Plants by Targeting Basic Helix-Loop-Helix Transcription Factors. *Plant Physiol.* **167**: 273–286.
- Shaw, P. and Brown, J.** (2012). Nucleoli: Composition, Function, and Dynamics. *Plant Physiol.* **158**: 44–51.
- Shaw, P.J. and Brown, J.W.** (2004). Plant nuclear bodies. *Curr. Opin. Plant Biol.* **7**: 614–620.
- Shen, H., Moon, J., and Huq, E.** (2005). PIF1 is regulated by light-mediated degradation through the ubiquitin-26S proteasome pathway to optimize photomorphogenesis of seedlings in Arabidopsis. *Plant J.* **44**: 1023–1035.
- Shen, Y., Khanna, R., Carle, C.M., and Quail, P.H.** (2007). Phytochrome Induces Rapid PIF5 Phosphorylation and Degradation in Response to Red-Light Activation. *Plant Physiol.* **145**: 1043–1051.
- Shimizu, T., Toumoto, A., Ihara, K., Shimizu, M., Kyogoku, Y., Ogawa, N., Oshima, Y., and Hakoshima, T.** (1997). Crystal structure of PHO4 bHLH domain–DNA complex: flanking base recognition. *EMBO J.* **16**: 4689–4697.
- Shin, L.-J., Lo, J.-C., Chen, G.-H., Callis, J., Fu, H., and Yeh, K.-C.** (2013). IRT1 DEGRADATION FACTOR1, a RING E3 Ubiquitin Ligase, Regulates the Degradation of IRON-REGULATED TRANSPORTER1 in Arabidopsis. *Plant Cell* **25**: 3039–3051.
- Shin, Y., Berry, J., Pannucci, N., Haataja, M.P., Toettcher, J.E., and Brangwynne, C.P.** (2017). Spatiotemporal Control of Intracellular Phase Transitions Using Light-Activated optoDroplets. *Cell* **168**: 159–171.
- Shuai, H., Chen, T., Wilk, T., Rozhon, W., Pimenta Lange, M.J., Sieberer, T., Lange, T., and Poppenberger, B.** (2022). SICESTA Is a Brassinosteroid-Regulated bHLH Transcription Factor of Tomato That Promotes Chilling Tolerance and Fruit Growth When Over-Expressed. *Front. Plant Sci.* **13**: 1–12.
- Sisó-Terraza, P., Luis-Villarroya, A., Fourcroy, P., Briat, J.F., Abadía, A., Gaymard, F., Abadía, J., and Álvarez-Fernández, A.** (2016). Accumulation and Secretion of Coumarinolignans and other Coumarins in Arabidopsis thaliana Roots in Response to Iron Deficiency at High pH. *Front. Plant Sci.* **7**: 1–22.
- Sivitz, A., Grinvalds, C., Barberon, M., Curie, C., and Vert, G.** (2011). Proteasome-mediated turnover of the

- transcriptional activator FIT is required for plant iron-deficiency responses. *Plant J.* **66**: 1044–1052.
- Sivitz, A.B., Hermand, V., Curie, C., and Vert, G.** (2012). Arabidopsis bHLH100 and bHLH101 Control Iron Homeostasis via a FIT-Independent Pathway. *PLoS One* **7**: 1–12.
- Sleeman, J.E. and Lamond, A.I.** (1999). Newly assembled snRNPs associate with coiled bodies before speckles, suggesting a nuclear snRNP maturation pathway. *Curr. Biol.* **9**: 1065–1074.
- Sperotto, R., Ricachenevsky, F.K., Stein, R.J., de Abreu Waldow, V., and Fett, J.P.** (2010). Iron stress in plants: dealing with deprivation and overload. *Plant Stress* **4**: 57–69.
- Stacey, M.G., Patel, A., McClain, W.E., Mathieu, M., Remley, M., Rogers, E.E., Gassmann, W., Blevins, D.G., and Stacey, G.** (2008). The Arabidopsis AtOPT3 Protein Functions in Metal Homeostasis and Movement of Iron to Developing Seeds. *Plant Physiol.* **146**: 589–601.
- Stoltzfus, R.J.** (2001). Defining Iron-Deficiency Anemia in Public Health Terms: A Time for Reflection. *J. Nutr.* **131**: 565S–567S.
- Strader, L., Weijers, D., and Wagner, D.** (2022). Plant transcription factors - being in the right place with the right company. *Curr. Opin. Plant Biol.* **65**: 102136.
- Sun, J., Qi, L., Li, Y., Zhai, Q., and Li, C.** (2013). PIF4 and PIF5 Transcription Factors Link Blue Light and Auxin to Regulate the Phototropic Response in Arabidopsis. *Plant Cell* **25**: 2102–2114.
- Takagi, S., Nomoto, K., and Takemoto, T.** (1984). Physiological aspect of mugineic acid, a possible phytosiderophore of graminaceous plants. *J. Plant Nutr.* **7**: 469–477.
- Tanabe, N., Noshi, M., Mori, D., Nozawa, K., Tamoi, M., and Shigeoka, S.** (2019). The basic helix-loop-helix transcription factor, bHLH11 functions in the iron-uptake system in Arabidopsis thaliana. *J. Plant Res.* **132**: 93–105.
- Tarczewska, A. and Greb-Markiewicz, B.** (2019). The Significance of the Intrinsically Disordered Regions for the Functions of the bHLH Transcription Factors. *Int. J. Mol. Sci.* **20**: 1–20.
- Tenekeci, U. et al.** (2016). K63-Ubiquitylation and TRAF6 Pathways Regulate Mammalian P-Body Formation and mRNA Decapping. *Mol. Cell* **62**: 943–957.
- Tian, Q., Zhang, X., Yang, A., Wang, T., and Zhang, W.H.** (2016). CIPK23 is involved in iron acquisition of Arabidopsis by affecting ferric chelate reductase activity. *Plant Sci.* **246**: 70–79.
- Tissot, N. et al.** (2019). Transcriptional integration of the responses to iron availability in Arabidopsis by the bHLH factor ILR3. *New Phytol.* **223**: 1433–1446.
- Tissot, N., Przybyla-Toscano, J., Reyt, G., Castel, B., Duc, C., Boucherez, J., Gaymard, F., Briat, J.F., and Dubos, C.** (2014). Iron around the clock. *Plant Sci.* **224**: 112–119.
- Toledo-Ortiz, G., Huq, E., and Quail, P.H.** (2003). The Arabidopsis Basic/Helix-Loop-Helix Transcription Factor Family. *Plant Cell* **15**: 1749–1770.
- Trinkle-Mulcahy, L. and Sleeman, J.E.** (2017). The Cajal body and the nucleolus: “In a relationship” or “It’s complicated”? *RNA Biol.* **14**: 739–751.
- Tsai, H.H., Rodriguez-Celma, J., Lan, P., Wu, Y.C., Vélez-Bermúdez, I.C., and Schmidt, W.** (2018). Scopoletin 8-Hydroxylase-Mediated Fraxetin Production Is Crucial for Iron Mobilization. *Plant Physiol.* **177**: 194–207.
- Tsai, H.H. and Schmidt, W.** (2017). Mobilization of Iron by Plant-Borne Coumarins. *Trends Plant Sci.* **22**: 538–548.
- Varotto, C., Maiwald, D., Pesaresi, P., Jahns, P., Salamini, F., and Leister, D.** (2002). The metal ion transporter IRT1 is necessary for iron homeostasis and efficient photosynthesis in Arabidopsis thaliana. *Plant J.* **31**: 589–599.
- Vert, G., Grotz, N., Dédaldéchamp, F., Gaymard, F., Guerinot, M. Lou, Briat, J.F., and Curie, C.** (2002). IRT1, an Arabidopsis Transporter Essential for Iron Uptake from the Soil and for Plant Growth. *Plant Cell* **14**: 1223–1233.
- Vert, G.A., Briat, J.F., and Curie, C.** (2003). Dual Regulation of the Arabidopsis High-Affinity Root Iron Uptake System by Local and Long-Distance Signals. *Plant Physiol.* **132**: 796–804.
- Wairich, A., de Oliveira, B.H.N., Arend, E.B., Duarte, G.L., Ponte, L.R., Sperotto, R.A., Ricachenevsky, F.K., and Fett, J.P.** (2019). The Combined Strategy for iron uptake is not exclusive to domesticated rice (*Oryza sativa*). *Sci. Rep.* **9**: 1–17.
- Wang, H.Y., Klatte, M., Jakoby, M., Bäumllein, H., Weisshaar, B., and Bauer, P.** (2007). Iron deficiency-mediated stress regulation of four subgroup Ib BHLH genes in Arabidopsis thaliana. *Planta* **226**: 897–908.
- Wang, N., Cui, Y., Liu, Y., Fan, H., Du, J., Huang, Z., Yuan, Y., Wu, H., and Ling, H.Q.** (2013). Requirement and Functional Redundancy of Ib Subgroup bHLH Proteins for Iron Deficiency Responses and Uptake in Arabidopsis thaliana. *Mol. Plant* **6**: 503–513.
- Wang, S., Li, L., Ying, Y., Wang, J., Shao, J.F., Yamaji, N., Whelan, J., Ma, J.F., and Shou, H.** (2020). A transcription factor OsbHLH156 regulates Strategy II iron acquisition through localising IRO2 to the nucleus in rice. *New Phytol.* **225**: 1247–1260.
- Wang, X., Jiang, B., Gu, L., Chen, Y., Mora, M., Zhu, M., Noory, E., Wang, Q., and Lin, C.** (2021). A photoregulatory mechanism of the circadian clock in Arabidopsis. *Nat. Plants* **7**: 1397–1408.
- Weber, S.C.** (2017). Sequence-encoded material properties dictate the structure and function of nuclear bodies. *Curr. Opin. Cell Biol.* **46**: 62–71.

- Wedepohl, K.H.** (1995). The composition of the continental crust. *Geochim. Cosmochim. Acta* **59**: 1217–1232.
- Wen, X., Zhang, C., Ji, Y., Zhao, Q., He, W., An, F., Jiang, L., and Guo, H.** (2012). Activation of ethylene signaling is mediated by nuclear translocation of the cleaved EIN2 carboxyl terminus. *Cell Res.* **22**: 1613–1616.
- Wild, M., Davière, J.M., Regnault, T., Sakvarelidze-Achard, L., Carrera, E., Lopez Diaz, I., Cayrel, A., Dubeaux, G., Vert, G., and Achard, P.** (2016). Tissue-Specific Regulation of Gibberellin Signaling Fine-Tunes Arabidopsis Iron-Deficiency Responses. *Dev. Cell* **37**: 190–200.
- Xu, G., Jiang, Z., Wang, H., and Lin, R.** (2019). The central circadian clock proteins CCA1 and LHY regulate iron homeostasis in Arabidopsis. *J. Integr. Plant Biol.* **61**: 168–181.
- Xu, X., Yuan, L., and Xie, Q.** (2022). The circadian clock ticks in plant stress responses. *Stress Biol.* **2**: 1–19.
- Xue, S., Gong, R., He, F., Li, Y., Wang, Y., Tan, T., and Luo, S.-Z.** (2019). Low-complexity domain of U1-70K modulates phase separation and aggregation through distinctive basic-acidic motifs. *Sci. Adv.* **5**: 1–9.
- Yang, J.L., Chen, W.W., Chen, L.Q., Qin, C., Jin, C.W., Shi, Y.Z., and Zheng, S.J.** (2013). The 14-3-3 protein GENERAL REGULATORY FACTOR11 (GRF11) acts downstream of nitric oxide to regulate iron acquisition in Arabidopsis thaliana. *New Phytol.* **197**: 815–824.
- Yang, Y., Ou, B., Zhang, J., Si, W., Gu, H., Qin, G., and Qu, L.-J.** (2014). The Arabidopsis Mediator subunit MED16 regulates iron homeostasis by associating with EIN3/EIL1 through subunit MED25. *Plant J.* **77**: 838–851.
- Yi, Y. and Guerinot, M. Lou** (1996). Genetic evidence that induction of root Fe(III) chelate reductase activity is necessary for iron uptake under iron deficiency. *Plant J.* **10**: 835–844.
- Yin, J., Yi, H., Chen, X., and Wang, J.** (2019). Post-Translational Modifications of Proteins Have Versatile Roles in Regulating Plant Immune Responses. *Int. J. Mol. Sci.* **20**: 1–17.
- Yu, X., Sayegh, R., Maymon, M., Warpeha, K., Klejnot, J., Yang, H., Huang, J., Lee, J., Kaufman, L., and Lin, C.** (2009). Formation of Nuclear Bodies of Arabidopsis CRY2 in Response to Blue Light Is Associated with Its Blue Light-Dependent Degradation. *Plant Cell* **21**: 118–130.
- Yuan, Y., Wu, H., Wang, N., Li, J., Zhao, W., Du, J., Wang, D., and Ling, H.Q.** (2008). FIT interacts with AtbHLH38 and AtbHLH39 in regulating iron uptake gene expression for iron homeostasis in Arabidopsis. *Cell Res.* **18**: 385–397.
- Yuan, Y.X., Zhang, J., Wang, D.W., and Ling, H.Q.** (2005). AtbHLH29 of Arabidopsis thaliana is a functional ortholog of tomato FER involved in controlling iron acquisition in strategy I plants. *Cell Res.* **15**: 613–621.
- Zhai, Z. et al.** (2014). OPT3 is a Phloem-Specific Iron Transporter That Is Essential for Systemic Iron Signaling and Redistribution of Iron and Cadmium in Arabidopsis. *Plant Cell* **26**: 2249–2264.
- Zhang, H., Li, Y., Yao, X., Liang, G., and Yu, D.** (2017). POSITIVE REGULATOR OF IRON HOMEOSTASIS1, OsPRI1, Facilitates Iron Homeostasis. *Plant Physiol.* **175**: 543–554.
- Zhang, H., Zhao, X., Li, J., Cai, H., Deng, X.W., and Li, L.** (2014a). MicroRNA408 Is Critical for the HY5-SPL7 Gene Network That Mediates the Coordinated Response to Light and Copper. *Plant Cell* **26**: 4933–4953.
- Zhang, J., Liu, B., Li, M., Feng, D., Jin, H., Wang, P., Liu, J., Xiong, F., Wang, J., and Wang, H.** (2015). The bHLH Transcription Factor bHLH104 Interacts with IAA-LEUCINE RESISTANT3 and Modulates Iron Homeostasis in Arabidopsis. *Plant Cell* **27**: 787–805.
- Zhang, Y., Wu, H., Wang, N., Fan, H., Chen, C., Cui, Y., Liu, H., and Ling, H.Q.** (2014b). Mediator subunit 16 functions in the regulation of iron uptake gene expression in Arabidopsis. *New Phytol.* **203**: 770–783.
- Zheng, L., Ying, Y., Wang, L., Wang, F., Whelan, J., and Shou, H.** (2010). Identification of a novel iron regulated basic helix-loop-helix protein involved in Fe homeostasis in *Oryza sativa*. *BMC Plant Biol.* **10**: 1–9.
- Zuo, Z.-C., Meng, Y.-Y., Yu, X.-H., Zhang, Z.-L., Feng, D.-S., Sun, S.-F., Liu, B., and Lin, C.-T.** (2012). A Study of the Blue-Light-Dependent Phosphorylation, Degradation, and Photobody Formation of Arabidopsis CRY2. *Mol. Plant* **5**: 726–733.
- Zuo, Z., Liu, H., Liu, B., Liu, X., and Lin, C.** (2011). Blue Light-Dependent Interaction of CRY2 with SPA1 Regulates COP1 activity and Floral Initiation in Arabidopsis. *Curr. Biol.* **21**: 841–847.

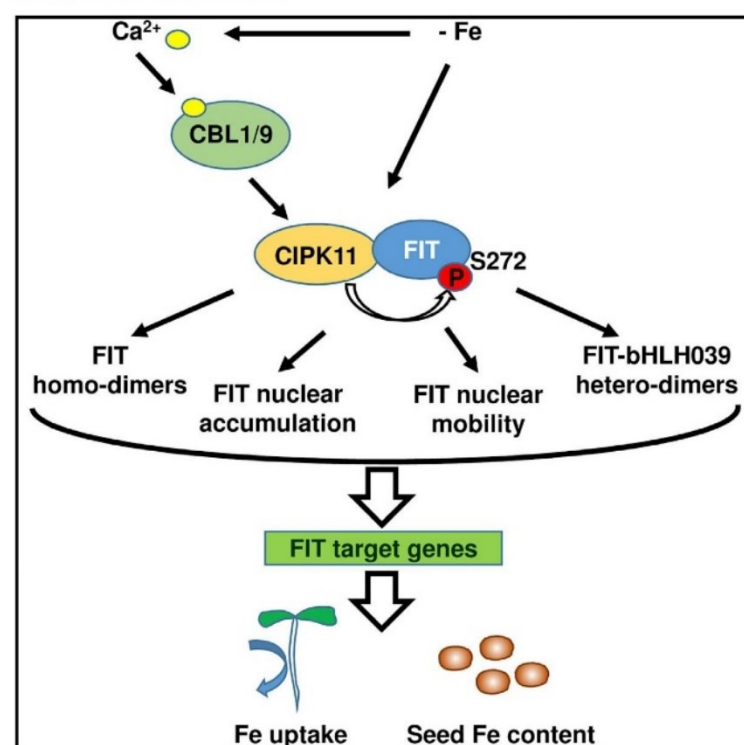
6 Paper I

CIPK11-Dependent Phosphorylation Modulates FIT Activity to Promote Arabidopsis Iron Acquisition in Response to Calcium Signaling

Developmental Cell

CIPK11-Dependent Phosphorylation Modulates FIT Activity to Promote Arabidopsis Iron Acquisition in Response to Calcium Signaling

Graphical Abstract



Authors

Regina Gratz, Prabha Manishankar, Rumen Ivanov, ..., Jörg Kudla, Petra Bauer, Tzvetina Brumbarova

Correspondence

petra.bauer@uni-duesseldorf.de (P.B.), tzvetina.brumberova@uni-duesseldorf.de (T.B.)

In Brief

Gratz et al. uncovered a phosphorylation-based mechanism for regulation of the central Arabidopsis root iron uptake transcription factor FIT. FIT is activated at the protein level. Phosphorylation at Ser272 by the calcium-dependent kinase CIPK11 activates FIT, highlighting the role of calcium signaling and post-translational modifications in plant iron nutrition responses.

Highlights

- Iron-regulated and calcium-dependent protein kinase CIPK11 interacts with FIT
- CIPK11 and calcium sensors CBL1/9 promote FIT-dependent Fe deficiency responses
- FIT is phosphorylated in plants, and CIPK11 phosphorylates FIT at Ser272
- Mutation at Ser272 modulates FIT activity, affecting seed iron content



Gratz et al., 2019, *Developmental Cell* 48, 726–740
 March 11, 2019 © 2019 Elsevier Inc.
<https://doi.org/10.1016/j.devcel.2019.01.006>

CellPress

CIPK11-Dependent Phosphorylation Modulates FIT Activity to Promote Arabidopsis Iron Acquisition in Response to Calcium Signaling

Regina Gratz,^{1,5} Prabha Manishankar,^{2,5} Rumen Ivanov,¹ Philipp Köster,² Inga Mohr,¹ Ksenia Trofimov,¹ Leonie Steinhorst,² Johannes Meiser,¹ Hans-Jörg Mai,¹ Maria Drerup,² Sibylle Arendt,² Michael Holtkamp,³ Uwe Karst,³ Jörg Kudla,² Petra Bauer,^{1,4,6,*} and Tzvetina Brumbarova^{1,6,*}

¹Institute of Botany, Heinrich-Heine University, Düsseldorf 40225, Germany

²Institute of Plant Biology and Biotechnology, University of Münster, Münster 48149, Germany

³Institute of Inorganic and Analytical Chemistry, University of Münster, Münster 48149, Germany

⁴Cluster of Excellence on Plant Sciences, Heinrich-Heine University, Düsseldorf 40225, Germany

⁵These authors contributed equally

⁶Lead Contact

*Correspondence: petra.bauer@uni-duesseldorf.de (P.B.), tzvetina.brumberova@uni-duesseldorf.de (T.B.)

<https://doi.org/10.1016/j.devcel.2019.01.006>

SUMMARY

Nutrient acquisition is entangled with growth and stress in sessile organisms. The bHLH transcription factor FIT is a key regulator of Arabidopsis iron (Fe) acquisition and post-translationally activated upon low Fe. We identified CBL-INTERACTING PROTEIN KINASE CIPK11 as a FIT interactor. Cytosolic Ca²⁺ concentration and *CIPK11* expression are induced by Fe deficiency. *cipk11* mutant plants display compromised root Fe mobilization and seed Fe content. Fe uptake is dependent on CBL1/CBL9. CIPK11 phosphorylates FIT at Ser272, and mutation of this target site modulates FIT nuclear accumulation, homo-dimerization, interaction with bHLH039, and transcriptional activity and affects the plant's Fe-uptake ability. We propose that Ca²⁺-triggered CBL1/9-mediated activation of CIPK11 and subsequent phosphorylation of FIT shifts inactive into active FIT, allowing regulatory protein interactions in the nucleus. This biochemical link between Fe deficiency and the cellular Ca²⁺ decoding machinery represents an environment-sensing mechanism to adjust nutrient uptake.

INTRODUCTION

Plant growth is influenced by a changing environment. This requires precise and coordinated decisions on plant development, physiology, and stress response. Iron (Fe) uptake regulation is a model system for investigating integration of signaling events. Nutrient, particularly Fe, availability is of crucial importance for plant growth and, hence, for the amount and quality of food available for humans. Fe is highly abundant in the soil but poorly accessible for plants (Guerinot and Yi, 1994). Plants can actively mobilize Fe in the soil. Many species, including Arabidopsis, use

a reduction-based strategy, where Fe is solubilized through active proton (H⁺) extrusion, reduced at the root surface and imported as bivalent Fe (Brumbarova et al., 2015). Lack of Fe triggers the induction of several gene clusters responsible for the maintenance of Fe homeostasis (Ivanov et al., 2012; Mai et al., 2016). The basic helix-loop-helix (bHLH) FER-LIKE IRON DEFICIENCY-INDUCED TRANSCRIPTION FACTOR (FIT) is a key regulator of Fe acquisition, balancing beneficial and potentially harmful effects of Fe in the cells. FIT upregulates the genes encoding the FERRIC REDUCTASE-OXIDASE2 (FRO2) and the metal transporter IRON-REGULATED TRANSPORTER1 (IRT1) (Colangelo and Guerinot, 2004; Jakoby et al., 2004).

FIT overexpression is not sufficient to induce downstream target genes. When overexpressed, FIT is very abundant but inactive upon Fe sufficiency, representing a large pool of inactive FIT. In Fe-deficient WT, FIT protein is hardly detectable but active in downstream gene activation, representing a small pool of active FIT (Lingam et al., 2011; Meiser et al., 2011). The same regulation is found for the tomato homolog, indicating a general mechanism (Ling et al., 2002; Brumbarova and Bauer, 2005). FIT 26S proteasome-mediated turnover is very pronounced under Fe deficiency, where FIT activity is crucial. Current models suggest that the active FIT form is rapidly degraded and replaced by new molecules from a pool of inactive FIT (Lingam et al., 2011; Meiser et al., 2011; Sivitz et al., 2011).

FIT activity responds to the plant Fe status but also to plant hormones, such as ethylene and gibberellin, and oxidative stress. The integration of this information flow occurs through post-translational regulation of FIT activity and results in adjusting Fe deficiency response to the environmental conditions. The same regulation is found for the tomato homolog, indicating a general mechanism (Brumbarova and Bauer, 2005; Brumbarova et al., 2015; Le et al., 2016; Wild et al., 2016). FIT activity is extensively regulated through protein-protein interactions. Four subgroup Ib bHLH proteins, bHLH038, bHLH039, bHLH100, and bHLH101, are upregulated by Fe deficiency (Wang et al., 2007). Their physical interaction with FIT activates it and induces FIT target genes (Yuan et al., 2008; Wang et al., 2013).



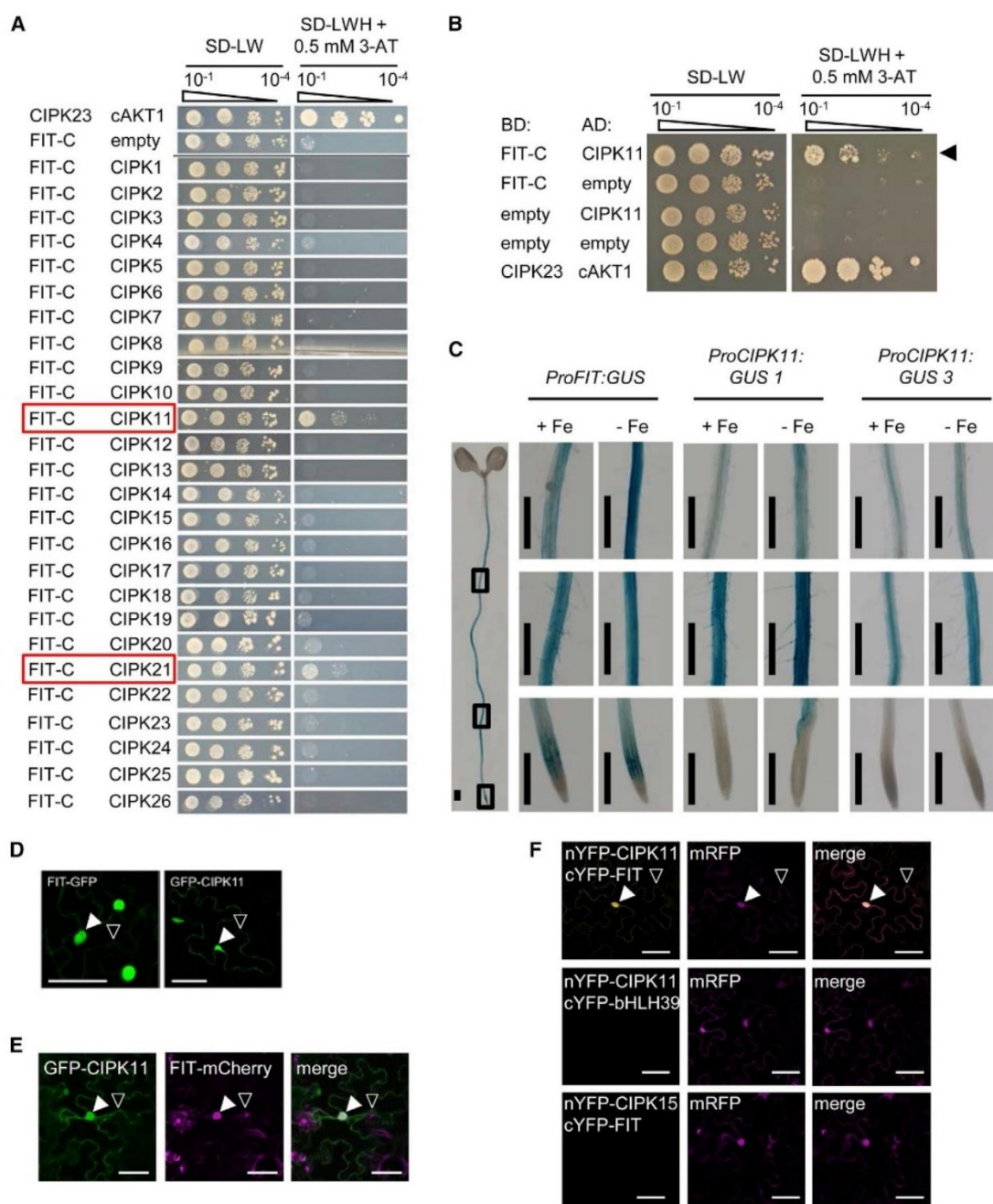


Figure 1. FIT and CIPK11 Co-localize and Interact with Each Other

(A) Targeted Y2H screen between the C-terminal part of FIT (FIT-C), fused to the GAL4 DNA-binding domain (BD), and the full 26-member CIPK family, fused to the GAL4 activation domain (AD). Yeast co-transformed with different BD and AD plasmid combinations were spotted in parallel in 10-fold dilution series ($A_{600} = 10^{-1}$ – 10^{-4}) on SD-LW (co-transformation control) and on SD-LWH + 0.5 mM 3-AT plates (selection for protein interaction). CIPK23/cAKT1, positive control, FIT-C/empty plasmid, negative control. The two strongest interactions are marked with red boxes.

(B) Targeted Y2H interaction assay between BD-FIT-C and AD-CIPK11, as in (A). Empty BD with empty AD, and empty BD with CIPK11-AD, negative controls. An arrow indicates the physical interaction between FIT-C and CIPK11.

(C) Promoter-driven GUS reporter activity in roots. Transgenic plants with *ProFIT::GUS* and *ProCIPK11::GUS* (lines 1 and 3) were grown in the 6-day system under sufficient (+ Fe) or deficient (– Fe) Fe supply and stained for GUS activity. Rectangles in the left side seedling picture indicate the positions of the enlarged images corresponding to, from top to bottom, differentiated root zone, early differentiation zone, and root tip. Bars: 1 mm. See also Figure S1A.

(D) Subcellular localization of FIT-GFP and GFP-CIPK11. Laser-scanning confocal images show the fluorescence of the GFP in FIT-GFP and GFP-CIPK11 in tobacco leaf epidermis cells. Arrowheads indicate nuclear and cytoplasmic GFP signals (filled and empty, respectively). Bars: 50 μ m. See also Figure S1B.

(legend continued on next page)

The ethylene-responsive transcription factors ETHYLENE-INSENSITIVE3 (EIN3) and EIN3-LIKE1 (EIL1) also interact with and activate FIT, linking Fe uptake regulation and ethylene signaling at the molecular level (Lingam et al., 2011). On the other hand, the abiotic stress-induced transcription factor ZINC FINGER OF ARABIDOPSIS THALIANA12 (ZAT12) negatively regulates FIT by scavenging it in an inactive complex to prevent reactive oxygen species (ROS) accumulation under prolonged Fe deficiency or excess Fe (Le et al., 2016). The gibberellin signaling DELLA proteins inhibit FIT activity by preventing FIT binding to its target promoters (Wild et al., 2016). It is tempting to speculate that active FIT molecules engage in functional interactions while interactions with negative FIT regulators keep FIT inactive. However, it is unclear how the pools of active and inactive FIT are molecularly distinguished and which mechanisms guide the formation of FIT protein complexes.

Increased cytosolic calcium concentration $[Ca^{2+}]_{cyt}$ is a second messenger in the plant response to many environmental changes. It is a versatile ancient mechanism to transmit information among cells and cellular compartments. CBL-INTERACTING PROTEIN KINASES (CIPKs), together with calcineurin B-like proteins (CBLs), are a class of Ca^{2+} signal decoders catalyzing serine/threonine protein phosphorylation elicited by environmental stimuli (Batistič and Kudla, 2012; Edel et al., 2017). CIPKs target enzymes and membrane transporters (Xu et al., 2006; Fuglsang et al., 2007; Ho et al., 2009; Drerup et al., 2013; Dubeaux et al., 2018) as well as transcription factors (Song et al., 2005; Lumba et al., 2014; Zhou et al., 2015).

Here, we identified the Fe deficiency-induced CIPK11 as FIT interactor. *cipk11* and *cbl1/9* mutant plants display *fit*-like phenotypes, suggesting that CIPK11 activation is triggered by an increased $[Ca^{2+}]_{cyt}$ sensed through plasma-membrane-localized CBL1/CBL9. We demonstrate that FIT is phosphorylated in plants. CIPK11 phosphorylates FIT at Ser272, and this target site impacts FIT activity. Phosphomutant analysis shows altered FIT mobility, protein interaction, and transcriptional activity in *planta*. The regulation of FIT phosphorylation status is a fundamental mechanism to dynamically adjust the pool of active FIT protein, thereby altering the plant's Fe utilization capacity in response to environmental cues.

RESULTS

FIT Interaction with CIPK Family Members Is Highly Selective

Observations that FIT exists in active and inactive forms prompted us to search for proteins involved in FIT modification. A previously reported yeast two-hybrid (Y2H) screen identified relevant FIT-interacting transcription factors (Lingam et al., 2011; Le et al., 2016). In the same screen, we retrieved a CIPK

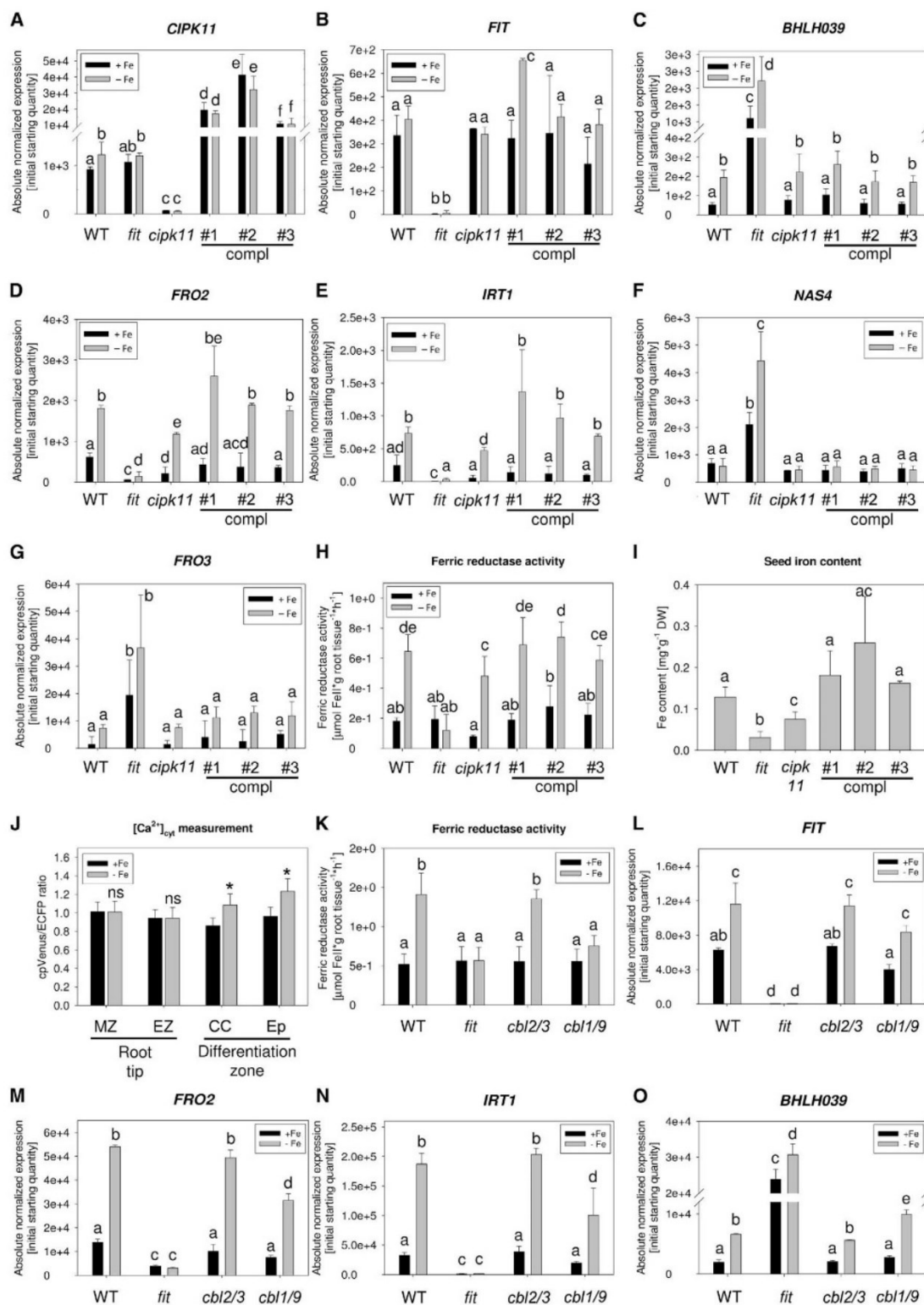
protein kinase. Apart from the currently known FIT-interacting transcription factors, a Ca^{2+} -responsive protein kinase as a FIT interactor suggests a new FIT regulation mechanism, linking Ca^{2+} signaling and Fe-deficiency responses. We addressed the interaction specificity of the C-terminal part of FIT (FIT-C) (Lingam et al., 2011) toward all 26 full-length CIPK family members (Weinl and Kudla, 2009) by targeted yeast two-hybrid (Y2H) assay. Only two of them, CIPK11 and CIPK21, clearly interacted with FIT (Figure 1A). Both *CIPK11* and *CIPK21* genes are Fe-regulated in seedlings. *CIPK11* is upregulated, while *CIPK21* is downregulated under Fe deficiency (Mai et al., 2016). A third member, *CIPK7* is also Fe-regulated but the protein did not interact with FIT in this assay. *CIPK11* is upregulated in the early root differentiation zone (Dinneny et al., 2008), which is primarily responsible for Fe uptake and where FIT activity is required most (Ivanov et al., 2012; Blum et al., 2014). Based on their expression, we figured that CIPK11 might be FIT-activating, while CIPK21 could have a negative impact on FIT-mediated Fe uptake. The result of the Y2H screen points out that the interaction of FIT with CIPK proteins is highly selective and involves Fe-regulated members of the family. With CIPK11, we identified a promising candidate for a phosphorylation-based FIT activation mechanism.

FIT and CIPK11 Interact in Plant Cells

To validate the FIT-CIPK11 interaction, we reconfirmed the interaction between FIT-C and CIPK11 in yeast (Figure 1B). We investigated whether *FIT* and *CIPK11* are expressed in similar parts of the plant by analyzing Arabidopsis stably transformed with *FIT* or *CIPK11* promoters driving β -glucuronidase (GUS) reporter gene. The spatial expression pattern revealed that *FIT* and *CIPK11* are expressed in similar root zones (Figures 1C and S1A). *ProFIT* activity was detected throughout the root differentiation zone, as reported (Jakoby et al., 2004). *ProCIPK11* was inactive at the root tip, but, similarly to *ProFIT*, active in the early root differentiation zone, where CIPK11 can affect FIT. The expression of the two genes in the central cylinder (Figures S1A and S1C) shown for *ProFIT* and *ProCIPK11* (Jakoby et al., 2004; Fuglsang et al., 2007) may be important, however, not central to the process of Fe acquisition. FIT and CIPK11 also share similar subcellular localization. Nuclear and cytoplasmic GFP signals were detected for both FIT-GFP and GFP-CIPK11 (Figure 1D), and expression of full-length fusion proteins was confirmed by immunoblot analysis (Figure S1B). Both proteins co-localize within plant cells, and their localization did not change when FIT-mCherry and GFP-CIPK11 were co-expressed (Figure 1E). In *planta* interaction between FIT and CIPK11 was confirmed by bimolecular fluorescence complementation (BiFC) (Figure 1F). Yellow fluorescent protein (YFP) fluorescent signals, indicative of FIT-CIPK11 interaction, were detected predominantly in the nucleus and weakly in the cytoplasm. No interaction was

(E) Co-localization of FIT-GFP and GFP-CIPK11 in tobacco leaf epidermis cells. Laser-scanning confocal images show co-localization of GFP-CIPK11 and FIT-mCherry. Arrowheads show examples of co-localized GFP and mCherry fluorescent signals in the nucleus (filled arrowheads) and in the cytoplasm (empty arrowheads). Bars: 50 μ m.

(F) BiFC with mRFP transformation control. Laser-scanning confocal images show BiFC signals of nYFP-CIPK11 and cYFP-FIT in tobacco leaf epidermis cells. nYFP-CIPK11 and cYFP-bHLH039, as well as nYFP-CIPK15 and cYFP-FIT, negative controls with a non-interacting related bHLH and a non-interacting CIPK, respectively. Reconstituted YFP signals are indicated by arrowheads (filled for nuclear YFP, empty for cytoplasmic YFP). FIT-CIPK11 interaction was detected predominantly in the nucleus. Bars: 50 μ m. See also Figure S1C.



(legend on next page)

observed between CIPK11 and the Fe-regulated FIT partner bHLH039 and between FIT and CIPK15 (Figure 1A), although the respective protein fusions were properly expressed (Figures 1F and S1C). These negative BiFC controls underline the specificity of the FIT-CIPK11 interaction. Thus, *FIT* and *CIPK11* are induced by Fe deficiency. The proteins interact with each other and function in the same subcellular compartments and root zones.

CIPK11 Is a Positive Regulator of FIT-Dependent Fe Deficiency Responses

To genetically address the function of CIPK11 in FIT-dependent Fe acquisition, we examined the Fe deficiency responses of *cipk11* loss-of-function mutant plants and three independent *cipk11*-complemented plant lines. The *cipk11* mutant used in our study is widely employed (Fuglsang et al., 2007; Yang et al., 2010; Lumba et al., 2014; Zhou et al., 2015). To assess the level of Fe responsiveness in *cipk11*, we compared it to wild-type (WT) and *fit* loss-of-function plants. *fit* mutants fail to induce Fe acquisition responses and do not acquire sufficient Fe, displaying severe leaf chlorosis and reduced growth unless supplemented with foliar Fe (Colangelo and Guerinot, 2004; Jakoby et al., 2004). Under Fe deficiency, WT plants had increased root length compared to +Fe conditions, potentially representing a foraging strategy of exploiting the medium for Fe, while at the same time, the severely Fe-deficient *fit* mutant was unable to sustain this growth response (Figures S2A and S2B). Main root length increase upon Fe deficiency was reported before for WT Arabidopsis and other eudicot species, while the opposite was the case upon FIT failure in Arabidopsis or its tomato ortholog (Ling et al., 2002; Zhang et al., 2015; Le et al., 2016). Compared with WT, *cipk11* displayed an even further increased root length under both Fe conditions, a phenotype that was reverted in *cipk11*-complemented lines (Figures S2A and S2B). The root phenotype of *cipk11* indicated a role of CIPK11 in Fe acquisition responses.

We tested the hypothesis that CIPK11 might affect Fe deficiency responses through regulating FIT. *FRO2* and *IRT1* are FIT target genes used as markers for the plant responsiveness to limited Fe supply (Colangelo and Guerinot, 2004; Jakoby et al., 2004). *CIPK11* gene expression was highly compromised in *cipk11*, while *CIPK11* in the three *cipk11*-complemented lines exceeded WT levels (Figure 2A). *CIPK11* was induced in WT roots upon -Fe and expressed at similar level in WT and *fit* (Figure 2A), confirming that *CIPK11* is not a FIT target gene (Mai et al., 2016). *FIT* transcript levels were not significantly deregulated in *cipk11*. One out of three complemented lines showed

enhanced *FIT* expression at -Fe versus +Fe condition (Figure 2B). *BHLH039* is upregulated by Fe deficiency (Wang et al., 2007), serving as a robust marker gene (Ivanov et al., 2012). Its transcript abundance is not dependent on FIT but increased in *fit* mutants due to their high level of Fe deficiency (Wang et al., 2007). We found that *BHLH039* expression was not dependent on CIPK11, indicating that the Fe deficiency signaling upstream of *FIT* and *BHLH039* was not perturbed in *cipk11* (Figure 2C). However, lack of functional CIPK11 led to the downregulation of the FIT targets *FRO2* (Figure 2D) and *IRT1* (Figure 2E) under -Fe, although not to the same extent as in *fit*. In the *cipk11*-complemented lines, *FRO2* and *IRT1* expression were restored to at least WT levels (Figures 2D and 2E). Fe homeostasis genes co-regulated with *BHLH039*, *NICOTIANAMINE SYNTHASE4* (*NAS4*), and *FERRIC REDUCTASE OXIDASE3* (*FRO3*) were not affected by the lack of functional CIPK11 (Figures 2F and 2G), similarly to *BHLH039*. These findings argue against a function of CIPK11 upstream of FIT and *bHLH039*. CIPK11 plays a positive role in regulating the FIT targets *IRT1* and *FRO2* but not in regulating Fe responsive genes that are not FIT targets.

Physiological analyses further confirmed the Fe deficiency response phenotype of *cipk11*. Root ferric reductase activity represents a physiological read-out to Fe limitation (Robinson et al., 1999). Indeed, *cipk11* plants had reduced Fe reductase activity in comparison to WT under Fe deficient conditions, whereas the activity in *cipk11*-complemented lines was similar to the WT, consistent with the *FRO2* transcript abundance in these plants (Figure 2H). Reduced Fe content per dry weight of *cipk11* seeds reflected the decreased capacity of the mutant to acquire Fe. Importantly, *cipk11*-complemented lines restored the seed Fe content to WT levels (Figure 2I).

Since CIPK11 decodes Ca^{2+} signals, we asked whether Fe deficiency alters $[Ca^{2+}]_{cyt}$ in our growth conditions. Using the genetically encoded Ca^{2+} sensor Yellow Cameleon 3.6 (YC3.6) (Krebs et al., 2012), we confirmed an Fe-deficiency-dependent $[Ca^{2+}]_{cyt}$ increase in the early root differentiation zone, both in the central cylinder and in the epidermis (Figures 2J, S2C, and S2D). The existence of a Ca^{2+} signal in the context of Fe deficiency suggests sensing at a certain subcellular compartment through a CBL. We examined the Fe mobilization capacity of the double loss-of-function mutants *cbi2/3* (Eckert et al., 2014) and *cbi1/9* (Xu et al., 2006), representing plants deficient in Ca^{2+} perception at the tonoplast and the plasma membrane (Battistic et al., 2010), respectively. The Fe reductase activity of *cbi2/3* was not significantly different from that of WT under both Fe supplies. However, *cbi1/9* was unable to induce Fe

Figure 2. CIPK11 Is a Positive Regulator of FIT-Dependent Fe Deficiency Responses

(A–I) Analysis of Fe deficiency responses of *cipk11* mutant and complemented lines. *cipk11* mutant, three *cipk11*-complemented lines (compl #1, #2, and #3) (see also Figures S2A and S2B) were analyzed in comparison to WT and *fit* mutant. Plants were grown in the 2-week system with sufficient (+Fe, black bars) or deficient (-Fe, gray bars) Fe supply. Data are represented as mean \pm SD. Different letters indicate statistically significant differences ($p < 0.05$).

(A–G) Gene expression analysis in roots, (A) *CIPK11*, (B) *FIT*, (C) *BHLH039*, (D) *FRO2*, (E) *IRT1*, (F) *NAS4*, and (G) *FRO3* ($n = 3$). (H) Root Fe reductase activity ($n = 4$). (I) Seed Fe content per dry weight ($n = 3$).

(J) Free $[Ca^{2+}]_{cyt}$ changes in response to Fe deficiency in roots by ratiometric imaging of the Ca^{2+} sensor YC3.6. cpVenus-to-ECFP emission ratios of fluorescence intensities indicative of free $[Ca^{2+}]_{cyt}$ were measured in roots of plants grown under sufficient (+Fe, black bars) or deficient (-Fe, gray bars) supply. $[Ca^{2+}]_{cyt}$ was measured in the meristematic (MZ) and elongation (EZ) zones of the root tip and in the central cylinder (CC) and epidermis (Epi) of the early root differentiation zone. Data are represented as mean \pm SD ($n = 12$). Asterisks indicate statistically significant differences ($p < 0.05$) to the respective Fe sufficient condition of the same genotype. See also Figures S2C and S2D.

(K–O) Analysis of Fe deficiency responses of *cbi* mutants. *cbi2/3* and *cbi1/9* double loss-of-function mutant plants were grown and analyzed, including statistics, as described in (A)–(H). (K) Root Fe reductase activity ($n = 4$). (L–O) Gene expression analysis in roots, (L) *FIT*, (M) *FRO2*, (N) *IRT1*, and (O) *BHLH039* ($n = 3$).

reductase activity under $-Fe$ (Figure 2K). In order to test whether the effect of CBL1/9 on Fe reductase activity reflected a change in FIT activity, we investigated the expression of FIT target genes. While *FIT* expression was not significantly affected in the *cb1* mutants (Figure 2L), both *FRO2* and *IRT1* transcript levels were significantly decreased in *cb1/9* compared to WT under $-Fe$ (Figures 2M and 2N). Consequently, *BHLH039* was significantly upregulated in *cb1/9* under $-Fe$ in comparison to WT (Figure 2O), underlining the inability of *cb1/9* to upregulate FIT-dependent Fe deficiency responses. These data suggest that the plasma-membrane-localized CBL1 and CBL9, similar to CIPK11, act as positive regulators of Fe uptake and are needed for proper FIT activation under Fe deficiency. In summary, CIPK11, potentially activated by CBL1/9-mediated Ca^{2+} sensing, positively affects FIT activity.

CIPK11 Phosphorylates FIT at Ser272

Since FIT interacts with a protein kinase affecting Fe acquisition, we asked whether differences in FIT activity could be attributed to differences in FIT phosphorylation status. We were unable to demonstrate FIT phosphorylation through peptide analysis because of the low FIT protein abundance. Instead, we employed phosphate affinity Zn^{2+} -Phos-tag SDS-PAGE, which leads to retarded electrophoretic mobility of phosphorylated proteins in comparison to their corresponding non-phosphorylated forms (Bekešová et al., 2015) in combination with HA-FIT immunodetection in transgenic HA₇-FIT plants. Standard SDS-PAGE resulted in a single HA-FIT protein band (Figure 3A), whereas Phos-tag analysis revealed a mobility shift with three distinct HA-FIT bands (Figure 3B). Calf intestinal phosphatase (CIP) treatment of the protein extracts prior to Phos-tag separation led to a decrease in the relative protein abundance of the low mobility (LM) FIT form versus the total FIT pool under both Fe supply conditions (Figure 3C), indicating the presence of phosphorylated HA-FIT in roots of Fe-sufficient and Fe-deficient plants. The HM FIT forms represented two bands at $+Fe$ and $-Fe$, whereby the upper HM bands were slightly shifted following CIP treatment. HM FIT bands were potentially non-phosphorylated or had a lower phosphorylation grade. Extracts from both $+Fe$ - and $-Fe$ -grown plants showed the presence of a phosphorylated LM HA-FIT form. It is likely that FIT is phosphorylated at different positions depending on the Fe supply, potentially by different protein kinases and with different outcomes for FIT activity.

A second proof for FIT phosphorylation *in planta* came from 2D SDS-PAGE and immunodetection (Figure 3D). Several HA-FIT forms with different isoelectric points (pI) were detected, a main group of FIT spots at the expected HA-FIT pI of 4.3 (Figure 3D, black ellipses) and several other spots spread further in the acidic pH range down to pH 3.4 (Figure 3D, red ellipses). In both $+Fe$ and $-Fe$ extracts, the acidic FIT isoforms disappeared after phosphatase treatment, confirming their phosphorylated nature. The presence of several main and weak HA-FIT spots in 2D-PAGE analysis correlates with main and weak HM bands in Phos-tag mobility shift assay. Thus, a small portion of FIT protein is highly phosphorylated, while a large portion of FIT might be not or less phosphorylated.

We next tested whether CIPK11 phosphorylates FIT. Since the FIT-CIPK11 interaction in yeast involved the C-terminal part of

FIT, we performed an *in silico* prediction of potential phosphorylation sites in this region (Figure 3E), considering site conservation between FIT and its tomato homolog SIFER. This led to the identification of Ser272 as a potential FIT/SIFER phosphorylation site (Figure 3E). Site-directed mutagenesis was used to create non-phosphorylatable, FITm(AA), and phospho-mimicking, FITm(E), FIT forms at the Ser272 position to investigate the potential impact of Ser272 phosphorylation (Figure 3E). We observed phosphorylation of FIT and FIT-C by CIPK11 *in vitro* (Figure 3F). CIPK11 also underwent auto-phosphorylation, which served as CIPK11 activity control. FIT or FIT-C, without exposure to CIPK11 and StrepII-GST protein incubated with CIPK11, were not phosphorylated, confirming the specificity of the detected FIT phosphorylation by CIPK11. FITm-C(AA) and FITm-C(E) displayed weaker radioactive signals than the non-mutagenized FIT-C when incubated with CIPK11 (Figure 3F), suggesting that Ser272 is a prominent CIPK11 target site. Taken together, we show that a small portion of FIT protein is phosphorylated *in planta*, and that FIT is phosphorylated at Ser272 by CIPK11.

Ser272 Phosphorylation Target Site Mutation Modulates FIT Localization, Mobility, and Activity

Next, we investigated whether Ser272 phosphorylation status impacts FIT function. For this, we generated plant lines constitutively expressing GFP-tagged FIT forms. FIT-GFP/*fit* plants (FIT/*fit*) expressed constitutively mRNA and full-length FIT-GFP protein under both Fe supply conditions (Figures S3A and S3B). Their root length response to Fe deficiency was similar to WT as was the *BHLH039* expression level (Figures S3C and S3D). *FRO2* and *IRT1* were similarly expressed and induced by $-Fe$ in FIT/*fit* and WT (Figures S3E and S3F). As a consequence, FIT/*fit* plants displayed WT-like Fe reductase activity and seed Fe content levels (Figures S3G and S3H), illustrating that FIT-GFP fusion can fully rescue the Fe-deficient phenotype of *fit* plants.

The presence of this functional FIT-GFP in the nucleus and in the cytoplasm described above (Figures 1D and 1E) was also seen in FIT/*fit* roots exposed to $+$ and $-Fe$ (Figure S3I). This implies that the amount of transcriptionally active nuclear FIT may be regulated through a partitioning between the nucleus and the cytoplasm. Interestingly, the non-phosphorylatable FITm(AA)-GFP displayed enhanced accumulation in the cytoplasm compared to FIT-GFP, while the phospho-mimicking FITm(E)-GFP form did not show a difference in subcellular distribution (Figure 4A). The expression of full-length GFP-fusion proteins for all three FIT forms was verified by immunoblotting (Figure S4A). In addition, fluorescent recovery after photobleaching (FRAP) revealed the increased mobility of the FITm(AA)-GFP form in comparison to FIT-GFP and FITm(E)-GFP (Figures 4B, S4B, and S4C). This suggests that FIT abundance and mobility in the nucleus are modulated by its phosphorylation status at Ser272.

We reported previously that full-length FIT coupled to the Gal4 binding domain (BD-FIT) has the capacity to self-activate reporter gene expression in yeast without requiring the Gal4 activation domain (Lingam et al., 2011). Interestingly, Ser272 mutations affected this self-activation capacity of BD-FIT. Indeed, BD-FITm(AA) caused a decreased transcriptional self-activation in

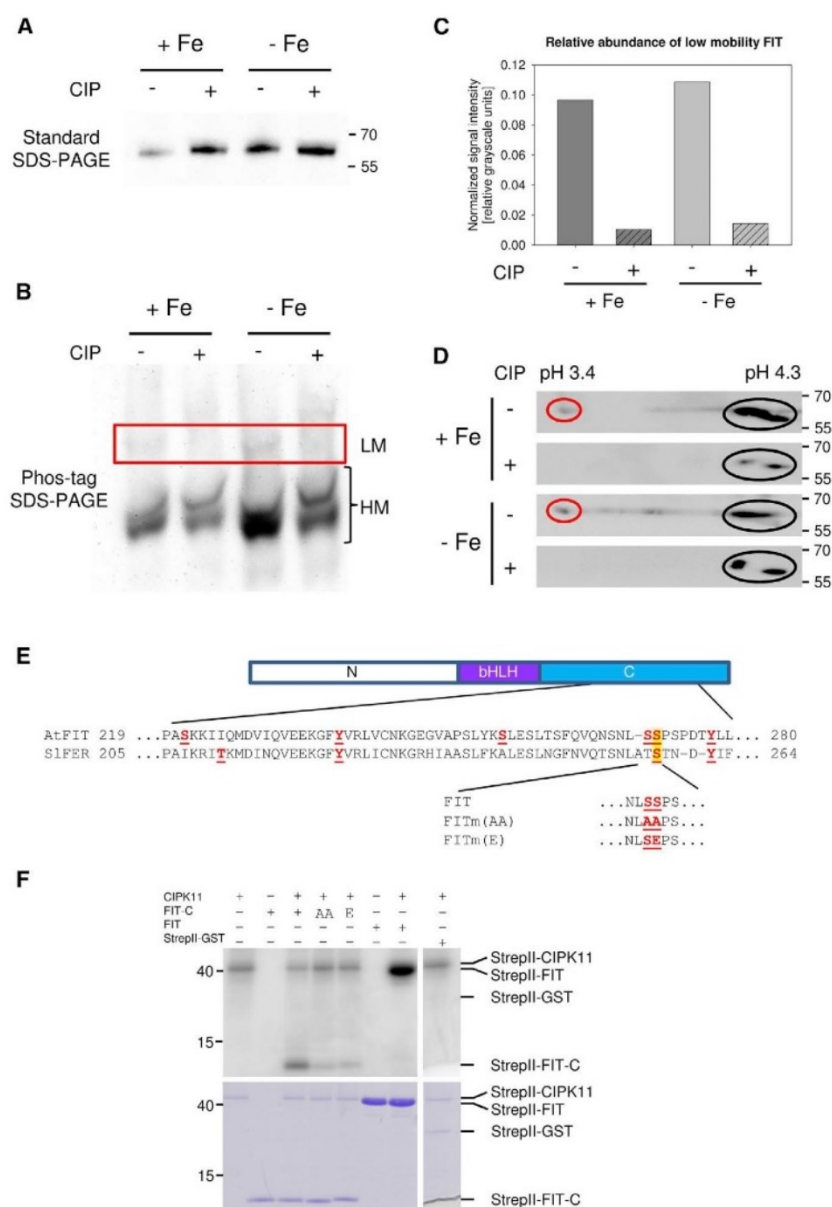


Figure 3. CIPK11 Phosphorylates FIT at Ser272

(A–D) Evidence for FIT phosphorylation in plants. HA₇-FIT plants were grown under sufficient (+Fe) or deficient (–Fe) Fe supply. Protein extracts were treated with or without calf intestinal phosphatase (CIP), subjected to electrophoresis, and subsequent immunoblot detection with anti-HA-HRP antibody. (A) Standard SDS-PAGE as control for FIT-GFP expression. The single band corresponds to HA₇-FIT. (B) Phos-tag mobility shift using Phos-tag SDS-PAGE. The same protein extracts as in (A) were used. Weak low-mobility (LM) and strong high-mobility (HM) bands are visible. The LM band disappears after phosphatase treatment, indicating a phosphorylated FIT isoform. Red rectangle, image area used for quantifying LM FIT forms in each sample. Bracket, image area used for quantifying HM FIT forms. The assay was performed two times showing similar results. (C) Quantification of Phos-tag results shown in (B). Relative LM FIT abundance was calculated versus total LM + HM FIT, as normalized LM FIT signal intensity. (D) Two-dimensional SDS-PAGE. Different FIT isoforms spread between the pI of HA₇-FIT (pH 4.3, black ellipses) and the more acidic pH. The FIT isoform at pH 3.4 (red ellipses) disappears after phosphatase treatment. The assay was performed two times showing similar results.

(E) Phosphorylation site prediction. FIT protein scheme with NetPhos2.0-predicted phosphorylation sites (highlighted in red and underlined). Serine S272 (in yellow) is conserved between AtFIT and SIFER, and was selected as target site for further investigations. Non-phosphorylatable, FITm(AA), and phosphomimicking, FITm(E), FITm forms created in this work are shown under the alignment.

(F) *In vitro* kinase assay. Affinity-purified recombinant StrepII-CIPK11 and StrepII-tagged substrates were incubated together, as specified. StrepII-FIT-C was assayed non-mutagenized and phospho-mutagenized as StrepII-FITm-C(AA) and StrepII-FITm(E) (AA and E). StrepII-GST, negative control. Lower panel, protein staining as loading control. Upper panel, auto-radiography image showing phosphorylation signals. Respective protein bands are indicated on the right side. CIPK11 auto-phosphorylation served as a positive control for CIPK11 activity. The assay was performed two times showing similar results.

(A, D, and F) Protein molecular weight (in kDa) is indicated.

comparison to BD-FITm(E) and BD-FIT (Figure 4C), pointing out the importance of Ser272 phosphorylation for BD-FIT transcription factor activity. Taken together, we demonstrate that Ser272 affects the cellular localization and nuclear mobility of FIT-GFP and the self-activation capacity of BD-FIT.

Ser272 Phosphorylation Target Site Mutation Disturbs FIT Homo- and Hetero-Dimerization

We investigated the functionality of FIT phosphomutants as transcription factors. Proteins from the bHLH transcription factor family are known to form dimers (Heim et al., 2003). FIT can

interact with itself, yet the function of FIT homo-dimerization is unknown (Yuan et al., 2008). Overexpression of FIT alone does not lead to enhanced Fe deficiency responses unless *BHLH039* is also present, indicating that FIT dimers are inactive (Jakoby et al., 2004; Meiser et al., 2011; Figure S3). *bHLH039* activates FIT (Yuan et al., 2008; Naranjo-Arcos et al., 2017). Since the protein interactions of FIT are crucial for FIT transcription factor activity, we figured that Ser272 could mediate the cellular decisions for non-activating and activating FIT interactions. Thus, FIT activity might be modulated through CIPK11 phosphorylation at Ser272. FIT-C, devoid of the bHLH domain,

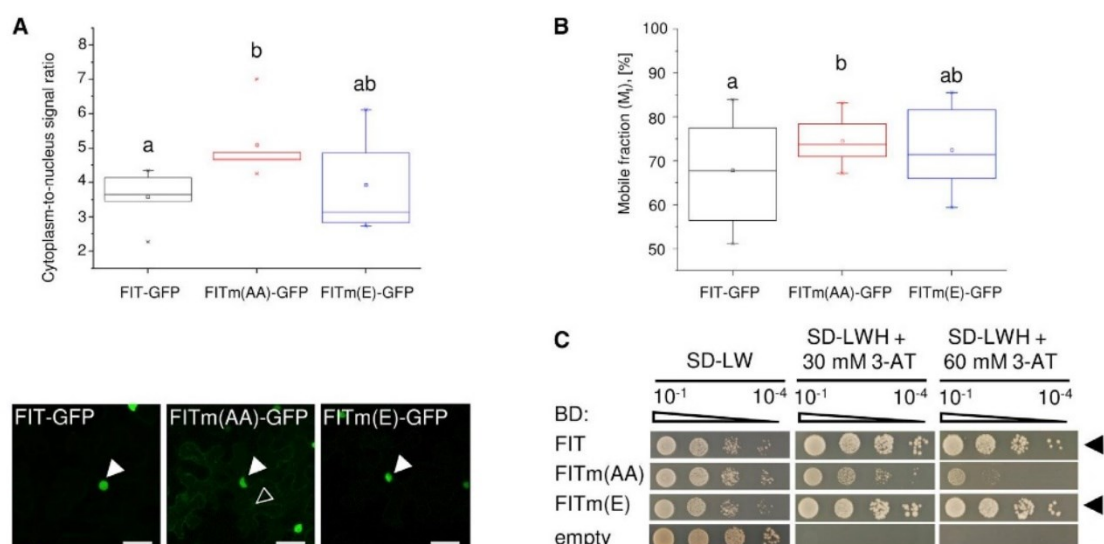


Figure 4. Mutation at Ser272 Alters FIT Cellular Localization, Protein Mobility, and Self-Activation

(A–B) Box plots; Inter-Quartile Range (IQR) 25 to 75%; whiskers, 25th percentile $-1.5 \times \text{IQR}$, 75th percentile $+1.5 \times \text{IQR}$; median, line within IQR box; mean, small square in IQR box; x, values outside $\pm 1.5 \times \text{IQR}$ range. Different letters indicate statistically significant differences ($p < 0.05$).

(A) Subcellular localization of FIT and FITm-GFP. Upper part, box plot showing quantification of cytoplasm-to-nucleus GFP signal ratios for FIT-GFP (black), FITm(AA)-GFP (red) and FITm(E)-GFP (blue) ($n = 3$). Lower part, representative laser-scanning confocal images of GFP signals in tobacco leaf epidermis cells. Full and empty arrowheads indicate nuclear and cytoplasmic GFP signals, respectively. Bars: 50 μm . See also Figure S4A.

(B) Protein mobility analysis of FIT-GFP and FITm-GFP by FRAP in plant cells. Box plot showing the percentage of the mobile protein fraction for FIT-GFP (black), FITm(AA)-GFP (red) and FITm(E)-GFP (blue) was calculated from the GFP fluorescence recovery rate ($n = 12-21$). See also Figures S4B and S4C.

(C) FIT and FITm transcriptional self-activation capacity assay in yeast. Yeast co-transformed with BD-FIT or BD-FITm and empty AD vector were spotted in parallel on SD-LW (co-transformation control) and on SD-LWH + 30 and 60 mM 3-AT plates (selection for self-activation), as described in Figure 1. Empty BD plasmid, negative control. Arrowheads indicate self-activation.

was sufficient for homo-dimerization in yeast. FITm(AA)-C showed a decreased, while FITm(E)-C had an increased homo-dimerization, compared to FIT-C (Figure 5A). FIT homo-dimer formation and its dependence on Ser272 phosphorylation status were further confirmed for full-length FIT forms *in planta* by Förster resonance energy transfer-acceptor photo bleaching (FRET-APB) in plant nuclei and BiFC analyses. FRET efficiency was scored as an indication of protein interaction. Non-phosphorylatable FITm(AA) displayed a reduced and phospho-mimicking FITm(E) an increased FRET efficiency compared to WT FIT (Figure 5B). BiFC assays showed homo-dimer formation for FIT and FITm(E) pairs but not for FITm(AA) (Figure S5A). In all cases, the respective nYFP- and cYFP-tagged proteins were detectable by immunoblot (Figure S5B).

Since the presence of bHLH039 is crucial for FIT target gene activation (Yuan et al., 2008; Naranjo-Arcos et al., 2017), we investigated the effect of Ser272 mutation on FIT-bHLH039 hetero-dimerization. The yeast assay did not show significant differences in interaction strength between FIT-C and bHLH039 or between any FITm-C and bHLH039 (Figure 5C). However, FRET-APB analysis in plant nuclei revealed a decrease in FRET efficiency for the bHLH039-GFP/FITm(AA)-mCherry but not the bHLH039-GFP/FITm(E)-mCherry pair (Figure 5D). This suggests that Ser272 phosphorylation positively affects FIT homo-dimerization and FIT-bHLH039 hetero-dimerization in plant nuclei. In summary, phospho-mimicking FITm(E) formed interactions similarly to WT. On the other hand, the non-phosphorylatable FITm(AA) form had decreased homo-dimerization and

bHLH039 interaction capacity, compared to WT FIT. This decreased ability of FITm(AA) to participate in protein-protein interactions may explain its reduced activity.

CIPK11 Target Site Mutation Affects FIT Target Gene Activation *In Vivo*

Based on their altered interaction affinity to bHLH039, we predicted that FITm protein forms may have different activity. To study this aspect at the whole-plant level, we performed a *fit* mutant complementation assay (Figure S3). Two FITm(AA)/*fit* (AA#1 and AA#2) and FITm(E)/*fit* (E#1 and E#2) lines were generated, constitutively expressing FITm(AA)-GFP or FITm(E)-GFP (Figures 6A, 6B, S6A, and S6B). The *fit* mutant phenotype of reduced root length at $-Fe$ supply versus $+Fe$ supply was not changed in AA#1 and AA#2, while it was rescued in E#1 and E#2 (Figures 6C and S6C). This indicates that FITm(AA) in contrast to FITm(E) does not complement *fit*. Consistently, target gene activation by FITm(AA), reflecting its transactivation capacity, was compromised. The AA#1 and AA#2 lines were not able to up-regulate *FRO2* and *IRT1* upon $-Fe$, contrary to WT, E#1 and E#2 (Figures 6D, 6E, S6D, and S6E). *BHLH039* expression levels were similar in AA#1, AA#2, and *fit* (Figure 6F). On the other hand, *BHLH039* expression was comparable between WT, E#1 and E#2 (Figure S6F). Consequently, ferric reductase activity remained low upon $-Fe$ in AA#1 and AA#2, as in *fit*, but was elevated in E#1 and E#2, as in WT (Figures 6G and S6G). Seed Fe contents of AA#1 and AA#2 were low as in *fit* seeds in contrast to WT, E#1 and E#2 (Figures 6H and S6H). Therefore, the FITm(E)-

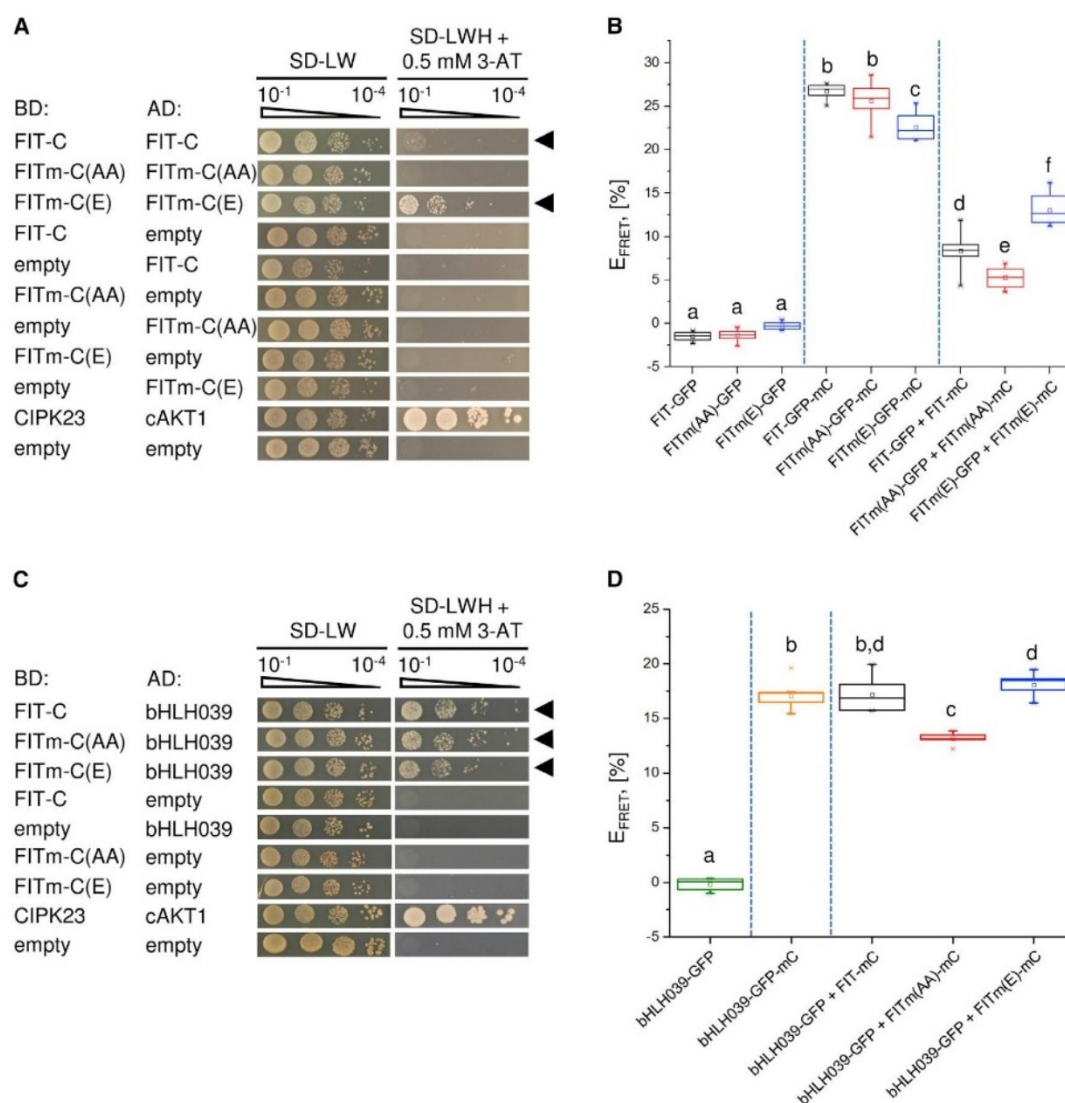


Figure 5. Mutation at Ser272 Alters FIT Homo-Dimerization and FIT-bHLH039 Interaction

(A and B) Mutant FIT protein homo-dimerization capacities. (A) FIT homo-dimerization assay in yeast. Yeast co-transformed with different combinations of non-mutagenized and mutagenized BD- and AD-FIT-C/FITm-C vectors were spotted in parallel as described in Figure 1. Arrowheads indicate homo-dimerization. (B) FIT and FITm homo-dimerization *in planta*. Box plot showing FRET-APB for GFP- and mCherry-tagged FIT and FITm pairs, measured to assess the strength of homo-dimer formation in plant cell nuclei. GFP-tagged fusions, donor-only (negative) controls. GFP-mCherry-tagged fusions for intra-molecular FRET, positive controls. Significant increase in FRET efficiency (E_{FRET}) is indicative of protein interaction. See also Figure S5.

(C and D) Mutant FIT-bHLH039 protein interaction capacities. (C) FIT-bHLH039 protein hetero-dimerization assay in yeast. Yeast co-transformed with different combinations of non-mutagenized and mutagenized BD-FIT-C/FITm-C and AD-bHLH039 vectors were spotted as in (A). Arrowheads indicate hetero-dimerization. (D) bHLH039 and FIT/FITm interaction *in planta*. Box plot showing FRET-APB for GFP-tagged bHLH039 and mCherry-tagged FIT/FITm pairs, measured as in (B) to assess the strength of hetero-dimer formation in plant cell nuclei.

(B–D) Box plots; Inter-Quartile Range (IQR) 25 to 75%; whiskers, 25th percentile $-1.5 \times \text{IQR}$, 75th percentile $+1.5 \times \text{IQR}$; median, line within IQR box; mean, small square in IQR box; x, values outside $\pm 1.5 \times \text{IQR}$ range. (n = 10). Different letters indicate statistically significant differences (p < 0.05). mC, mCherry; GFP-mC, and GFP-mCherry.

GFP fusion fully complemented the *fit* phenotype, indicating an active FIT form, while FITm(AA)-GFP represented an inactive form. Similar to the observations in tobacco leaf epidermis cells, FITm(AA)-GFP in both AA#1 and AA#2 lines showed quantitatively increased GFP fluorescence in the cytoplasm in comparison to WT FIT-GFP. The fluorescence and localization of FITm(E)-GFP

in E#1 and E#2 was similar to non-mutagenized FIT-GFP (Figures 6I, S6I, and S7). These results support the conclusion that non-phosphorylatable mutation at Ser272 renders FIT less active, impeding its role as a transcriptional activator. FITm(E), on the other hand, is active upon Fe deficiency. When overexpressed, FITm(E) does not have an enhancing effect on Fe uptake. This is

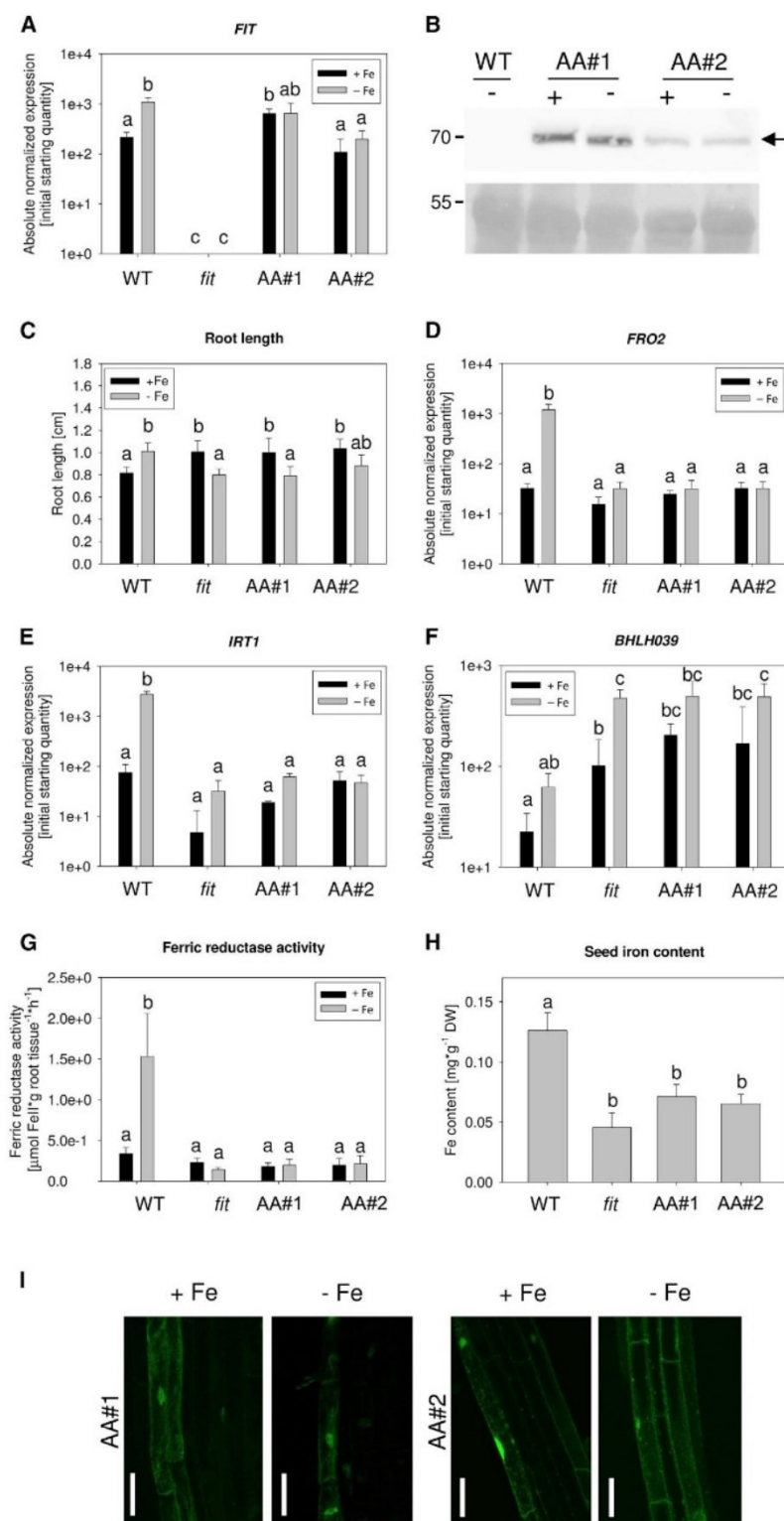


Figure 6. Non-phosphorylatable FITm(AA) at Ser272 Has Reduced Activity in Arabidopsis

The *fit* mutant complementation assay with FITm(AA)-GFP. Two FITm(AA)-GFP/*fit* lines (AA#1 and AA#2) were analyzed in comparison with WT and *fit* plants. Plants were grown with sufficient (+Fe, black bars) or deficient (-Fe, gray bars) Fe supply in 6 days (C and I) and 2-week growth assays (A, B, and D-G). See also Figures S3 and S6.

(A) *FIT* gene expression in roots, represented in base-10 logarithmic scale ($n = 3$).

(B) Anti-GFP immunodetection of full-length FITm(AA)-GFP fusion protein (indicated by an arrow) in plants. WT plants, negative control. PonceauS staining of the membrane, loading control. Protein molecular weight (in kDa) is indicated.

(C) Root lengths of plants ($n = 10$).

(D-F) Gene expression analysis in roots of *FRO2* (D), *IRT1* (E) and *BHLH039* (F) ($n = 3$).

(G) Root Fe reductase activity ($n = 4$).

(H) Seed Fe content per dry weight ($n = 3$).

(I) Laser-scanning confocal images of GFP-FITm(AA) in roots. Bars: 50 μm . See also Figure S7.

(A and C-H) Data are represented as mean \pm SD. Different letters indicate statistically significant differences ($p < 0.05$).

likely due to the regulated presence of the activating partner bHLH039. In summary, our data show that phosphorylation of FIT at Ser272 under Fe deficient conditions may prime FIT for participation in an active transcriptional complex with bHLH039.

DISCUSSION

Here, we identified the protein kinase CIPK11 as a positive regulator of Fe acquisition, phosphorylating FIT and priming it for interaction with bHLH039 for downstream target gene activation. This is consistent with the existence of two pools of FIT protein, active and inactive. In this study, we distinguish two pools of FIT based on its phosphorylation and show that FIT phosphorylated at position Ser272 has characteristics that would allow discriminating it as active FIT from the non-phosphorylated inactive FIT.

CIPK11 Acts as a Positive Regulator of Fe Acquisition by Forming a Pool of Active FIT

CIPK11 exerts its positive function in Fe deficiency response regulation by acting predominantly on FIT. This is supported by three findings. First, CIPK11 specifically interacts with FIT and phosphorylates it at Ser272. Second, CIPK11 and FIT act in the same root tissues and cell compartments. Upon Fe deficiency, *CIPK11* is expressed similarly to *FIT* in the early differentiation root zone, where Fe uptake predominantly takes place. Third, genetic analyses show that *cipk11*, *cb11/9* and the non-complementing FITm(AA)-GFP/*fit* (#AA1 and #AA2) lines share the same phenotypes of inability to fully induce Fe uptake, suggesting that in these lines FIT cannot achieve full activation. WT and complemented FITm(E)/*fit* (#E1 and #E2) plants had active FIT. FITm(E) does not increase Fe uptake alone, due to the independent regulation of bHLH039 partner of the active FIT complex. Therefore, FIT phosphorylation at Ser272 primes FIT for participation in an active transcriptional complex with bHLH039 under Fe deficiency, for activating Fe uptake. The identification of CIPK11 as an enzyme, that interacts with and post-translationally modifies FIT, allows better understanding of the mechanisms leading to the attachment of regulatory marks on FIT.

FIT Activation via CIPK11 Involves Nucleocytoplasmic Redistribution and Differential Protein Interaction Capacity

Subcellular localization studies found both FIT and CIPK11 in the nucleus and in the cytoplasm. The interaction between the two proteins was detected predominantly in the nucleus but also in the cytoplasm. Therefore, it is possible that FIT phosphorylation by CIPK11 occurs at both cellular locations. Nevertheless, active FITm(E) had a preference for nuclear localization compared to the more mobile and cytoplasmically-enriched inactive FITm(AA), which was particularly evident in root cells. The consequence of the interaction among active FIT molecules is currently unclear. FIT dimerization or FIT multimerization is facilitated upon CIPK11-mediated phosphorylation at Ser272 and the FIT-FIT complex formation could be at the origin of nuclear accumulation and decreased mobility of FIT. Protein phosphorylation is one of the potential mechanisms involved in regulated nucleocytoplasmic partitioning of transcription factors (Meier and Somers, 2011). Phosphorylation may lead to a conformational change that either masks or exposes a nuclear localization signal

(NLS) or a nuclear exclusion signal (NES). Phosphorylation may also affect FIT interaction with a nuclear shuttle protein or with a protein that retains FIT in the cytoplasm. One of these or a combination of these mechanisms may be responsible for the observed increased mobility and decreased nuclear accumulation of the non-phosphorylatable FITm(AA) form. In addition, FIT-FIT interaction could be a prerequisite for further attraction of bHLH subgroup Ib proteins such as bHLH039 into this complex. We could show that in yeast FIT homo-dimerization and interaction with bHLH039 can occur through the FIT C-terminus. This suggests that phosphorylation-induced alterations in FIT-C conformation may contribute, together with the bHLH domain, to the overall strength of FIT homo- and hetero-dimer formation. Subsequently, bHLH039-FIT complexes further stimulate *FIT* gene induction and Fe acquisition (Naranjo-Arcos et al., 2017). FIT, FITm(AA), and FITm(E) proteins were detectable upon sufficient and deficient Fe supply in roots of the transgenic lines, indicating that protein stability is not directly dependent on this phosphorylation site. The tobacco cells used for transient expression experiments have proven a good model system to study FIT localization and interactions, probably because a CIPK11-like activity is present there. In Arabidopsis, *CIPK11* is expressed in leaves and the CIPK11 activity is reduced in *cipk11* mutants but reconstituted in complemented *cipk11* lines (Fuglsang et al., 2007). This indicates that leaf cells do contain CIPK11-like activity explaining the different behavior of FIT and FITm forms in the leaf epidermis assays. In summary, the regulation of FIT phosphorylation status presents a mechanism to dynamically adjust the pool of functionally active FIT protein in the nucleus where it is available for protein-protein interactions, affecting the plant's Fe utilization capacity (Figure 7).

CIPK11-Mediated FIT Activation Is Integrated with the Plant Stress Response Networks

The mechanism of CIPK11 activation by Fe deficiency is an interesting aspect of the role of this protein kinase in Fe acquisition. *CIPK11* is upregulated by Fe deficiency, irrespective of FIT, possibly by subgroup IVc bHLH transcription factors that positively regulate Fe homeostasis upstream of FIT and bHLH038/039/100/101 (Zhang et al., 2015; Li et al., 2016; Liang et al., 2017). At post-translational level, CIPK11 is likely activated by one of the 10 CBLs (Weinl and Kudla, 2009) in response to Fe deficiency-induced elevation of cytosolic Ca^{2+} concentration. A variety of extracellular stimuli lead to the generation of Ca^{2+} transients to regulate cellular responses (Steinhorst and Kudla, 2014). We observed an increase in $[Ca^{2+}]_{cyt}$ in the early root differentiation zone after several days of Fe deficiency, consistent with the report by Tian et al. (2016). The perception of Fe deficiency is not as rapid as responses to chemical stimuli. Physiological and molecular data on the *cb11/9*, *cipk11*, and FITm/*fit* complementation lines demonstrate that active FIT is needed after 3 days of Fe deficiency. This is not surprising since in a previous study (Le et al., 2016), we could show that FIT activity regulation is still needed even after 10 days of Fe deficiency. Therefore, our data demonstrate the need for Ca^{2+} , CBL, and CIPK involvement in FIT activity regulation upon 3 days of Fe deficiency. Interestingly, the increase in $[Ca^{2+}]_{cyt}$ upon -Fe is significant in both epidermis and central cylinder, where both *FIT* (Jakoby et al., 2004) and *IRT1* (Marqués-Bueno et al., 2016)

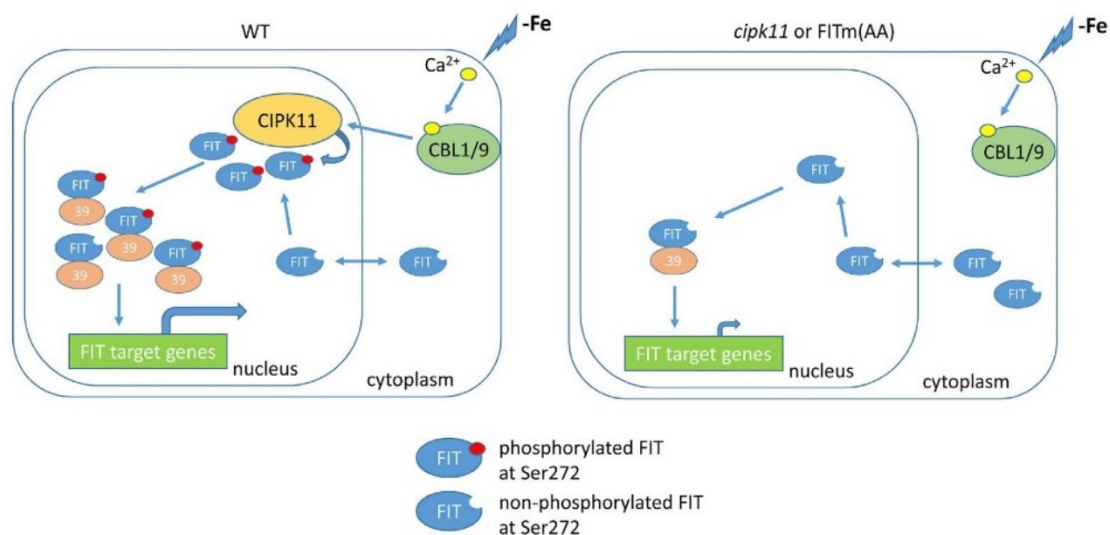


Figure 7. CIPK11-Mediated FIT Phosphorylation Promotes FIT Activity and Fe Acquisition

Model on the role of CIPK11 as a positive regulator of FIT target gene expression. Left side, in WT, Fe deficiency leads to elevated $[Ca^{2+}]_{\text{cyt}}$ perceived by Ca^{2+} sensors CBL1/9. CBL1/9 in turn activate CIPK11. Lack of Fe up-regulates independently CIPK11, BHLH039, and FIT. CIPK11 interacts with and phosphorylates FIT at Ser272. We propose that this phosphorylation discriminates between two FIT protein pools, namely a small pool of active FIT (Ser272-phosphorylated) and a large pool of inactive FIT (non-Ser272-phosphorylated). Phosphorylation at Ser272 triggers nucleocytoplasmic redistribution and FIT mobility changes toward higher nuclear accumulation. Due to increased amount of FIT in the nucleus, FIT can form homo-dimers and interact with bHLH039. Enhanced Ser272-phosphorylated FIT-bHLH039 interaction activates FIT transcriptional activity resulting in higher level of FIT target gene expression. Right side, in the *cipk11* mutant or in FITm(AA)/*fit* plants less FIT primed for bHLH039 interaction is available in the nucleus. Consequently, less FIT-bHLH039 hetero-dimers form, leading to decreased FIT target gene induction under Fe deficiency. The regulation of FIT phosphorylation is a mechanism to dynamically adjust the pool of functionally active FIT protein in the cell, altering the plant's Fe utilization capacity.

are expressed, though may be regulated by different cell-type-specific mechanisms (Brumbarova et al., 2016; Brumbarova and Ivanov, 2018). Still, a lack of IRT1 from either the epidermis or the central cylinder compromises the capacity of the plant to mobilize Fe (Marqués-Bueno et al., 2016). This makes it likely that FIT-dependent Fe uptake regulation responds to Ca^{2+} signals in both root zones.

Plants deficient in plasma membrane (*cb1/9*) but not tonoplast CBL function (*cb1/3*) showed altered Fe responses under $-Fe$ conditions, pointing toward an involvement of the plasma membrane-localized and CIPK11-interacting (Albrecht et al., 2001; Kolukisaoglu et al., 2004) CBL1 and CBL9 in perceiving Fe deficiency. Consistently, *cb1/9* has reduced shoot Fe content (Tian et al., 2016). Apart from their subcellular localization, CBL1/9 and CBL2/3 differ also in their number of canonical EF hands that bind Ca^{2+} ions. While CBL1 and CBL9 contain two canonical and two non-canonical EF hands, CBL2 and CBL3 have only a single canonical EF hand (Kolukisaoglu et al., 2004). This implies different affinities of the proteins for Ca^{2+} and, therefore, their participation in decoding Ca^{2+} signals with different strengths at different subcellular compartments, providing spatiotemporal specificity (Steinhorst and Kudla, 2014). Under alkaline stress, CIPK11 acts as a negative regulator of AHA2 activity, an effect surprisingly mediated by the tonoplast-localized CBL2 (Fuglsang et al., 2007). The role of CBL2 might be specific to high external pH stress, which is different from Fe deficiency. Different signaling read-out could explain why the activity of AHA2 is increased under Fe deficiency, despite the activation of CIPK11. In this context, it is interesting to note that CBL2/3

affect CIPK21 activity (Pandey et al., 2015). An interaction of CIPK21 with FIT, as suggested by our work, would be interesting to study. Presumably, different CBLs and different places of FIT phosphorylation in the cell could explain how Ca^{2+} can affect FIT-dependent processes in opposite ways. Seemingly contradictory physiological reactions might be relevant for fine-tuning of responses. Such is the case in ABA signaling. Several CIPK targets participate in the ABA response (Sanyal et al., 2015). In these cases, CIPKs play a dual role in the phosphorylation of plasma membrane and transcription factor proteins, causing both activation and repression of ABA responses. Fe signaling in root cells, similarly to ABA signaling in young seedlings, also involves communication between the plasma membrane and the nucleus. CIPK11 targets different proteins relevant in ABA and Fe signaling to confer positive and negative responses (this work; Fuglsang et al., 2007; Lumba et al., 2014; Zhou et al., 2015). Additionally, CIPK11 was proposed to be a regulatory hub in the ABA signaling network (Lumba et al., 2014; Zhou et al., 2015). This opens up the possibility that CIPK11 may serve as a connecting point to coordinate Fe acquisition with adverse abiotic stress conditions via ABA signaling, involving Ca^{2+} waves.

STAR★METHODS

Detailed methods are provided in the online version of this paper and include the following:

- KEY RESOURCES TABLE
- CONTACT FOR REAGENT AND RESOURCE SHARING

● EXPERIMENTAL MODEL AND SUBJECT DETAILS

- Plant Material
- Plant Growth Conditions

● METHOD DETAILS

- Yeast Two-Hybrid Screens
- Histochemical β -glucuronidase (GUS) Assay
- FIT Mutagenesis
- Generation of Fluorescent Protein Fusions
- Bimolecular Fluorescence Complementation (BiFC)
- Confocal Microscopy
- Root Length Measurement
- Gene Expression Analysis by RT-qPCR
- Fe Reductase Activity Assay
- Seed Fe Content Determination
- $[Ca^{2+}]_{cyt}$ Measurement and Ratiometric Imaging
- *In Vivo* FIT Phosphorylation Detection (Phos-Tag Mobility Shift Assay)
- *In Vivo* FIT Phosphorylation Detection (2D SDS-PAGE)
- Immunoblot Analysis
- Expression and Affinity Purification of Recombinant Proteins
- *In Vitro* Kinase Assay
- Cytoplasm-to-Nucleus Ratio Determination
- Fluorescence Recovery after Photobleaching (FRAP) Analysis
- Transcriptional Self-Activation Capacity Assay
- Protein Homo- and Hetero-Dimerization Assay in Yeast
- Protein Homo- and Hetero-Dimerization Assays *In Planta* (FRET-APB)
 - *fit* Mutant Complementation Assay

● QUANTIFICATION AND STATISTICAL ANALYSIS

● DATA AND SOFTWARE AVAILABILITY

● ACCESSION NUMBERS

SUPPLEMENTAL INFORMATION

Supplemental Information includes seven figures and one table and can be found with this article online at <https://doi.org/10.1016/j.devcel.2019.01.006>.

ACKNOWLEDGMENTS

We thank Angelika Anna, Ulrike Ellersiek, Gintaute Matthäi, and Elke Wieneke (Heinrich-Heine University) for excellent technical assistance. We acknowledge the contributions of Julia Mohrbacher, Florence Hermal, and Dana Wiebel. We are thankful to Stefanie Weidtkamp-Peters and members of the CAI imaging platform at Heinrich Heine University. R.G. and P.M. are members of graduate schools iGRAD-Plant, Düsseldorf, and CiM-IMPRS, Münster, Germany. Funding from the German Research Foundation is greatly acknowledged (grants Ba1610/5-2 and Ba1610/7-1 to P. B. and Ku931/18-1 to J. K.).

AUTHOR CONTRIBUTIONS

Conceptualization, T.B., R.G., P.M., R.I., J.K., and P.B.; Investigation, T.B., R.G., P.M., R.I., P.K., I.M., K.T., H.-J.M., and M.H.; Resources, L.S., J.M., M.D., S. A., and U.K.; Writing – Original Draft, T.B. and R.G.; Writing – Review & Editing, T.B., R.G., P.M., R.I., J.K., and P.B.; Supervision, T.B., J.K., and P.B.; Project Administration, T.B. and L.S.; Funding Acquisition, J.K. and P.B.

DECLARATION OF INTERESTS

The authors declare no competing interests.

Received: November 7, 2017

Revised: November 27, 2018

Accepted: December 31, 2018

Published: January 31, 2019

REFERENCES

- Abdallah, H.B., and Bauer, P. (2016). Quantitative reverse transcription-qPCR-based gene expression analysis in plants. *Methods Mol. Biol.* **1363**, 9–24.
- Albrecht, V., Ritz, O., Linder, S., Harter, K., and Kudla, J. (2001). The NAF domain defines a novel protein-protein interaction module conserved in Ca^{2+} -regulated kinases. *EMBO J.* **20**, 1051–1063.
- Bancaud, A., Huet, S., Rabut, G., and Ellenberg, J. (2010). Fluorescence perturbation techniques to study mobility and molecular dynamics of proteins in live cells: FRAP, photoactivation, photoconversion, and FLIP. *Cold Spring Harb. Protoc.* **2010**, pdb.top90.
- Batistić, O., and Kudla, J. (2012). Analysis of calcium signaling pathways in plants. *Biochim. Biophys. Acta* **1820**, 1283–1293.
- Batistić, O., Waadt, R., Steinhorst, L., Held, K., and Kudla, J. (2010). CBL-mediated targeting of CIPKs facilitates the decoding of calcium signals emanating from distinct cellular stores. *Plant J.* **67**, 211–222.
- Behera, S., Krebs, M., Loro, G., Schumacher, K., Costa, A., and Kudla, J. (2013). Ca^{2+} imaging in plants using genetically encoded Yellow Cameleon Ca^{2+} indicators. *Cold Spring Harb. Protoc.* **2013**, 700–703.
- Behera, S., Long, Y., Schmitz-Thom, I., Wang, X.P., Zhang, C., Li, H., Steinhorst, L., Manishankar, P., Ren, X.L., Offenborn, J.N., et al. (2017). Two spatially and temporally distinct Ca^{2+} signals convey Arabidopsis thaliana responses to K^{+} deficiency. *New Phytol.* **213**, 739–750.
- Bekešová, S., Komis, G., Krěnek, P., Vyplelová, P., Ovečka, M., Luptovciak, I., Illés, P., Kuchařová, A., and Šamaj, J. (2015). Monitoring protein phosphorylation by acrylamide pendant Phos-Tag in various plants. *Front. Plant Sci.* **6**, 336.
- Bleckmann, A., Weidtkamp-Peters, S., Seidel, C.A., and Simon, R. (2010). Stem cell signaling in Arabidopsis requires CRN to localize CLV2 to the plasma membrane. *Plant Physiol.* **152**, 166–176.
- Blum, A., Brumbarova, T., Bauer, P., and Ivanov, R. (2014). Hormone influence on the spatial regulation of IRT1 expression in iron-deficient Arabidopsis thaliana roots. *Plant Signal. Behav.* **9**, e28787.
- Brumbarova, T., and Bauer, P. (2005). Iron-mediated control of the basic helix-loop-helix protein fer, a regulator of iron uptake in tomato. *Plant Physiol.* **137**, 1018–1026.
- Brumbarova, T., and Ivanov, R. (2016). Differential gene expression and protein phosphorylation as factors regulating the state of the Arabidopsis SNX1 protein complexes in response to environmental stimuli. *Front. Plant Sci.* **7**, 1456.
- Brumbarova, T., and Ivanov, R. (2018). SNX1-mediated protein recycling: piecing together the tissue-specific regulation of Arabidopsis iron acquisition. *Plant Signal. Behav.* **13**, e1411451.
- Brumbarova, T., Bauer, P., and Ivanov, R. (2015). Molecular mechanisms governing Arabidopsis iron uptake. *Trends Plant Sci.* **20**, 124–133.
- Brumbarova, T., Le, C.T., Ivanov, R., and Bauer, P. (2016). Regulation of ZAT12 protein stability: the role of hydrogen peroxide. *Plant Signal. Behav.* **11**, e1137408.
- Clough, S.J., and Bent, A.F. (1998). Floral dip: a simplified method for Agrobacterium-mediated transformation of Arabidopsis thaliana. *Plant J.* **16**, 735–743.
- Colangelo, E.P., and Guerinot, M.L. (2004). The essential basic helix-loop-helix protein FIT1 is required for the iron deficiency response. *Plant Cell* **16**, 3400–3412.
- Curtis, M.D., and Grossniklaus, U. (2003). A gateway cloning vector set for high-throughput functional analysis of genes in planta. *Plant Physiol.* **133**, 462–469.
- Dinneny, J.R., Long, T.A., Wang, J.Y., Jung, J.W., Mace, D., Pointer, S., Barron, C., Brady, S.M., Schiefelbein, J., and Benfey, P.N. (2008). Cell identity

- mediates the response of Arabidopsis roots to abiotic stress. *Science* 320, 942–945.
- Drerup, M.M., Schlücking, K., Hashimoto, K., Manishankar, P., Steinhorst, L., Kuchitsu, K., and Kudla, J. (2013). The calcineurin B-like calcium sensors CBL1 and CBL9 together with their interacting protein kinase CIPK26 regulate the Arabidopsis NADPH oxidase RBOHF. *Mol. Plant* 6, 559–569.
- Dubeaux, G., Neveu, J., Zelazny, E., and Vert, G. (2018). Metal sensing by the IRT1 transporter-receptor orchestrates its own degradation and plant metal nutrition. *Mol. Cell* 69, 953–964.
- Eckert, C., Offenbom, J.N., Heinz, T., Armarego-Marriott, T., Schülte, S., Zhang, C., Hillmer, S., Heilmann, M., Schumacher, K., Bock, R., et al. (2014). The vacuolar calcium sensors CBL2 and CBL3 affect seed size and embryonic development in Arabidopsis thaliana. *Plant J.* 78, 146–156.
- Edel, K.H., Marchadier, E., Brownlee, C., Kudla, J., and Hetherington, A.M. (2017). The evolution of calcium-based signalling in plants. *Curr. Biol.* 27, R667–R679.
- Fuglsang, A.T., Guo, Y., Cui, T.A., Qiu, Q., Song, C., Kristiansen, K.A., Bych, K., Schulz, A., Shabala, S., Schumaker, K.S., et al. (2007). Arabidopsis protein kinase PKS5 inhibits the plasma membrane H⁺-ATPase by preventing interaction with 14-3-3 protein. *Plant Cell* 19, 1617–1634.
- Grefen, C., and Blatt, M.R. (2012). A 2in1 cloning system enables ratio-metric bimolecular fluorescence complementation (rBIFC). *Biotechniques* 53, 311–314.
- Guerinot, M.L., and Yi, Y. (1994). Iron: nutritious, noxious, and not readily available. *Plant Physiol.* 104, 815–820.
- Hashimoto, K., Eckert, C., Anshütz, U., Scholz, M., Held, K., Waadt, R., Reyer, A., Hippler, M., Becker, D., and Kudla, J. (2012). Phosphorylation of calcineurin B-like (CBL) calcium sensor proteins by their CBL-interacting protein kinases (CIPKs) is required for full activity of CBL-CIPK complexes toward their target proteins. *J. Biol. Chem.* 287, 7956–7968.
- Heim, M.A., Jakoby, M., Werber, M., Martin, C., Weisshaar, B., and Bailey, P.C. (2003). The basic helix-loop-helix transcription factor family in plants: a genome-wide study of protein structure and functional diversity. *Mol. Biol. Evol.* 20, 735–747.
- Ho, C.H., Lin, S.H., Hu, H.C., and Tsay, Y.F. (2009). CHL1 functions as a nitrate sensor in plants. *Cell* 138, 1184–1194.
- Holtkamp, M., Elseberg, T., Wehe, C.A., Sperling, M., and Karst, U. (2013). Complexation and oxidation strategies for improved TXRF determination of mercury in vaccines. *J. Anal. At. Spectrom.* 28, 719–723.
- Holtkamp, M., Wehe, C.A., Blaske, F., Holtschulte, C., Sperling, M., and Karst, U. (2012). Nitrogen purged TXRF for the quantification of silver and palladium. *J. Anal. At. Spectrom.* 27, 1799–1802.
- Hotzer, B., Ivanov, R., Brumbarova, T., Bauer, P., and Jung, G. (2012). Visualization of Cu(2+)(+) uptake and release in plant cells by fluorescence lifetime imaging microscopy. *FEBS J.* 279, 410–419.
- Ivanov, R., Brumbarova, T., and Bauer, P. (2012). Fitting into the harsh reality: regulation of iron deficiency responses in dicotyledonous plants. *Mol. Plant* 5, 27–42.
- Ivanov, R., Brumbarova, T., Blum, A., Jantke, A.M., Fink-Straube, C., and Bauer, P. (2014). SORTING NEXIN1 is required for modulating the trafficking and stability of the Arabidopsis IRON-REGULATED TRANSPORTER1. *Plant Cell* 26, 1294–1307.
- Jakoby, M., Wang, H.Y., Reidt, W., Weisshaar, B., and Bauer, P. (2004). FRU (bHLH029) is required for induction of iron mobilization genes in Arabidopsis thaliana. *FEBS Lett.* 577, 528–534.
- Kolukisaoglu, U., Weinl, S., Blazevic, D., Baticic, O., and Kudla, J. (2004). Calcium sensors and their interacting protein kinases: genomics of the Arabidopsis and rice CBL-CIPK signaling networks. *Plant Physiol.* 134, 43–58.
- Krebs, M., Held, K., Binder, A., Hashimoto, K., Den Herder, G., Pamiske, M., Kudla, J., and Schumacher, K. (2012). FRET-based genetically encoded sensors allow high-resolution live cell imaging of Ca²⁺ dynamics. *Plant J.* 69, 181–192.
- Kudla, J., and Bock, R. (2016). Lighting the way to protein-protein interactions: recommendations on best practices for bimolecular fluorescence complementation analyses. *Plant Cell* 28, 1002–1008.
- Le, C.T., Brumbarova, T., Ivanov, R., Stoof, C., Weber, E., Mohrbacher, J., Fink-Straube, C., and Bauer, P. (2016). Zinc FINGER of Arabidopsis THALIANA12 (ZAT12) interacts with fer-LIKE iron DEFICIENCY-INDUCED transcription factor (FIT) linking iron deficiency and oxidative stress responses. *Plant Physiol.* 170, 540–557.
- Li, X., Zhang, H., Ai, Q., Liang, G., and Yu, D. (2016). Two bHLH transcription factors, bHLH34 and bHLH104, regulate iron homeostasis in Arabidopsis thaliana. *Plant Physiol.* 170, 2478–2493.
- Liang, G., Zhang, H., Li, X., Ai, Q., and Yu, D. (2017). bHLH transcription factor bHLH115 regulates iron homeostasis in Arabidopsis thaliana. *J. Exp. Bot.* 68, 1743–1755.
- Ling, H.Q., Bauer, P., Berczky, Z., Keller, B., and Ganai, M. (2002). The tomato fer gene encoding a bHLH protein controls iron-uptake responses in roots. *Proc. Natl. Acad. Sci. U S A* 99, 13938–13943.
- Lingam, S., Mohrbacher, J., Brumbarova, T., Potuschak, T., Fink-Straube, C., Blondet, E., Genschik, P., and Bauer, P. (2011). Interaction between the bHLH transcription factor FIT and ethylene INSENSITIVE3/ETHYLENE INSENSITIVE3-LIKE1 reveals molecular linkage between the regulation of iron acquisition and ethylene signaling in Arabidopsis. *Plant Cell* 23, 1815–1829.
- Lumba, S., Toh, S., Handfield, L.F., Swan, M., Liu, R., Youn, J.Y., Cutler, S.R., Subramaniam, R., Provart, N., Moses, A., et al. (2014). A mesoscale abscisic acid hormone interactome reveals a dynamic signaling landscape in Arabidopsis. *Dev. Cell* 29, 360–372.
- Mai, H.J., Pateyron, S., and Bauer, P. (2016). Iron homeostasis in Arabidopsis thaliana: transcriptomic analyses reveal novel FIT-regulated genes, iron deficiency marker genes and functional gene networks. *BMC Plant Biol.* 16, 211.
- Mai, H.J., Lindermayr, C., von Toerne, C., Fink-Straube, C., Durner, J., and Bauer, P. (2015). Iron and fer-LIKE iron DEFICIENCY-INDUCED transcription factor-dependent regulation of proteins and genes in Arabidopsis thaliana roots. *Proteomics* 15, 3030–3047.
- Marqués-Bueno, M.D.M., Morao, A.K., Cayrel, A., Platre, M.P., Barberon, M., Caillieux, E., Colot, V., Jaillais, Y., Roudier, F., and Vert, G. (2016). A versatile Multisite Gateway-compatible promoter and transgenic line collection for cell type-specific functional genomics in Arabidopsis. *Plant J.* 85, 320–333.
- Meier, I., and Somers, D.E. (2011). Regulation of nucleocytoplasmic trafficking in plants. *Curr. Opin. Plant Biol.* 14, 538–546.
- Meiser, J., Lingam, S., and Bauer, P. (2011). Posttranslational regulation of the iron deficiency basic helix-loop-helix transcription factor FIT is affected by iron and nitric oxide. *Plant Physiol.* 157, 2154–2166.
- Naranjo-Arcos, M.A., Maurer, F., Meiser, J., Pateyron, S., Fink-Straube, C., and Bauer, P. (2017). Dissection of iron signaling and iron accumulation by overexpression of subgroup Ib bHLH039 protein. *Sci. Rep.* 7, 10911.
- Pandey, G.K., Kanwar, P., Singh, A., Steinhorst, L., Pandey, A., Yadav, A.K., Tokas, I., Sanyal, S.K., Kim, B.G., Lee, S.C., et al. (2015). Calcineurin B-like protein-interacting protein kinase CIPK21 regulates osmotic and salt stress responses in Arabidopsis. *Plant Physiol.* 169, 780–792.
- Robinson, N.J., Procter, C.M., Connolly, E.L., and Guerinot, M.L. (1999). A ferric-chelate reductase for iron uptake from soils. *Nature* 397, 694–697.
- Sanyal, S.K., Pandey, A., and Pandey, G.K. (2015). The CBL-CIPK signaling module in plants: a mechanistic perspective. *Physiol. Plant* 155, 89–108.
- Sivitz, A., Grinvalds, C., Barberon, M., Curie, C., and Vert, G. (2011). Proteasome-mediated turnover of the transcriptional activator FIT is required for plant iron-deficiency responses. *Plant J.* 66, 1044–1052.
- Song, C.P., Agarwal, M., Ohta, M., Guo, Y., Halfter, U., Wang, P., and Zhu, J.K. (2005). Role of an Arabidopsis AP2/EREBP-type transcriptional repressor in abscisic acid and drought stress responses. *Plant Cell* 17, 2384–2396.
- Steinhorst, L., and Kudla, J. (2014). Signaling in cells and organisms - calcium holds the line. *Curr. Opin. Plant Biol.* 22, 14–21.
- Tian, Q., Zhang, X., Yang, A., Wang, T., and Zhang, W.H. (2016). CIPK23 is involved in iron acquisition of Arabidopsis by affecting ferric chelate reductase activity. *Plant Sci.* 246, 70–79.

- Walter, M., Chaban, C., Schütze, K., Batistic, O., Weckermann, K., Näke, C., Blazevic, D., Grefen, C., Schumacher, K., Oecking, C., et al. (2004). Visualization of protein interactions in living plant cells using bimolecular fluorescence complementation. *Plant J.* *40*, 428–438.
- Wang, H.Y., Klatte, M., Jakoby, M., Bäumllein, H., Weisshaar, B., and Bauer, P. (2007). Iron deficiency-mediated stress regulation of four subgroup Ib BHLH genes in *Arabidopsis thaliana*. *Planta* *226*, 897–908.
- Wang, N., Cui, Y., Liu, Y., Fan, H., Du, J., Huang, Z., Yuan, Y., Wu, H., and Ling, H.Q. (2013). Requirement and functional redundancy of Ib subgroup bHLH proteins for iron deficiency responses and uptake in *Arabidopsis thaliana*. *Mol. Plant* *6*, 503–513.
- Weinl, S., and Kudla, J. (2009). The CBL-CIPK Ca²⁺-decoding signaling network: function and perspectives. *New Phytol.* *184*, 517–528.
- Wild, M., Davière, J.M., Regnault, T., Sakvarelidze-Achard, L., Carrera, E., Lopez Diaz, I., Cayrel, A., Dubeaux, G., Vert, G., and Achard, P. (2016). Tissue-specific regulation of gibberellin signaling fine-tunes Arabidopsis iron-deficiency responses. *Dev. Cell* *37*, 190–200.
- Xu, J., Li, H.D., Chen, L.Q., Wang, Y., Liu, L.L., He, L., and Wu, W.H. (2006). A protein kinase, interacting with two calcineurin B-like proteins, regulates K⁺ transporter AKT1 in Arabidopsis. *Cell* *125*, 1347–1360.
- Yang, T.J., Lin, W.D., and Schmidt, W. (2010). Transcriptional profiling of the Arabidopsis iron deficiency response reveals conserved transition metal homeostasis networks. *Plant Physiol.* *152*, 2130–2141.
- Yuan, Y., Wu, H., Wang, N., Li, J., Zhao, W., Du, J., Wang, D., and Ling, H.Q. (2008). FIT interacts with AtbHLH38 and AtbHLH39 in regulating iron uptake gene expression for iron homeostasis in Arabidopsis. *Cell Res.* *18*, 385–397.
- Zhang, J., Liu, B., Li, M., Feng, D., Jin, H., Wang, P., Liu, J., Xiong, F., Wang, J., and Wang, H.B. (2015). The bHLH transcription factor bHLH104 interacts with IAA-leucine RESISTANT3 and modulates iron homeostasis in Arabidopsis. *Plant Cell* *27*, 787–805.
- Zhou, X., Hao, H., Zhang, Y., Bai, Y., Zhu, W., Qin, Y., Yuan, F., Zhao, F., Wang, M., Hu, J., et al. (2015). SOS2-LIKE PROTEIN KINASE5, an SNF1-RELATED PROTEIN KINASE3-type protein kinase, is important for abscisic acid responses in Arabidopsis through phosphorylation of abscisic acid-INSENSITIVE5. *Plant Physiol.* *168*, 659–676.

STAR★METHODS

KEY RESOURCES TABLE

REAGENT or RESOURCE	SOURCE	IDENTIFIER
Antibodies		
Mouse anti-GFP	Roche	Cat# 11814460001; RRID: AB_390913
Goat anti-mouse IgG horseradish peroxidase conjugate	Promega	Cat# W4021; RRID: AB_430834
Anti-HA-peroxidase high-affinity monoclonal rat antibody	Roche	Cat# 12013819001; RRID: AB_390917
Critical Commercial Assays		
Spectrum Plant Total RNA Kit	Sigma-Aldrich	Cat# STRN250-1KT
RevertAid First Strand cDNA Synthesis Kit	Fermentas	Cat# K1622
RTS 500 Wheat Germ CECF Kit	5 PRIME	Cat# 2402100
Strep-Tactin® Macro Prep	IBA	Cat# 2-1505-002
Mini-PROTEAN® TGX™ Precast Gel	BioRad	Cat# 4561086
SuperSep Phos-tag™ gel	Wako Laboratory Chemicals	Cat# 195-17991
SERVA IPG BlueStrip 3-6 / 7 cm	Serva Electrophoresis GmbH	Cat# 43005.01
Experimental Models: Organisms/Strains		
<i>S. cerevisiae</i> strain AH109	Clontech	Cat# 630439
<i>Rhizobium radiobacter</i> strain C58 (pGV2260)	Institute of Plant Biology and Biotechnology, University of Münster	N/A
<i>Tobacco (Nicotiana benthamiana)</i>	Botanical garden, Heinrich-Heine University	N/A
<i>Arabidopsis</i> wild-type ecotype Col-0	Institute of Botany, Heinrich-Heine University	N/A
<i>Arabidopsis</i> ProFIT:GUS	(Jakoby et al., 2004)	N/A
<i>Arabidopsis</i> ProCIPK11:GUS line 1	This study	N/A
<i>Arabidopsis</i> ProCIPK11:GUS line 3	This study	N/A
<i>Arabidopsis</i> fit-3 (<i>fit</i>)	(Jakoby et al., 2004)	TAIR: GABI_108C10
<i>Arabidopsis</i> 2x35S:gFIT-GFP/ <i>fit</i> -3 (<i>FIT/fit</i>)	This study	N/A
<i>Arabidopsis</i> pks5-1, <i>cipk11</i> -1 (<i>cipk11</i>)	(Fuglsang et al., 2007)	TAIR: SALK_108074
<i>Arabidopsis</i> ProCIPK11:CIPK11/ <i>cipk11</i> line 1 (compl #1)	This study	N/A
<i>Arabidopsis</i> ProCIPK11:CIPK11/ <i>cipk11</i> line 2 (compl #2)	This study	N/A
<i>Arabidopsis</i> ProCIPK11:CIPK11/ <i>cipk11</i> line 3 (compl #3)	This study	N/A
<i>E. coli</i> BL21(DE3)pLysS	Promega	Cat# L1191
<i>Arabidopsis</i> FITm(AA)-GFP/ <i>fit</i> line AA#1	This study	N/A
<i>Arabidopsis</i> FITm(AA)-GFP/ <i>fit</i> line AA#2	This study	N/A
<i>Arabidopsis</i> FITm(E)-GFP/ <i>fit</i> line E#1	This study	N/A
<i>Arabidopsis</i> FITm(E)-GFP/ <i>fit</i> line E#2	This study	N/A
<i>Arabidopsis</i> HA ₇ -FIT/Col-0 line 8	(Meiser et al., 2011)	N/A
<i>Arabidopsis</i> ProUBQ10:YC3.6 (YC3.6)	(Krebs et al., 2012)	N/A
<i>Arabidopsis</i> <i>cbi2/3</i>	(Eckert et al., 2014)	N/A
<i>Arabidopsis</i> <i>cbi1/9</i>	(Xu et al., 2006)	N/A
Oligonucleotides		
Primers are listed in Table S1	N/A	N/A
Recombinant DNA		
pGBKT7:FIT-C	(Lingam et al., 2011)	N/A
pGAD.GH	(Kolukisaoglu et al., 2004)	N/A

(Continued on next page)

Continued

REAGENT or RESOURCE	SOURCE	IDENTIFIER
pGAD.GH:CIPK1	(Kolukisaoglu et al., 2004)	N/A
pGAD.GH:CIPK2	(Kolukisaoglu et al., 2004)	N/A
pGAD.GH:CIPK3	(Kolukisaoglu et al., 2004)	N/A
pGAD.GH:CIPK4	(Kolukisaoglu et al., 2004)	N/A
pGAD.GH:CIPK5	(Kolukisaoglu et al., 2004)	N/A
pGAD.GH:CIPK6	(Kolukisaoglu et al., 2004)	N/A
pGAD.GH:CIPK7	(Kolukisaoglu et al., 2004)	N/A
pGAD.GH:CIPK8	(Kolukisaoglu et al., 2004)	N/A
pGAD.GH:CIPK9	(Kolukisaoglu et al., 2004)	N/A
pGAD.GH:CIPK10	(Kolukisaoglu et al., 2004)	N/A
pGAD.GH:CIPK11	(Kolukisaoglu et al., 2004)	N/A
pGAD.GH:CIPK12	(Kolukisaoglu et al., 2004)	N/A
pGAD.GH:CIPK13	(Kolukisaoglu et al., 2004)	N/A
pGAD.GH:CIPK14	(Kolukisaoglu et al., 2004)	N/A
pGAD.GH:CIPK15	(Kolukisaoglu et al., 2004)	N/A
pGAD.GH:CIPK16	(Kolukisaoglu et al., 2004)	N/A
pGAD.GH:CIPK17	(Kolukisaoglu et al., 2004)	N/A
pGAD.GH:CIPK18	(Kolukisaoglu et al., 2004)	N/A
pGAD.GH:CIPK19	(Kolukisaoglu et al., 2004)	N/A
pGAD.GH:CIPK20	(Kolukisaoglu et al., 2004)	N/A
pGAD.GH:CIPK21	(Kolukisaoglu et al., 2004)	N/A
pGAD.GH:CIPK22	(Kolukisaoglu et al., 2004)	N/A
pGAD.GH:CIPK23	(Kolukisaoglu et al., 2004)	N/A
pGAD.GH:CIPK24	(Kolukisaoglu et al., 2004)	N/A
pGAD.GH:CIPK25	(Kolukisaoglu et al., 2004)	N/A
pGAD.GH:CIPK26	(Drerup et al., 2013)	N/A
pGBT9.BS:CIPK23	(Xu et al., 2006)	N/A
pGAD.GH:cAKT1	(Xu et al., 2006)	N/A
pKS II Bluescript:ProCIPK11	This study	N/A
pGPTV-II-KOZ-BAR	(Walter et al., 2004)	N/A
pGPTV-II-KOZ-BAR:ProCIPK11	This study	N/A
pGPTV-II-BAR-pUBQ10-GFP	(Batistic et al., 2010)	N/A
pGPTV-II-BAR-pUBQ10-GFP:CIPK11	This study	N/A
pDONR207:gFIT	This study	N/A
pJNC1	(Ivanov et al., 2014)	N/A
pJNC1:gFIT	This study	N/A
pMDC83	(Curtis and Grossniklaus, 2003)	N/A
pMDC83:gFIT	This study	N/A
pDONR221 P3-P2:CIPK11	This study	N/A
pDONR221 P1-P4:FIT	This study	N/A
pBiFC-2in1-NN	(Grefen and Blatt, 2012)	N/A
pBiFC-2in1-NN:CIPK11-FIT	This study	N/A
pDONR221 P1-P4:BHLH039	This study	N/A
pBiFC-2in1-NN:CIPK11-BHLH039	This study	N/A
pDONR221 P3-P2:CIPK15	This study	N/A
pBiFC-2in1-NN:CIPK15-FIT	This study	N/A
pKS II Bluescript:CIPK11	This study	N/A
pKS II Bluescript:ProCIPK11:CIPK11	This study	N/A
pGPTV-II-MCS-BAR:ProCIPK11:CIPK11	This study	N/A

(Continued on next page)

Continued

REAGENT or RESOURCE	SOURCE	IDENTIFIER
pIVEX-WG-StrepII	(Hashimoto et al., 2012)	N/A
pIVEX-WG-StrepII:CIPK11	This study	N/A
pET-24a(+)	Novagen	Cat# 69749
pET-24a(+):FIT	This study	N/A
pET-24a(+):FIT-C	This study	N/A
pET-24a(+):FITm(AA)-C	This study	N/A
pET-24a(+):FITm(E)-C	This study	N/A
pIVEX-WG-StrepII:GST	This study	N/A
pET-24b(+)	Novagen	Cat# 69750
pET-24b(+):StrepII-GST	This study	N/A
pDONR207:cFIT	This study	N/A
pDONR207:cFITm(AA)	This study	N/A
pDONR207:cFITm(E)	This study	N/A
pGBKT7-GW	Dr. Yves Jacob	N/A
pGBKT7-GW:cFIT	This study	N/A
pGBKT7-GW:cFITm(AA)	This study	N/A
pGBKT7-GW:cFITm(E)	This study	N/A
pACT2-GW	Dr. Yves Jacob	N/A
pGBKT7-GW:cFIT-C	This study	N/A
pGBKT7-GW:cFITm(AA)-C	This study	N/A
pGBKT7-GW:cFITm(E)-C	This study	N/A
pACT2-GW:cFIT-C	This study	N/A
pACT2-GW:cFITm(AA)-C	This study	N/A
pACT2-GW:cFITm(E)-C	This study	N/A
pABindGFP	(Bleckmann et al., 2010)	N/A
pABindmCherry	(Bleckmann et al., 2010)	N/A
pABindGFPmCherry	(Bleckmann et al., 2010)	N/A
pABindGFP:cFIT	This study	N/A
pABindGFP:cFITm(AA)	This study	N/A
pABindGFP:cFITm(E)	This study	N/A
pABindmCherry:cFIT	This study	N/A
pABindmCherry:cFITm(AA)	This study	N/A
pABindmCherry:cFITm(E)	This study	N/A
pABindGFPmCherry:cFIT	This study	N/A
pABindGFPmCherry:cFITm(AA)	This study	N/A
pABindGFPmCherry:cFITm(E)	This study	N/A
pDONR221 P3-P2:FIT	This study	N/A
pDONR221 P3-P2:FITm(AA)	This study	N/A
pDONR221 P3-P2:FITm(E)	This study	N/A
pDONR221 P1-P4:FITm(AA)	This study	N/A
pDONR221 P1-P4:FITm(E)	This study	N/A
pBiFC-2in1-NN:FIT-FIT	This study	N/A
pBiFC-2in1-NN:FITm(AA)-FITm(AA)	This study	N/A
pBiFC-2in1-NN:FITm(E)-FITm(E)	This study	N/A
Software and Algorithms		
ZEN 2 Blue Edition software	Zeiss	https://www.zeiss.com
ZEN 2 Black Edition software	Zeiss	https://www.zeiss.com
JMicroVision software, version 1.2.7	JMicroVision	http://www.jmicrovision.com
Bruker Spectra software (version 6.1.5.0)	Bruker Nano	https://www.bruker.com

(Continued on next page)

Continued

REAGENT or RESOURCE	SOURCE	IDENTIFIER
Bio-Rad SFX Manager™ (version 3.1) software	Bio-Rad	http://www.bio-rad.com
AlphaView software	ProteinSimple	https://www.proteinsimple.com/
ImageJ software		https://imagej.net
Origin Lab software	OriginLab Corporation	http://www.originlab.de/
SPSS Statistics software	IBM	https://www.ibm.com
Other		
Plant growth chambers	CLF Plant Climatics	http://www.plantclimatics.de/
Axio Imager.M2 microscope	Zeiss	https://www.zeiss.com
LSM 780 laser-scanning microscope	Zeiss	https://www.zeiss.com
IEF system Amersham Ettan IPGphor III	GE Healthcare Life Sciences	https://www.gelifesciences.com
2D electrophoresis system Amersham Ettan DALTsix	GE Healthcare Life Sciences	https://www.gelifesciences.com
FluorChem Q System	ProteinSimple	https://www.proteinsimple.com/
Tecan Safire2 plate reader	Thermo Fisher Scientific	https://www.thermofisher.com
S2-PICOFOX TXRF-Spektrometer	Bruker Nano	https://www.bruker.com
SFX96 Touch™ Real-Time PCR Detection System	Bio-Rad	http://www.bio-rad.com
Branson Sonifier®W-250 D	Fisher Scientific	https://www.fishersci.com
Molecular Dynamics Typhoon 9200 Variable Mode Imager	Amersham Biosciences	www.gelifesciences.com

CONTACT FOR REAGENT AND RESOURCE SHARING

Further information and requests for resources and reagents should be directed to and will be fulfilled by the Lead Contact, Petra Bauer (petra.bauer@uni-duesseldorf.de).

EXPERIMENTAL MODEL AND SUBJECT DETAILS**Plant Material**

The *Arabidopsis* (*Arabidopsis thaliana*) ecotype Col-0 was used as WT. The *fit* loss-of-function mutant allele *fit-3* (GABI_108C10, abbreviated as *fit* in the text) was described previously (Jakoby et al., 2004). The *cipk11* loss-of-function mutant allele *pks5-1* (named here *cipk11-1*, SALK_108074, briefly termed *cipk11* in the text) was previously reported (Fuglsang et al., 2007). Three independent *cipk11*-complemented lines were obtained by transforming *cipk11* mutant plants with *ProCIPK11:CIPK11* cloned into pGPTV-II-MCS-BAR and selecting them until homozygous. In order to obtain the *ProCIPK11:CIPK11* construct, 1882 bp *CIPK11* promoter fragment was amplified using CIPK11_forSpe and pCIPK11_reBam_2 (Table S1), and cloned into pKS II Bluescript. The full-length *CIPK11* intron-containing coding sequence followed by the 3' UTR was amplified using the primers CIPK11_for_Bam and CIPK11UTRreXho (Table S1), and cloned also into pKS II Bluescript. The *CIPK11* promoter and the *CIPK11*+3'UTR sequence were then subcloned into pGPTV-II-MCS-BAR. HA₇-FIT plants were previously described (HA-FIT 8; Meiser et al., 2011). The line stably expressing the genetically encoded Ca²⁺ sensor Yellow Cameleon 3.6 (YC3.6) under the control of the *UBQ10* promoter has been described previously by Krebs et al. (2012). The *cbl2/3* and *cbl1/9* double loss-of-function mutants were previously described (Xu et al., 2006; Eckert et al., 2014).

Tobacco (*Nicotiana benthamiana*) plants were used for protein subcellular localization and interaction studies.

Plant Growth Conditions

Arabidopsis seeds were sterilized and seedlings grown on upright sterile plates containing modified half-strength Hoagland medium [1.5 mM Ca(NO₃)₂, 1.25 mM KNO₃, 0.75 mM MgSO₄, 0.5 mM KH₂PO₄, 50 μM KCl, 50 μM H₃BO₃, 10 μM MnSO₄, 2 μM ZnSO₄, 1.5 μM CuSO₄, 0.075 μM (NH₄)₆Mo₇O₂₄, 1% sucrose, pH 5.8, supplemented with 1.4 % Plant agar (Duchefa)] with sufficient (50 μM FeNaEDTA, + Fe) or deficient (0 μM FeNaEDTA, - Fe) Fe supply under long-day conditions, as described previously (Lingam et al., 2011). Plants were grown in plant growth chambers (CLF Plant Climatics) either for 6 days directly on sufficient or Fe-deficient medium (6-day system) or for 14 days at sufficient Fe supply and then transferred for three days to either sufficient or deficient Fe supply (2-week system). For 2D SDS-PAGE, seedlings were grown on +Fe or -Fe for ten days. For [Ca²⁺]_{cyt} measurements and ratiometric imaging, plants were grown for five days at sufficient Fe supply and then transferred for three days to either sufficient or deficient Fe supply.

Tobacco plants were grown on soil for 3-4 weeks in a greenhouse facility under long day conditions (16-hour light/8-hour dark).

METHOD DETAILS

Yeast Two-Hybrid Screens

For targeted Y2H interaction assays between FIT and the 26 members of the CIPK family, the GAL4 DNA binding domain (BD)-containing construct pGBKT7:FIT-C (BD-FIT-C; [Lingam et al., 2011](#)) was used as a bait and co-transformed in the yeast strain AH109 together with prey pGAD.GH, providing the GAL4 activation domain (AD)-containing full-length CIPK fusion constructs. pGAD.GH:CIPK1 to pGAD.GH:CIPK26 were described previously ([Kolukisaoglu et al., 2004](#); [Drerup et al., 2013](#)). FIT-C was used since full-length BD-FIT triggers self-activation. The combination of pGBT9.BS:CIPK23 and pGAD.GH:cAKT1 was used as a positive control ([Xu et al., 2006](#)). BD-FIT-C co-transformed with empty AD plasmid was used as a negative control. In the targeted Y2H interaction assay combining FIT and CIPK11, empty BD and AD-CIPK11 plasmids, and empty BD with empty AD plasmids, were used as additional negative controls. Yeast transformation and subsequent cultivation were performed as previously described ([Le et al., 2016](#)). In short, aliquots of ten-fold serial dilutions ($A_{600} = 10^{-1}$ – 10^{-4}) of the transformed AH109 cells were spotted on synthetic defined (SD) agar plates lacking Leu (pGBKT7 auxotrophy selection) and Trp (pACT2-GW auxotrophy selection) (SD-LW, co-transformation control). In parallel, aliquots of the same serial dilutions were spotted on SD agar plates lacking Leu, Trp, and His, and supplemented with 0.5 mM 3-amino-1,2,4-triazole (SD-LWH + 0.5 mM 3-AT, selection for interaction). The parallel spotting of defined amounts of yeast cells on control and interaction selective media allowed the semi-quantitative comparison of yeast growth between different co-transformation events. Plates were photographed after one-week incubation at 30 °C.

Histochemical β -glucuronidase (GUS) Assay

ProFIT:GUS transgenic plants have been described previously ([Jakoby et al., 2004](#)). *ProCIPK11:GUS* plants were generated as follows: a 1882 bp *CIPK11* promoter fragment was amplified using the primers pCIPK11_forSpe and pCIPK11_reXho ([Table S1](#)), cloned into pKS II Bluescript (Stratagene), and then subcloned into pGPTV-II-KOZ-BAR ([Walter et al., 2004](#)). The resulting *ProCIPK11:GUS* construct was transformed into Col-0 plants using the floral dip procedure ([Clough and Bent, 1998](#)). Positive transformants were identified by BASTA selection, selfed, and propagated until homozygous lines were obtained. Two independent *ProCIPK11:GUS* lines (1 and 3) were selected for detailed analysis. GUS plants were grown in the 6-day system and assayed for histochemical GUS activity using the substrate 5-bromo-4-chloro-3-indolyl- β -D-glucuronic acid (X-Gluc). Chlorophyll was removed by a 16-hour incubation in 100 % ethanol. Seedlings were stored in 70 % ethanol before imaging. GUS staining was documented on an Axio Imager.M2 microscope (Zeiss). Single images obtained with 10x objective magnification were assembled using the Stitching function of the ZEN 2 Blue Edition software (Zeiss).

FIT Mutagenesis

pDONR207:gFIT was used as a template for FIT mutagenesis. To mutate FIT at position Ser272 to Glu and create a phosphomimicking FIT form, termed gFITm(E), the primers FITmS272E-1 and FITmS272E-2 ([Table S1](#)) were used. To create a non-phosphorylatable gFITm(AA) form for position Ser272, the amino acid was mutated to Ala together with the adjacent Ser271 in order to exclude redundancy, using the primers FITmSS271AA-1 and FITmSS271AA-2 ([Table S1](#)). The PCR conditions were as follows: 95°C, 30 s; 18 cycles of: 95°C, 30 s/ 55°C, 1 min/ 72°C for 2 min per 1kb of plasmid length; 72°C, 7 min. After the PCR, the reaction was treated with 10 units Dpn I for 1 h at 37°C before *E. coli* transformation. The mutagenized *gFITm* forms in pDONR207 were subsequently used for creating plant expression constructs for C-terminal GFP fusions in the pMDC83 vector.

Generation of Fluorescent Protein Fusions

Generation of plant transformation vectors for fluorescent protein-fusion expression was performed as follows: *CIPK11* cDNA was amplified using primers CIPK11 SpeI forward and CIPK11 XhoI reverse ([Table S1](#)) and inserted into pGPTV-II-BAR-pUBQ10-GFP for translational N-terminal GFP fusion. For cloning genomic *FIT* fragment (*gFIT*) into the Gateway-compatible plasmids pJNC1 ([Ivanov et al., 2014](#)) and pMDC83 ([Curtis and Grossniklaus, 2003](#)) for translational C-terminal fusion of mCherry, and GFP, respectively, the entry clone pDONR207:gFIT was generated after amplification of *gFIT* from Col-0 gDNA using the primers FIT B1 and FITns B2 ([Table S1](#)) (BP reaction; Life Technologies). *gFIT*-mCherry and *gFIT*-GFP fusions were created by subcloning *gFIT* (LR reaction; Life Technologies) into pJNC1 and pMDC83, respectively. The *Agrobacterium* (*Rhizobium radiobacter*) strain C58 (pGV2260) carrying pGPTV-II-BAR-pUBQ10-GFP:CIPK11, pJNC1:gFIT or pMDC83:gFIT, was used to transiently transform tobacco leaves as previously described ([Hotzer et al., 2012](#)). In short, *Rhizobium* cultures carrying the plasmid of interest were resuspended in infiltration solution (2 mM NaH₂PO₄, 0.5% glucose, 50 mM MES, 100 mM acetosyringone, pH 5.6) at $A_{600} = 0.8$. The suspension was infiltrated with a syringe applied to the abaxial side of the leaf. Transformed plants were kept for 48 h at 25 °C in long day conditions (16-hour light/8-hour dark) before being analyzed for transgene expression.

Bimolecular Fluorescence Complementation (BiFC)

The verification of FIT-CIPK11 interaction *in planta* was performed using the BiFC 2in1 system with mRFP transformation control ([Grefen and Blatt, 2012](#)). *CIPK11* and *FIT* coding sequences were amplified using the primers CIPK11 B3 and CIPK11 B2, and FIT B1 and FITstop B4 ([Table S1](#)). The resulting *CIPK11* and *FIT* PCR fragments were cloned by BP reaction (Life Technologies) into pDONR221 P3-P2 (Invitrogen) and pDONR221 P1-P4 (Invitrogen), respectively. Following LR reaction (Life Technologies) with the obtained vectors and pBiFC-2in1-NN ([Grefen and Blatt, 2012](#)), *CIPK11* and *FIT* were cloned together into

pBiFC-2in1-NN:CIPK11-FIT. Following the recommendations for appropriate negative BiFC controls (Kudla and Bock, 2016), two pBiFC-2in1-NN constructs were created – *CIPK11* together with *BHLH039* and *FIT* together with *CIPK15*. *BHLH039* was amplified using the primers 39 B1 and 39st B4 (Table S1). *CIPK15* was amplified using CIPK15 B3 and CIPK15st B2 (Table S1). The obtained constructs were transformed into agrobacteria and used for tobacco leaf infiltration as described above. After 48 h, YFP fluorescent signals were detected by confocal microscopy. The BiFC experiments were performed in three independent repetitions on a total of 6 infiltrated leaves. Transformed cells were verified by mRFP fluorescence. The vector pBiFC-2in1-NN was kindly provided by Dr. Christopher Grefen, Tübingen, Germany.

For FIT and FITm homo-dimer formation analysis, full-length *FIT*, *FITm(AA)* and *FITm(E)* coding sequences were amplified using the primers FIT B3 and FITstop B2 (Table S1) for cloning into pDONR221 P3-P2, and the primers FIT B1 and FITstop B4 (Table S1) for cloning into pDONR221 P1-P4. pDONR207:cFIT, pDONR207:cFITm(AA) and pDONR207:cFITm(E) were used as templates, respectively. *FIT* and *FITm* were subcloned into pBiFC-2in1-NN:FIT-FIT, pBiFC-2in1-NN:FITm(AA)-FITm(AA) and pBiFC-2in1-NN:FITm(E)-FITm(E).

Confocal Microscopy

Laser-scanning confocal microscopy (LSM 780, Zeiss) controlled by ZEN 2 Black Edition software (Zeiss) was used for fluorescence imaging of YFP and GFP at an excitation wavelength of 488 nm and emission wavelength of 500 to 530 nm as previously described (Brumbarova and Ivanov, 2016; Le et al., 2016). mRFP and mCherry were detected 48 h after Agrobacterium leaf infiltration of tobacco plants (as described above) with an excitation wavelength at 563 nm and emission wavelength of 560 to 615 nm. Pinholes for each channel were set at 1 Airy Unit with optical slices equivalent to 0.8 μm . Images were recorded in a 1,024 pixel format.

Root Length Measurement

Images of plants grown on agar plates were taken and primary root lengths of individual seedlings were measured using the JMicroVision software, version 1.2.7 (<http://www.jmicrovision.com>), as described previously (Ivanov et al., 2014). In short, special calibration was performed for converting pixel values into centimeters. Then, 1D measurements of the roots were performed using the free-hand drawing tool. The line lengths were used for calculating average root length and standard deviations. Root lengths of 16 to 46 plants per condition were measured. ($n = 16-46$).

Gene Expression Analysis by RT-qPCR

Gene expression analysis was performed as described previously (Abdallah and Bauer, 2016). In short, total RNA was isolated from roots of plants grown in the 2-week system using the Spectrum Plant Total RNA kit (Sigma-Aldrich). Reverse transcription with oligo(dT) primer was performed using the RevertAid first-strand cDNA synthesis kit (Fermentas). RT-qPCR was performed on SFX96 Touch™ Real-Time PCR Detection System (Bio-Rad). The results were processed on Bio-Rad SFX Manager™ (version 3.1) software. Primer pairs used in this study are listed in Table S1. Absolute gene expression was determined by mass standard curve analysis and normalized to elongation factor *EF1B α* expression as a reference. The assay was performed in three biological replicates ($n = 3$), each with two technical replicates.

Fe Reductase Activity Assay

Fe reductase activity was determined as described in (Le et al., 2016) with some modifications. Plants grown in the 2-week system, were washed in 100 mM $\text{Ca}(\text{NO}_3)_2$ solution followed by incubation at room temperature in 1 mL of Fe reductase solution (300 μM ferrozine and 100 μM FeNaEDTA) in the dark. After 1 h, the absorbance of the Fe reductase solution was measured at 562 nm using the Safire2 plate reader (Tecan). The Fe reductase activity normalized to root weight was calculated using the extinction coefficient $\epsilon = 28.6 \text{ mM}^{-1}\text{cm}^{-1}$. The assay was performed in four replicates ($n = 4$), each representing a pool of two plants.

Seed Fe Content Determination

For Fe content determination in seeds, plants were grown in parallel on soil under long-day conditions (16 h day, 8 h night, 21°C). Harvested seeds were dried overnight at 120 °C, followed by 2 days exposure to 60 °C. Their Fe content was determined using Total Reflection X-Ray Fluorescence (TXRF) (Holtkamp et al., 2012; Holtkamp et al., 2013). TXRF was carried out on a S2-PICOFOX instrument (Bruker Nano) with an air-cooled molybdenum anode for X-ray generation. The excitation settings were 50 kV and 750 μA and quartz glass disks were used as sample carriers. As internal standard, arsenic (As, Fluka Chemie) with a concentration of 10 mg/L was applied. The samples of plant material were weighed into a vial and digested with nitric acid (70 %; Primar Plus®, Trace Analysis Grade, Fisher Scientific) over night at 95 °C. The dried samples were redissolved in 1 mL purified water (Aquatron A4000D system, Barloworld Scientific) and aliquots of 100 μL were mixed with the same volume of the 10 mg/L As standard solution. Aliquots of 5 μL of the samples were placed on the sample carriers and evaporated to dryness. The analysis was performed by signal integration over 500 s. For the determination, the signals of Fe ($K\alpha_1 = 6.405 \text{ keV}$) and As ($K\alpha_1 = 10.543 \text{ keV}$), as internal standard, were used. Quantification was performed by the Bruker Spectra software (version 6.1.5.0) and based on the known concentration of the internal As standard. The assay was performed in three biological replicates ($n = 3$). Each biological replicate was measured two times.

[Ca²⁺]_{cyt} Measurement and Ratiometric Imaging

For monitoring Fe supply dependent changes in free cytosolic [Ca²⁺], 6 days-old Arabidopsis seedlings stably expressing the genetically encoded Ca²⁺ sensor *ProUBQ10:YC3.6* were transferred to microscopic slides in liquid Hoagland medium containing the same amount of Fe as on the Hoagland agar plates where the plants grew for three days on + Fe (50 μM FeNaEDTA) or – Fe (0 μM FeNaEDTA) supply prior to imaging. Imaging was performed using LSM780 confocal laser-scanning microscope (Zeiss) essentially as described in (Behera et al., 2013). In brief, fluorescence was excited at 458 nm and detected at 465–499 nm for ECFP, and 520–570 nm for cpVenus. 1024 x 1024 pixel images were acquired with 10x objective (pinhole 7 airy units) every 10 s for 12 min. ImageJ (<http://rsbweb.nih.gov/ij/>) was used to quantify changes in [Ca²⁺] in different root zones and tissues. Regions of interest (ROIs) were defined in the meristematic (MZ) and elongation (EZ) zones of the root tip, and in the central cylinder (CC) and epidermis with cortex (Ep) region of the early root differentiation zone. For each zone, a ROI with the same size was used to calculate background fluorescence in the ECFP and cpVenus channels. Background-corrected cpVenus and ECFP fluorescent intensities in the defined ROIs were used to calculate cpVenus/ECFP ratios. In order to exclude unspecific responses of the root to the mounting on the microscopic slide, the ratio values of the first 3 min were excluded from the subsequent analysis. The rest of the values were averaged for each zone and compared. The measurement was performed on 12 seedlings in two independent experiments. Ratiometric Ca²⁺ imaging was performed as previously described (Behera et al., 2017).

In Vivo FIT Phosphorylation Detection (Phos-Tag Mobility Shift Assay)

HA₇-FIT plants were grown in the 2-week system. Total protein was extracted from roots as previously described (Bekešová et al., 2015) by using RIPA buffer. Protein concentration was determined by Bradford Assay. 200 μg total root protein was precipitated with 80% v/v acetone for 4 h at -20 °C and pelleted at 15.000 x g at 4 °C for ten minutes. The protein pellet was solubilized in 100 μl 1x CIP reaction buffer (Sigma-Aldrich) to a final concentration of 2 mg/ml. The samples were treated with 60 units of CIP or reaction buffer (mock treated) and incubated overnight at 37 °C. The reaction was stopped by adding 5x Laemmli buffer (250 mM Tris-Cl pH6.8, 10% SDS, 30% glycerol, 5% β-mercaptoethanol, 0,02% bromophenol blue), denatured at 95 °C for 10 min and kept on ice until loading. Approximately 20 μg root total protein was separated in a standard Mini-PROTEAN® TGX™ Precast Gel (BioRad). In parallel, the same samples were loaded on precast SuperSep Phos-tag™ gels (Wako Laboratory Chemicals), containing 50 μmol/L Phos-tag and 7.5% polyacrylamide. Electrophoresis was performed as described in Bekešová et al. (2015) (following instructions for Zn²⁺-Phos-tag™ gels). HA₇-FIT protein detection was performed as previously described (Le et al., 2016). See also “Immunoblot detection”. The assay was performed two times.

In Vivo FIT Phosphorylation Detection (2D SDS-PAGE)

Two-dimensional (2D) gel electrophoresis (SDS-PAGE) was performed as in Mai et al., (2015). Whole seedlings were harvested and ground in liquid N₂. Proteins were precipitated by adding 10 volumes of ice-cold precipitation solution (10 % TCA and 0.07 % 2-mercaptoethanol in acetone) and incubation at -20 °C for 30 min. The suspension was centrifuged at maximum speed for 30 min at 4 °C and the pellet was washed three times with 10 volumes of washing solution (0.07 % 2-mercaptoethanol in acetone). Finally, the pellet was dried and resuspended in 1 volume of extraction buffer (7 M urea, 2 M thiourea, 4 % CHAPS, 50 mM dithiothreitol, 0.5 % Servalyt™ pH 3-10 Iso-Dalt). 50 μl of 10 x dephosphorylation buffer (5 mM Tris pH 7.9, 10 mM NaCl, 1 mM MgCl₂, and 0.1 mM DTT) were added to 800 μg of total protein and then diluted to a volume of 460 μl. 40 μl of 10 IU/μl phosphatase from bovine mucosa (+AP) or AP storage buffer without AP (-AP) were added to the solution. The samples were incubated at 37 °C for 2 h. The proteins were then precipitated by adding 2 % (v/v) of 20 mg/ml cold sodium deoxycholate and incubating on ice for 30 min, followed by addition of 1/9 volume of 100 % trichloroacetic acid to the solution and incubation at 4 °C overnight. The solution was centrifuged at 24 000 g for 30 min at 4 °C. The pellet was washed 3 times with ice-cold acetone, dried in a vacuum centrifuge and resolubilized in 150 μl extraction buffer (protein solution 1). 150 μg of the resolubilized and mock or phosphatase treated total protein were loaded on 7 cm IPG strips pH 3-6 (SERVA IPG BlueStrip). The respective volume of protein solution 1 was diluted to final volume of 120 μl with rehydration solution pH 3-6 (8 M urea, 2% CHAPS, 50 mM DTT, 0.5 % Servalyt™ pH 3-10 Iso-Dalt, 0.75 % Servalyt™ pH 3-6 and a trace of bromophenol blue). IPG strip rehydration was performed overnight. Isoelectric focusing was performed with a slow voltage gradient and a total of ca. 22 000 Vh (gradient to 150 V for 150 Vh, gradient to 300 V for 300 Vh, gradient to 600 V for 600 Vh, gradient to 1500 V for 1500 Vh, gradient to 3000 V for 3000 Vh, hold 3000 V for 16000 Vh, hold 250 V forever). Prior to the second dimension separation, the isoelectrically focused samples were reduced in reduction buffer (6 M urea, 30 % glycerol, 10 % 0.5 M Tris pH 6.8, 2 % SDS, 2 % DTT) for 35 min. Alkylation of cysteins was performed by incubating the strips in alkylation buffer (6 M urea, 30 % glycerol, 10 % 0.5 M Tris pH 6.8, 2 % SDS, 2.5 % iodoacetamide) for 35 min. Then the strips were briefly rinsed with running buffer and placed on top of a vertical 12.5 % polyacrylamide gel. The 2D SDS-PAGE was run with 100 V for 45 min.

Immunoblot Analysis

Total protein extraction from Arabidopsis plants grown in the 2-week system or from tobacco leaves, sample separation on SDS-PAGE and immunodetection were performed as previously described (Le et al., 2016). In short, plant material was grinded under liquid N₂ and proteins were extracted with SDG buffer (62mM Tris-HCl, pH 8.6, 2.5 % (w/v) SDS, 2 % (w/v) DTT, 10 % (w/v) glycerol). Samples containing 5 mg of protein were separated on 12 % (w/v) SDS-PAGE gels. Following electrophoresis, the proteins were transferred to a Protran nitrocellulose membrane (Schleicher & Schuell) and stained with Ponceau S (Sigma-Aldrich) as a loading control. Immunodetection was performed as follows: Membranes were blocked for 1 hour in 5 % (w/v) milk solution (Roth), dissolved in

TBST (20 mM Tris-HCl, pH 7.4, 180 mM NaCl, and 0.1 % (v/v) Tween 20), followed by 1-hour incubation in a dilution of the primary antibody in TBST containing 2.5 % (w/v) milk. After three washes with TBST, 15 min each, the membrane was incubated in a dilution of the secondary antibody in TBST containing 2.5 % (w/v) milk. The membrane was washed three times with TBST, 15 min each, before detection using the enhanced chemiluminescence system (GE Healthcare). GFP- or cYFP-tagged fusion proteins were probed with mouse anti-GFP (Roche, catalog no. 11814460001, 1:1000) followed by goat anti-mouse IgG horseradish peroxidase conjugate (Promega, catalog no. W4021, 1:5000). HA- and nYFP-tagged (due to the presence of an HA-tag in the same expression cassette) fusion proteins were detected in a single-step immunoblot with anti-HA-peroxidase high-affinity monoclonal rat antibody (3F10, Roche, catalog no. 12013819001, 1:1000). Chemiluminescence detection and image analysis were performed using the FluorChem Q System for quantitative Western blot imaging (ProteinSimple) with the AlphaView software (ProteinSimple) allowing signal recording in the dynamic detection range.

Expression and Affinity Purification of Recombinant Proteins

CIPK11 and kinase target proteins were generated as follows: *CIPK11* coding sequence was amplified using the primers CIPK11 SpeI forward and CIPK11 XhoI reverse (Table S1), and cloned into the pIVEX-WG-StrepII vector (Hashimoto et al., 2012). StrepII-tagged CIPK11 protein was generated using wheat germ-based cell-free protein synthesis with the RTS 500 Wheat Germ CECF Kit (5 PRIME) following the manufacturer's instructions. The purification of the StrepII-CIPK11 protein was performed as previously described (Hashimoto et al., 2012). In short, each *in vitro* translation reaction (1 ml) was mixed with 0.8 ml of Strep-Tactin Macroprep (IBA) and incubated for 30 min at 4°C. StrepII-tagged proteins were eluted by gravity flow in elution buffer (100 mM Tris pH 8.0, 150 mM NaCl, 2.5 mM desthiobiotin).

Constructs for recombinant protein expression of full-length and C-terminal part of non-mutated and mutagenized FIT forms were produced as follows: Full-length *FIT* coding sequence was amplified from Col-0 -Fe root cDNA using primers SpeI-noATG-FIT and FITstop-SacI (Table S1). The C-terminal part of *FIT* or mutagenized *FIT* forms were amplified from cDNA prepared from tobacco leaves infiltrated with pMDC83:gFIT, pMDC83:gFITm(AA) or pMDC83:gFITm(E), respectively, using primers SpeI-FIT-C and FITstop-SacI (Table S1). The obtained *FIT*, *FIT-C*, *FITm-C(AA)* and *FITm-C(E)* products were subsequently cloned into the pET-24a(+) plasmid (Novagen). The resulting constructs were transformed into the *E. coli* bacterial strain BL21(DE3)pLysS (Promega).

In order to obtain StrepII-tagged glutathione S-transferase (GST) protein, the *GST* coding sequence was amplified using primers GST_XbaI.for and GST_SpeI_BamHI_Sall.rev (Table S1) and subcloned into the pIVEX-WG-StrepII vector (Hashimoto et al., 2012). The resulting StrepII-GST fusion was subsequently cloned into pET-24b(+) plasmid. The resulting construct was transformed into BL21(DE3)pLysS cells.

Recombinantly expressed StrepII-FIT, StrepII-FIT-C, StrepII-FITm-C(AA) and StrepII-FITm-C(E) proteins were produced from BL21(DE3)pLysS cell cultures carrying the pET-24a(+) plasmid containing the respective StrepII-tagged FIT form as described in (Hashimoto et al., 2012) with the exception that bacterial cultures were induced by 0.5mM isopropyl β -D-thiogalactopyranoside (IPTG) at 30°C for 3 h. Afterwards, cells were harvested by centrifugation, and resuspended in lysis buffer (100 mM Tris pH 8.0, 150 mM NaCl, 1 mg/ml lysozyme). After 1 hour incubation on ice, the lysate was sonicated and centrifuged at 14,000 x g for 5 min at 4°C. The affinity purification of the StrepII-tagged FIT forms was performed using Strep-Tactin® Macro Prep (IBA) following the manufacturer's instructions. The protein amount in the fractions was estimated using BSA standards on Coomassie-stained SDS gels.

The StrepII-GST protein was produced in a similar manner, with the following exception: after cell lysis and centrifugation, StrepII-GST protein remained in the supernatant, which was then directly used for affinity purification using Strep-Tactin® Macro Prep (IBA) following the manufacturer's instructions.

In Vitro Kinase Assay

In vitro kinase assays were performed according to (Hashimoto et al., 2012). In short, StrepII-tagged purified CIPK11 (150 ng per reaction) and different substrate proteins (500 ng per reaction) were mixed according to the experimental setup in 24 μ l in reaction buffer containing 5mM MnSO₄, 0.5mM CaCl₂, 2mM DTT, 10 μ M ATP and 4 μ Ci of [γ -³²P] ATP (3000 Ci/mmol) for 30 min at 30°C. Following the kinase assay, the samples were subjected to SDS-PAGE and Coomassie staining. The SDS gels were exposed to phosphorimager screens and the radioactively labelled protein bands were visualized by auto-radiography using a Molecular Dynamics Typhoon 9200 Variable Mode Imager (Amersham Biosciences). The *in vitro* kinase assays were repeated two times, showing similar results.

Cytoplasm-to-Nucleus Ratio Determination

The localization of FIT-GFP and FITm-GFP fusion proteins was detected in tobacco 48 h post infiltration by laser-scanning confocal microscopy (LSM 780, Zeiss). Cells were imaged using a 40x C-Apochromat water immersion objective at an excitation wavelength of 488 nm and an emission wavelength of 500 to 530 nm, pinhole diameter 90 μ m, pixel resolution of 0.208 μ m in X and Y, and 1 μ m in Z. Z-stacks typically consisted of 20 - 40 slices ensuring the recording full cell dimensions. For nucleus-to-cytoplasm ratio analysis, a maximum intensity projection of the Z-stack was made in the ZEN 2 Blue Edition software. Images were exported to tiff files and each image was analyzed in ImageJ software after conversion to 12-bit grayscale format. Signal intensity values were obtained for the whole cell without the nucleus and for the nucleus separately. The nucleus-to-cytoplasm ratio was calculated for each cell separately. Six tobacco cells were imaged per construct per experiment. Three independent experiments were performed. The

cytoplasm-to-nucleus ratio of FIT- and FITm-GFP fusion proteins in Arabidopsis root epidermis cells of plants grown under sufficient and deficient Fe supply was calculated from fifteen cells per genotype and growth condition per biological replicate.

Fluorescence Recovery after Photobleaching (FRAP) Analysis

The mobility of FIT-GFP and FITm-GFP fusion proteins, transiently expressed in tobacco was quantified using laser-scanning confocal microscopy (LSM 780, Zeiss) as described above. Data was recorded with a pinhole diameter of 41 μm and pixel resolution of 0.208 μm . Successive control scans were made to ensure that no acquisition bleaching occurred during imaging. After 20 scans, a bleach with 50 iterations of maximum laser intensity was performed of a rectangular region of interest (ROI) of 46 x 14 pixels in the nucleus. This was followed by 280 post-bleaching scans within 100 s. For each single acquisition, the background fluorescence was subtracted from the FRAP values, which were then normalized to the mean of the pre-bleach values. The kinetic parameter final fluorescence intensity (F_{end}) was determined after applying Exponential curve fitting in the Origin Lab software, taking into account the initial fluorescence intensity (F_{pre}) and the fluorescence intensity after photobleaching (F_{post}). The percentage of mobile (M_f) and immobile (I_f) fractions of FIT-GFP, FITm(AA)-GFP and FITm(E)-GFP was determined according to the following equations: $M_f = [(F_{\text{end}} - F_{\text{post}}) / (F_{\text{pre}} - F_{\text{post}})] * 100$ and $I_f = 100 - M_f$ (Bancaud et al., 2010). Twelve to 21 nuclei were quantified per construct.

Transcriptional Self-Activation Capacity Assay

In order to investigate the self-activation capacity of FIT and mutagenized FIT forms, full-length *FIT*, *FITm(AA)* and *FITm(E)* were amplified using primers FIT B1 and FITns B2 (Table S1) from cDNA prepared from tobacco leaves transiently transformed with pMDC83:gFIT, pMDC83:gFITm(AA) and pMDC83:gFITm(E). The PCR products were cloned into pDONR207 (BP reaction; Life Technologies) and subcloned into the BD-containing yeast two-hybrid destination vector pGBKT7-GW (LR reaction; Life Technologies). The resulting constructs were co-transformed into AH109 yeast cells together with an empty AD-containing pACT2-GW plasmid. Growth of yeast colonies was assayed on SD-LWH media with two different high 3-AT concentrations (30 and 60 mM) after spotting in ten-fold serial dilutions. Growth on selective SD-LW media was used as a co-transformation control. pGBKT7-GW and pACT2-GW plasmids were kindly provided by Dr. Yves Jacob.

Protein Homo- and Hetero-Dimerization Assay in Yeast

For assaying the homo-dimerization ability of FIT-C and FIT-C phosphomutant forms, *FITm-C(AA)* and *FITm-C(E)* coding sequences were amplified from tobacco cDNA (primers FIT-C B1 and FITst B2, Table S1) and the amplicons were transferred into the BD- and AD-containing vectors pGBKT7-GW and pACT2-GW, respectively, to obtain the final destination constructs. These constructs were used to co-transform yeast AH109 cells with the combinations BD-FIT-C with AD-FIT-C, BD-FITm-C(AA) with AD-FITm-C(AA), and BD-FITm-C(E) with AD-FITm-C(E). Growth of yeast colonies was assayed on SD-LWH media with 0.5 mM 3-AT (selection for interaction) after spotting in ten-fold serial dilutions. Growth on selective SD-LW media was used as a co-transformation control.

For assaying the ability of FIT-C and FIT-C phosphomutant forms to form hetero-dimers with bHLH039, the coding sequence of *BHLH039* was amplified using the primers 39 B1 and 39st B2 (Table S1) and subcloned into pACT2-GW to obtain AD-bHLH039. AD-bHLH039 was co-transformed with AD-FIT-C, BD-FITm-C(AA) and AD-FITm-C(AA) in AH109 cells and the strength of their interaction was assayed as described above.

Protein Homo- and Hetero-Dimerization Assays In Planta (FRET-APB)

Full-length coding sequences of FIT and FITm were cloned into the pABind vector set [pABindGFP, pABindmCherry, and pABindFRET (named here pABindGFPmCherry)] (Bleckmann et al., 2010) by LR reaction (Life Technologies) using the constructs pDONR207:cFIT, pDONR207:cFITm(AA) and pDONR207:cFITm(E). The Agrobacterium (*Rhizobium radiobacter*) strain C58 (pGV2260) carrying one of the obtained constructs was used to transiently transform tobacco leaf epidermis cells as previously above. Direct application of β -estradiol allowed the inducible expression of GFP-, mCherry- and GFP-mCherry-tagged FIT, FITm(AA) and FITm(E) fusion proteins 24 h post infiltration. Förster Resonance Energy Transfer - Acceptor Photo Bleaching (FRET-APB) for GFP and mCherry-tagged pairs was measured to assess the strength of homo-dimer formation in epidermis cell nuclei. GFP-tagged fusions were used as donor-only (negative) controls. Fusions of the respective proteins with both GFP and mCherry for intra-molecular FRET were used as positive controls. Similarly, bHLH039 coding sequence was also cloned into the pABind vector set to produce bHLH039-GFP and bHLH039-GFP-mCherry fusions. bHLH039-GFP FRET pairs with FIT/FITm(AA)/FITm(E)-mCherry were assayed for their FRET efficiency. bHLH039-GFP was used as a donor-only control. bHLH039-GFP-mCherry was used as a positive control. Laser-scanning confocal microscopy (LSM 780, Zeiss) controlled by ZEN 2 Black Edition software (Zeiss) was used for GFP and mCherry detection as described above. Series of images were acquired in a 256 x 256 pixel format. After the fifth image, mCherry was photobleached in a region within the nucleus using 80 iterations of 100 % laser power. FRET efficiency (E_{FRET}) in percent was calculated as the relative increase of GFP intensity following photobleaching of the mCherry acceptor. Only plant nuclei with similar GFP and mCherry fluorescence levels were considered for the FRET efficiency measurements. Ten nuclei were measured per construct. Two independent experiments were performed.

fit Mutant Complementation Assay

Arabidopsis *fit* mutant plants were transformed with full-length FIT and full-length FITm forms fused to GFP, resulting in FIT-GFP, FITm(AA)-GFP and FITm(E)-GFP, by floral dip (Clough and Bent, 1998). Positive transformants, selected based on hygromycin

resistance, GFP fluorescence, immunoblot analysis and PCR genotyping, were selfed and multiplied until homozygous lines were obtained. Lines in the T3 generation were used for further analysis, named FIT/ *fit* for FIT-GFP/*fit*, AA#1 and AA#2 for FITm(AA)-GFP/*fit* and E#1 and E#2 for FITm(E)-GFP/*fit*.

QUANTIFICATION AND STATISTICAL ANALYSIS

Statistical details of experiments, such as number of technical and biological repetitions, can be found in the respective Methods section and in the Figure legends. For statistical analysis, P values were obtained via one-way ANOVA followed by Fisher's LSD using the SPSS Statistics software (IBM). Different lower-case letters on the graphs were used to indicate statistically significant differences ($P < 0.05$), distributed in the graphs from left to right.

DATA AND SOFTWARE AVAILABILITY

Software used in this study is listed in the [Key Resources Table](#).

ACCESSION NUMBERS

Sequence data from this article can be found in the TAIR and GenBank data libraries under accession numbers:

AKT1 (TAIR: AT2G26650), *BHLH039* (TAIR: AT3G56980), *CIPK1* (TAIR: AT3G17510), *CIPK2* (TAIR: AT5G07070), *CIPK3* (TAIR: AT2G26980), *CIPK4* (TAIR: AT4G14580), *CIPK5* (TAIR: AT5G10930), *CIPK6* (TAIR: AT4G30960), *CIPK7* (TAIR: AT3G23000), *CIPK8* (TAIR: AT4G24400), *CIPK9* (TAIR: AT1G01140), *CIPK10* (TAIR: AT5G58380), *CIPK11* (TAIR: AT2G30360), *CIPK12* (TAIR: AT4G18700), *CIPK13* (TAIR: AT2G34180), *CIPK14* (TAIR: AT5G01820), *CIPK15* (TAIR: AT5G01810), *CIPK16* (TAIR: AT2G25090), *CIPK17* (TAIR: AT1G48260), *CIPK18* (TAIR: AT1G29230), *CIPK19* (TAIR: AT5G45810), *CIPK20* (TAIR: AT5G45820), *CIPK21* (TAIR: AT5G57630), *CIPK22* (TAIR: AT2G38490), *CIPK23* (TAIR: AT1G30270), *CIPK24* (TAIR: AT5G35410), *CIPK25* (TAIR: AT5G25110), *CIPK26* (TAIR: AT5G21326), *CBL1* (TAIR: AT4G17615), *CBL2* (TAIR: AT5G55990), *CBL3* (TAIR: AT4G26570), *CBL9* (TAIR: AT5G47100), *FIT* (TAIR: AT2G28160), *FRO2* (TAIR: AT1G01580), *FRO3* (TAIR: AT1G23020), *IRT1* (TAIR: AT4G19690), *NAS4* (TAIR: AT1G56430), *SIFER* (GenBank: AF437878).

Developmental Cell, Volume 48

Supplemental Information

**CIPK11-Dependent Phosphorylation Modulates FIT
Activity to Promote Arabidopsis Iron Acquisition
in Response to Calcium Signaling**

Regina Gratz, Prabha Manishankar, Rumen Ivanov, Philipp Köster, Inga Mohr, Ksenia Trofimov, Leonie Steinhorst, Johannes Meiser, Hans-Jörg Mai, Maria Drerup, Sibylle Arendt, Michael Holtkamp, Uwe Karst, Jörg Kudla, Petra Bauer, and Tzvetina Brumbarova

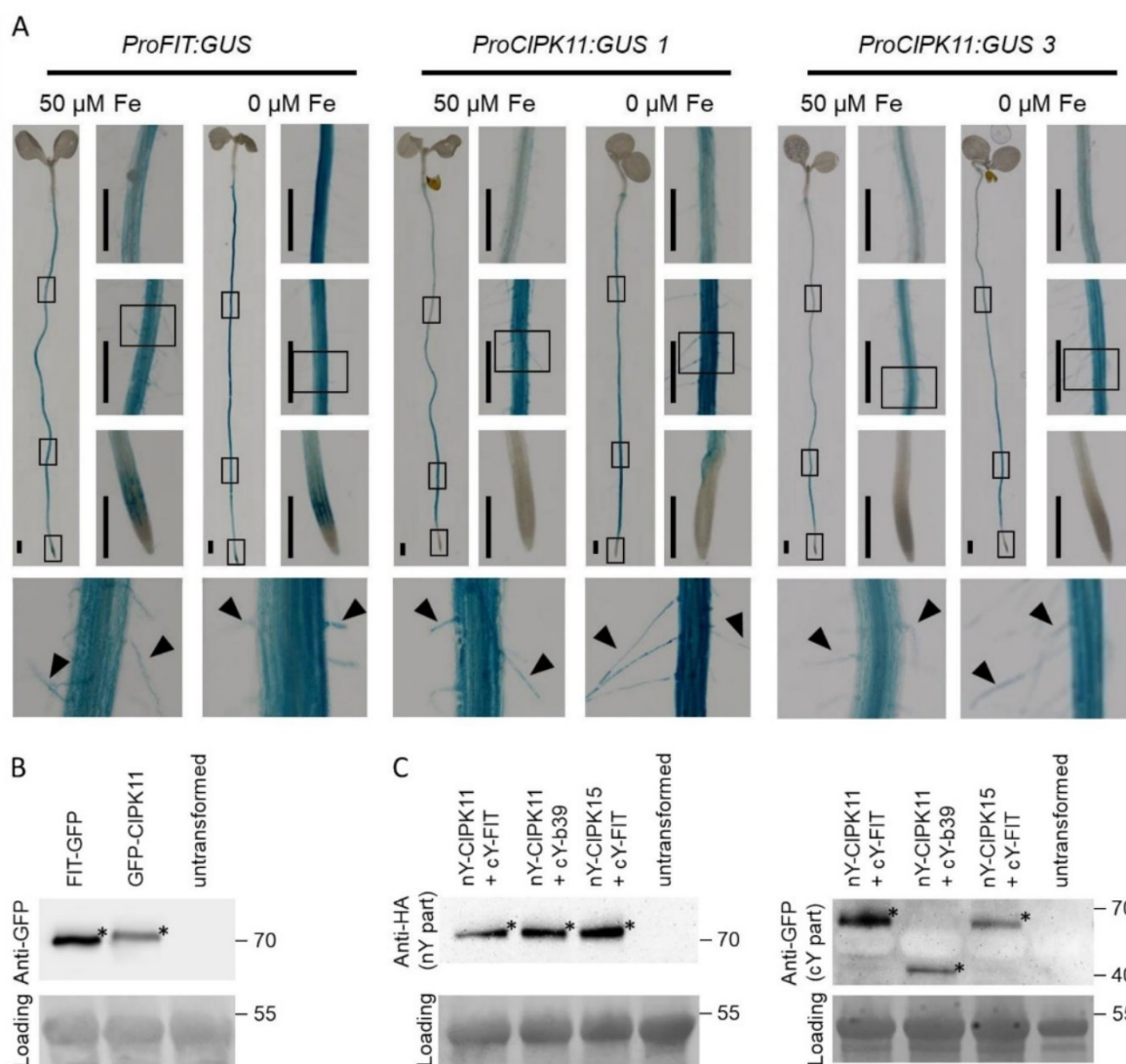


Figure S1. Overlapping Fe deficiency-induced *FIT* and *CIPK11* promoter activities and immunodetection controls for protein localization and BiFC experiments. Related to Figure 1.

(A) Promoter-driven GUS reporter staining in whole seedlings and roots. *ProFIT:GUS* and *ProCIPK11:GUS* plants (lines 1 and 3) were grown in the 6-day system under sufficient (+ Fe) or deficient (- Fe) Fe supply. Rectangles in the respective seedling image indicate the positions of the enlarged images along the root for each genotype and condition, and correspond to, from top to bottom, the differentiated cell zone, the early differentiation zone and the root tip. Lowest row –

corresponding close-ups of regions from the early root differentiation zone (marked with rectangles). Filled arrowheads indicate GUS staining (promoter activity) in root hairs. Bars: 1 mm.

(B) Immunodetection control of fluorescently tagged FIT- and CIPK11-GFP fusion proteins in tobacco leaf cells, used in protein localization experiments in [Figure 1D](#). Anti-GFP antibody was used for detection.

(C) Immunodetection control of split YFP-tagged fusion proteins in tobacco leaf cells, used in BiFC experiments in [Figure 1F](#). Anti-HA antibody detected nYFP- and anti-GFP antibody detected cYFP-tagged fusion proteins.

(B, C) Untransformed tobacco leaf extract was used as a negative control. PonceauS staining of the membrane was used as a loading control. Asterisks indicate the protein bands corresponding to the respective full-length fusion protein. Protein molecular weight (in kDa) is indicated.

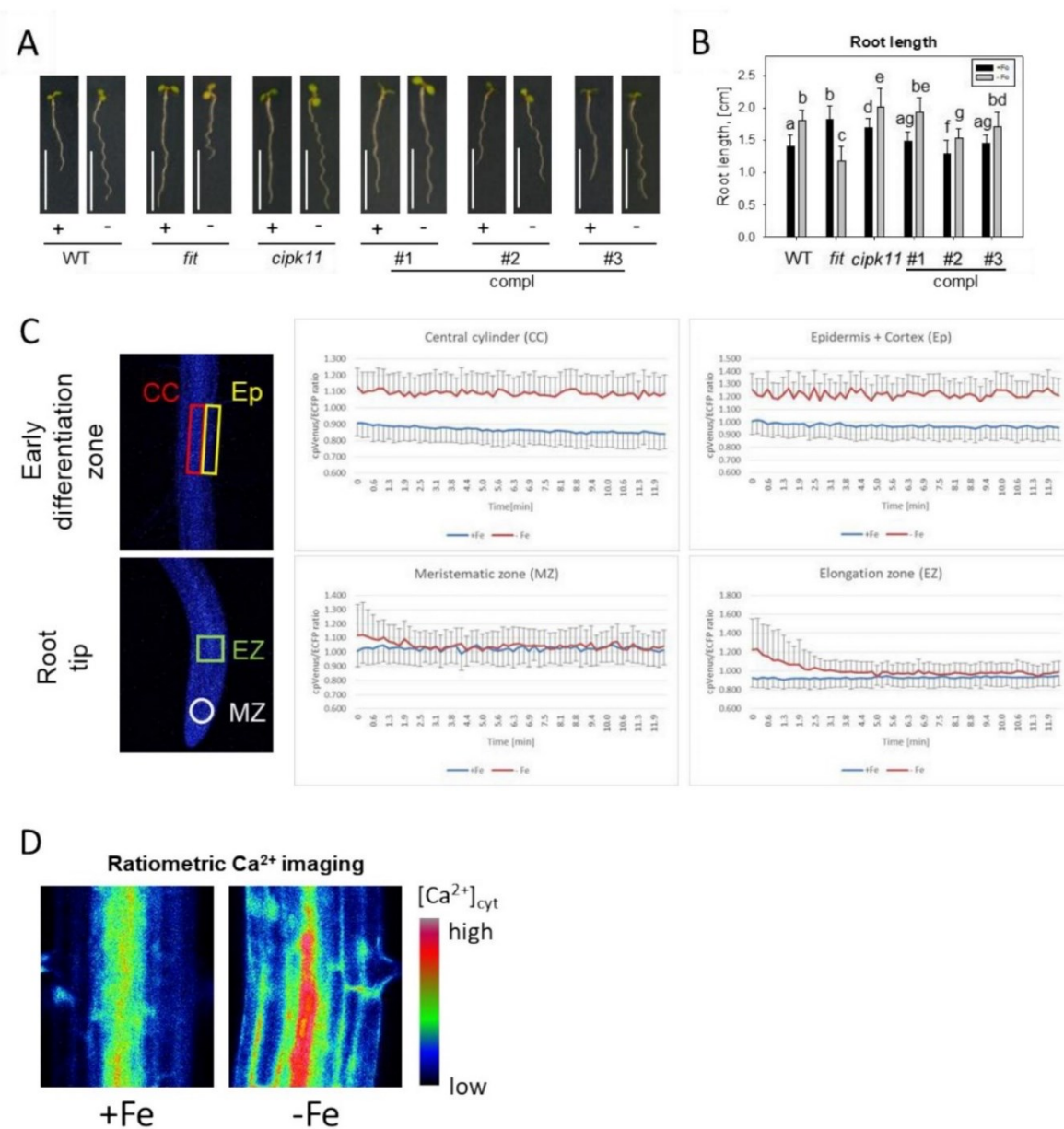


Figure S2. *cipk11* root length phenotype and additional information on $[\text{Ca}^{2+}]_{\text{cyt}}$ measurements. Related to Figure 2.

(A, B) Growth phenotypes of *cipk11* mutant and three *cipk11*-complemented lines (compl #1, #2, and #3). Plants were grown in the 6-day system under sufficient (+ Fe) or deficient (- Fe) Fe supply in comparison with wild type (WT) and *fit* mutant.

(A) Phenotypes of plants. Bars: 1 mm.

(B) Quantification of primary root lengths. Data are represented as mean \pm SD (n = 16-46). Different letters indicate statistically significant differences (P < 0.05).

(C, D) Additional information for $[\text{Ca}^{2+}]_{\text{cyt}}$ measurements.

(C) Changes in free $[\text{Ca}^{2+}]_{\text{cyt}}$ concentrations in roots of 5 day-old plants grown for three further days under sufficient (+Fe, blue line) or deficient (-Fe, red line) Fe supply. Left, Indication of root areas for $[\text{Ca}^{2+}]_{\text{cyt}}$ change measurements in the meristematic (MZ) and elongation (EZ) zones of the root tip, central cylinder (CC) and epidermis with cortex (Ep) of the early root differentiation zone. Right, Emission ratios between cpVenus and ECFP fluorescence intensities indicative of $[\text{Ca}^{2+}]_{\text{cyt}}$ changes, measured for 12 min in the indicated root areas. The ratio values after 3.3 min (to exclude unspecific responses to the mounting) were averaged and represented in [Figure 2J](#). Error bars represent standard deviations (n = 12).

(D) Changes in $[\text{Ca}^{2+}]_{\text{cyt}}$ under Fe deficiency visualized by ratiometric Ca^{2+} imaging of the early root differentiation zone of plants grown as in (C).

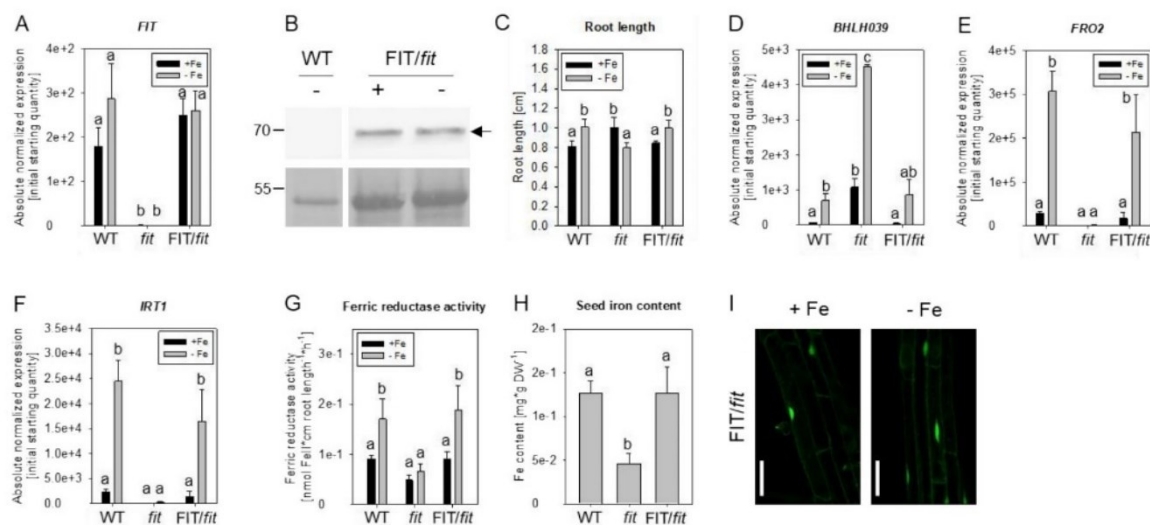


Figure S3. FIT-GFP rescues the Fe deficient *fit* mutant phenotype. Related to Figure 6, S6 and S7.

fit mutant complementation assay with wild-type FIT-GFP. FIT-GFP/*fit* plants (FIT/*fit*) were analyzed in comparison with wild-type (WT) and *fit* mutant plants grown in response to sufficient (+Fe, black bars) and deficient (-Fe, gray bars) Fe supply in the six-day (C, I) and two-week growth assays (A, B, D-G). Data are represented as mean \pm SD. Different letters indicate statistically significant differences ($P < 0.05$).

(A) Gene expression analysis in roots of *FIT*, represented in base-10 logarithmic scale ($n = 3$).

(B) Immunodetection of full-length FIT-GFP fusion protein (indicated by an arrow) in plants, detected with anti-GFP antibody. WT, negative control, PonceauS staining, loading control. WT samples were on the same membrane as FIT/*fit* samples. Excluded lanes, indicated by a white bar.

(C) Root lengths of plants ($n = 10$).

(D-F) Gene expression analysis in roots of *BHLH039* (D), *FRO2* (E) and *IRT1* (F) ($n = 3$).

(G) Root Fe reductase activity of plants ($n = 4$).

(F) Fe contents per dry weight (DW) of seeds, collected from soil-grown plants ($n = 3$).

(I) Laser-scanning confocal images of roots. Bars: 50 μm . See also Figure S7.

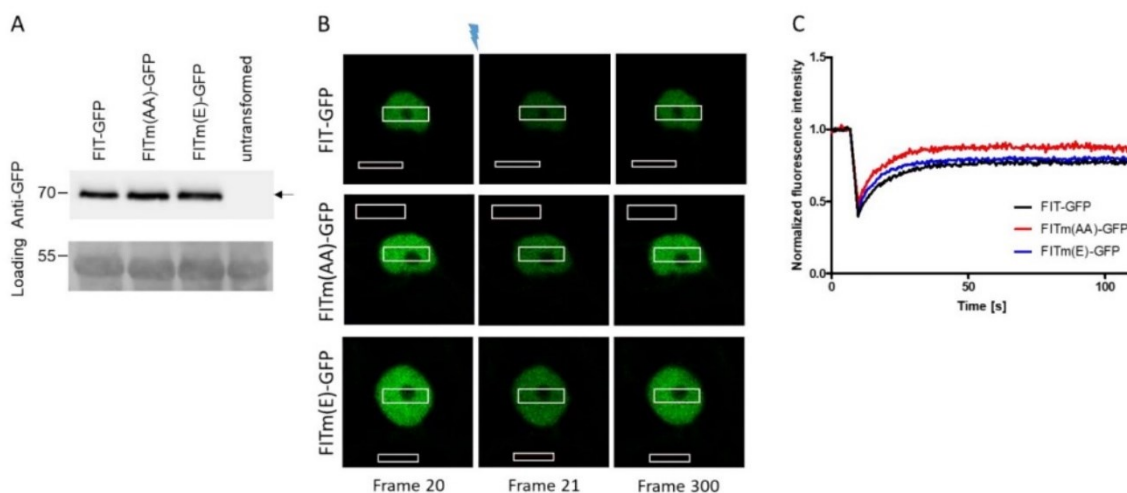


Figure S4. Control experiments for protein localization and FRAP experiments using FIT-GFP and FITm-GFP. Related to Figure 4.

(A) Immunodetection control of fluorescently tagged FIT-, FITm(AA)- and FIT(E)-GFP fusion proteins in tobacco leaf cells, used in [Figure 4A and 4B](#). Anti-GFP antibody was used for detection. Untransformed tobacco leaf extract was used as a negative control. PonceauS staining of the membrane was used as a loading control. An arrow indicates the protein bands corresponding to the respective full-length fusion protein. Protein molecular weight (in kDa) is indicated.

(B) Representative FIT- and FITm-GFP fluorescence images obtained in FRAP experiments. The GFP signal intensities are shown just before bleaching (marked by a lightning sign) (left vertical panels, frame 20), immediately after bleaching (middle vertical panels, frame 21) and at the end of the GFP acquisition time (right vertical panels, frame 300). White rectangular shapes indicate the measured regions of interest (ROIs), bleached inside the nucleus, outside the nucleus used for background fluorescence subtraction (see quantified data in [Figure 4B](#)).

(C) Background-corrected, normalized fluorescence intensities plotted as a function of time. One representative curve is shown for each FIT form. The pre-bleach fluorescence intensities are set to 100 %. During the bleaching of the nuclei, a strong decline of the fluorescence signals by more than 50 % is indicative of bleaching. GFP fluorescence signal recovery of the non-phosphorylatable FITm(AA)-GFP form (red) is accelerated in comparison to the recovery of non-mutagenized FIT-GFP (black) and phosphomimicking FITm(E)-GFP (blue) forms (see quantified data in [Figure 4B](#)).

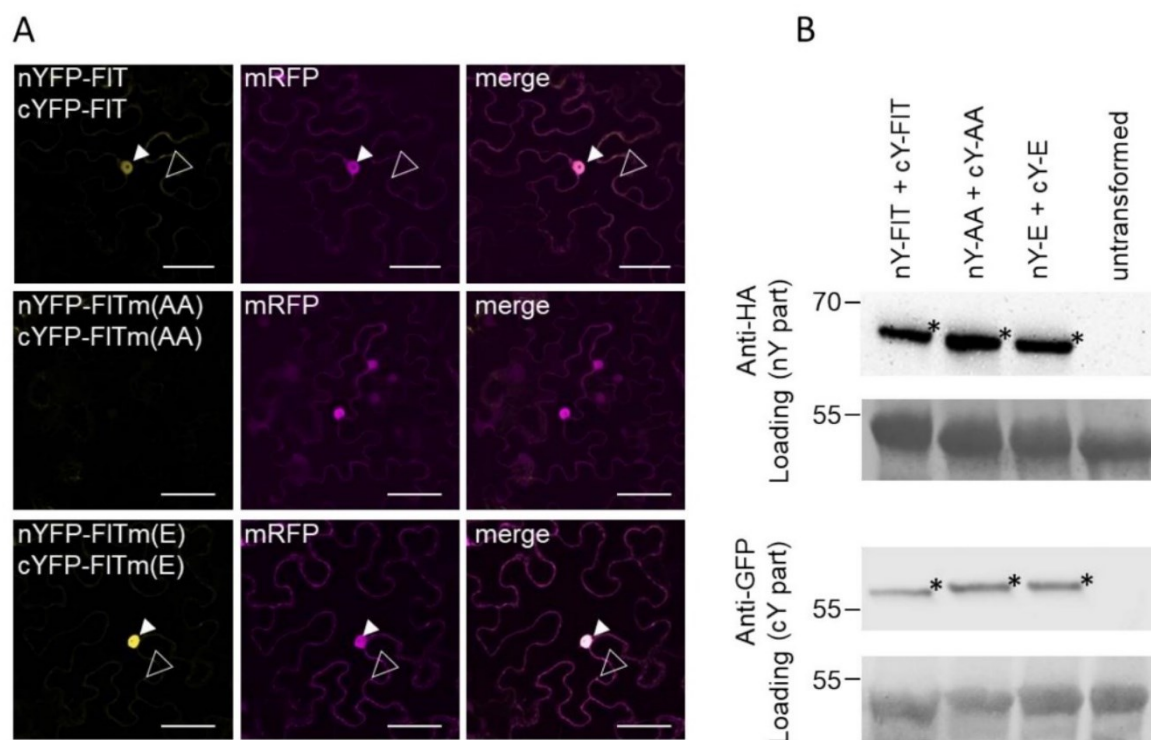


Figure S5. FIT and FITm homo-dimerization analysis *in planta*. Related to Figure 5.

(A) Laser-scanning confocal images showing Bimolecular Fluorescence Complementation (BiFC) of nYFP- and cYFP-tagged FIT and FITm homo-dimer couples in tobacco leaf epidermis cells. Successful homo-dimer formation (YFP signal) was detected for FIT (nYFP-FIT and cYFP-FIT, upper horizontal panels) and FITm(E) (nYFP-FITm(E) and cYFP-FITm(E), lower horizontal panels), whereas FITm(AA) (nYFP-FITm(AA) and cYFP-FITm(AA), middle horizontal panels) homo-dimerization was barely detectable. Reconstituted YFP signals are indicated by arrowheads (filled for nuclear YFP, empty for cytoplasmic YFP). Positive mRFP signal served as transformation control. Bars: 50 μ m. The immunodetection of split YFP proteins is shown in B.

(B) Immunodetection control of split YFP-tagged fusion proteins in tobacco leaf cells, used in BiFC experiments in (A). Anti-HA antibody detected nYFP- and anti-GFP antibody detected cYFP-tagged fusion proteins. Untransformed tobacco leaf extract was used as a negative control. PonceauS staining of the membrane was used as a loading control. Asterisks indicate the protein bands corresponding to the respective full-length fusion proteins. Protein molecular weight (in kDa) is indicated.

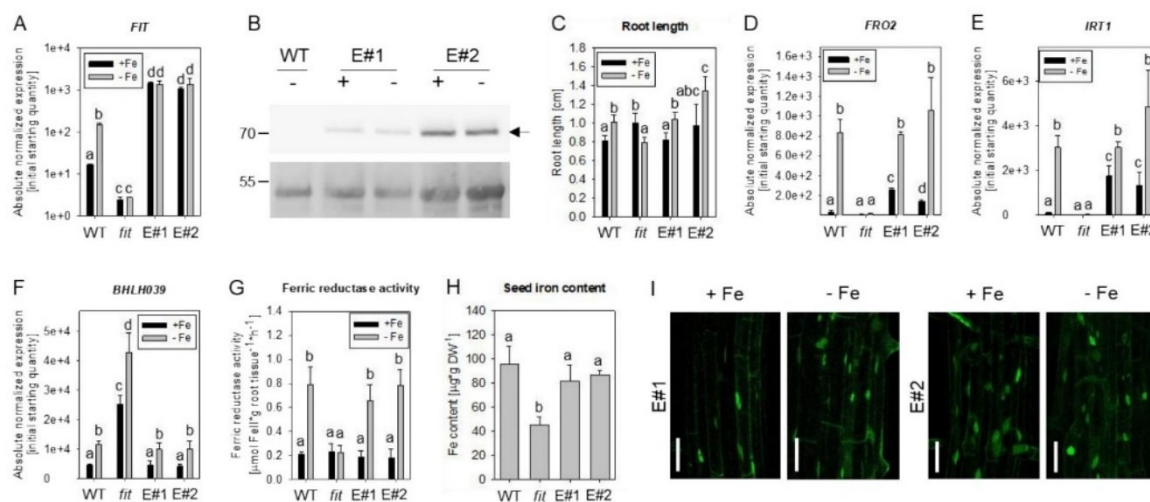


Figure S6. Phospho-mimicking FITm(E) at Ser272 complements the *fit* mutant. Related to Figure 6, S3 and S7.

fit mutant complementation assay with FITm(E)-GFP. Two FITm(E)-GFP/*fit* lines (E#1 and E#2) were analyzed in comparison with wild-type (WT) and *fit* mutant plants, grown in response to sufficient (+Fe, black bars) and deficient (-Fe, gray bars) Fe supply in the six-day A-C, I) and two-week growth assays (D-G).

(A) *FIT* gene expression analysis in roots, represented in base-10 logarithmic scale ($n = 3$).

(B) Immunodetection of full-length FITm(E)-GFP fusion protein (indicated by an arrow) with anti-GFP antibody in plants. WT plants served as negative control. PonceauS staining of the membrane was used as loading control. Protein molecular weight (in kDa) is indicated.

(C) Root lengths of plants ($n = 10$).

(D-F) Gene expression analysis in roots of *FRO2* (D), *IRT1* (E) and *BHLH039* (F) ($n = 3$).

(G) Root Fe reductase activity ($n = 4$).

(H) Fe contents per dry weight (DW) of seeds, collected from soil-grown plants ($n = 3$).

(I) Laser-scanning confocal images of FITm(E)-GFP in roots. Bars: 50 μm . See also Figure S7.

Data are represented as mean \pm SD. Different letters indicate statistically significant differences ($P < 0.05$).

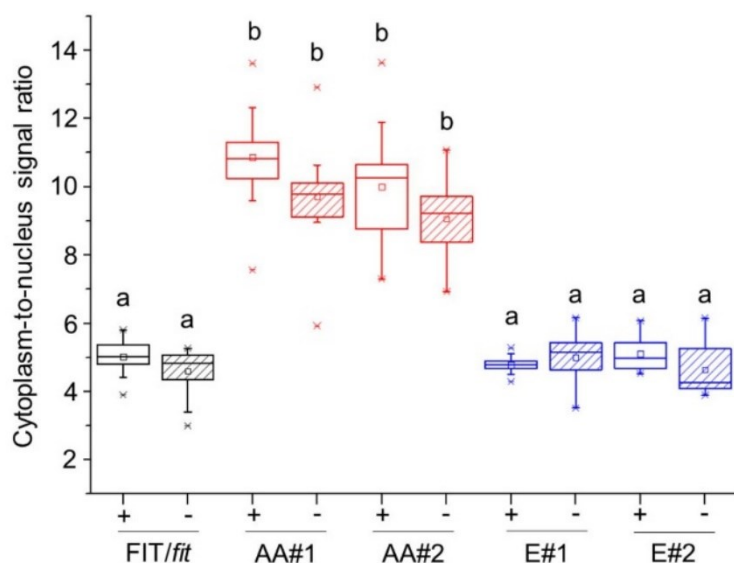


Figure S7. Nucleocytoplasmic partitioning of wild-type and phospho-mutant FITm(AA) and FITm(E) forms in Arabidopsis root epidermis cells. Related to Figure 6, Figure S3 and Figure S6.

Quantification of the cytoplasm-to-nucleus GFP signal ratios for FIT-GFP and FITm-GFP in Arabidopsis roots. FIT-GFP (black), FITm(AA)-GFP (red) and FITm(E)-GFP (blue) signals were recorded in root epidermis cells of the Arabidopsis lines FIT/*fit*, AA#1 and #2, E#1 and #2, grown in the 6-day system under sufficient (+Fe, open boxes) or deficient (-Fe, shaded boxes) Fe supply (n=3). Different letters indicate statistically significant differences ($P < 0.05$). Corresponding representative laser-scanning confocal imaging of the subcellular GFP fluorescence in Arabidopsis roots is shown for FIT-GFP in [Figure S3I](#), for FITm(AA)-GFP in [Figure 6I](#), for FITm(E) in [Figure S6I](#).

Table S1. Primers used in this study, related to STAR Methods.

Primer name	Primer sequence	Purpose	Origin
pCIPK11_forSpe	TTTACTAGTCAACGTGAAACTT TTGCTGATAAA	Cloning of ProCIPK11:GUS and pKS II Bluescript:ProCIPK11	This study
pCIPK11_reXho	TTTCTCGAGGATTGATGAATCC AGAGATTGATT	Cloning of ProCIPK11:GUS	This study
CIPK11 SpeI forward	TTTACTAGTATGCCAGAGATCG AGATTGC	Cloning of pGPTV-II- BAR-pUBQ10- GFP:CIPK11 and pIVEX- WG-StrepII:CIPK11	This study
CIPK11 XhoI reverse	TTTCTCGAGAATAGCCGCGTTT GTTGACG	Cloning of pGPTV-II- BAR-pUBQ10- GFP:CIPK11 and pIVEX- WG-StrepII:CIPK11	This study
FIT B1	GGGGACAAGTTTGTACAAAAA AGCAGGCTTAATGGAAGGAAG AGTCAACGC	Cloning of pDONR207:gFIT and pDONR221 P1-P4:cFIT	Le et al., 2016
FITns B2	GGGGACCACTTTGTACAAGAA AGCTGGGTTAGTAAATGACTT GATGAATTC	Cloning of pDONR207:gFIT	This study
CIPK11 B3	GGGGACAACCTTTGTATAATAA AGTTGTAATGCCAGAGATCGA GATTGC	Cloning of pDONR221 P3- P2:CIPK11	This study
CIPK11 B2	GGGGACCACTTTGTACAAGAA AGCTGGGTTTTAAATAGCCGC GTTTGTG	Cloning of pDONR221 P3- P2:CIPK11	This study
FITstop B4	GGGGACAACCTTTGTATAGAAA AGTTGGGTGTCAAGTAAATGA CTTGATGA	Cloning of pDONR221 P1- P4:cFIT	Le et al., 2016
39 B1	GGGGACAAGTTTGTACAAAAA AGCAGGCTTAATGTGTGCATTA GTACCTCC	Cloning of pDONR221 P1- P4:BHLH039	Le et al., 2016

39st B4	GGGGACAACCTTTGTATAGAAA AGTTGGGTGTCATATATATGAG TTTCCAC	Cloning of pDONR221 P1- P4:BHLH039	Le et al., 2016
CIPK15 B3	GGGGACAACCTTTGTATAATAA AGTTGTAATGGAGAAGAAAGG ATCTGT	Cloning of pDONR221 P3- P2:CIPK15	This study
CIPK15st B2	GGGGACCACTTTGTACAAGAA AGCTGGGTTTCAGTGCCAAGCT AATACAA	Cloning of pDONR221 P3- P2:CIPK15	This study
pCIPK11_reBam_2	TTTGGATCCGATTGATGAATCC AGAGATTGATT	Cloning of pKS II Bluescript:ProCIPK11	This study
CIPK11_for_Bam	TTTGGATCCATGCCAGAGATCG AGATTGC	Cloning of pKS II Bluescript:gCIPK11+3'UT R	This study
CIPK11UTRreXho	TTTCTCGAGGGAAAATCCAAA CTATAAATAGAAGA	Cloning of pKS II Bluescript:gCIPK11+3'UT R	This study
EFg1	TCCGAACAATACCAGAACTAC G	<i>EF1Balpha</i> (genomic) RT-PCR	Wang et al., 2007
EFg2	CCGGGACATATGGAGGTAAG	<i>EF1Balpha</i> (genomic) RT-PCR	Wang et al., 2007
EFc1	ACTTGTACCAGTTGGTTATGGG	<i>EF1Balpha</i> RTPCR	Wang et al., 2007
EFc2	CTGGATGTACTCGTTGTTAGGC	<i>EF1Balpha</i> RTPCR	Wang et al., 2007
FITrt1	GGAGAAGGTGTTGCTCCATC	<i>FIT</i> RT-PCR	Wang et al., 2007

FITrt2	TCCGGAGAAGGAGAGCTTAG	<i>FIT</i> RT-PCR	Wang et al., 2007
BHLH39rt1	GACGGTTTCTCGAAGCTTG	<i>BHLH039</i> RT-PCR	Wang et al., 2007
BHLH39rt2	GGTGGCTGCTAACGTAACAT	<i>BHLH039</i> RT-PCR	Wang et al., 2007
IRT1rt1	AAGCTTTGATCACGGTTGG	<i>IRT1</i> RT-PCR	Wang et al., 2007
IRT1rt2	TTAGGTCCCATGAACTCCG	<i>IRT1</i> RT-PCR	Wang et al., 2007
FRO2rt1	CTTGGTCATCTCCGTGAGC	<i>FRO2</i> RT-PCR	Wang et al., 2007
FRO2rt2	AAGATGTTGGAGATGGACGG	<i>FRO2</i> RT-PCR	Wang et al., 2007
C11 RT-F	GGATTTGTATTTTCGCGGTTG	<i>CIPK11</i> RT-PCR	This study
C11 RT-R	GTCAACAAACGCGGCTATTT	<i>CIPK11</i> RT-PCR	This study
FITmS272E-1	AACTCTAACCTAAGCGAACCTT CTCCGGACACA	Cloning of pDONR2017:gFITm(E)	This study
FITmS272E-2	TGTGTCCGGAGAAGGTTTCGCTT AGGTTAGAGTT	Cloning of pDONR2017:gFITm(E)	This study
FITmSS271AA-1	CAGAACTCTAACCTAGCCGCTC CTTCTCCGGACA	Cloning of pDONR207:gFITm(AA)	This study
FITmSS271AA-2	TGTCCGGAGAAGGAGCGGCTA GGTTAGAGTTCTG	Cloning of pDONR207:gFITm(AA)	This study
SpeI-noATG-FIT	TTTTACTAGTGAAGGAAGAGT CAACGCTCT	Cloning pET-24a(+):FIT/ FITm(AA)/FITm(E)	This study

FITstop-SacI	AAAAGAGCTCTCAAGTAAATG ACTTGATGA	Cloning pET-24a(+):FIT/ FITm(AA)/FITm(E) and pET-24a(+):FIT-C/ FITm-C(AA)/FITm-C(E)	This study
SpeI-FIT-C	TTTTACTAGTACTCAACCTTTT CGCGGTAT	Cloning pET-24a(+):FIT-C/ FITm-C(AA)/FITm-C(E)	This study
GST_XbaI.for	AAATCTAGAATGTCCCCTATAC TAGGTTATTG	Cloning pET-24a(+):GST	This study
GST_SpeI_Bam HI_ SalI.rev	TTTTGTCGACGGATCCACTAGT ATCCGATTTTGGAGG	Cloning pET-24a(+):GST	This study
FIT-C B1	GGGGACAAGTTTGTACAAAAA AGCAGGCTTAACTCAACCTTTT CGCGGTATC	Cloning pGBKT7-GW: and pACT2-GW:FIT-C/ FITm- C(AA)/FITm-C(E)	This study
FITst B2	GGGGACCACTTTGTACAAGAA AGCTGGGTTCAAGTAAATGAC TTGATGA	Cloning pGBKT7-GW: and pACT2-GW:FIT-C/ FITm- C(AA)/FITm-C(E)	This study

Author contributions to Paper IKsenia Trofimov

Performed and analyzed following experiments: confocal imaging of BiFC (Figure 1F, S5A), FRET-APB measurements (Figure 5B, 5D). Contributed to following experiments: confocal imaging (Figure 1D), cytoplasm-to-nucleus signal ratio quantification (Figure 4A). Contributed to the writing of the methods section.

Regina Gratz

Conceptualization of study. Designed, performed, and analyzed following experiments: yeast assays, cytoplasm-to-nucleus signal ratio quantification, FRAP, phospho-mutant line analysis, Phos-tag assay. Contributed to kinase assay. Contributed to the writing of the manuscript, prepared figures and reviewed/edited the manuscript.

Prabha Manishankar, Rumen Ivanov

Conceptualization of study. Designed, performed, and analyzed remaining experiments. Reviewed/edited the manuscript.

Inga Mohr

Designed, performed, and analyzed remaining experiments.

Tzvetina Brumbarova

Conceptualization of study. Designed, performed, and analyzed remaining experiments. Designed the outline of the manuscript, supervised the study. Wrote the manuscript, prepared final figures, and reviewed/edited the manuscript.

Michael Holtkamp, Uwe Karst

Performed total reflection X-Ray fluorescence experiments.

Philipp Köster, Leonie Steinhorst, Johannes Meiser, Maria Drerup, Sibylle Arendt

Contributed key material.

Hans-Jörg Mai

Performed 2D SDS-PAGE.

Jörg Kudla, Petra Bauer

Conceptualization of study. Designed the outline of the manuscript, supervised the study, provided funding, and reviewed/edited the manuscript.

7 Paper II

Phospho-mutant activity assays provide evidence for alternative phospho-regulation pathways of the transcription factor FER-LIKE IRON DEFICIENCY-INDUCED TRANSCRIPTION FACTOR

Phospho-mutant activity assays provide evidence for alternative phospho-regulation pathways of the transcription factor FER-LIKE IRON DEFICIENCY-INDUCED TRANSCRIPTION FACTOR

Regina Gratz¹ , Tzvetina Brumbarova^{1,2} , Rumen Ivanov^{1,2} , Ksenia Trofimov¹, Laura Tünnermann¹, Rocio Ochoa-Fernandez³, Tim Blomeier³, Johannes Meiser^{2,4} , Stefanie Weidtkamp-Peters⁵ , Matias D. Zurbriggen^{3,6}  and Petra Bauer^{1,2,6} 

¹Institute of Botany, Heinrich-Heine University, 40225, Düsseldorf, Germany; ²Department of Biosciences-Plant Biology, Saarland University, 66123, Saarbrücken, Germany; ³Institute of Synthetic Biology, Heinrich-Heine University, 40225, Düsseldorf, Germany; ⁴Department of Oncology, Luxembourg Institute of Health, 1445, Strassen, Luxembourg; ⁵Center for Advanced Imaging, Heinrich-Heine University, 40225, Düsseldorf, Germany; ⁶Cluster of Excellence on Plant Sciences, Heinrich-Heine University, 40225, Düsseldorf, Germany

Summary

Author for correspondence:

Petra Bauer

Tel: +49 211 8113479

Email: petra.bauer@hhu.de

Received: 20 May 2019

Accepted: 16 August 2019

New Phytologist (2020) **225**: 250–267

doi: 10.1111/nph.16168

Key words: *Arabidopsis*, bHLH039, FIT, iron uptake, *IRT1*, serine phosphorylation, transcription factor, tyrosine phosphorylation.

- The key basic helix–loop–helix (bHLH) transcription factor in iron (Fe) uptake, FER-LIKE IRON DEFICIENCY-INDUCED TRANSCRIPTION FACTOR (FIT), is controlled by multiple signaling pathways, important to adjust Fe acquisition to growth and environmental constraints. FIT protein exists in active and inactive protein pools, and phosphorylation of serine Ser272 in the C-terminus, a regulatory domain of FIT, provides a trigger for FIT activation.
- Here, we use phospho-mutant activity assays and study phospho-mimicking and phospho-dead mutations of three additional predicted phosphorylation sites, namely at Ser221 and at tyrosines Tyr238 and Tyr278, besides Ser 272.
- Phospho-mutations at these sites affect FIT activities in yeast, plant, and mammalian cells. The diverse array of cellular phenotypes is seen at the level of cellular localization, nuclear mobility, homodimerization, and dimerization with the FIT-activating partner bHLH039, promoter transactivation, and protein stability. Phospho-mimicking Tyr mutations of FIT disturb *fit* mutant plant complementation.
- Taken together, we provide evidence that FIT is activated through Ser and deactivated through Tyr site phosphorylation. We therefore propose that FIT activity is regulated by alternative phosphorylation pathways.

Introduction

Acquisition of trace elements such as iron (Fe) is indispensable for metabolic pathways, crop yield, and high-quality nutritious food. Biofortification offers the chance to reduce Fe-deficiency anemia in humans but relies on elaborate knowledge of nutrient sensing, uptake, and signaling (Connorton *et al.*, 2017). Most Fe is not soluble, and therefore not bioavailable in the soil. Plants must therefore mobilize Fe in the soil before they can take it up through their roots. For that, plants balance the need for Fe in their metabolism and the toxic effects that heavy metal ions can have in cells (Connorton *et al.*, 2017). *Arabidopsis thaliana* serves as model for uncovering regulatory events for Fe acquisition. As a representative of nongraminaceous angiosperm species, it uses the so-called Strategy I. Hallmarks of this strategy in *Arabidopsis* are reduction of ferric (Fe³⁺) to ferrous Fe (Fe²⁺) by FERRIC REDUCTION OXIDASE2 (FRO2) (Robinson *et al.*, 1999) and

uptake of Fe²⁺ ions by IRON-REGULATED TRANSPORTER1 (IRT1) (Eide *et al.*, 1996; Vert *et al.*, 2002). In contrast, Strategy II Fe acquisition is mediated by phytosiderophore-based Fe³⁺ chelation (Marschner *et al.*, 1986).

The expression of *FRO2*, *IRT1*, and more than 30 other Fe-deficiency-induced genes is controlled from early to late vegetative growth stages by the essential subgroup IIIa basic helix–loop–helix (bHLH) FER-LIKE IRON DEFICIENCY-INDUCED TRANSCRIPTION FACTOR (FIT; Heim *et al.*, 2003; Colangelo & Guerinot, 2004; Jakoby *et al.*, 2004; Yuan *et al.*, 2005; Mai *et al.*, 2016). *fit* mutant plants with complete FIT failure, homozygous for the *fit-3* loss-of-function allele, develop a strong Fe-deficiency leaf chlorosis, a phenotype caused by the inability to take up sufficient amounts of environmental Fe by roots (Jakoby *et al.*, 2004). This displays the pivotal role of FIT in the Fe-deficiency response, and particularly in upregulating Fe acquisition genes in roots.

FIT activity is mainly controlled at protein level through protein–protein interactions. Upon low Fe (–Fe), subgroup Ib bHLH proteins bHLH038/039/100/101 are induced and heterodimerize with FIT, which enhances *FIT* expression and FIT protein activity for inducing downstream FIT target gene expression (Wang *et al.*, 2007, 2013; Yuan *et al.*, 2008; Naranjo-Arcos *et al.*, 2017). Among subgroup Ib *BHLH* genes, *BHLH039* serves as a robust marker for Fe-deficiency responses (Ivanov *et al.*, 2012) and promotes Fe acquisition via FIT when overexpressed (Naranjo-Arcos *et al.*, 2017). Although the amount of FIT protein in a FIT overexpression situation can by far exceed that of FIT protein in wild-type (WT), FIT target gene induction remains comparable and restricted to –Fe (Jakoby *et al.*, 2004; Meiser *et al.*, 2011). FIT protein is thus present in a rather small active and in a large inactive pool. FIT is also controlled at the level of protein abundance and stability. FIT undergoes proteasomal degradation, and both FIT pools are targets of the proteasome (Lingam *et al.*, 2011; Meiser *et al.*, 2011). Despite that, FIT abundance is often lower at –Fe than at +Fe when overexpressed (Lingam *et al.*, 2011; Meiser *et al.*, 2011; Sivitz *et al.*, 2011). Presumably, in order to maintain Fe-deficiency responses, FIT must become activated and active FIT is being degraded to ‘refresh’ target sites, which could be beneficial for the cell to remain responsive to quick changes in nutrient abundance (Meiser *et al.*, 2011; Sivitz *et al.*, 2011). Posttranslational modification differentiates between active and inactive FIT. A small pool of FIT protein is phosphorylated, and calcium-sensing CBL-INTERACTING PROTEIN KINASE11 (CIPK11) targets position Ser272 of FIT and activates it. Ser272 is crucial for FIT to localize in the nucleus, interact with bHLH039, and activate FIT targets so that plants ultimately take up Fe and transport it to seeds (Gratz *et al.*, 2019). Interestingly, Ser272 is present in the C-terminal part of FIT, which can be regarded as a regulatory domain of FIT, FIT-C. A dynamic protein interaction network, particularly involving the FIT-C domain, enables the cell to quickly react to changes in Fe availability and adapt Fe uptake to environmental constraints by fine-tuning FIT protein activity beyond phosphorylation (Lingam *et al.*, 2011; Le *et al.*, 2016; Wild *et al.*, 2016; Cui *et al.*, 2018).

Phosphorylation events contribute to protein activation, and antagonistic mechanisms often ensure responsiveness to quickly changing conditions by a balanced protein activity. For example, cold-responsive bHLH protein INDUCER OF CBF EXPRESSION1 (ICE1; Chinnusamy *et al.*, 2003) is cold activated by phosphorylation of Ser278 through SnRK2.6/OPEN STOMATA 1 (OST1; Ding *et al.*, 2015). MITOGEN-ACTIVATED PROTEIN KINASES 3 and 6 (MAPK3 and -6) facilitate additional ICE1 phosphorylation with diametrically opposite effects on stability, causing proteasomal degradation of ICE1 (Li H. *et al.*, 2017; Zhao *et al.*, 2017).

Plant tyrosine (Tyr) phosphorylation is mainly associated with proteins having kinase or transferase activity (Sugiyama *et al.*, 2008). Only a few transcription factors were identified to be Tyr-phosphorylated until today. One of them, *Coptis japonica* WRKY-type transcription factor CjWRKY1 for alkaloid biosynthesis, displays enhanced cytosolic localization, reduced

transactivation activity, and a protein turnover phenotype of its Tyr phospho-mimicking mutant (Yamada & Sato, 2016).

In vivo studies of the mechanisms leading to FIT phosphorylation are very difficult. Owing to the low amounts of FIT protein *in planta* and the small fractions of phosphorylated forms thereof, individual phosphorylation sites of FIT cannot be identified directly (Gratz *et al.*, 2019). Proving phosphorylation by kinases requires prior knowledge of the concrete interacting protein kinase, but another kinase type besides a calcium-dependent CIPK is not known (Gratz *et al.*, 2019).

We therefore used an alternative approach and show here that a phospho-mutant activity screening approach can be successfully applied to overcome the obstacles described and to determine the functional importance of novel predicted phosphorylation sites in cellular biochemical activity assays. Synthetic biology plays a fundamental role in elucidating functional modules in mammalian and insect cell signaling. The circumstance that complex plant signaling modules with multiple endogenous connections between physiological, developmental, hormonal, and environmental pathways can be studied in experimental systems with reduced complexity is becoming increasingly recognized as an advantage to quantify properties of plant signaling modules (Samodelov & Zurbriggen, 2017). We demonstrate that phospho-mimicking and phospho-dead Ser and Tyr mutations affect diverse cellular FIT transcription factor activities in an opposite manner. We conclude that phosphorylation of Ser sites in FIT-C activates FIT, whereas that of Tyr sites deactivates FIT. These findings render future examination of Ser and Tyr modification of FIT possible to manipulate Fe acquisition regulation and to investigate novel Tyr phosphorylation control mechanisms in plants.

Materials and Methods

Multiple sequence alignment of FIT orthologues

Arabidopsis full-length FIT protein sequence was blasted against protein sequences of every order of the angiosperms and several families among Brassicales (Cole *et al.*, 2019). Hits with highest maximum score were re-blasted against the *Arabidopsis* TAIR10 protein sequence collection, using The Arabidopsis Information Resource BLAST v.2.2.8. (Phoenix Bioinformatics Corp., Fremont, CA, USA) FIT was aligned to the two other members of *A. thaliana* bHLH subgroup IIIa, AT2G16910 and AT4G21330, using the MUSCLE algorithm (Heim *et al.*, 2003; Edgar, 2004).

Site-directed mutagenesis and generation of plasmids for cellular assays

Plasmids with genomic DNA or complementary DNA (cDNA) sequences for intermediate cloning steps and experiments were generated by PCR, subsequent Gateway (Life Technologies), Gibson assembly cloning (New England Biolabs, Ipswich, MA, USA), or AQUA cloning (Beyer *et al.*, 2015) and verified by sequencing (see list of recombinant plasmids used/constructed in Supporting Information Table S1; primers for plasmid generation are in Table S2). Site-directed mutagenesis was conducted by

PCR with genomic FIT to create phospho-mutant *gFITm* forms, namely FITm(S221A), FITm(S221E), FITm(S221E/SS271/272AA), FITm(Y238F), FITm(Y238E), FITm(Y278F), and FITm(Y278E), as described previously (Gratz *et al.*, 2019) for FITm(SS271/272AA). Briefly, methylated template plasmid DNA was eliminated by *DpnI* treatment before DH5 α *Escherichia coli* transformation. *FIT* and *FITm* coding sequences without introns were obtained from cDNA prepared from transiently transformed *Nicotiana benthamiana* leaves with expression plasmids containing *gFIT-GFP* and *gFITm-GFP* forms (GFP, green fluorescent protein).

Transient expression in tobacco leaf epidermis cells

Tobacco (*N. benthamiana*) leaf epidermal cells were transiently transformed by infiltration with *Agrobacterium* (*Rhizobium radiobacter*) GV3101 (pMP90) strain containing the respective plant expression vectors, as described (Gratz *et al.*, 2019).

Subcellular localization of GFP fusion proteins

The cytoplasm-to-nucleus ratio for FIT-GFP and FITm-GFP was determined 48 h after tobacco leaf infiltration with agrobacteria containing pMDC83:gFITns-GFP or pMDC83:gFITmns-GFP forms (Table S1), as described previously (Gratz *et al.*, 2019). Briefly, Z-stack images taken with an LSM780 laser-scanning confocal microscope (Zeiss) were exported to .tiff and converted to grayscale format. The cytoplasm-to-nucleus ratio was calculated by accessing the fluorescence signal intensity once for the nucleus, and once for the cell while excluding the nucleus, with IMAGEJ software (US National Institutes of Health, Bethesda, MD, USA). For each independent experiment, several cells from one or two leaves of a transiently transformed tobacco plant were imaged and the fluorescence ratios quantified ($n = 6-11$ cells). Three experiments using independently transformed plants were performed.

Nuclear mobility of GFP fusion proteins

Fluorescence recovery after photobleaching (FRAP) experiments were conducted 48 h after tobacco leaf infiltration with agrobacteria containing pMDC83:gFITns-GFP or pMDC83:gFITmns-GFP forms, as described (Gratz *et al.*, 2019). In brief, using an LSM780 laser-scanning confocal microscope (Zeiss), a rectangular region of interest in the nucleus of a tobacco cell was chosen to determine initial GFP signal intensity and intensity after bleaching to monitor fluorescence recovery. Background fluorescence was subtracted from FRAP values, which were normalized to the mean of pre-bleach values. Nonlinear curve fitting was performed (PRISM; GraphPad Software, San Diego, CA, USA) in order to assess the fluorescence intensities (Fig. S1). Using the initial fluorescence intensity F_{pre} and the fluorescence intensity after photobleaching F_{post} the percentages of mobile fractions M_f of FIT-GFP and FITm-GFP forms were calculated: $M_f = [(F_{end} - F_{post}) / (F_{pre} - F_{post})] \times 100$ (Bancaud *et al.*, 2010). For each construct, several nuclei were analyzed from two leaves of transiently transformed plants ($n = 10-17$ nuclei).

Homo- and heterodimerization using targeted yeast two-hybrid assays

Yeast strain AH109 was co-transformed with respective plasmids, pGBKT7-GW:FIT-C, pGBKT7-GW:FIT-Cm forms or pGBKT7-GW:bHLH039 with N-terminal fusion of GAL4 DNA binding domain (BD-FIT or BD-FITm forms), and pACT2-GW:FIT-C, pACT2-GW:FIT-Cm forms or pACT2-GW:bHLH039 with N-terminal fusion of GAL4 activation domain (AD-FIT, AD-FITm forms, AD-bHLH039) (Table S1). Positive transformants were selected on synthetic defined (SD) medium lacking Leu and Trp (SD-LW) and verified by colony-PCR. To obtain appropriate negative controls, cells were co-transformed with respective empty AD or BD plasmid controls. The combination of pGBT9.BS:CIPK23 and pGAD.GH:cAKT1 served as a positive control (Xu *et al.*, 2006; Le *et al.*, 2016). The screening for positive protein-protein interactions was performed on SD medium lacking Leu, Trp and His (SD-LWH) in the presence of 0.5 mM 3-amino-1,2,4-triazole (3-AT), selective for interaction, in comparison with co-transformation controls on SD-LW medium, after spotting serial dilutions, as previously described and indicated in the text (Le *et al.*, 2016). Plates were photographed after incubation at 30°C for 1 wk (heterodimerization) or 2 wk (homodimerization).

Homo- and heterodimerization assay by Förster resonance energy transfer-acceptor photobleaching *in planta*

Förster resonance energy transfer-acceptor photobleaching (FRET-APB) experiments were conducted 48 h after tobacco leaf infiltration with agrobacteria containing pABindGFP, pABindmCherry, and pABindFRET vectors recombinant for FIT, FITm forms, and BHLH039 to measure the homo- (FIT-GFP + FIT-mCherry or FITm-GFP + FITm-mCherry) or the heterodimerization (bHLH039-GFP + FIT-mCherry or bHLH039-GFP and FITm-mCherry) efficiency (Table S1). Donor proteins were additionally transformed single-tagged with GFP and double-tagged with GFP-mCherry to serve as a negative and positive control. Gene expression was induced by spraying the leaves with a 20 μ M β -estradiol solution 16 h before FRET-APB measurements.

Measurements were operated with ZEN2 black edition software (Zeiss) at the confocal laser-scanning-microscope LSM780 (Zeiss). Fluorescence intensity for both fluorophores was detected within 20 frames in a 128 \times 128 pixel format and a pixel time of 2.55 μ s. After the fifth frame, 100% laser power (561 nm) was used to bleach mCherry using 80 iterations. FRET efficiency was calculated in percent as relative increase of GFP intensity after acceptor photobleaching. At least two independent experiments with 10 measured nuclei each were performed ($n = 10$ nuclei).

FIT transcriptional self-activation assay in yeast

Yeast strain AH109 was co-transformed with either pGBKT7-GW:FIT (BD-FIT) or pGBKT7-GW:FITm (BD-FITm) forms, as well as pACT2-GW (empty AD) (Table S1), selected on SD-

LW media and verified by colony-PCR. The screening for autoactivation was performed by assaying the growth on SD-LWH media, containing either 0.5 or 90 mM 3-AT in 10-fold dilution series compared with SD-LW co-transformation controls. pGBT9.BS:CIPK23 and pGAD.GH:cAKT1 were used as a positive control (Xu *et al.*, 2006; Le *et al.*, 2016). Growth of colonies was recorded after incubation at 30°C for 1 wk.

Quantitative transactivation reporter gene assay for FIT in mammalian cells

The mammalian cell transactivation assay was conducted according to Muller *et al.* (2014). Briefly, Chinese hamster ovary (CHO) cells were seeded to a density of 40 000 cells per well in 500 µl of medium in 24-well plates and transfected with a solution of 100 µl per well, containing pMZ333:FIT or pMZ333:FITm, pKM195:IRT1pro, and pMZ333:bHLH039, as indicated. 1 µg of plasmids in total was mixed, if necessary by adding stuffer plasmid pHB007:BFP (Table S1). The mix was exchanged 4 h after transfection and the supernatant collected 48 h after transfection for analysis of recombinant secreted alkaline phosphatase (SEAP) activity using a colorimetric assay and *Gaussia* luciferase activity as described (Schlatter *et al.*, 2002; Remy & Michnick, 2006; Muller *et al.*, 2014).

For immunoblot analysis, CHO cells were transfected with the same plasmid combinations, but replacing the aforementioned pMZ333 plasmids with the respective tagged pMZ333:FIT-GFP, pMZ333:FITm-GFP forms and pMZ333:HA₃-bHLH039 (Table S1). Protein extraction was performed according to Silva *et al.* (2018). Sample separation on sodium dodecyl sulfate (SDS) polyacrylamide gel electrophoresis (PAGE), immunodetection, and chemiluminescence signal recording were performed as previously described (Gratz *et al.*, 2019), using mouse anti-GFP (catalog no. 11814460001, 1 : 1000; Roche) followed by goat anti-mouse immunoglobulin G horseradish peroxidase conjugate (catalog no. W4021, 1 : 5000; Promega) or anti-HA-peroxidase high-affinity monoclonal rat antibody (3F10, catalog no. 12013819001, 1 : 1000; Roche) for immunodetection.

Quantitative cell-free degradation assay

pMDC83:gFIT-GFP and mutant pMDC83:gFITm-GFP forms (Table S1) were transiently expressed in tobacco leaf epidermal cells. At 48 h post-infiltration, leaves were ground in liquid nitrogen, weighed, and combined with ×2 Protein Loading Buffer in a 1.5 ml reaction tube (124 mM Tris-Cl pH 6.8, 5% SDS, 4% dithiothreitol, 20% glycerol, 0.002% bromophenol blue), incubated on a rotating wheel for 10 min at room temperature, and subsequently pelleted by centrifugation at full speed (21 000 g) and 4°C. Then, 25 µl supernatant was aliquoted in four individual reaction tubes and incubated for 0, 60, 120 or 240 min at 25°C. Samples were then processed for SDS-PAGE and immunoblot analysis as already described. Three individual tobacco transformations and degradation assays were performed. For proteasomal arrest, 100 µM MG132 (AbMole BioScience, Houston, TX, USA), prepared from a 100 mM stock dissolved in

dimethyl sulfoxide (DMSO), was added to the protein extract before incubation at 25°C; DMSO alone was used as a control.

Quantification of the chemiluminescence signal was performed with the 'Band Analysis' module of the ALPHAVIEW software (Cell Biosciences, Santa Clara, CA, USA), according to manufacturer's instructions for background-corrected signal average. The signal value obtained from the first sample (0 min incubation at 25°C) was set to 100% and used to calculate the signal intensities of the remaining samples (60, 120 and 240 min). Means (± SD) of the values obtained were displayed as fitted curves using nonlinear regression (GraphPad PRISM). Individual curve fitting of single replicates was used to calculate half-life times.

Arabidopsis fit complementation assay

Arabidopsis thaliana fit-3 (fit) mutant and complemented pMDC83:gFIT-GFP-transformed pro35S::gFIT-GFP/*fit-3* (FIT-GFP/*fit*) plants are described (Jakoby *et al.*, 2004; Gratz *et al.*, 2019). *Arabidopsis fit* mutant plants were transformed with Tyr phospho-mimicking pMDC83:gFITm(Y238E)-GFP and pMDC83:gFITm(Y278E)-GFP, resulting in the lines pro35S::gFITm(Y238E)-GFP/*fit-3* (FITm(Y238E)-GFP/*fit*) and pro35S::gFITm(Y278E)-GFP/*fit-3* (FITm(Y278E)-GFP/*fit*) by floral dip (Clough & Bent, 1998). Lines were multiplied by selfing until homozygous lines were obtained for analysis. Positive transformants and lines were selected based on hygromycin resistance, GFP fluorescence, immunoblot analysis and PCR genotyping.

For plant experiments, *Arabidopsis* seeds were sterilized and seedlings grown on upright sterile plates containing modified half-strength Hoagland medium for 14 d. Then, plants were transferred for 3 d to new Hoagland plates with sufficient (50 µM FeNaEDTA, +Fe) or deficient (0 µM FeNaEDTA, -Fe) Fe supply, as described previously (Gratz *et al.*, 2019). Roots were harvested.

Immunoblot analysis of FIT-GFP/FITm-GFP was conducted as described earlier. Gene expression analysis was performed by reverse transcription quantitative PCR using the procedures and primers as described (Ben Abdallah & Bauer, 2016; Gratz *et al.*, 2019). Briefly, analysis was performed with SYBR Green detection. Absolute gene expression was determined by mass standard curve analysis and normalized to reference gene *EF1B* expression. The assay was performed in three biological replicates ($n = 3$), each with two technical replicates.

Statistical analysis

Statistical analysis was performed using a two-tailed, unpaired Student's *t*-test ($P < 0.05$) when comparing an individual phospho-mutant with WT. When comparing WT and phospho-mutants among themselves, *P*-values were obtained using one-way ANOVA, followed by a Tukey's post-hoc test performed with OriginLab (Northampton, MA, USA). Different letters indicate statistically significant values ($P < 0.05$).

For box plot representation, outlier identification was based on the calculation of the interquartile range and determination of the inner and outer fences within a data set. A value

that was located above the outer fence or below the inner fence was excluded from the analysis (Jacobs & Dinman, 2004). Outlier calculations were applied to the subcellular localization, nuclear mobility, FRET-based protein–protein interaction, and to the FIT transactivation reporter gene assay dataset.

Results

Three-step analysis of FIT protein sequence predicts novel phosphorylation target sites

Several bHLH transcription factors, including SPEECHLESS, are phosphorylated at multiple sites (Lampard *et al.*, 2008; Gudesblat *et al.*, 2012; Yang *et al.*, 2015). Phosphorylatable amino acid residues usually occur as part of phosphorylation motifs and are often conserved in the protein amino acid sequence. This concept was applied to predict FIT phosphorylation sites.

In a first step, NETPHOS 2.0 (Blom *et al.*, 1999) *in silico* phospho-site prediction in the FIT sequence resulted in a total of 21 amino acid hits, of which six residues were located in the C-terminal part of FIT following the bHLH domain (FIT-C; Fig. 1a). These six residues were of high interest, as several FIT protein–protein interactions are facilitated via FIT-C, which we therefore consider to be a regulatory domain of FIT (Lingam *et al.*, 2011; Le *et al.*, 2016; Gratz *et al.*, 2019).

The number of potential phosphorylation sites was narrowed down by evolutionary conservation using a multiple sequence alignment between full-length *Arabidopsis* FIT and respective FIT orthologues from angiosperms (Fig. 1b). Out of the six putative phosphorylation sites in FIT-C, Ser256 is conserved exclusively in the order of the Brassicales, representing the least conserved position among the candidates. Ser221 is conserved within the family of Brassicaceae, as well as in species belonging to the commelinids and fabids. The two serines Ser271 and Ser272, previously characterized by us as FIT phosphorylation targets (Gratz *et al.*, 2019), are conserved among the Brassicaceae. Interestingly, however, only one of the two Sers is conserved among members of the monocots, superasterids, and the remaining superrosids. Furthermore, two Tyrs are highly conserved throughout the angiosperms. FIT orthologues, ranging from the most distant order of Amborellales to the order of Apiales, possess a Tyr that aligns to Tyr238. Tyr278 was found to be conserved among the order of Brassicales as well as among the commelinids and the lamiids.

We included a full-length sequence alignment between FIT and two *A. thaliana* bHLH proteins, ABORTED MICROSPORES (AT2G16910) and DYSFUNCTIONAL TAPETUM (AT4G21330), which together with FIT belong to the subgroup IIIa bHLH proteins (Heim *et al.*, 2003; Fig. 1c). Both proteins do not show substantial sequence similarity with FIT in their C-termini. Also, neither of these two bHLH proteins contains conserved residues that align with predicted FIT phosphorylation target sites. This suggests a specific function for the predicted sites in the FIT protein.

Finally, we identified phosphorylation motifs for four out of the six predicted phosphorylation target sites (Fig. 1d). The motif [pS/pT]X[R/K] (Pearson & Kemp, 1991) encompasses Ser221, which strengthens the assumption of Ser phosphorylation at this position. The additional phosphorylation motifs XXpSPX (Kemp & Pearson, 1990; Beausoleil *et al.*, 2004; Luo *et al.*, 2005; Schwartz & Gygi, 2005) and SXXXpS (Fiol *et al.*, 1990) were found to enclose Ser271 and Ser272. This suggests that only one of the two neighboring Sers undergoes phosphorylation, to which we refer here as Ser272, which is concordant with our previous results (Gratz *et al.*, 2019). The highly conserved Tyr238 is part of the motif pYXX[L/I/V] (Argetsinger *et al.*, 2004). Another phosphorylation motif, SX[D/E]XpY, was assigned to Tyr278 (Amanchy *et al.*, 2011), which reinforces the hypothesis of Tyr phosphorylation for both residues.

In summary, the three-step *in silico* prediction, multiple-sequence alignment, and phosphorylation motif identification permitted us to identify four most promising phosphorylation target sites in FIT-C, namely Ser221, Tyr238, Tyr278, and the previously characterized Ser272 (Gratz *et al.*, 2019).

To conduct a functional FIT phospho-mutant activity screening, we generated phospho-dead FITm mutations with Ser to Ala and Tyr to Phe substitutions and phospho-mimicking FITm mutations with Ser or Tyr to Glu substitutions (Fig. 1d). With such a mutational approach, we recently showed relevance of Ser272 for FIT activity (Gratz *et al.*, 2019). In the course of our work presented here, FITm(S221E) turned out to be more active than WT FIT, whereas FITm(S221A) behaved rather neutrally. Ser221 and Ser272 might be both used for phosphorylation. To investigate the effect of FITm(S221E) alone, we therefore included additionally the triple phospho-mutant FITm(S221E/SS271/2AA) and compared it with single-mutant FITm(S221E) and as a control to the previously characterized FITm(SS271/2AA) – also known as FITm(AA) in Gratz *et al.* (2019). These eight phospho-mutants were tested for their effects on several FIT regulatory properties and cellular activities.

Cellular localization and nuclear mobility depend on FIT phospho-mutant forms

Posttranslational phosphorylation affects protein properties, including subcellular localization (Ju *et al.*, 2012; Ren *et al.*, 2017; Takeo & Ito, 2017), and this is also the case for FIT (Gratz *et al.*, 2019). The cytoplasm-to-nucleus ratio of FIT localization is in the range of 3–5 (Fig. 2). Out of the eight mutants tested, six FIT phospho-mutants showed a significant increase of the cytoplasm-to-nucleus ratio. FITm(SS271/2AA) resulted in a significant increase, as expected (Gratz *et al.*, 2019), whereas FITm(S221E) and FITm(S221E/SS271/2AA) cytoplasm-to-nucleus ratios increased greatly, by 180% and 300%, respectively (Fig. 2a,c). FITm(Y238F), FITm(Y278F), and FITm(Y278E) showed significantly increased ratios, by 150% to 350% compared with WT (Fig. 2b,c). There was no significant increase observed for FITm(S221A) and FITm(Y238E). Thus, depending on the phospho-mutation, FIT protein is retained in the cytoplasm.

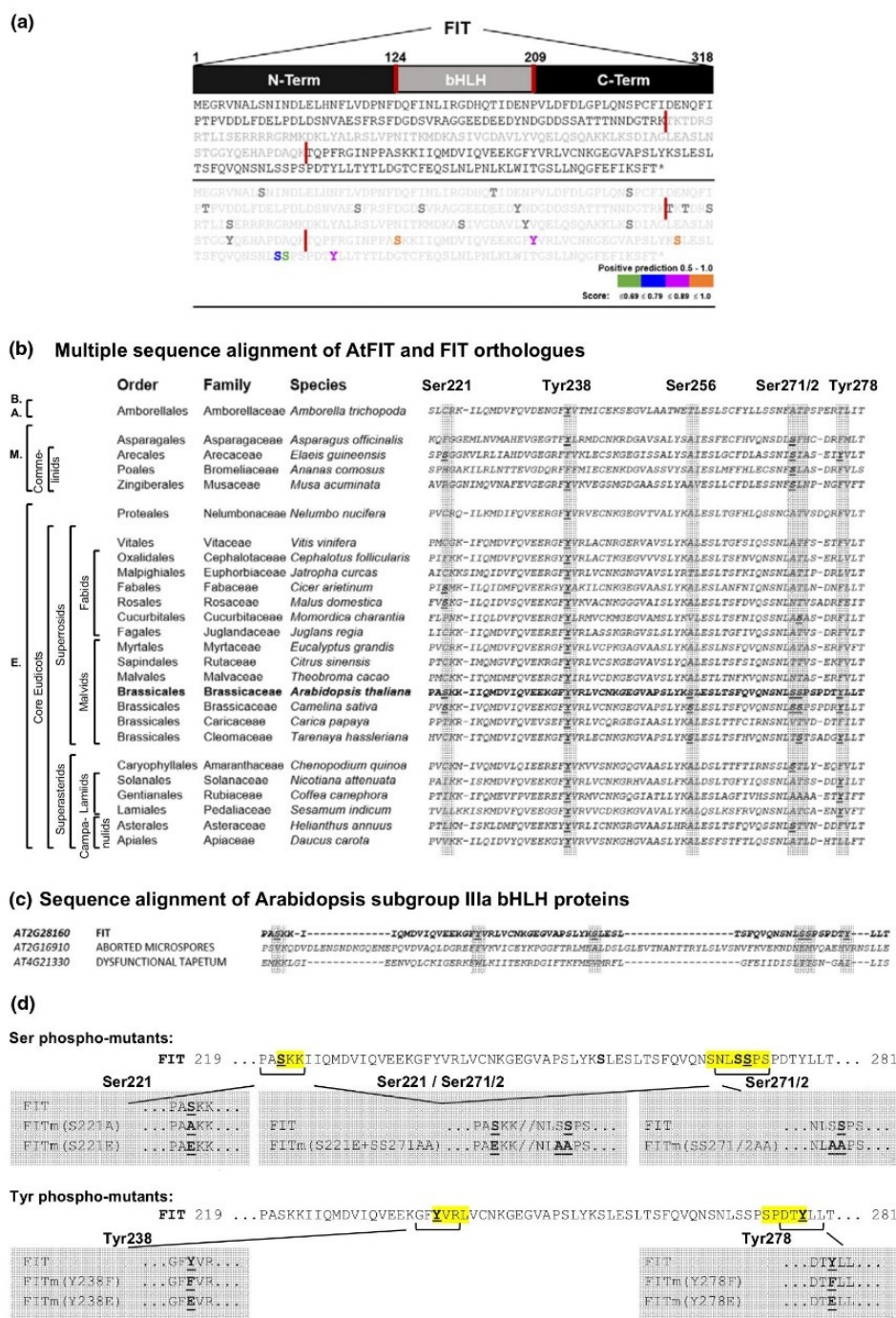


Fig. 1 Analysis of FER-LIKE IRON DEFICIENCY-INDUCED TRANSCRIPTION FACTOR (FIT) protein sequence reveals novel putative phosphorylation target sites in FIT-C. (a) Phosphorylation site prediction of FIT. Full-length amino acid sequence of FIT (top), composed of an amino-terminal (N-term), basic helix–loop–helix (bHLH; gray), and carboxyl-terminal (C-term) region, also known as FIT-C, divided by red bars. *In silico* prediction by NetPhos2.0 identified potential phosphorylation sites (bottom, bold), of which six are located in FIT-C (bold, colored). Colors reflect the confidence score of the prediction. (b) Multiple sequence alignment, showing the FIT-C region with putative phosphorylation sites, compared with orthologues in angiosperms. AtFIT is presented in bold, conserved putative phosphorylation sites are bold and underlined, and these sites are highlighted for comparison in gray. B.A., basal angiosperms, M., monocots, E., eudicots. (c) Sequence alignment of subgroup IIIa bHLH proteins, showing the FIT-C region with putative phosphorylation sites. AtFIT full-length protein sequence was aligned with bHLH proteins AT2G16910 and AT4G21330 (subgroup IIIa). FIT target sites are not conserved between the bHLH proteins. (d) Identification of phosphorylation motifs and phospho-mutants of FIT-C. Predicted phosphorylated amino acids are presented in bold, underlined; known phosphorylation motifs are highlighted in yellow. FIT target site phospho-mutants are shown in gray boxes, with phospho-dead (serine to alanine/S to A, tyrosine to phenylalanine/Y to F) and phospho-mimicking (S, Y to glutamate/S, Y to E) FIT forms.

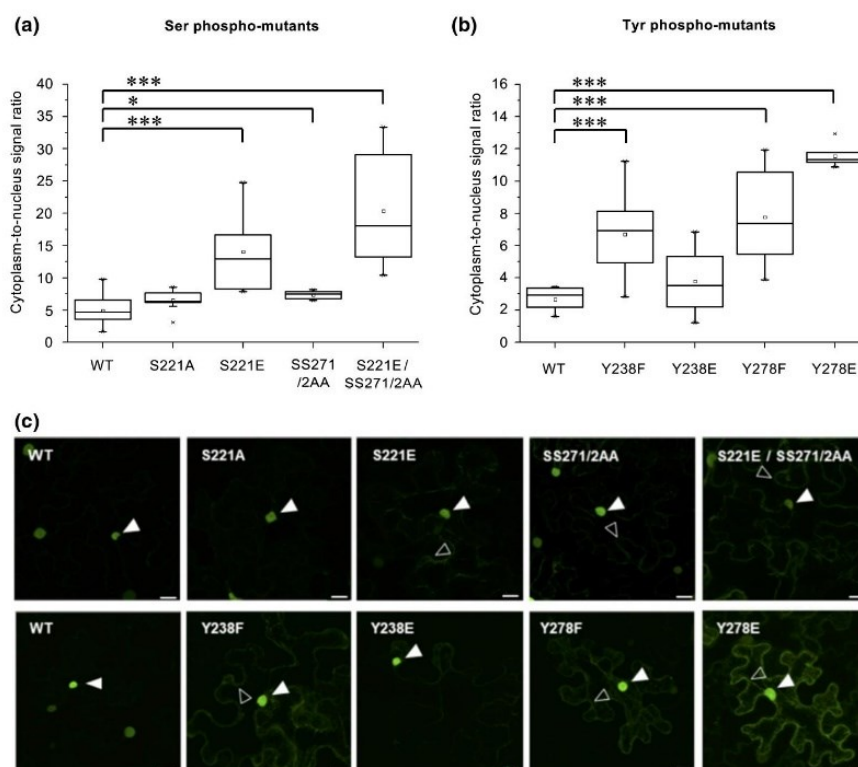


Fig. 2 FER-LIKE IRON DEFICIENCY-INDUCED TRANSCRIPTION FACTOR (FIT) subcellular compartmentalization is altered in FITm phospho-mutants. (a, b) Quantification of cytoplasmic to nuclear fluorescence ratio of FIT-green fluorescent protein (GFP) in comparison with (a) serine (Ser) and (b) tyrosine (Tyr) FITm forms. The subcellular localization was analyzed following transient expression in tobacco leaf epidermis cells by laser-scanning confocal microscopy. Data are presented in box plots; interquartile range (IQR) 25th–75%; whiskers: 25th percentile, $-1.5 \times$ IQR; 75th percentile, $+1.5 \times$ IQR; median, horizontal line within IQR box; mean, small square in IQR box; x, values outside $\pm 1.5 \times$ IQR range. Asterisks indicate statistical significance between WT and individual mutants, determined by Student's *t*-test ($n = 6-11$; *, $P < 0.05$; ***, $P < 0.001$). (c) Representative confocal images of leaf epidermis cells, expressing FIT-GFP and FITm-GFP. Empty arrowheads indicate significantly enhanced cytoplasmic GFP signal accumulation of FITm-GFP compared with FIT-GFP. Filled arrowheads highlight nuclear signals. Bar, 20 μm.

Nuclear architecture is complex, and the motion of molecules in the nucleus could be coupled to their activity status (Reits & Neefjes, 2001). In FRAP experiments, the mobile fraction of nonmutagenized FIT within the nucleus represented roughly 70% (Fig. 3; see also Gratz *et al.*, 2019, Fig. 4B). This mobile fraction was significantly increased by 10–20% in FITm(SS271/2AA), as reported (Gratz *et al.*, 2019, Fig. 4B) and FITm(S221E/SS271/2AA) (Fig. 3a), whereas it was significantly decreased in FITm(Y238E) by 10%, compared with the control (Fig. 3b; see also the kinetic plots in Fig. S1).

In summary, subcellular localization and nuclear mobility of FIT are affected in FIT phospho-mutants.

FIT phospho-mutants display altered dimerization capacity

FIT forms nuclear homodimers and heterodimers with bHLH039, depending on Ser272 phosphorylation (Gratz *et al.*, 2019). Functional relevance of FIT homodimerization is unclear. Yet, heterodimerization with subgroup Ib bHLH proteins is an activating mechanism stimulating FIT downstream responses (Yuan *et al.*, 2008; Wang *et al.*, 2013). Because of its robustness and our previous work, we focus on bHLH039 as representative

for a subgroup Ib bHLH protein (Naranjo-Arcos *et al.*, 2017; Gratz *et al.*, 2019). These protein interactions are detectable for WT FIT-C in semi-quantitative targeted yeast two-hybrid assays (Figs 4a, 5a; controls in Figs S2, S3; note that, in the yeast assays, use of full-length FIT-BD is excluded because of autoactivation, as explained by Gratz *et al.* (2019)). Protein interactions of full-length WT FIT are shown in plant cell quantitative FRET-APB experiments (FRET efficiency of 8% for FRET pair WT-G + WT-C, corresponding to FIT-GFP/FIT-mCherry, in Fig. 4b,c, and of *c.* 15% for FRET pair bHLH039-G + WT-C, corresponding to bHLH039-GFP/FIT-mCherry, in Fig. 5b,c).

Less homodimerization was found for FITm-C/FITm with S221E, SS271/2AA, and combined S221E/SS271/2AA mutations and there was no significant difference with S221A mutation relative to controls in both assays (Fig. 4a,b). A slight reduction in dimerization capacity was found for FITm-C/FITm with Y238F and a stronger reduction with Y238E and Y278F mutations (Fig. 4a,c). Only Y278E showed opposing effects in both systems, as homodimerization was inhibited in yeast, but FRET efficiency increased vs the nonmutagenized forms.

In FIT-bHLH039 heterodimerization experiments, phospho-mutant interactions were either not affected in either of the two

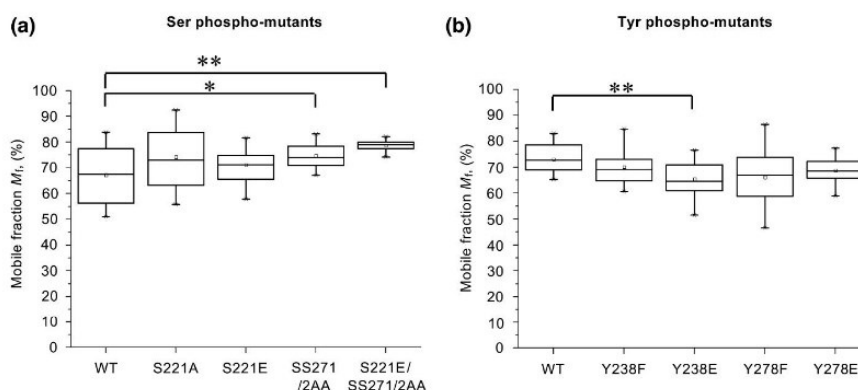


Fig. 3 FER-LIKE IRON DEFICIENCY-INDUCED TRANSCRIPTION FACTOR (FIT) phospho-mutants display altered nuclear mobility. Quantification of the mobile nuclear fraction M_f of FIT-green fluorescent protein (GFP) in comparison with (a), serine (Ser) FITm and (b), tyrosine (Tyr) FITm phospho-mutants. Nuclear mobility was quantified following leaf infiltration in tobacco by fluorescence recovery after photobleaching. Data are represented in box plots; interquartile range (IQR) 25–75%; whiskers: 25th percentile, $-1.5 \times$ IQR; 75th percentile, $+1.5 \times$ IQR; median, horizontal line within IQR box; mean, small square in IQR box; x, values outside $\pm 1.5 \times$ IQR range. Statistical significance between FIT-GFP and FITm-GFP forms was calculated with Student's *t*-test and is denoted by asterisks ($n = 10$ –17; *, $P < 0.05$; **, $P < 0.01$). The data for FIT-GFP (wild-type, WT) and FITm(SS271/2AA) were reported in Gratz *et al.* (2019). Kinetic plots are shown in Supporting Information Fig. S1.

systems or reduced in only one assay: SS271/2AA and Y238E in FRET-APB vs Y278F in yeast. Y278E was the only mutation causing reduced heterodimerization in both assays (Fig. 5a,c).

Taken together, with two independent approaches, FIT homodimerization was found significantly affected in seven out of eight phospho-mutants. FIT heterodimerization was changed in three out of eight phospho-mutants. The previous FITm (SS271/2AA) data (Gratz *et al.*, 2019) were confirmed. Thus, the ability of FIT to interact with itself or bHLH039 depends on the phosphorylation status.

Phospho-mutants affect FIT transactivation ability

Promoter activation is a crucial FIT function. Intriguingly, full-length FIT and FITm had varying abilities to autoactivate the reporter in the targeted yeast two hybrid assay. Nonmutagenized FIT and several mutants self-activated the system even in the presence of 90 mM 3-AT. However, FITm(SS271/2AA), FITm(S221E/SS271/2AA) and FITm(Y278E) showed reduced autoactivation (Fig. S4). Altered FIT autoactivation might have been a consequence of the phosphorylation status.

Synthetic cellular systems are becoming increasingly popular to study gene regulatory modules and the impact of functional variants in the absence of interfering secondary effectors present in plant cells (Samodelov & Zurbriggen, 2017). Low-level *IRT1* promoter induction in a *fit* mutant background indicates that other plant factors can, to some extent, replace FIT function for promoter control in plants (Jakoby *et al.*, 2004). We thus exploited transactivation of the target *IRT1* promoter by FIT and bHLH039 in a quantifiable mammalian assay, based on normalized human SEAP reporter expression, driven by *IRT1_{pro}*. Neither expression of FIT nor bHLH039 protein alone initiated *IRT1_{pro}* activation beyond background, but their combination led to an approximately seven-fold activation of *IRT1_{pro}* (Fig. 6a). This demonstrates that the mammalian transactivation assay is reliable and quantitative. We observed a statistically significant

increase in *IRT1_{pro}* activity for FITm(S221E) of 25% compared with WT, whereas a decrease of 25–30% was detectable for FITm(SS271/2AA) and FITm(S221E/SS271/2AA). FITm(S221A) activity was comparable to the control (Fig. 6b). FITm(Y238F) and FITm(Y278F) showed a significant increase in *IRT1_{pro}* activity by 20% and *c.* 70%, respectively. However, FITm(Y238E) and FITm(Y278E) displayed a significant decrease in activity by *c.* 75% (Fig. 6c). Immunoblot analyses in combination with promoter activity demonstrated that transcription factor proteins were expressed in the system, even in cases where only weak protein bands (FITm(S221E)) were detected (Fig. 6).

In summary, the altered transactivation activity of FIT provides evidence that predicted phospho-sites are crucial for fine-tuning transcriptional FIT activity. Indeed, for the three mutant forms FITm(SS271/2AA), FITm(Y238E) and FITm(Y278E), which interacted less with bHLH039 in plant cells, transactivation capacities were lower than for WT FIT. Accordingly, phospho-mutant forms interacting with bHLH039 similar to WT showed mostly at least the same level of transactivation capacity as FIT.

A FIT phospho-mutant has altered protein stability

Protein phosphorylation can be a signal for initiation or decrease of protein turnover (Ni *et al.*, 2013), and phosphorylation of FIT might also be linked with proteasomal degradation. FIT-GFP protein, expressed in plant cells, was nearly completely degraded over a 240 min time course, as shown by a quantified cell-free degradation assay (Fig. 7). Proteasomal inhibitor MG132 antagonized this degradation and confirmed proteasomal involvement in FIT protein turnover (Figs 7, S5a). The Ser221, Ser271/2 and Tyr238 phospho-mutants, as well as FITm(Y278F) phospho-mutant, were not degraded in a significantly different time from WT, whereas FITm(Y278E) displayed a decrease in protein stability, confirmed by half-life rates (Figs 7, S5b,d).

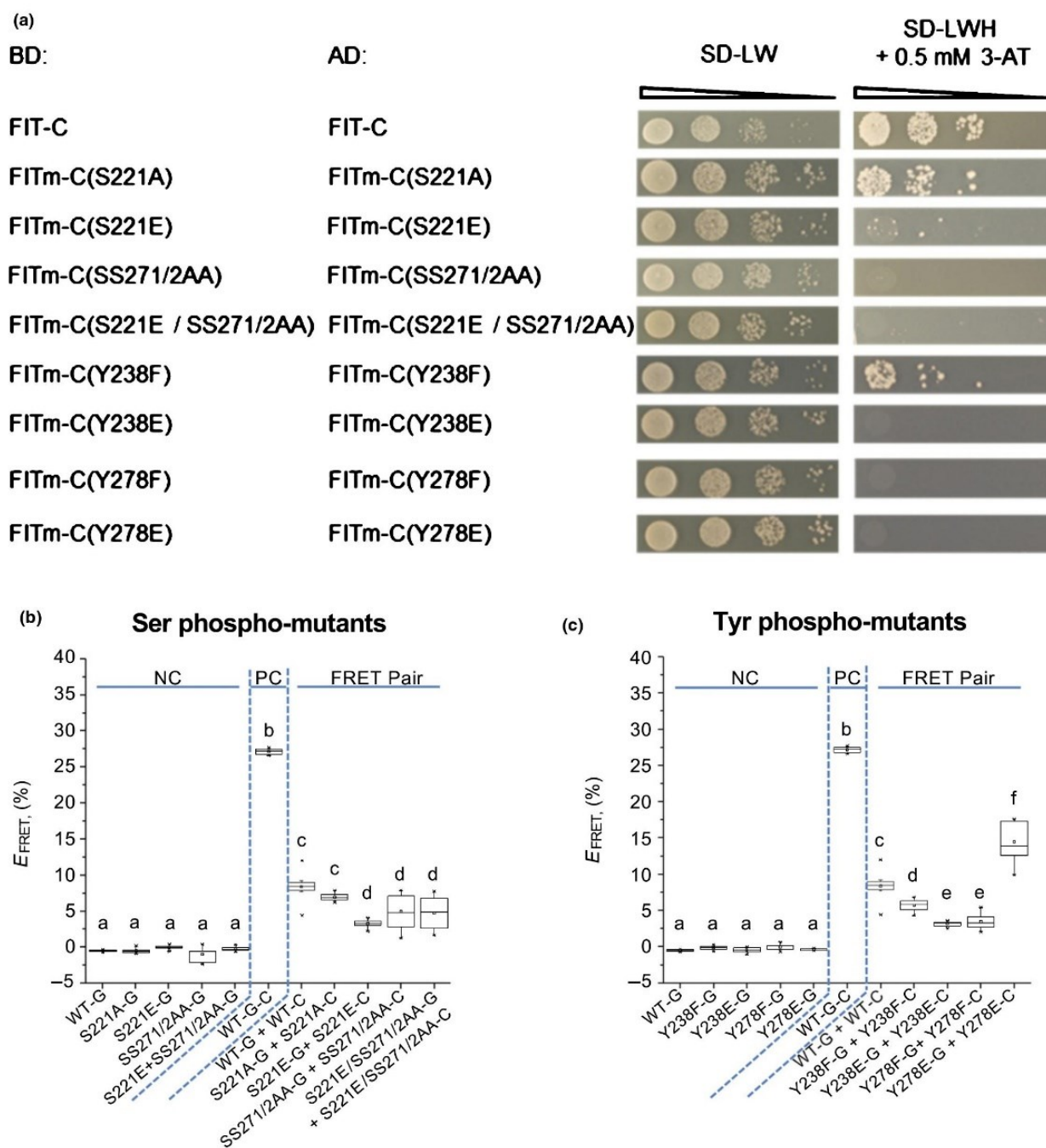


Fig. 4 FER-LIKE IRON DEFICIENCY-INDUCED TRANSCRIPTION FACTOR (FIT) homodimerization capacity is affected in phospho-mutants. (a) FIT-C and FITm-C homodimerization by targeted yeast two-hybrid assays. Yeast cells were co-transformed with GAL4-binding domain BD-FIT-C or BD-FITm-C and GAL4-activation domain AD-FIT-C or AD-FITm-C plasmids. A 10-fold dilution series was spotted onto synthetic defined –leucine, –tryptophan (SD-LW) plates as growth control ($OD_{600} = 1-10^{-3}$). To analyze the interaction capacity, yeast was spotted onto SD-LW, –histidine (SD-LWH) plates, containing 0.5 mM 3-amino-1,2,4-triazole (3-AT), representing selective growth conditions indicative of interaction. Controls of the assays are shown in Supporting Information Fig. S2. (b, c) Quantification of homo-dimerization of FIT compared to (b) Serine (Ser) FITm phospho-mutants and (c) tyrosine (Tyr) FITm phospho-mutants following Förster resonance energy transfer (FRET)–acceptor photobleaching assays in plant cells. Green fluorescent protein (GFP) (G)- and mCherry (C)-tagged FIT and FITm pairs were measured in plant cell nuclei (FRET pairs) following tobacco leaf infiltration and induction of gene expression. GFP-fusion proteins serve as donor-only negative controls (NC). Fusion proteins with dual GFP-mCherry (G–C) serve as positive controls (PC). FRET efficiency E_{FRET} is the relative increase of GFP intensity following photobleaching of the mCherry acceptor. Elevated E_{FRET} for the FRET pair compared with NC is indicative of protein interaction. Data are presented in box plots; inter-quartile range (IQR) 25–75%; whiskers, 25th percentile –1.5 × IQR, 75th percentile +1.5 × IQR; median, horizontal line within IQR box; mean, small square in IQR box; x, values outside ± 1.5 × IQR range. Statistically different values are highlighted by different letters. Statistical significance was calculated using one-way ANOVA ($P < 0.05$) and Tukey post-hoc test ($n = 10$). At least two independent experiments were performed. One representative experiment is shown.

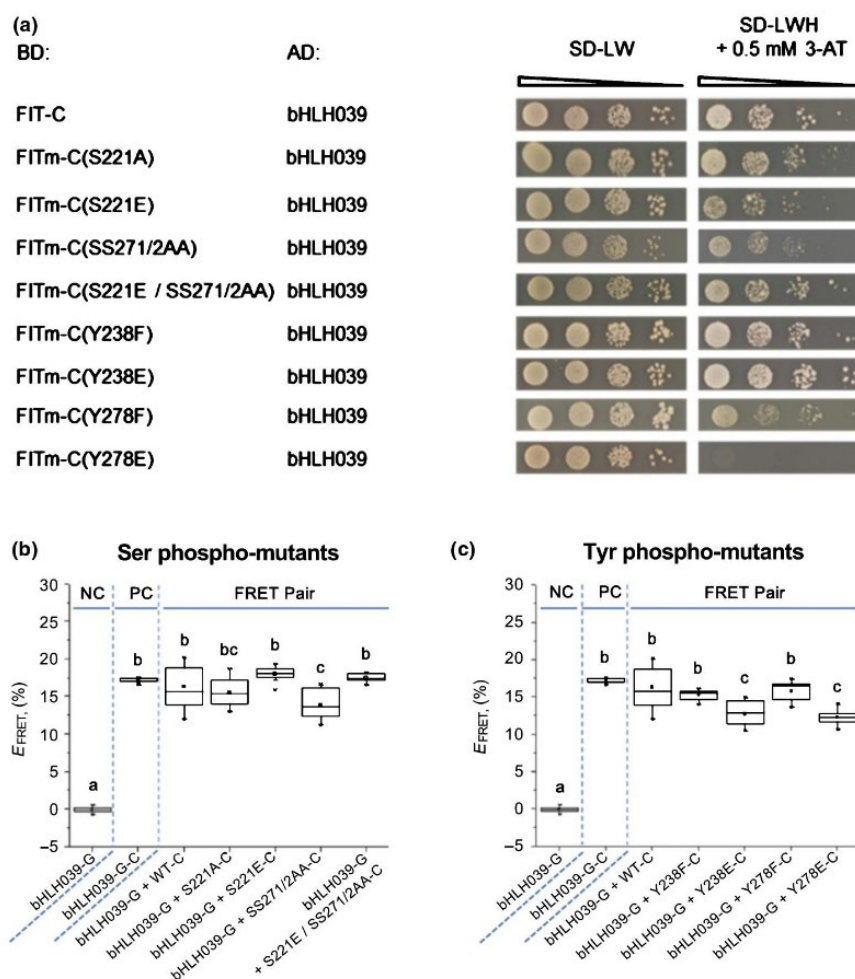


Fig. 5 FER-LIKE IRON DEFICIENCY-INDUCED TRANSCRIPTION FACTOR (FIT)-basic helix-loop-helix 39 (bHLH039) heterodimerization capacity is affected in phospho-mutants. (a) FIT-C or FITm-C and bHLH039 heterodimerization by targeted yeast two-hybrid assays. The yeast assay was conducted as described for Fig. 4(a) using BD-FIT-C or BD-FITm-C and AD-bHLH039 plasmids for co-transformation. Controls of the assays are shown in Supporting Information Fig. S3. (b, c) Quantification of heterodimerization of FIT, following Förster resonance energy transfer (FRET)-acceptor photobleaching assays in plant cells, compared with (b) serine (Ser) FITm phospho-mutants and (c) tyrosine (Tyr) FITm phospho-mutants with bHLH039. FRET efficiency and statistical significance were assessed as described in Fig. 4(b,c), using as FRET pairs green fluorescent protein (GFP)-tagged bHLH039 (bHLH039-G) together with mCherry-tagged FIT or -FITm (FIT-C or FITm-C) as negative control (NC) bHLH039-G and as positive control (PC) bHLH039-G-C. FRET efficiency E_{FRET} is the relative increase of GFP intensity following photobleaching of the mCherry acceptor. Elevated E_{FRET} for the FRET pair compared with NC is indicative of protein interaction. Data are represented in box plots; interquartile range (IQR) 25–75%; whiskers: 25th percentile, $-1.5 \times$ IQR; 75th percentile, $+1.5 \times$ IQR; median, horizontal line within IQR box; mean, small square in IQR box; x, values outside $\pm 1.5 \times$ IQR range. Statistically different values are highlighted by different letters. Statistical significance was calculated using one-way ANOVA ($P < 0.05$) and Tukey post-hoc test ($n = 10$). At least two independent experiments were performed. One representative experiment is shown.

These results suggest that Tyr278 phosphorylation could be a trigger for faster degradation of the protein.

Phospho-mimicking Tyr mutants do not complement the *fit-3* mutant

The aforementioned functional phospho-mutant screen has revealed that FITm(Y238E) and FITm(Y278E) displayed a majority of phenotypes among phospho-mutant FIT forms. To generate a proof of concept for identification of meaningful new phospho-sites using the phospho-mutant screen, we used these two phospho-mimicking Tyr mutants to demonstrate

phenotypes *in planta*, using a *fit-3* mutant complementation assay (Fig. 8). *FITm* mRNA and FITm protein were expressed at a comparable level to nonmutagenized FIT-GFP in the lines analyzed (Fig. 8a,b; note that FIT and FITm-GFP are driven by a constitutive promoter). In the line FITm(Y238E)-GFP/*fit-3*, the FIT target genes *FRO2* and *IRT1* were not induced to the same high level at $-Fe$ as in FIT-GFP/*fit-3*. In the line FITm(Y278E)-GFP/*fit-3*, *FRO2* was similarly expressed as in FIT-GFP/*fit-3*, but *IRT1* levels were lower. Also, FITm(Y278E)-GFP/*fit-3* expressed *IRT1* to a higher level than FITm(Y238E)-GFP/*fit-3* did at $-Fe$. In both Tyr-mutated FIT lines, *FRO2* and *IRT1* were expressed at higher level than in *fit-3* plants (Fig. 8c,d). We

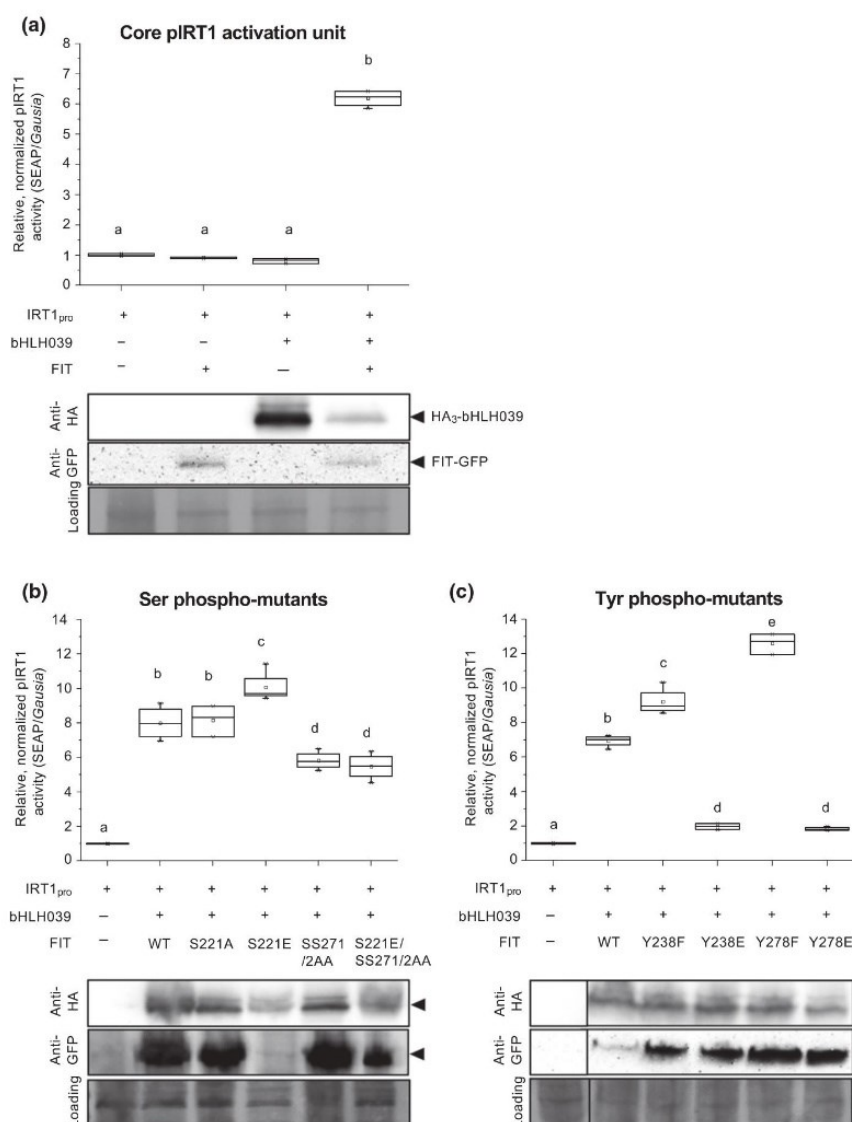


Fig. 6 FER-LIKE IRON DEFICIENCY-INDUCED TRANSCRIPTION FACTOR (FIT) phospho-mutants differ in transactivation of the IRON-REGULATED TRANSPORTER1 (*IRT1*) target promoter. (a) Proof-of-concept demonstration of the quantifiable cellular transactivation assay in Chinese hamster ovary (CHO) cells to quantify the ability of FIT and) basic helix-loop-helix 39 (bHLH039) to induce the target promoter *IRT1*_{pro} resulting in induced activity of the secreted alkaline phosphatase (SEAP) reporter. Upper part, quantified promoter induction relative to the baseline control of *IRT1*_{pro} in the absence of bHLH039 and FIT, normalized to co-transfected *Gaussia* luciferase activity. Lower part, immunoblot analysis showing protein expression of hemagglutinin (HA)-tagged HA₃-bHLH039 (Anti-HA, 36 kDa, arrowhead) and FIT-GFP (Anti-GFP, 62 kDa, arrowhead) in transfected CHO cells; as control for protein transfer, we used Ponceau S staining of the membrane (Loading). Both FIT and bHLH039 are required to activate *IRT1*_{pro}, defining the minimal framework needed for promoter activation. Data are presented in box plots; interquartile range (IQR) 25–75%; whiskers: 25th percentile, $-1.5 \times$ IQR; 75th percentile $+1.5 \times$ IQR; median, horizontal line within IQR box; mean, small square in IQR box; x, values outside $\pm 1.5 \times$ IQR range. Statistical significance is highlighted by different letters and was calculated using one-way ANOVA ($P < 0.05$) and Tukey post-hoc test ($n = 3$). One representative experiment is shown. (b, c) Cellular transactivation assay to quantify the ability of (b) serine (Ser) FITm and (c) tyrosine (Tyr) FITm phospho-mutants compared with FIT. The assay, statistical analysis, immunoblot analysis, and labeling of protein bands were carried out as described for (a).

therefore conclude that the Tyr phospho-mimicking mutations cause decreased FIT activity, which confirms results of the cellular assays. However, Tyr phospho-mimicked FIT still retains sufficient functionality for target gene activation. Elevated *BHLH039* expression indicates Fe deficiency. At +Fe, *BHLH039* expression was similarly low between Tyr mutant- and WT FIT-complementing plants (Fig. 8e), whereas it was high in *fit-3*.

Therefore, Tyr phospho-mimicked FIT is less active than WT FIT, but its function is not knocked out.

Discussion

Phospho-dead and phospho-mimicking mutants of four Ser and Tyr sites caused different molecular and cellular phenotypes in

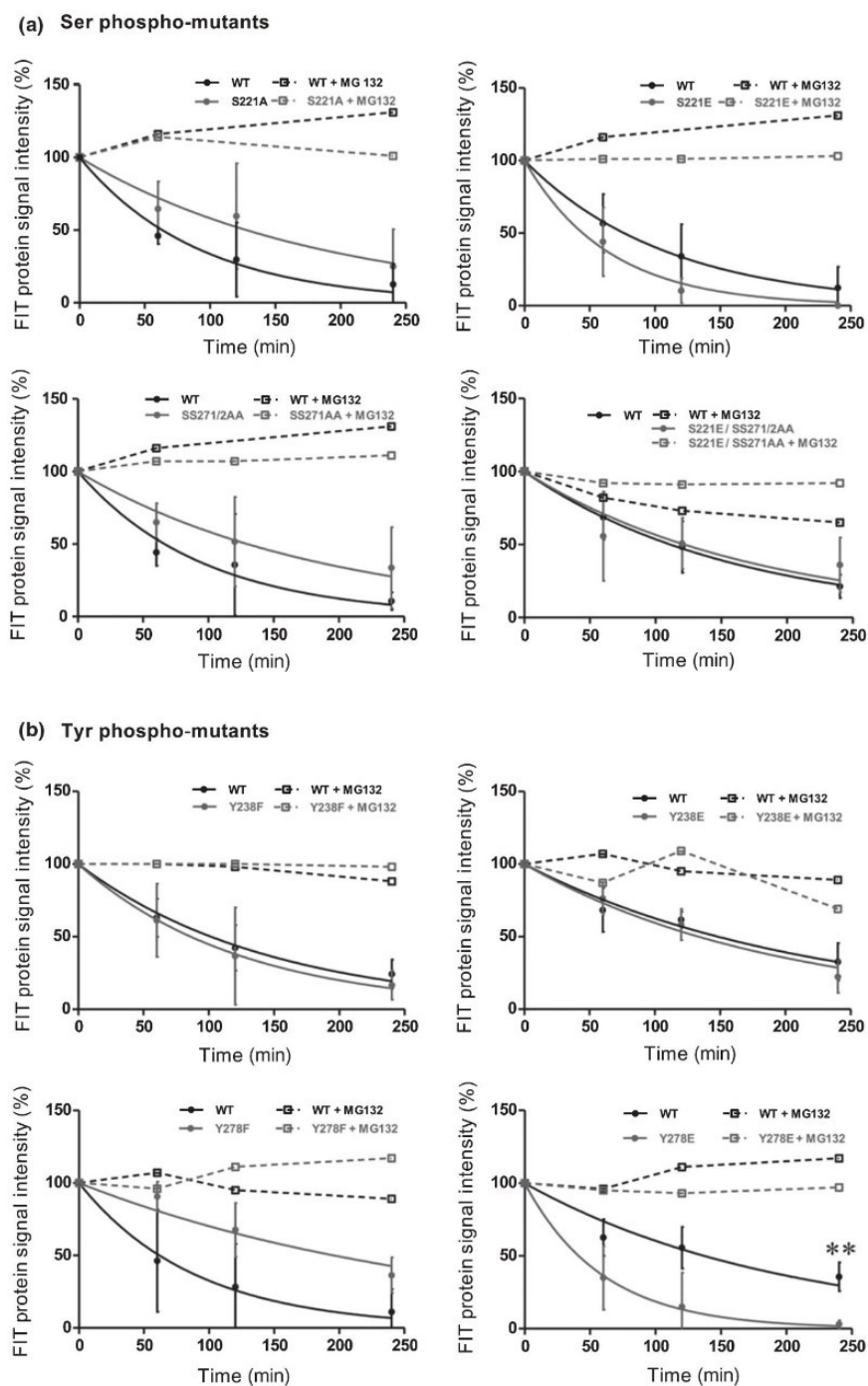


Fig. 7 A FER-LIKE IRON DEFICIENCY-INDUCED TRANSCRIPTION FACTOR (FIT) tyrosine (Tyr) phospho-mutant is degraded faster than other phospho-mutants. Quantified cell-free protein degradation assay for (a) serine (Ser) and (b) Tyr phospho-mutant FITm-green fluorescent protein (GFP) in comparison with FIT-GFP. The assay was conducted following transient expression in tobacco leaf epidermis cells. Equal amounts of total protein extract were incubated at 25°C for 0, 60, 120 and 240 min, partly treated with the proteasomal inhibitor MG132 (+MG132). Protein abundance was determined by quantitative immunoblot analysis of FIT-GFP and FITm-GFP. Wild-type (WT) is represented as solid black, FITm-GFP as solid gray curves, dashed lines are +MG132 samples. Data are means \pm SD (+MG132, one replicate). Statistically significant differences between mutant and WT at each individual time-point are highlighted by asterisks (Student's *t*-test, **, $P < 0.01$, $n = 3$). Immunoblots and calculated half-life times of FIT-GFP and FITm-GFP are presented in Supporting Information Fig. S5.

phospho-mutant activity assays of FIT. Whereas Ser phosphorylation, with predominance at the previously identified Ser272 site, would activate FIT, Tyr phosphorylation would deactivate it, and this also in plants. We suggest that alternative pathways exert multifaceted phosphorylation control of FIT.

All four predicted phosphorylation target residues were relevant for cellular FIT activities. Three of them were validated through transgenic plant experiments (this work) and our previous work (Gratz *et al.*, 2019), showing suitability of the three-

step NETPhos prediction, phylogenetic sequence analysis, and phosphorylation motif searches in combination with a subsequent mutant activity screening.

Clear sequence similarity of monocot and basal angiosperm FIT C-termini was not evident. FIT regulation via FIT-C may, therefore, have been acquired in eudicots. Phosphorylated amino acids, especially Tyr, are often conserved across plant species (Maathuis, 2008; Sugiyama *et al.*, 2008; Nakagami *et al.*, 2010; Mithoe *et al.*, 2012). Because of the high conservation, Tyr

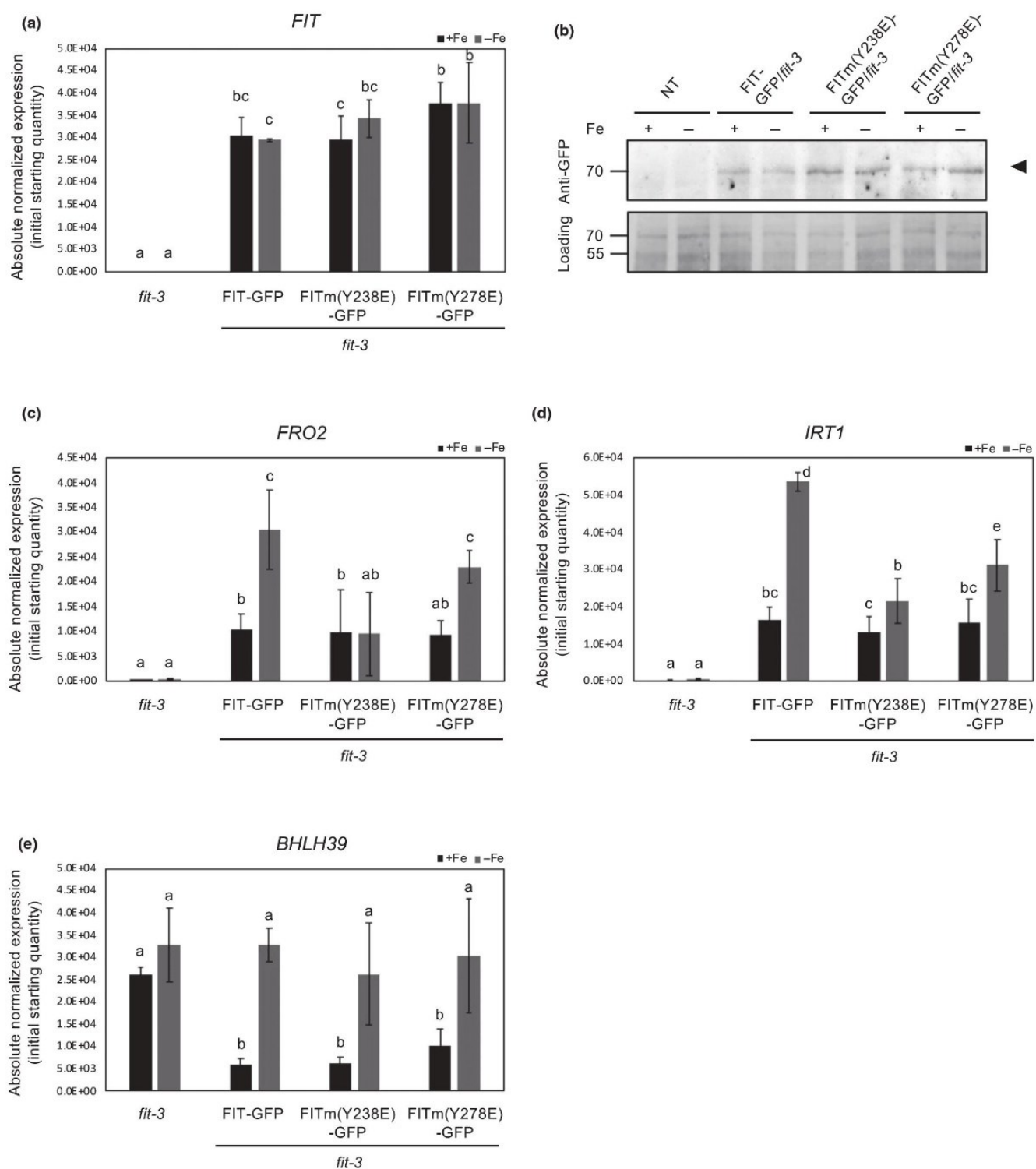


Fig. 8 Phospho-mimicking FITm(Y238E) and FITm(Y278E) have reduced activity in *Arabidopsis thaliana*. *fit* mutant complementation assay with FITm (Y238E)-GFP/*fit-3* and FITm(Y278E)-GFP/*fit-3* lines in comparison to FIT-GFP/*fit-3* (FIT, FER-LIKE IRON DEFICIENCY-INDUCED TRANSCRIPTION FACTOR; GFP, green fluorescent protein). Plants were grown with sufficient iron (+Fe, black bars) or deficient iron (-Fe, gray bars) supply in 2-wk growth assays. (a) *FIT* gene expression analysis in roots. (b) Immunoblot analysis of FIT-GFP and FITm-GFP protein expression (upper, FIT-GFP and FITm-GFP 63 kDa), Ponceau S membrane loading control (lower). FIT-GFP/*fit-3* lines have similar expression levels to the FIT-GFP/*fit-3* line. (c–e) Gene expression analysis in roots of (c) *FRO2*, (d) IRON-REGULATED TRANSPORTER1 (*IRT1*), and (e) basic helix-loop-helix 39 (*BHLH39*). Data are represented as mean \pm SD. Statistical significance is highlighted by different letters and was calculated using one-way ANOVA ($P < 0.05$) and Tukey post-hoc test ($n = 3$).

	S221A	S221E	SS271/272AA	S221E/ SS271/272AA	Y238F	Y238E	Y278F	Y278E
Phospho-mimicking		x		x		x		x
Phospho-dead	x		x	x	x		x	
Nuclear (vs cytoplasmic) localization (Fig. 2)		Blue	Blue	Blue	Blue	Blue	Blue	Blue
Nuclear mobility (Fig. 3)			Red	Red		Blue		
Homodimerization in yeast (Fig. 4a)		Blue	Blue	Blue	Blue	Blue	Blue	Blue
Homodimerization in planta (Fig. 4b, c)		Blue	Blue	Blue	Blue	Blue	Blue	Red
Heterodimerization in yeast (Fig. 5a)								Blue
Heterodimerization in planta (Fig. 5b, c)			Blue			Blue		Blue
Transcriptional self-activation in yeast (Supporting Information Fig. S4)				Blue				Blue
Transactivation assay (Fig. 6)		Red	Blue	Blue	Red	Blue	Red	Blue
Protein stability (Fig. 7)								Blue

Less than WT < No difference < More than WT

Fig. 9 Summary of FER-LIKE IRON DEFICIENCY-INDUCED TRANSCRIPTION FACTOR (FIT) phospho-mutant phenotype screening using cellular assays. A color code was applied, highlighting altered regulatory properties and cellular activities between FIT (wild-type, WT) and FITm forms. Red shading indicates a stronger effect, and blue shading a reduced effect in the respective FITm form compared with FIT for the experiment conducted, referred to by figure numbers. Increase of the individual color indicates a stronger effect. The absence of differences between FIT and FITm is marked in gray. A mathematical correlation analysis conducted with the data matrix showed significant correlation between heterodimerization of FIT and basic helix–loop–helix 39, transactivation capability, and protein stability.

regulation of FIT might be evolutionarily older than Ser regulation and potentially older than the role of FIT in regulating Strategy I. Perhaps the high pressure to survive on dry land was a selective factor for eudicots during the Cretaceous period to evolve more efficient Fe acquisition regulation with better integration into plant growth. This way, new protein interactions and protein modifications could have occurred. FIT might have acquired this function via FIT-C, keeping some of its regulatory properties.

Phospho-mutant analyses are widely accepted to identify and characterize functional phosphorylation patterns (Yang *et al.*, 2015; Li H. *et al.*, 2017; Li S. *et al.*, 2017), and the cellular FIT mutant activities (summarized in Fig. 9) can be explained by differential phosphorylation. Local charge differences lead to conformational changes that allow or impede regulatory protein interactions. Shuttling of FIT from the cytoplasm to the nucleus is mediated by the presence of a nuclear localization signal (Zhang *et al.*, 2006). Phosphorylation could alter this signal, and hence nuclear translocation, via a conformational change or interaction with a regulatory protein, as shown for 14-3-3 protein binding to phospho-sites (Moorhead *et al.*, 2006). Changes in FIT phospho-mutant mobility might be due to the binding of FIT to subnuclear structures and nuclear protein complexes. FIT protein interactions are needed for target promoter

transactivation, and protein stability control regulates the responsiveness of the signaling system. In 13 out of 16 cases, yeast and plant systems gave fully concordant results for FIT phospho-mutant protein interactions, underlining the general reliability of protein interaction assays. Differences can be explained by differing regulatory mechanisms in the two systems, and likely by lack of regulatory contributions of the N-terminal and bHLH subdomains of FIT. Yeast interaction assays were conducted with FIT-C, in contrast to plant assays performed with full-length FIT.

Interestingly, heterodimerization of FIT and bHLH039 was correlated with transactivation capability and protein stability (see Fig. 9). On the other hand, FIT transactivation ability did not correlate with nucleo-cytoplasmic partitioning and homodimerization, in line with the failure of FIT alone to activate *IRT1_{pro}*. A higher cytoplasmic-to-nuclear ratio of FIT (lower nuclear vs cytoplasmic localization, as indicated in Fig. 9) seems linked with homodimerization, but the values were not significant in correlation (Fig. 9). Perhaps FIT homodimerization affects nuclear localization. Taken together, phospho-mutant activity screening of FIT opens up a way to connect Fe acquisition regulation to new cellular signaling pathways, including cytoplasmic-to-nuclear partitioning and Tyr phosphorylation.

Positive effects of phospho-mimicking Ser (Gratz *et al.*, 2019; this work) and phospho-dead Tyr (this work), in contrast to

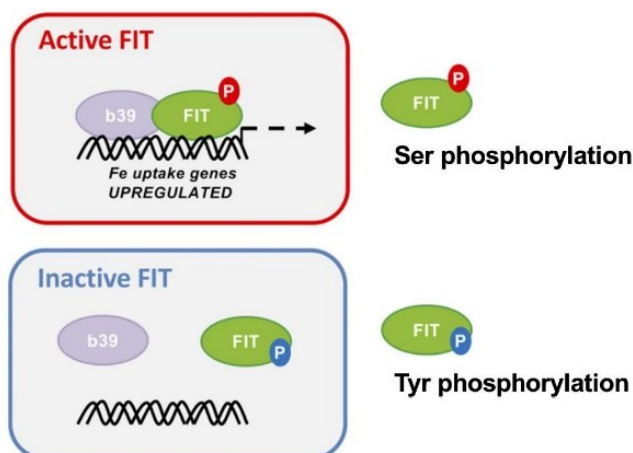


Fig. 10 Model of two-step regulation of FER-LIKE IRON DEFICIENCY-INDUCED TRANSCRIPTION FACTOR (FIT) activity by protein phosphorylation. Active FIT (upper): serine (Ser) phosphorylation promotes FIT activity. Phosphorylation (P) at Ser221 and Ser272 in FIT-C favors basic helix–loop–helix 39 (bHLH039) interaction and expression of *IRON-REGULATED TRANSPORTER1* promoter (*IRT1_{pro}*). Inactive FIT (lower): tyrosine (Tyr) phosphorylation (P) reduces FIT activity in a situation where no active FIT protein is needed or even could be detrimental. Phosphorylation at Tyr238 and Tyr278 in FIT-C reduces bHLH039 heterodimerization and expression of *IRT1_{pro}* and partly promotes FIT degradation.

negative effects of the phospho-dead Ser272 (Gratz *et al.*, 2019) and phospho-mimicking Tyr (this work) mutations, are indicators for multiple phosphorylation triggers for FIT. We therefore suggest that FIT is controlled via different phosphorylation pathways, leading to activation by Ser and deactivation by Tyr phosphorylation (Fig. 10).

Ser272 phosphorylation by CIPK11 activates FIT to accumulate in the nucleus, dimerize with bHLH039, and activate target promoters (Gratz *et al.*, 2019). CIPK11 also phosphorylates FIT-Cm(SS271/2AA) protein to a minor extent (Gratz *et al.*, 2019), possibly at Ser221. Mutant comparisons between FITm(SS21E SS271/2AA) and the respective single mutants indicated that the multiple mutant behaved more similar to FITm(SS271/2AA), suggesting that Ser221 appears less important than Ser272. In this sense, phosphorylation of position Ser272 plays a pivotal role. Loss of phosphorylation in phospho-dead FITm(SS271/2AA) has more dramatic effects than loss of FITm(SS21A), and FITm(SS271/2AA) is not rescued by nearby phospho-mimicking FITm(SS21E) regarding nuclear mobility, transcriptional self-activation in yeast, and transactivation. Besides CIPK11, other Fe-regulated *CIPK* genes and another CIPK interactor of FIT are known, but their roles in Fe-deficiency responses or FIT regulation remain to be determined (Gratz *et al.*, 2019). CIPK23, on the other hand, affects FIT downstream targets *FRO2* and *IRT1* proteins (Tian *et al.*, 2016; Dubeaux *et al.*, 2018). Furthermore, other Ser/Thr kinase families are connected to Fe deficiency and could target FIT, such as MAPK3 and MAPK6, upregulated under Fe deficiency (Ye *et al.*, 2015). *mapk3* and *mapk6* loss-of-function mutants have decreased gene expression levels of *FRO2* and *IRT1* (Ye *et al.*, 2015). Both kinases are involved in the expression of *ACC SYNTHASE (ACS)* genes (Li *et al.*, 2012; Li

S. et al., 2017) and they could positively influence Fe acquisition through phosphorylation-based stabilization of ACS proteins, needed for ethylene production (Liu & Zhang, 2004). Ethylene-induced transcription factor EIN3 is phosphorylated and stabilized by MAPK3 and MAPK6 (Yoo *et al.*, 2008). MAPK3 and MAPK6 could thus play a dual role in possibly activating FIT by Ser phosphorylation and via stabilization of EIN3, known to interact and activate FIT (Lingam *et al.*, 2011). Recently, the involvement of serine/threonine kinases CALCIUM-DEPENDENT PROTEIN KINASES (CPKs) CPK5 and CPK6 in *ACS* expression has been shown (Li *S. et al.*, 2017), and these could also represent kinase candidates for FIT Ser phosphorylation.

The presence of two regulatory Tyr sites is very intriguing. Tyr phosphorylation has been rarely described to date in plant transcription factors, whereas based on phospho-proteomics it could be quite important (Sugiyama *et al.*, 2008; van Wijk *et al.*, 2014; Lu *et al.*, 2015). Tyr can also be involved in other protein modifications; for example, nitration, and generally in hydrogen bond formation. However, the fact that Tyr phospho-mimicking and phospho-dead mutations yielded contrasting phenotypes in several assays speaks in favor for different activities in the phosphorylated vs nonphosphorylated state. Tyr phospho-mimicking mutants have a decreased bHLH039 interaction and transactivation ability, and the phospho-mimicking mutant of Tyr278 also has a lower protein stability in plant cells. Interestingly, the phospho-mimicking Tyr mutants of FIT display very similar features to phospho-mimicked CjWRKY1(Y115E), which is impaired in induction of target genes and shows increased cytosolic localization, where it is degraded subsequently (Yamada & Sato, 2016). Thus, Tyr phosphorylation is likely a multi-inhibitory mechanism, rendering FIT inactive by inhibition of protein interaction with bHLH039, inhibition of transactivation, and enhanced protein degradation.

Presently, we cannot distinguish where in the cell FIT phosphorylation events occur. For example, Tyr phosphorylation could be relevant at the promoter target site in the nucleus to eliminate ‘used FIT’ and make the system responsive to ‘fresh’ FIT again, as proposed (Sivitz *et al.*, 2011). On the other hand, only a small fraction of FIT protein is needed for being ‘used’ at the target promoters, yet the inhibitory Tyr phosphorylation affects all FIT protein (‘used’ and ‘fresh’). An alternative possibility, therefore, is that Tyr phosphorylation takes place in the cytoplasm, where Tyr kinases or dual-specificity kinases could be present. A very interesting follow-up question is to identify a kinase for Tyr phosphorylation of FIT. Potential Tyr kinases might belong to Raf-like subfamilies of MAPKKKs in plants (Jouannic *et al.*, 1999; Ichimura *et al.*, 2002). The phosphorylation motif spanning FIT Tyr238 is a kinase substrate motif of human JANUS KINASE 2 (Argetsinger *et al.*, 2004). The closest plant homologue is the MAPKKK Raf10, which is expressed in roots, responsive to abiotic stresses, and classified as plant Tyr kinase (Jouannic *et al.*, 1999; Ichimura *et al.*, 2002; Rudrabhatla *et al.*, 2006; Lee *et al.*, 2015). Alternatively, brassinosteroids (BRs) are negative regulators of Fe uptake (Wang *et al.*, 2012), and BR signaling might be involved in FIT Tyr phosphorylation

via dual-specificity kinases of BR signaling, even though transcription factor substrates remain to be proven (Oh *et al.*, 2009; Kim & Wang, 2010; Jaillais *et al.*, 2011).

Conclusions

The three-step prediction of phosphorylation target sites in FIT-C was validated by phospho-mutant activity assays. The contrasting effects of Ser and Tyr phospho-mutations suggest alternative regulation of FIT activity by different phosphorylation pathways. This multiple regulation of FIT activity underlines the importance of FIT as a central hub for regulating Fe acquisition in dicots. It may serve to integrate changes in environmental conditions and to quickly adjust Fe acquisition at the transcriptional level. FIT can serve as a model to characterize the rare Tyr phosphorylation event in plants and to identify a Tyr kinase.

Acknowledgements

We are grateful to Elke Wieneke, Gintaute Matthäi, and Kai Kirchhoff for excellent technical assistance. We are thankful for contributions of Daniela Lichtblau, Christopher Endres, and Büsra Acaroglu. RG and RO-F are members of iGRAD Plant Graduate School, Düsseldorf. Funding from the German Research Foundation grants Ba1610/5-2 and Ba1610/7-1 to PB is greatly acknowledged. TB was supported for this research through the International Max Planck Research School (IMPRS) on Understanding Complex Plant Traits using Computational and Evolutionary Approaches at the Max Planck Institute for Plant Breeding Research and the universities of Düsseldorf and Cologne. This work received funding from Germany's Excellence Strategy, EXC 2048/1, Project ID: 390686111, and from Deutsche Forschungsgemeinschaft – Project no. 267205415 – SFB 1208 (CRC 1208) Project B05 to PB.

Author contributions

RG, TB, RI, MDZ and PB designed the study, RG, TB, RI, KT, LT, RO-F, TB and JM performed research, RG, TB, RI, KT, LT, RO-F, TB, MDZ and PB analyzed data, RG wrote the original draft, RG, TB and PB reviewed and edited the article, TB, SW-P, MDZ and PB supervised the study, and PB and MDZ acquired funding.

ORCID

Petra Bauer  <https://orcid.org/0000-0002-0404-4532>
Tzvetina Brumbarova  <https://orcid.org/0000-0002-3104-6795>
Regina Gratz  <https://orcid.org/0000-0002-8820-7211>
Rumen Ivanov  <https://orcid.org/0000-0001-7909-4123>
Johannes Meiser  <https://orcid.org/0000-0002-9093-6210>
Stefanie Weidtkamp-Peters  <https://orcid.org/0000-0001-7734-3771>
Matias D. Zurbriggen  <https://orcid.org/0000-0002-3523-2907>

References

- Amanchy R, Kandasamy K, Mathivanan S, Periaswamy B, Reddy R, Yoon WH, Joore J, Beer MA, Cope L, Pandey A. 2011. Identification of novel phosphorylation motifs through an integrative computational and experimental analysis of the human phosphoproteome. *Journal of Proteomics and Bioinformatics* 4: 22–35.
- Argetsinger LS, Kouadio JLK, Steen H, Stensballe A, Jensen ON, Carter-Su C. 2004. Autophosphorylation of JAK2 on tyrosines 221 and 570 regulates its activity. *Molecular and Cellular Biology* 24: 4955–4967.
- Bancaud A, Huet S, Rabut G, Ellenberg J. 2010. Fluorescence perturbation techniques to study mobility and molecular dynamics of proteins in live cells: FRAP, photoactivation, photoconversion, and FLIP. *Cold Spring Harbor Protocols* 2010: pdb.top90.
- Beausoleil SA, Jedrychowski M, Schwartz D, Elias JE, Villen J, Li J, Cohn MA, Cantley LC, Gygi SP. 2004. Large-scale characterization of HeLa cell nuclear phosphoproteins. *Proceedings of the National Academy of Sciences, USA* 101: 12130–12135.
- Ben Abdallah H, Bauer P. 2016. Quantitative reverse transcription-qPCR-based gene expression analysis in plants. *Methods in Molecular Biology* 1363: 9–24.
- Beyer HM, Gonschorek P, Samodelov SL, Meier M, Weber W, Zurbriggen MD. 2015. AQUA cloning: a versatile and simple enzyme-free cloning approach. *PLoS ONE* 10: e0137652.
- Blom N, Gammeltoft S, Brunak S. 1999. Sequence and structure-based prediction of eukaryotic protein phosphorylation sites. *Journal of Molecular Biology* 294: 1351–1362.
- Chinnusamy V, Ohta M, Kanrar S, Lee BH, Hong X, Agarwal M, Zhu JK. 2003. ICE1: a regulator of cold-induced transcriptome and freezing tolerance in *Arabidopsis*. *Genes Development* 17: 1043–1054.
- Clough SJ, Bent AF. 1998. Floral dip: a simplified method for *Agrobacterium*-mediated transformation of *Arabidopsis thaliana*. *The Plant Journal* 16: 735–743.
- Colangelo EP, Guerinot ML. 2004. The essential basic helix–loop–helix protein FIT1 is required for the iron deficiency response. *Plant Cell* 16: 3400–3412.
- Cole TCH, Hilger HH, Stevens PF. 2019. Angiosperm phylogeny poster (APP) – flowering plant systematics, 2019. *PeerJ Preprints* 7: e23206.
- Connorton JM, Balk J, Rodriguez-Celma J. 2017. Iron homeostasis in plants – a brief overview. *Metallomics* 9: 813–823.
- Cui Y, Chen CL, Cui M, Zhou WJ, Wu HL, Ling HQ. 2018. Four IVa bHLH transcription factors are novel interactors of FIT and mediate JA inhibition of iron uptake in *Arabidopsis*. *Molecular Plant* 11: 1166–1183.
- Ding Y, Li H, Zhang X, Xie Q, Gong Z, Yang S. 2015. OST1 kinase modulates freezing tolerance by enhancing ICE1 stability in *Arabidopsis*. *Developmental Cell* 32: 278–289.
- Dubeaux G, Neveu J, Zelazny E, Vert G. 2018. Metal sensing by the IRT1 transporter-receptor orchestrates its own degradation and plant metal nutrition. *Molecular Cell* 69: 953–964.
- Edgar RC. 2004. MUSCLE: a multiple sequence alignment method with reduced time and space complexity. *BMC Bioinformatics* 5: e113.
- Eide D, Broderius M, Fett J, Guerinot ML. 1996. A novel iron-regulated metal transporter from plants identified by functional expression in yeast. *Proceedings of the National Academy of Sciences, USA* 93: 5624–5628.
- Fiol CJ, Wang AQ, Roeske RW, Roach PJ. 1990. Ordered multisite protein-phosphorylation – analysis of glycogen-synthase kinase-3 action using model peptide-substrates. *Journal of Biological Chemistry* 265: 6061–6065.
- Gratz R, Manishankar P, Ivanov R, Koster P, Mohr I, Trofimov K, Steinhorst L, Meiser J, Mai HJ, Drerup M *et al.* 2019. CIPK11-dependent phosphorylation modulates FIT activity to promote *Arabidopsis* iron acquisition in response to calcium signaling. *Developmental Cell* 48: 726–740.
- Gudesblat GE, Schneider-Pizon J, Betti C, Mayerhofer J, Vanhoutte I, van Dongen W, Boeren S, Zhiponova M, de Vries S, Jonak C *et al.* 2012. SPEECHLESS integrates brassinosteroid and stomata signalling pathways. *Nature Cell Biology* 14: 548–558.
- Heim MA, Jakoby M, Werber M, Martin C, Weisshaar B, Bailey PC. 2003. The basic helix–loop–helix transcription factor family in plants: a genome-wide

- study of protein structure and functional diversity. *Molecular Biology and Evolution* 20: 735–747.
- Ichimura K, Shinozaki K, Tena G, Sheen J, Henry Y, Champion A, Kreis M, Zhang S, Hirt H, Wilson C. 2002. Mitogen-activated protein kinase cascades in plants: a new nomenclature. *Trends in Plant Science* 7: 301–308.
- Ivanov R, Brumbarova T, Bauer P. 2012. Fitting into the harsh reality: regulation of iron deficiency responses in dicotyledonous plants. *Molecular Plant* 5: 27–42.
- Jacobs JL, Dinman JD. 2004. Systematic analysis of bicistronic reporter assay data. *Nucleic Acids Research* 32: e160.
- Jaillais Y, Hothorn M, Belkhadir Y, Dabi T, Nimchuk ZL, Meyerowitz EM, Chory J. 2011. Tyrosine phosphorylation controls brassinosteroid receptor activation by triggering membrane release of its kinase inhibitor. *Genes & Development* 25: 232–237.
- Jakoby M, Wang HY, Reidt W, Weisshaar B, Bauer P. 2004. FRU (BHLH029) is required for induction of iron mobilization genes in *Arabidopsis thaliana*. *FEBS Letters* 577: 528–534.
- Jouanin S, Hamal A, Leprince A-S, Tregear J, Kreis M, Henry Y. 1999. Plant MAP kinase structure, classification and evolution. *Gene* 233: 1–11.
- Ju CL, Yoon GM, Shemansky JM, Lin DY, Ying ZI, Chang JH, Garrett WM, Kessenbrock M, Groth G, Tucker ML *et al.* 2012. CTR1 phosphorylates the central regulator EIN2 to control ethylene hormone signaling from the ER membrane to the nucleus in *Arabidopsis*. *Proceedings of the National Academy of Sciences, USA* 109: 19486–19491.
- Kemp BE, Pearson RB. 1990. Protein-kinase recognition sequence motifs. *Trends in Biochemical Sciences* 15: 342–346.
- Kim T-W, Wang Z-Y. 2010. Brassinosteroid signal transduction from receptor kinases to transcription factors. *Annual Review of Plant Biology* 61: 681–704.
- Lampard GR, Macalister CA, Bergmann DC. 2008. *Arabidopsis* stomatal initiation is controlled by MAPK-mediated regulation of the bHLH SPEECHLESS. *Science* 322: 1113–1116.
- Le CTT, Brumbarova T, Ivanov R, Stoof C, Weber E, Mohrbacher J, Fink-Straube C, Bauer P. 2016. ZINC FINGER OF ARABIDOPSIS THALIANA12 (ZAT12) interacts with FER-LIKE IRON DEFICIENCY-INDUCED TRANSCRIPTION FACTOR (FIT) linking iron deficiency and oxidative stress responses. *Plant Physiology* 170: 540–557.
- Lee S-J, Lee MH, Kim J-I, Kim SY. 2015. *Arabidopsis* putative MAP kinase kinases Raf10 and Raf11 are positive regulators of seed dormancy and ABA response. *Plant and Cell Physiology* 56: 84–97.
- Li GJ, Meng XZ, Wang RG, Mao GH, Han L, Liu YD, Zhang SQ. 2012. Dual-level regulation of ACC synthase activity by MPK3/MPK6 cascade and its downstream WRKY transcription factor during ethylene induction in *Arabidopsis*. *PLoS Genetics* 8: e1002767.
- Li H, Ding Y, Shi Y, Zhang X, Zhang S, Gong Z, Yang S. 2017. MPK3- and MPK6-mediated ICE1 phosphorylation negatively regulates ICE1 stability and freezing tolerance in *Arabidopsis*. *Developmental Cell* 43: 630–642.
- Li S, Han X, Yang L, Deng X, Wu H, Zhang M, Liu Y, Zhang S, Xu J. 2017. Mitogen-activated protein kinases and calcium-dependent protein kinases are involved in wounding-induced ethylene biosynthesis in *Arabidopsis thaliana*. *Plant, Cell & Environment* 41: 134–147.
- Lingam S, Mohrbacher J, Brumbarova T, Potuschak T, Fink-Straube C, Blondet E, Genschik P, Bauer P. 2011. Interaction between the bHLH transcription factor FIT and ETHYLENE INSENSITIVE3/ETHYLENE INSENSITIVE3-LIKE1 reveals molecular linkage between the regulation of iron acquisition and ethylene signaling in *Arabidopsis*. *Plant Cell* 23: 1815–1829.
- Liu YD, Zhang SQ. 2004. Phosphorylation of L-aminocyclopropane-L-carboxylic acid synthase by MPK6, a stress-responsive mitogen-activated protein kinase, induces ethylene biosynthesis in *Arabidopsis*. *Plant Cell* 16: 3386–3399.
- Lu Q, Helm S, Rödiger A, Baginsky S. 2015. On the extent of tyrosine phosphorylation in chloroplasts. *Plant Physiology* 169: 996–1000.
- Luo ML, Reyna S, Wang LS, Yi ZP, Carroll C, Dong LQ, Langlais P, Weintraub ST, Mandarino LJ. 2005. Identification of insulin receptor substrate 1 serine/threonine phosphorylation sites using mass spectrometry analysis: regulatory role of serine 1223. *Endocrinology* 146: 4410–4416.
- Maathuis FJ. 2008. Conservation of protein phosphorylation sites within gene families and across species. *Plant Signaling & Behavior* 3: 1011–1013.
- Mai HJ, Pateyron S, Bauer P. 2016. Iron homeostasis in *Arabidopsis thaliana*: transcriptomic analyses reveal novel FIT-regulated genes, iron deficiency marker genes and functional gene networks. *BMC Plant Biology* 16: e211.
- Marschner H, Romheld V, Kissel M. 1986. Different strategies in higher-plants in mobilization and uptake of iron. *Journal of Plant Nutrition* 9: 695–713.
- Meiser J, Lingam S, Bauer P. 2011. Posttranslational regulation of the iron deficiency basic helix–loop–helix transcription factor FIT is affected by iron and nitric oxide. *Plant Physiology* 157: 2154–2166.
- Mithoe SC, Boersema PJ, Berke L, Snel B, Heck AJR, Menke FLH. 2012. Targeted quantitative phosphoproteomics approach for the detection of phospho-tyrosine signaling in plants. *Journal of Proteome Research* 11: 438–448.
- Moorhead GW, Templeton GT, Tran H. 2006. Role of protein kinases, phosphatases and 14-3-3 proteins in the control of primary plant metabolism. In: Plaxton WC, McManus MT, eds. *Annual plant reviews volume 22: control of primary metabolism in plants*. Oxford, UK: Blackwell Publishing, 121–149.
- Muller K, Zurbriggen MD, Weber W. 2014. Control of gene expression using a red- and far-red light-responsive bi-stable toggle switch. *Nature Protocols* 9: 622–632.
- Nakagami H, Sugiyama N, Mochida K, Daudi A, Yoshida Y, Toyoda T, Tomita M, Ishihama Y, Shirasu K. 2010. Large-scale comparative phosphoproteomics identifies conserved phosphorylation sites in plants. *Plant Physiology* 153: 1161–1174.
- Naranjo-Arcos MA, Maurer F, Meiser J, Pateyron S, Fink-Straube C, Bauer P. 2017. Dissection of iron signaling and iron accumulation by overexpression of subgroup Ib bHLH039 protein. *Scientific Reports* 7: e10911.
- Ni WM, Xu SL, Chalkley RJ, Pham TND, Guan SH, Maltby DA, Burlingame AL, Wang ZY, Quail PH. 2013. Multisite light-induced phosphorylation of the transcription factor PIF3 is necessary for both its rapid degradation and concomitant negative feedback modulation of photoreceptor phyB levels in *Arabidopsis*. *Plant Cell* 25: 2679–2698.
- Oh M-H, Wang X, Kota U, Goshe MB, Clouse SD, Huber SC. 2009. Tyrosine phosphorylation of the BR11 receptor kinase emerges as a component of brassinosteroid signaling in *Arabidopsis*. *Proceedings of the National Academy of Sciences, USA* 106: 658–663.
- Pearson RB, Kemp BE. 1991. Protein-kinase phosphorylation site sequences and consensus specificity motifs – tabulations. *Methods in Enzymology* 200: 62–81.
- Reits EA, Neeffes JJ. 2001. From fixed to FRAP: measuring protein mobility and activity in living cells. *Nature Cell Biology* 3: E145.
- Remy I, Michnick SW. 2006. A highly sensitive protein–protein interaction assay based on *Gaussia* luciferase. *Nature Methods* 3: 977–979.
- Ren YJ, Li YY, Jiang YQ, Wu BH, Miao Y. 2017. Phosphorylation of WHIRLY1 by CIPK14 shifts its localization and dual functions in *Arabidopsis*. *Molecular Plant* 10: 749–763.
- Robinson NJ, Procter CM, Connolly EL, Guerinot ML. 1999. A ferric-chelate reductase for iron uptake from soils. *Nature* 397: 694–697.
- Rudrabhatla P, Reddy MM, Rajasekharan R. 2006. Genome-wide analysis and experimentation of plant serine/threonine/tyrosine-specific protein kinases. *Plant Molecular Biology* 60: 293–319.
- Samodelov SL, Zurbriggen MD. 2017. Quantitatively understanding plant signaling: novel theoretical–experimental approaches. *Trends in Plant Sciences* 22: 685–704.
- Schlatter S, Rimann M, Kelm J, Fussenegger M. 2002. *SAMY*, a novel mammalian reporter gene derived from *Bacillus stearothermophilus* α -amylase. *Gene* 282: 19–31.
- Schwartz D, Gygi SP. 2005. An iterative statistical approach to the identification of protein phosphorylation motifs from large-scale data sets. *Nature Biotechnology* 23: 1391–1398.
- Silva RC, Castilho BA, Sattlegger E. 2018. A rapid extraction method for mammalian cell cultures, suitable for quantitative immunoblotting analysis of proteins, including phosphorylated GCN2 and eIF2 α . *MethodsX* 5: 75–82.
- Sivitz A, Grinvalds C, Barberon M, Curie C, Vert G. 2011. Proteasome-mediated turnover of the transcriptional activator FIT is required for plant iron-deficiency responses. *The Plant Journal* 66: 1044–1052.

- study of protein structure and functional diversity. *Molecular Biology and Evolution* 20: 735–747.
- Ichimura K, Shinozaki K, Tena G, Sheen J, Henry Y, Champion A, Kreis M, Zhang S, Hirt H, Wilson C. 2002. Mitogen-activated protein kinase cascades in plants: a new nomenclature. *Trends in Plant Science* 7: 301–308.
- Ivanov R, Brumbarova T, Bauer P. 2012. Fitting into the harsh reality: regulation of iron deficiency responses in dicotyledonous plants. *Molecular Plant* 5: 27–42.
- Jacobs JL, Dinman JD. 2004. Systematic analysis of bicistronic reporter assay data. *Nucleic Acids Research* 32: e160.
- Jaillais Y, Hothorn M, Belkhadir Y, Dabi T, Nimchuk ZL, Meyerowitz EM, Chory J. 2011. Tyrosine phosphorylation controls brassinosteroid receptor activation by triggering membrane release of its kinase inhibitor. *Genes & Development* 25: 232–237.
- Jakoby M, Wang HY, Reidt W, Weisshaar B, Bauer P. 2004. FRU (BHLH029) is required for induction of iron mobilization genes in *Arabidopsis thaliana*. *FEBS Letters* 577: 528–534.
- Jouanin S, Hamal A, Leprince A-S, Tregear J, Kreis M, Henry Y. 1999. Plant MAP kinase kinases structure, classification and evolution. *Gene* 233: 1–11.
- Ju CL, Yoon GM, Shemansky JM, Lin DY, Ying ZI, Chang JH, Garrett WM, Kessenbrock M, Groth G, Tucker ML *et al.* 2012. CTR1 phosphorylates the central regulator EIN2 to control ethylene hormone signaling from the ER membrane to the nucleus in *Arabidopsis*. *Proceedings of the National Academy of Sciences, USA* 109: 19486–19491.
- Kemp BE, Pearson RB. 1990. Protein-kinase recognition sequence motifs. *Trends in Biochemical Sciences* 15: 342–346.
- Kim T-W, Wang Z-Y. 2010. Brassinosteroid signal transduction from receptor kinases to transcription factors. *Annual Review of Plant Biology* 61: 681–704.
- Lampard GR, Macalister CA, Bergmann DC. 2008. *Arabidopsis* stomatal initiation is controlled by MAPK-mediated regulation of the bHLH SPEECHLESS. *Science* 322: 1113–1116.
- Le CTT, Brumbarova T, Ivanov R, Stoof C, Weber E, Mohrbacher J, Fink-Straube C, Bauer P. 2016. ZINC FINGER OF ARABIDOPSIS THALIANA12 (ZAT12) interacts with FER-LIKE IRON DEFICIENCY-INDUCED TRANSCRIPTION FACTOR (FIT) linking iron deficiency and oxidative stress responses. *Plant Physiology* 170: 540–557.
- Lee S-J, Lee MH, Kim J-I, Kim SY. 2015. *Arabidopsis* putative MAP kinase kinases Raf10 and Raf11 are positive regulators of seed dormancy and ABA response. *Plant and Cell Physiology* 56: 84–97.
- Li GJ, Meng XZ, Wang RG, Mao GH, Han L, Liu YD, Zhang SQ. 2012. Dual-level regulation of ACC synthase activity by MPK3/MPK6 cascade and its downstream WRKY transcription factor during ethylene induction in *Arabidopsis*. *PLoS Genetics* 8: e1002767.
- Li H, Ding Y, Shi Y, Zhang X, Zhang S, Gong Z, Yang S. 2017. MPK3- and MPK6-mediated ICE1 phosphorylation negatively regulates ICE1 stability and freezing tolerance in *Arabidopsis*. *Developmental Cell* 43: 630–642.
- Li S, Han X, Yang L, Deng X, Wu H, Zhang M, Liu Y, Zhang S, Xu J. 2017. Mitogen-activated protein kinases and calcium-dependent protein kinases are involved in wounding-induced ethylene biosynthesis in *Arabidopsis thaliana*. *Plant, Cell & Environment* 41: 134–147.
- Lingam S, Mohrbacher J, Brumbarova T, Potuschak T, Fink-Straube C, Blondet E, Genschik P, Bauer P. 2011. Interaction between the bHLH transcription factor FIT and ETHYLENE INSENSITIVE3/ETHYLENE INSENSITIVE3-LIKE1 reveals molecular linkage between the regulation of iron acquisition and ethylene signaling in *Arabidopsis*. *Plant Cell* 23: 1815–1829.
- Liu YD, Zhang SQ. 2004. Phosphorylation of 1-aminocyclopropane-1-carboxylic acid synthase by MPK6, a stress-responsive mitogen-activated protein kinase, induces ethylene biosynthesis in *Arabidopsis*. *Plant Cell* 16: 3386–3399.
- Lu Q, Helm S, Rödiger A, Baginsky S. 2015. On the extent of tyrosine phosphorylation in chloroplasts. *Plant Physiology* 169: 996–1000.
- Luo ML, Reyna S, Wang LS, Yi ZP, Carroll C, Dong LQ, Langlais P, Weintraub ST, Mandarino LJ. 2005. Identification of insulin receptor substrate 1 serine/threonine phosphorylation sites using mass spectrometry analysis: regulatory role of serine 1223. *Endocrinology* 146: 4410–4416.
- Maathuis FJ. 2008. Conservation of protein phosphorylation sites within gene families and across species. *Plant Signaling & Behavior* 3: 1011–1013.
- Mai HJ, Pateyron S, Bauer P. 2016. Iron homeostasis in *Arabidopsis thaliana*: transcriptomic analyses reveal novel FIT-regulated genes, iron deficiency marker genes and functional gene networks. *BMC Plant Biology* 16: e211.
- Marschner H, Romheld V, Kissel M. 1986. Different strategies in higher-plants in mobilization and uptake of iron. *Journal of Plant Nutrition* 9: 695–713.
- Meiser J, Lingam S, Bauer P. 2011. Posttranslational regulation of the iron deficiency basic helix–loop–helix transcription factor FIT is affected by iron and nitric oxide. *Plant Physiology* 157: 2154–2166.
- Mithoe SC, Boersema PJ, Berke L, Snel B, Heck AJR, Menke FLH. 2012. Targeted quantitative phosphoproteomics approach for the detection of phospho-tyrosine signaling in plants. *Journal of Proteome Research* 11: 438–448.
- Moorhead GW, Templeton GT, Tran H. 2006. Role of protein kinases, phosphatases and 14-3-3 proteins in the control of primary plant metabolism. In: Plaxton WC, McManus MT, eds. *Annual plant reviews volume 22: control of primary metabolism in plants*. Oxford, UK: Blackwell Publishing, 121–149.
- Muller K, Zurbriggen MD, Weber W. 2014. Control of gene expression using a red- and far-red light-responsive bi-stable toggle switch. *Nature Protocols* 9: 622–632.
- Nakagami H, Sugiyama N, Mochida K, Daudi A, Yoshida Y, Toyoda T, Tomita M, Ishihama Y, Shirasu K. 2010. Large-scale comparative phosphoproteomics identifies conserved phosphorylation sites in plants. *Plant Physiology* 153: 1161–1174.
- Naranjo-Arcos MA, Maurer F, Meiser J, Pateyron S, Fink-Straube C, Bauer P. 2017. Dissection of iron signaling and iron accumulation by overexpression of subgroup Ib bHLH039 protein. *Scientific Reports* 7: e10911.
- Ni WM, Xu SL, Chalkley RJ, Pham TND, Guan SH, Maltby DA, Burlingame AL, Wang ZY, Quail PH. 2013. Multisite light-induced phosphorylation of the transcription factor PIF3 is necessary for both its rapid degradation and concomitant negative feedback modulation of photoreceptor phyB levels in *Arabidopsis*. *Plant Cell* 25: 2679–2698.
- Oh M-H, Wang X, Kota U, Goshe MB, Clouse SD, Huber SC. 2009. Tyrosine phosphorylation of the BRI1 receptor kinase emerges as a component of brassinosteroid signaling in *Arabidopsis*. *Proceedings of the National Academy of Sciences, USA* 106: 658–663.
- Pearson RB, Kemp BE. 1991. Protein-kinase phosphorylation site sequences and consensus specificity motifs – tabulations. *Methods in Enzymology* 200: 62–81.
- Reits EA, Neeffjes JJ. 2001. From fixed to FRAP: measuring protein mobility and activity in living cells. *Nature Cell Biology* 3: E145.
- Remy I, Michnick SW. 2006. A highly sensitive protein–protein interaction assay based on *Gussia* luciferase. *Nature Methods* 3: 977–979.
- Ren YJ, Li YY, Jiang YQ, Wu BH, Miao Y. 2017. Phosphorylation of WHIRLY1 by CIPK14 shifts its localization and dual functions in *Arabidopsis*. *Molecular Plant* 10: 749–763.
- Robinson NJ, Procter CM, Connolly EL, Guerinot ML. 1999. A ferric-chelate reductase for iron uptake from soils. *Nature* 397: 694–697.
- Rudrabhatla P, Reddy MM, Rajasekharan R. 2006. Genome-wide analysis and experimentation of plant serine/threonine/tyrosine-specific protein kinases. *Plant Molecular Biology* 60: 293–319.
- Samodelov SL, Zurbriggen MD. 2017. Quantitatively understanding plant signaling: novel theoretical–experimental approaches. *Trends in Plant Sciences* 22: 685–704.
- Schlatter S, Rimann M, Kelm J, Fussenegger M. 2002. *SAMY*, a novel mammalian reporter gene derived from *Bacillus stearotheophilus* α -amylase. *Gene* 282: 19–31.
- Schwartz D, Gygi SP. 2005. An iterative statistical approach to the identification of protein phosphorylation motifs from large-scale data sets. *Nature Biotechnology* 23: 1391–1398.
- Silva RC, Castilho BA, Sattlegger E. 2018. A rapid extraction method for mammalian cell cultures, suitable for quantitative immunoblotting analysis of proteins, including phosphorylated GCN2 and eIF2 α . *MethodsX* 5: 75–82.
- Sivitz A, Grinvalds C, Barberon M, Curie C, Vert G. 2011. Proteasome-mediated turnover of the transcriptional activator FIT is required for plant iron-deficiency responses. *The Plant Journal* 66: 1044–1052.



New Phytologist Supporting Information Supplemental Figures Fig. S1-Fig. S5

Article title: **Phospho-mutant activity assays provide evidence for alternative phospho-regulation pathways of the transcription factor FIT**

Authors: Regina Gratz, Tzvetina Brumbarova, Rumen Ivanov, Ksenia Trofimov, Laura Tünnermann, Rocio Ochoa-Fernandez, Tim Blomeier, Johannes Meiser, Stefanie Weidtkamp-Peters, Matias Zurbriggen and Petra Bauer

Article acceptance date: 16 August 2019

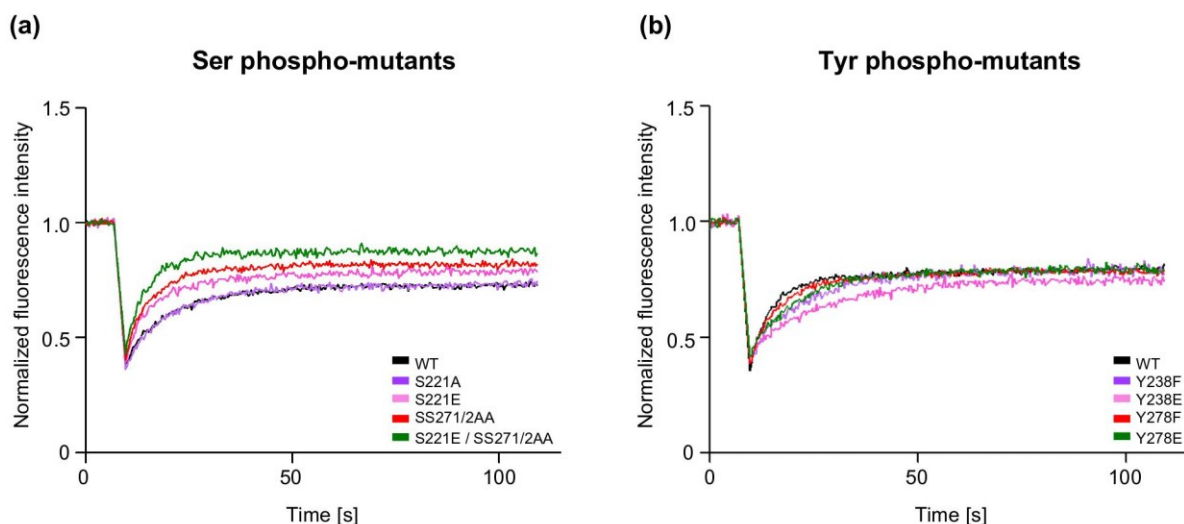


Figure S1. Kinetic plots and representative recordings for nuclear mobility assays of phospho-mutant FITm-GFP forms, as supplemental information for Fig. 3. Fluorescence Recovery after Photobleaching (FRAP) for (a), serine (Ser) and (b), tyrosine (Tyr) FITm-GFP phospho-mutants, compared to FIT-GFP. For every mutant, one recording of a representative bleach is shown. The background-corrected and normalized curve comprises the fluorescence intensity as a function of time. The fluorescence intensity is initially stable during the pre-bleach phase, reduced by more than 50 % during the bleach after 10 seconds and recovers during 10-15 seconds to reach a stable value. Nuclear mobility (Fig. 3) is calculated according to an equation presented by Bancaud et al. (2010), taking into account the intensity values (initial, postbleach, half recovered at half-time of recovery following the bleach, and end value of recovered).

Bancaud A, Huet S, Rabut G, Ellenberg J. 2010. Fluorescence perturbation techniques to study mobility and molecular dynamics of proteins in live cells: FRAP, photoactivation, photoconversion, and FLIP. *Cold Spring Harbor Protocols* **2010**(12): pdb.top90.

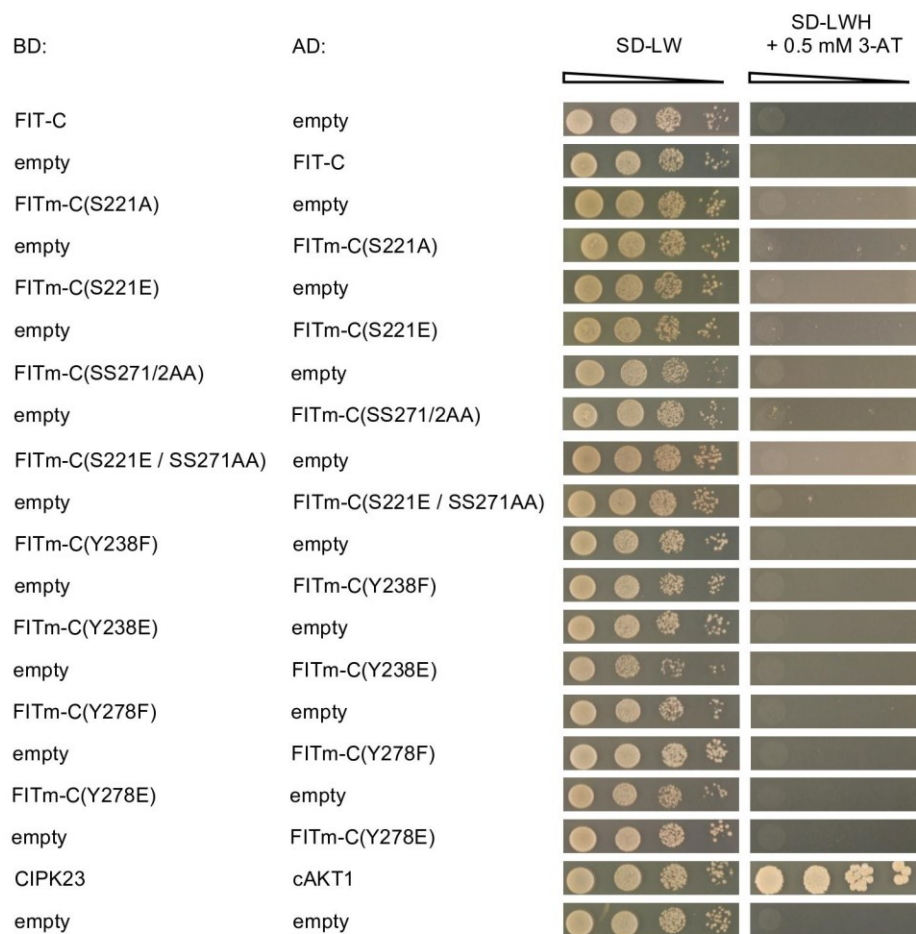


Figure S2. Controls for FIT and FITm homo-dimerization targeted yeast two-hybrid assays, as supplemental information for Fig. 4a. As negative controls for the yeast two hybrid assay, empty AD controls were used together with BD-FIT-C and BD-FITm-C, and empty BD controls together with AD-FIT-C and AD-FITm-C, using the procedure as described for Fig. 4a. BD-CIPK23 and AD-cAKT1 served as positive control.

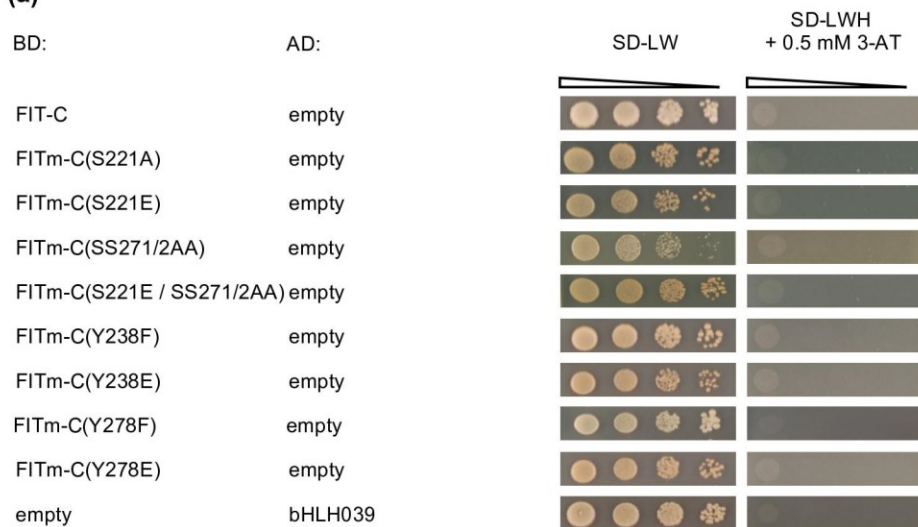
(a)**(b)**

Figure S3. Controls for FIT- and FITm-bHLH039 hetero-dimerization targeted yeast two-hybrid assays, as supplemental information for Fig. 5a. **(a)** Negative controls for the yeast two hybrid assays were conducted using empty AD together with BD-FIT-C, and BD-FITm-C and empty BD together with AD-bHLH039 plasmids for co-transformation, using the procedure as described for Fig. 5a. **(b)** FIT-C or FITm-C and bHLH039 hetero-dimerization by alternative BD/AD combination in a targeted yeast two-hybrid assay. The yeast assay was conducted as described for Fig. 5a using BD-bHLH039 and AD-FIT-C and AD-FITm-C plasmids for co-transformation. Negative controls of the assay are empty BD together with AD-FIT-C and AD-FITm-C, and both empty vectors. A positive control is BD-CIPK23 and AD-cAKT1.

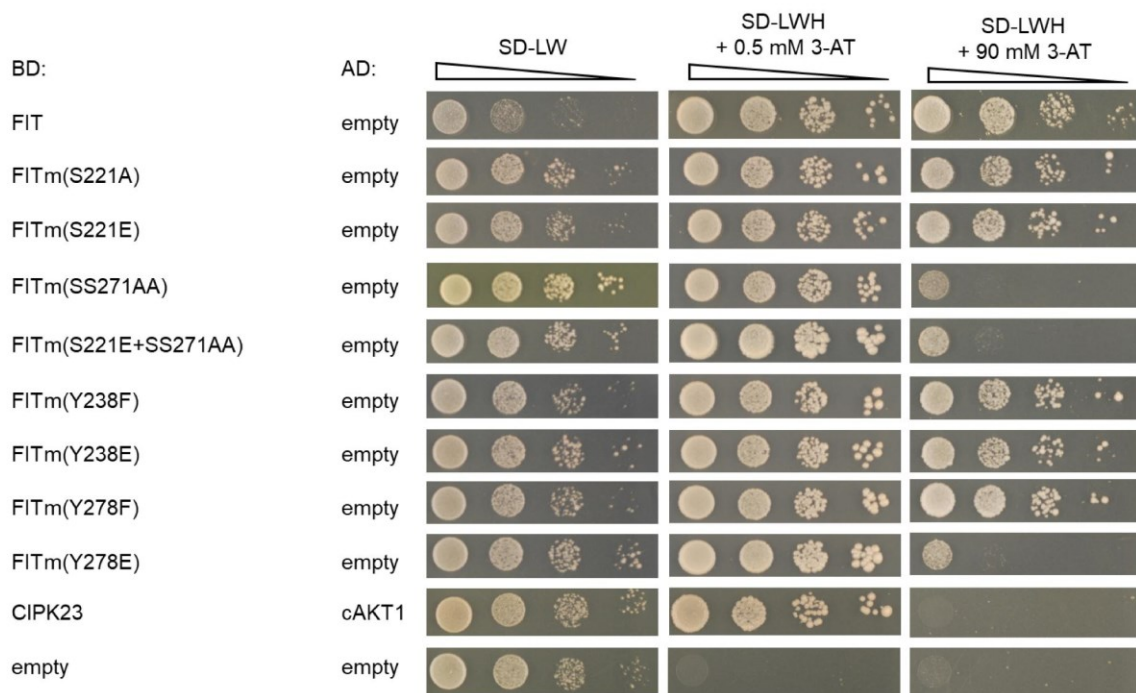


Figure S4. Transcriptional self-activation capacity differs in FIT phospho-mutants. A modified yeast two hybrid assay was conducted to test for self-activation of BD-FIT and BD-FITm phospho-mutant forms. Yeast strain AH109 was co-transformed with full-length BD-FIT or BD-FITm and AD-empty plasmids. A 10-fold dilution series was spotted ($OD_{600} = 1 \cdot 10^{-3}$) on selection media. Growth on synthetic defined media, lacking leucine and tryptophane (SD-LW), demonstrates a successful co-transformation. Media lacking L, W and histidine (SD-LWH,) supplemented with 3-amino-1,2,4-triazole (3-AT, 0.5 mM, 90 mM), selects for self-activation of the GAL4-transcription machinery by BD-FIT or BD-FITm at 90 mM 3-AT. BD-CIPK23 and AD-cAKT1 act as positive control at 0.5 mM 3-AT. Empty plasmids served as negative control.

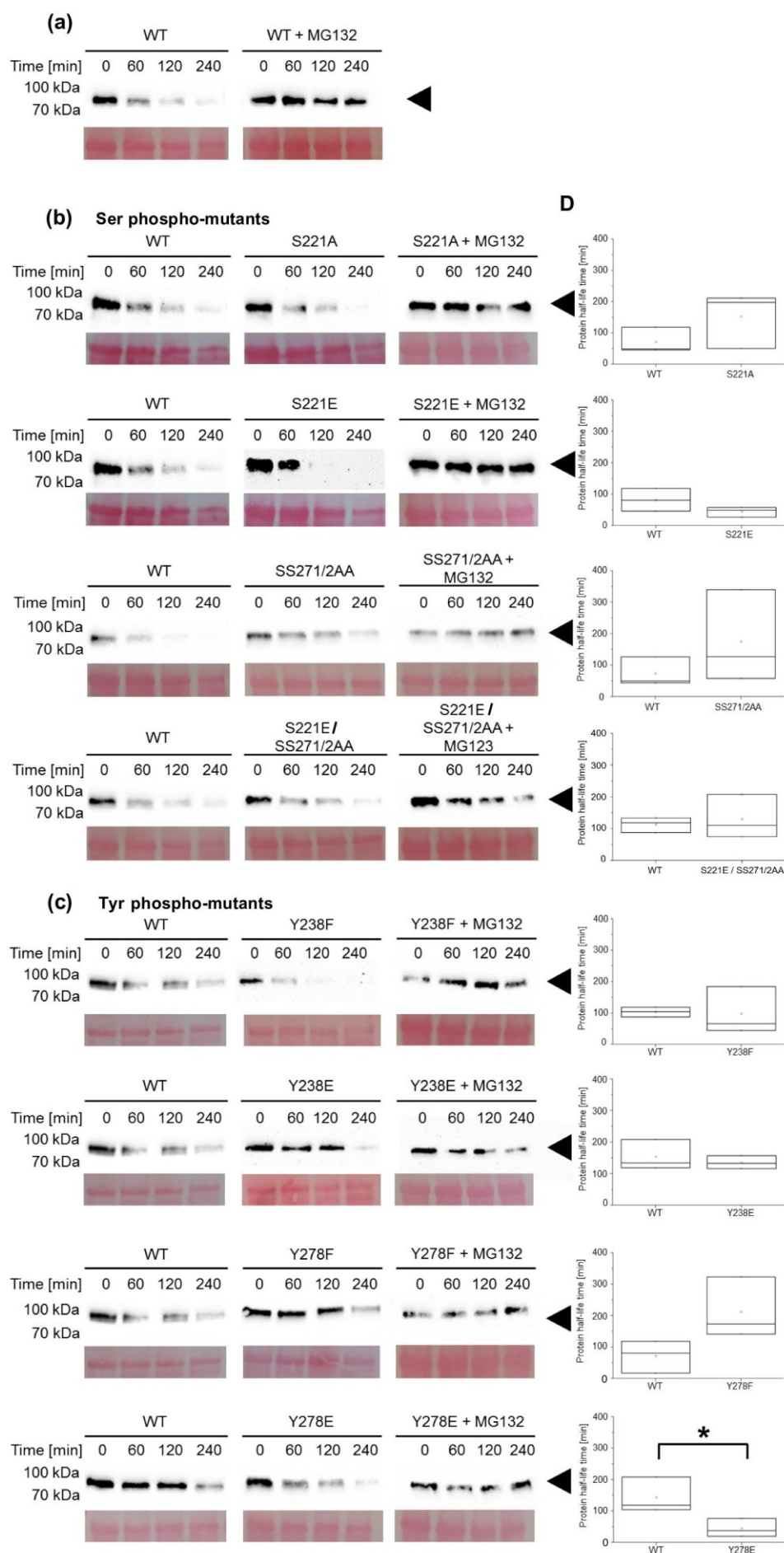


Figure S5. Immuno-blot analysis and half-life times for FIT-GFP and FITm-GFP forms in the quantified cell-free protein degradation assay, as supplemental information to Fig. 7. **(a-c)** One representative immunoblot experiment is shown, to follow protein degradation of **(a)**, FIT-GFP, **(b)**, serine (Ser) and, **(c)**, tyrosine (Tyr) FITm-GFP phospho-mutants, partially treated with the proteasomal-inhibitor MG132 (+MG132) and incubated at room temperature for 0, 60, 120 or 240 minutes. Equal amounts of protein were used for immunoblotting, FIT-GFP/FITm-GFP bands at 63 kDa. Ponceau S staining served as equal loading control. **(d)** Quantification of the immunoblot signal and calculation of half-life times for FIT-GFP and FITm-GFP. Data are represented as box-plots (n=3). Statistical significance was calculated using Student's *t*-test, and statistical differences are highlighted by asterisks ($P \leq 0.05$, n= 3).



New Phytologist Supporting Information Table S1

Article title: **Phospho-mutant activity assays provide evidence for alternative phospho-regulation pathways of the transcription factor FIT**

Authors: Regina Gratz, Tzvetina Brumbarova, Rumen Ivanov, Ksenia Trofimov, Laura Tünnermann, Rocio Ochoa-Fernandez, Tim Blomeier, Johannes Meiser, Stefanie Weidtkamp-Peters, Matias Zurbriggen and Petra Bauer

Article acceptance date: 16 August 2019

1

Table S1: List of recombinant plasmids and cloning procedures				
Site-directed Mutagenesis				
Plasmid name	Cloning method	Original plasmid	Primers for PCR	Template for PCR
pDONR207:gFITns ¹	Gateway	pDONR207 ²	FIT B1 FITns B2	Col-0 gDNA
pDONR207:gFITm(S221A)	S.-d. m.*	pDONR207:gFITns	FITm(S221A) Fw FITm(S221A)ns Rv	pDONR207:gFITns
pDONR207:gFITm(S221E)	S.-d. m.*	pDONR207:gFITns	FITm(S221E) Fw FITm(S221E)ns Rv	pDONR207:gFITns
pDONR207:gFITm(SS271/2AA) ¹	S.-d. m.*	pDONR207:gFITns	FITm(SS271/2AA) Fw FITm(SS271/2AA)ns Rv	pDONR207:gFITns
pDONR207:gFITm(Y238F)	S.-d. m.*	pDONR207:gFITns	FITm(Y238F) Fw FITm(Y238F)ns Rv	pDONR207:gFITns
pDONR207:gFITm(Y238E)	S.-d. m.*	pDONR207:gFITns	FITm(Y238E) Fw FITm(Y238E)ns Rv	pDONR207:gFITns
pDONR207:gFITm(Y278F)	S.-d. m.*	pDONR207:gFITns	FITm(Y278F) Fw FITm(Y278F)ns Rv	pDONR207:gFITns
pDONR207:gFITm(Y278E)	S.-d. m.*	pDONR207:gFITns	FITm(Y278E) Fw FITm(Y278E)ns Rv	pDONR207:gFITns
pDONR207:gFITm(S221E/SS271/2AA)	S.-d. m.*	pDONR207:gFITm(SS271/2AA)ns	FITm(S221E)Fw FITm(S221E)ns Rv	pDONR207:gFITns
Tobacco transient expression of fluorescent protein fusions				
Plasmid name	Cloning method	Original plasmid	- (= Gateway LR)	Template for Gateway LR
pMDC83:gFITns-GFP ¹	Gateway	pMDC83 ³	-	pDONR207:gFITns
pMDC83:gFITm(S221A)ns-GFP	Gateway	pMDC83 ³	-	pDONR207:gFITm(S221A)ns
pMDC83:gFITm(S221E)ns-GFP	Gateway	pMDC83 ³	-	pDONR207:gFITm(S221E)ns
pMDC83:gFITm(SS271/2AA)ns-GFP ¹	Gateway	pMDC83 ³	-	pDONR207:gFITm(SS271/2AA)ns
pMDC83:gFITm(Y238F)ns-GFP	Gateway	pMDC83 ³	-	pDONR207:gFITm(Y238F)ns

2

pMDC83:gFITm(Y238E)ns-GFP	Gateway	pMDC83 ³	-	pDONR207:gFITm(Y238E)ns
pMDC83:gFITm(Y278F)ns-GFP	Gateway	pMDC83 ³	-	pDONR207:gFITm(Y278F)ns
pMDC83:gFITm(Y278E)ns-GFP	Gateway	pMDC83 ³	-	pDONR207:gFITm(Y278E)ns
pMDC83:gFITm(S221E/SS271/2AA)ns-GFP	Gateway	pMDC83 ³	-	pDONR207:gFITm(S221E/SS271/2AA)ns
Tobacco transient expression FRET experiments				
Plasmid name	Cloning method	Original plasmid	Primers for PCR or – (= Gateway LR)	Template for PCR or Gateway LR
pDONR207:FITns ¹	Gateway	pDONR207 ²	FIT B1 FITns B2	cDNA tobacco/ transformed with pMDC83:gFITns-GFP
pDONR207:FITm(S221A)ns	Gateway	pDONR207 ²	FIT B1 FITns B2	cDNA tobacco/ transformed with pMDC83:gFITm(S221A)ns-GFP
pDONR207:FITm(S221E)ns	Gateway	pDONR207 ²	FIT B1 FITns B2	cDNA tobacco/ transformed with pMDC83:gFITm(S221E)ns-GFP
pDONR207:FITm(SS271/2AA)ns ¹	Gateway	pDONR207 ²	FIT B1 FITns B2	cDNA tobacco/ transformed with pMDC83:gFITm(SS271/2AA)ns-GFP
pDONR207:FITm(Y238F)ns	Gateway	pDONR207 ²	FIT B1 FITns B2	cDNA tobacco/ transformed with pMDC83:gFITm(Y238F)ns-GFP
pDONR207:FITm(Y238E)ns	Gateway	pDONR207 ²	FIT B1 FITns B2	cDNA tobacco/ transformed with pMDC83:gFITm(Y238E)ns-GFP
pDONR207:FITm(Y278F)ns	Gateway	pDONR207 ²	FIT B1 FITns B2	cDNA tobacco/ transformed with pMDC83:gFITm(Y278F)ns-GFP
pDONR207:FITm(Y278E)ns	Gateway	pDONR207 ²	FIT B1 FITns B2	cDNA tobacco/ transformed with pMDC83:gFITm(Y278E)ns-GFP
pDONR207:gFITm(S221E/SS271/2AA)ns	Gateway	pDONR207 ²	FIT B1 FITns B2	cDNA tobacco/ transformed with pMDC83:gFITm(S221E/SS271/2AA) ns-GFP
pABind:FIT-GFP ¹	Gateway	pABindGFP ⁴	-	pDONR207:FITns
pABind:FITm(S221A)-GFP	Gateway	pABindGFP ⁴	-	pDONR207:FITm(S221A)ns
pABind:FITm(S221E)-GFP	Gateway	pABindGFP ⁴	-	pDONR207:FITm(S221E)ns
pABind:FITm(SS271/2AA)-GFP ¹	Gateway	pABindGFP ⁴	-	pDONR207:FITm(SS271/2AA)ns
pABind:FITm(Y238F)-GFP	Gateway	pABindGFP ⁴	-	pDONR207:FITm(Y238F)ns
pABind:FITm(Y238E)-GFP	Gateway	pABindGFP ⁴	-	pDONR207:FITm(Y238E)ns

3

pABind:FITm(Y278F)-GFP	Gateway	pABindGFP ⁴	-	pDONR207:FITm(Y278F)ns
pABind:FITm(Y278E)-GFP	Gateway	pABindGFP ⁴	-	pDONR207:FITm(Y278E)ns
pABind:FITm(S221E/SS271/2AA)-GFP	Gateway	pABindGFP ⁴	-	pDONR207:gFITm(S221E/SS271/2AA)ns
pABind:FIT-mCherry ¹	Gateway	pABindmCherry ⁴	-	pDONR207:FITns
pABind:FITm(S221A)-mCherry	Gateway	pABindmCherry ⁴	-	pDONR207:FITm(S221A)ns
pABind:FITm(S221E)-mCherry	Gateway	pABindmCherry ⁴	-	pDONR207:FITm(S221E)ns
pABind:FITm(SS271/2AA)-mCherry ¹	Gateway	pABindmCherry ⁴	-	pDONR207:FITm(SS271/2AA)ns
pABind:FITm(Y238F)-mCherry	Gateway	pABindmCherry ⁴	-	pDONR207:FITm(Y238F)ns
pABind:FITm(Y238E)-mCherry	Gateway	pABindmCherry ⁴	-	pDONR207:FITm(Y238E)ns
pABind:FITm(Y278F)-mCherry	Gateway	pABindmCherry ⁴	-	pDONR207:FITm(Y278F)ns
pABind:FITm(Y278E)-mCherry	Gateway	pABindmCherry ⁴	-	pDONR207:FITm(Y278E)ns
pABind:FITm(S221E/SS271/2AA)-mCherry	Gateway	pABindmCherry ⁴	-	pDONR207:gFITm(S221E/SS271/2AA)ns
pABind:FIT-GFP-mCherry ¹	Gateway	pABindFRET ⁴	-	pDONR207:FITns
pABind:FITm(S221A)-GFP-mCherry	Gateway	pABindFRET ⁴	-	pDONR207:FITm(S221A)ns
pABind:FITm(S221E)-GFP-mCherry	Gateway	pABindFRET ⁴	-	pDONR207:FITm(S221E)ns
pABind:FITm(SS271/2AA)-GFP-mCherry ¹	Gateway	pABindFRET ⁴	-	pDONR207:FITm(SS271/2AA)ns
pABind:FITm(Y238F)-GFP-mCherry	Gateway	pABindFRET ⁴	-	pDONR207:FITm(Y238F)ns
pABind:FITm(Y238E)-GFP-mCherry	Gateway	pABindFRET ⁴	-	pDONR207:FITm(Y238E)ns
pABind:FITm(Y278F)-GFP-mCherry	Gateway	pABindFRET ⁴	-	pDONR207:FITm(Y278F)ns
pABind:FITm(Y278E)-GFP-mCherry	Gateway	pABindFRET ⁴	-	pDONR207:FITm(Y278E)ns

4

pABind:FITm(S221E/SS271/2AA)-GFP-mCherry	Gateway	pABindFRET ⁴	-	pDONR207:gFITm(S221E/SS271/2AA)ns
pDONR207:bHLH039ns ¹	Gateway	pDONR207 ²	bHLH039 B1 bHLH039ns B2	Fe-deficient Col-0 root cDNA
pABind:bHLH039-GFP ¹	Gateway	pABindGFP ⁴	-	pDONR207:bHLH039ns
pABind:bHLH039-GFP-mCherry ¹	Gateway	pABindFRET ⁴	-	pDONR207:bHLH039ns
Yeast assays				
Plasmid name	Cloning method	Original plasmid	Primers for PCR or – (Gateway LR)	Template for PCR or Gateway LR
pDONR207:FIT-Cst ¹	Gateway	pDONR207 ²	FIT-C B1 FITst B2	pDONR207:FITns
pDONR207:FIT-Cm(S221A)st	Gateway	pDONR207 ²	FIT-C B1 FITst B2	pDONR207:FITm(S221A)ns
pDONR207:FIT-Cm(S221E)st	Gateway	pDONR207 ²	FIT-C B1 FITst B2	pDONR207:FITm(S221E)ns
pDONR207:FIT-Cm(SS271/2AA)st ¹	Gateway	pDONR207 ²	FIT-C B1 FITst B2	pDONR207:FITm(SS271/2AA)ns
pDONR207:FIT-Cm(Y238F)st	Gateway	pDONR207 ²	FIT-C B1 FITst B2	pDONR207:FITm(Y238F)ns
pDONR207:FIT-Cm(Y238E)st	Gateway	pDONR207 ²	FIT-C B1 FITst B2	pDONR207:FITm(Y238E)ns
pDONR207:FIT-Cm(Y278F)st	Gateway	pDONR207 ²	FIT-C B1 FITst B2	pDONR207:FITm(Y278F)ns
pDONR207:FIT-Cm(Y278E)st	Gateway	pDONR207 ²	FIT-C B1 FITst B2	pDONR207:FITm(Y278E)ns
pDONR207: FIT-Cm(S221E/SS271/2AA)st	Gateway	pDONR207 ²	FIT-C B1 FITst B2	pDONR207:FITm(S221E/SS271/2AA)ns
pDONR207:FITst ¹	Gateway	pDONR207 ²	FIT B1 FITst B2	pDONR207:FITns
pDONR207:FITm(S221A)st	Gateway	pDONR207 ²	FIT B1 FITst B2	pDONR207:FITm(S221A)ns
pDONR207:FITm(S221E)st	Gateway	pDONR207 ²	FIT B1	pDONR207:FITm(S221E)ns

5

pDONR207:FITm(SS271/2AA)st ¹	Gateway	pDONR207 ²	FITst B2 FIT B1 FITst B2	pDONR207:FITm(SS271/2AA)ns
pDONR207:FITm(Y238F)st	Gateway	pDONR207 ²	FIT B1 FITst B2	pDONR207:FITm(Y238F)ns
pDONR207:FITm(Y238E)st	Gateway	pDONR207 ²	FIT B1 FITst B2	pDONR207:FITm(Y238E)ns
pDONR207:FITm(Y278F)st	Gateway	pDONR207 ²	FIT B1 FITst B2	pDONR207:FITm(Y278F)ns
pDONR207:FITm(Y278E)st	Gateway	pDONR207 ²	FIT B1 FITst B2	pDONR207:FITm(Y278E)ns
pDONR207:FITm(S221E/SS271/2AA)st	Gateway	pDONR207 ²	FIT B1 FITst B2	pDONR207:gFITm(S221E/SS271/2AA)ns
pDONR207:bHLH039st ¹	Gateway	pDONR207 ²	bHLH039 B1 bHLH039st B2	pDONR207:bHLH039ns
pGBKT7-GW:FIT-C ¹	Gateway	pGBKT7-GW ⁵	-	pDONR207:FIT-Cst
pGBKT7-GW:FIT-Cm(S221A)	Gateway	pGBKT7-GW ⁵	-	pDONR207:FIT-Cm(S221A)st
pGBKT7-GW:FIT-Cm(S221E)	Gateway	pGBKT7-GW ⁵	-	pDONR207:FIT-Cm(S221E)st
pGBKT7-GW:FIT-Cm(SS271/2AA) ¹	Gateway	pGBKT7-GW ⁵	-	pDONR207:FIT-Cm(SS271/2AA)st
pGBKT7-GW:FIT-Cm(Y238F)	Gateway	pGBKT7-GW ⁵	-	pDONR207:FIT-Cm(Y238F)st
pGBKT7-GW:FIT-Cm(Y238E)	Gateway	pGBKT7-GW ⁵	-	pDONR207:FIT-Cm(Y238E)st
pGBKT7-GW:FIT-Cm(Y278F)	Gateway	pGBKT7-GW ⁵	-	pDONR207:FIT-Cm(Y278F)st
pGBKT7-GW:FIT-Cm(Y278E)	Gateway	pGBKT7-GW ⁵	-	pDONR207:FIT-Cm(Y278E)st
pGBKT7-GW:FIT-Cm(S221E/SS271/2AA)	Gateway	pGBKT7-GW ⁵	-	pDONR207: FIT-Cm(S221E/SS271/2AA)st
pGBKT7-GW:bHLH039 ¹	Gateway	pGBKT7-GW ⁵	-	pDONR207:bHLH039st
pACT2-GW:FIT-C ¹	Gateway	pACT2-GW ⁵	-	pDONR207:FITst
pACT2-GW:FIT-Cm(S221A)	Gateway	pACT2-GW ⁵	-	pDONR207:FITm(S221A)st
pACT2-GW:FIT-Cm(S221E)	Gateway	pACT2-GW ⁵	-	pDONR207:FITm(S221E)st
pACT2-GW:FIT-Cm(SS271/2AA) ¹	Gateway	pACT2-GW ⁵	-	pDONR207:FITm(SS271/2AA)st
pACT2-GW:FIT-Cm(Y238F)	Gateway	pACT2-GW ⁵	-	pDONR207:FITm(Y238F)st

6

pACT2-GW:FIT-Cm(Y238E)	Gateway	pACT2-GW ⁵	-	pDONR207:FITm(Y238E)st
pACT2-GW:FIT-Cm(Y278F)	Gateway	pACT2-GW ⁵	-	pDONR207:FITm(Y278F)st
pACT2-GW:FIT-Cm(Y278E)	Gateway	pACT2-GW ⁵	-	pDONR207:FITm(Y278E)st
pACT2-GW:FIT-Cm(SS21E/SS271/2AA)	Gateway	pACT2-GW ⁵	-	pDONR207:gFITm(SS21E/SS271/2AA)st
pACT2-GW:bHLH039 ¹	Gateway	pACT2-GW ⁵	-	pDONR207:bHLH039st
pGBKT7-GW:FIT ¹	Gateway	pGBKT7-GW ⁵	-	pDONR207:FITst
pGBKT7-GW:FITm(S221A)	Gateway	pGBKT7-GW ⁵	-	pDONR207:FITm(S221A)st
pGBKT7-GW:FITm(S221E)	Gateway	pGBKT7-GW ⁵	-	pDONR207:FITm(S221E)st
pGBKT7-GW:FITm(SS271/2AA) ¹	Gateway	pGBKT7-GW ⁵	-	pDONR207:FITm(SS271/2AA)st
pGBKT7-GW:FITm(Y238F)	Gateway	pGBKT7-GW ⁵	-	pDONR207:FITm(Y238F)st
pGBKT7-GW:FITm(Y238E)	Gateway	pGBKT7-GW ⁵	-	pDONR207:FITm(Y238E)st
pGBKT7-GW:FITm(Y278F)	Gateway	pGBKT7-GW ⁵	-	pDONR207:FITm(Y278F)st
pGBKT7-GW:FITm(Y278E)	Gateway	pGBKT7-GW ⁵	-	pDONR207:FITm(Y278E)st
pGBKT7-GW:FITm(SS21E/SS271/2AA)	Gateway	pGBKT7-GW ⁵	-	pDONR207:FITm(SS21E/SS271/2AA)st
Mammalian transactivation assay				
Plasmid name	Cloning method	Original plasmid	Primers for PCR or – (Gateway LR)	Template for PCR or Gateway LR
pMZ333:FIT	AQUA	pMZ333 ⁶	aqFIT Fw aqFIT Rv	pDONR207:FITns
pMZ333:FITm(S221A)	AQUA	pMZ333 ⁶	aqFIT Fw aqFIT Rv	pDONR207:FITm(S221A)ns
pMZ333:FITm(S221E)	AQUA	pMZ333 ⁶	aqFIT Fw aqFIT Rv	pDONR207:FITm(S221E)ns
pMZ333:FITm(SS271/2AA)	AQUA	pMZ333 ⁶	aqFIT Fw aqFIT Rv	pDONR207:FITm(SS271/2AA)ns
pMZ333:FITm(Y238F)	AQUA	pMZ333 ⁶	aqFIT Fw aqFIT Rv	pDONR207:FITm(Y238F)ns
pMZ333:FITm(Y238E)	AQUA	pMZ333 ⁶	aqFIT Fw aqFIT Rv	pDONR207:FITm(Y238E)ns

7

pMZ333:FITm(Y278F)	AQUA	pMZ333 ⁶	aqFIT Fw aqFIT Rv	pDONR207:FITm(Y278F)ns
pMZ333:FITm(Y278E)	AQUA	pMZ333 ⁶	aqFIT Fw aqFIT Rv	pDONR207:FITm(Y278E)ns
pMZ333:gFITm(SS21E/SS271/2AA)	AQUA	pMZ333 ⁶	aqFIT Fw aqFIT Rv	pDONR207:gFITm(SS21E/SS271/2AA)ns
pMZ333:bHLH039	AQUA	pMZ333 ⁶	aqBHLH039 Fw aqBHLH039 Rv	pDONR207:bHLH039ns
pHB007:BF ⁶	Gibson	pMZ333 ⁶	oHB018 oHB019	h-mTagBF ² cDNA
pKM195:IRT1 _{pro}	AQUA	pKM195 ⁶	aqIRT1 _{pro} Fw aqIRT1 _{pro} Rv	Col-0 gDNA
pMZ333:FIT-GFP	AQUA	pMZ333 ⁶	aqFIT Fw aqGFP Rv	pMDC83:gFITns-GFP
pMZ333:FITm(S221A)-GFP	AQUA	pMZ333 ⁶	aqFIT Fw aqGFP Rv	pMDC83:gFITm(S221A)ns-GFP
pMZ333:FITm(S221E)-GFP	AQUA	pMZ333 ⁶	aqFIT Fw aqGFP Rv	pMDC83:gFITm(S221E)ns-GFP
pMZ333:FITm(SS271/2AA)-GFP	AQUA	pMZ333 ⁶	aqFIT Fw aqGFP Rv	pMDC83:gFITm(SS271/2AA)ns-GFP
pMZ333:FITm(Y238F)-GFP	AQUA	pMZ333 ⁶	aqFIT Fw aqGFP Rv	pMDC83:gFITm(Y238F)ns-GFP
pMZ333:FITm(Y238E)-GFP	AQUA	pMZ333 ⁶	aqFIT Fw aqGFP Rv	pMDC83:gFITm(Y238E)ns-GFP
pMZ333:FITm(Y278F)-GFP	AQUA	pMZ333 ⁶	aqFIT Fw aqGFP Rv	pMDC83:gFITm(Y278F)ns-GFP
pMZ333:FITm(Y278E)-GFP	AQUA	pMZ333 ⁶	aqFIT Fw aqGFP Rv	pMDC83:gFITm(Y278E)ns-GFP
pMZ333:gFITm(SS21E/SS271/2AA)-GFP	AQUA	pMZ333 ⁶	aqFIT Fw aqGFP Rv	pMDC83:gFITm(SS21E/SS271/2AA)ns-GFP
pMZ333:HA ₃ -bHLH039	AQUA	pMZ333 ⁶	aqHA ₃ Fw aqBHLH039 Rv	pAlligator:HA ₃ -gBHLH039 ⁷

8

*S.-d. m.= Site-directed mutagenesis

References for plasmids:

- ¹Gratz R, Manishankar P, Ivanov R, Koster P, Mohr I, Trofimov K, Steinhorst L, Meiser J, Mai HJ, Drerup M, et al. 2019. CIPK11-Dependent Phosphorylation Modulates FIT Activity to Promote Arabidopsis Iron Acquisition in Response to Calcium Signaling. *Dev Cell* 48: 726-740 e710.
- ²Thermo Fisher Scientific, Gateway cloning
- ³Curtis MD and Grossniklaus U. 2003. A Gateway cloning vector set for high-throughput functional analysis of genes in planta. *Plant Physiology* 133: 562-469.
- ⁴Hecker A, Wallmeroth N, Peter S, Blatt MR, Harter K, Grefen C. 2015. Binary 2in1 Vectors Improve in Planta (Co)localization and Dynamic Protein Interaction Studies. *Plant Physiology* 168: 776–787
- ⁵provided by Dr. Yves Jacob
- ⁶Beyer HM, Gonschorek P, Samodelov SL, Meier M, Weber W, Zurbriggen MD. 2015. AQUA Cloning: A Versatile and Simple Enzyme-Free Cloning Approach. *PLoS One* 10: e0137652.
- ⁷Naranjo-Arcos MA, Maurer F, Meiser J, Pateyron S, Fink-Straube C, Bauer P. 2017. Dissection of iron signaling and iron accumulation by overexpression of subgroup Ib bHLH039 protein. *Scientific Reports* 7:10911.

All other recombinant plasmids were generated in this work. Descriptions and references for the cloning methods are provided in the Materials and Methods section of the main text.



New Phytologist Supporting Information Table S2

Article title: **Phospho-mutant activity assays provide evidence for alternative phosphoregulation pathways of the transcription factor FIT**

Authors: Regina Gratz, Tzvetina Brumbarova, Rumen Ivanov, Ksenia Trofimov, Laura Tünnermann, Rocio Ochoa-Fernandez, Tim Blomeier, Johannes Meiser, Stefanie Weidtkamp-Peters, Matias Zurbriggen and Petra Bauer

Article acceptance date: 16 August 2019

Table S2: List of primers for recombinant vector generation in alphabetical order	
Primer Name	Primer Sequence (5' ... 3')
aqBHLH039 Fw	TTTGTCTTTTATTTTCAGGTCCCGGATCGAATTATGT GTGCATTAGTACCTCC
aqBHLH039st Rv	TGTCTGGATCGAAGCTTGGGCTGCAGGTCGACTCA TATATATGAGTTTCCAC
aqFIT Fw	TTTGTCTTTTATTTTCAGGTCCCGGATCGAATTATGG AAGGAAGAGTCAACGC
aqFITst Rv	TGTCTGGATCGAAGCTTGGGCTGCAGGTCGACTCA AGTAAATGACTTGATGA
aqGFP Rv	TGTCTGGATCGAAGCTTGGGCTGCAGGTCGACTTA GTGGTGGTGGTGGTGGT
aqHA ₃ Fw	TTTGTCTTTTATTTTCAGGTCCCGGATCGAATTATGG CATACCCATACGACGT
aqIRT1 _{pro} Fw	TTCCCCGAAAAGTGCCACCTGACGTCGTCGACTAG GAGCACATGGATTGACACAT
aqIRT1 _{pro} Rv	CACTAAACGAGCTCTGCTTATATAGGGCTAGCAG ATTGTTTAATGTTTGTGT
bHLH039 B1	GGGGACAAGTTTGTACAAAAAAGCAGGCTTCATG TGTGCATTAGTACCTC
bHLH039ns B2	GGGGACCACTTTGTACAAGAAAGCTGGGTCTATA TATGAGTTTCCAC
bHLH039st B2	GGGGACCACTTTGTACAAGAAAGCTGGGTCTCAT ATATATGAGTTTCCAC
FIT B1	GGGGACAAGTTTGTACAAAAAAGCAGGCTTAATG GAAGGAAGAGTCAACGC
FIT-C B1	GGGGACAAGTTTGTACAAAAAAGCAGGCTTAACT CAACCTTTTCGCGGTATC
FITm(S221A) Fw	TATCAATCCTCCTGCAGCCAAAAAATCATTCA
FITm(S221A)ns Rv	TGAATGATTTTTTTGGCTGCAGGAGGATTGATA
FITm(S221E) Fw	TATCAATCCTCCTGCAGAGAAAAAATCATTCA

FITm(S221E)ns Rv	TGAATGATTTTTTCTCTGCAGGAGGATTGATA
FITm(SS271/2AA) Fw	CAGAACTCTAACCTAGCCGCTCCTTCTCCGGACA
FITm(SS271/2AA)ns Rv	TGTCCGGAGAAGGAGCGGCTAGGTTAGAGTTCTG
FITm(Y238E) Fw	GAGGAGAAAGGGTTTGAAGTGAGATTGGTGTGT
FITm(Y238E)ns Rv	ACACACCAATCTCACTTCAAACCCTTTCTCCTC
FITm(Y238F) Fw	GAGGAGAAAGGGTTTTTTGTGAGATTGGTGTGT
FITm(Y238F)ns Rv	ACACACCAATCTCACAAAAACCCTTTCTCCTC
FITm(Y278E) Fw	CCTTCTCCGGACACAGAGCTCTTAACATATAACC
FITm(Y278E)ns Rv	GGTATATGTTAAGAGCTCTGTGTCCGGAGAAGG
FITm(Y278F) Fw	CCTTCTCCGGACACATTCCTCTTAACATATAACC
FITm(Y278F)ns Rv	GGTATATGTTAAGAGGAATGTGTCCGGAGAAGG
FITns B2	GGGGACCACTTTGTACAAGAAAGCTGGGTTAGTA AATGACTTGATGAATTC
FITst B2	GGGGACCACTTTGTACAAGAAAGCTGGGTTTCAA GTAAATGACTTGATGA
oHB018 Fw	CTTTTTGTCTTTTATTTTCAGGTCCCGGATCGAATTG CGGCCGCAGGAGGCGCCACCATGAGCGAGGAACT GATCAAAGAAAACATGC
oHB019 Rv	TCATGTCTGGATCGAAGCTTGGGCTGCAGGTCGAC TCTAGATTAGTTCAGCTTGTGGCCCAGCTTAGAAG

Author contributions to Paper IIKsenia Trofimov

Performed and analyzed following experiments: FRET-APB measurements (Figure 4B, 4C, 5B, 5C). Contributed to following experiments: cytoplasm-to-nucleus signal ratio quantification (Figure 2A, 2B). Contributed to the writing of the methods section.

Regina Gratz

Conceptualization of study. Designed, performed, and analyzed remaining experiments. Wrote the manuscript, prepared final figures, and reviewed/edited the manuscript.

Tzvetina Brumbarova, Rumen Ivanov

Conceptualization of study. Helped in designing, performing, and analyzing experiments, supervised the study, and reviewed/edited the manuscript.

Laura Tünnermann

Performed and analyzed degradation assays.

Rocio Ochoa-Fernandez, Tim Blomeier

Helped designing, performing, and analyzing the quantitative transactivation reporter gene assay.

Johannes Meiser

Helped designing the phospho-mutants approach.

Stefanie Weidtkamp-Peters

Supervised the study and assisted in microscopy.

Matias Zurbriggen

Conceptualization of study. Supervised and provided help for the quantitative transactivation reporter gene assay. Provided funding.

Petra Bauer

Conceptualization of study. Analyzed data. Designed the outline of the manuscript, supervised the study, provided funding, and reviewed/edited the manuscript.

8 Paper III

Mobility and localization of the iron deficiency-induced transcription factor bHLH039 change in the presence of FIT

Received: 6 November 2019 | Accepted: 12 November 2019

DOI: 10.1002/pld3.190

ORIGINAL RESEARCH

American Society
of Plant Biologists
Celebrating a better future through plant biology research

WILEY

Mobility and localization of the iron deficiency-induced transcription factor bHLH039 change in the presence of FIT

Ksenia Trofimov¹ | Rumen Ivanov¹ | Monique Eutebach¹ | Büsra Acaroglu¹ |
Inga Mohr¹ | Petra Bauer^{1,2} | Tzvetina Brumbarova¹

¹Institute of Botany, Heinrich Heine University, Düsseldorf, Germany

²Cluster of Excellence on Plant Sciences, Heinrich Heine University, Düsseldorf, Germany

Correspondence

Petra Bauer and Tzvetina Brumbarova, Institute of Botany, Heinrich Heine University, Düsseldorf 40225, Germany. Emails: Petra.Bauer@uni-duesseldorf.de (P.B.); Tzvetina.Brumbarova@uni-duesseldorf.de (T.B.)

Funding information

Deutsche Forschungsgemeinschaft, Grant/Award Number: 267205415; Germany's Excellence Strategy, Grant/Award Number: EXC 2048 and /1

Abstract

Regulation of iron (Fe) acquisition and homeostasis is critical for plant survival. In Arabidopsis, Fe deficiency-induced bHLH039 forms a complex with the master regulator FIT and activates it to upregulate Fe acquisition genes. FIT is partitioned between cytoplasm and nucleus, whereby active FIT accumulates more in the nucleus than inactive FIT. At the same time, there is so far no information on the subcellular localization of bHLH039 protein and how it is controlled. We report here that the bHLH039 localization pattern changes depending on the presence of FIT in the cell. When expressed in cells lacking FIT, bHLH039 localizes predominantly in the cytoplasm, including cytoplasmic foci in close proximity to the plasma membrane. The presence of FIT enhances the mobility of bHLH039 and redirects the protein toward primarily nuclear localization, abolishing its accumulation in cytoplasmic foci. This FIT-dependent change in localization of bHLH039 found in transient fluorescent protein expression experiments was confirmed in both leaves and roots of Arabidopsis transgenic plants, stably expressing hemagglutinin-tagged bHLH039 in wild-type or *fit* mutant background. This posttranslational mechanism for intracellular partitioning of Fe-responsive transcription factors suggests a signaling cascade that translates Fe sensing at the plasma membrane to nuclear accumulation of the transcriptional regulators.

KEYWORDS

bHLH039, Fer-like iron deficiency-induced transcription factor, iron deficiency, nucleocytoplasmic partitioning, transcription factor regulation

1 | INTRODUCTION

Iron (Fe) is an essential element in plants as it participates in key redox reactions. Changes in metabolism due to execution of developmental programs or in response to environmental cues result in major rebalancing of the cellular and plant Fe homeostasis. Fe acquisition

in Arabidopsis (*Arabidopsis thaliana*) and other Strategy I plants requires active proton extrusion to solubilize Fe in the soil, the reduction of Fe³⁺ to Fe²⁺ by the ferric reductase-oxidase 2 (FRO2) and the subsequent uptake of Fe²⁺ in the root epidermis cells by the metal transporter iron-regulated transporter 1 (IRT1) (Brumbarova, Bauer, & Ivanov, 2015; Jeong, Merkovich, Clyne, & Connolly, 2017). The

Trofimov and Ivanov contributed equally to this article.

This is an open access article under the terms of the Creative Commons Attribution-NonCommercial License, which permits use, distribution and reproduction in any medium, provided the original work is properly cited and is not used for commercial purposes.

© 2019 The Authors. *Plant Direct* published by American Society of Plant Biologists and the Society for Experimental Biology and John Wiley & Sons Ltd

execution of this strategy under Fe deficiency requires the essential basic helix–loop–helix (bHLH) transcription factor Fer-like iron deficiency-induced transcription factor (FIT) (Colangelo & Guerinot, 2004; Jakoby, Wang, Reidt, Weisshaar, & Bauer, 2004). Members of the bHLH subgroup Ib, *BHLH038*, *BHLH039*, *BHLH100*, and *BHLH101* (Heim et al., 2003) are induced by Fe deficiency in roots and leaves (Vorwieger et al., 2007; Wang et al., 2007), controlled by a network of transcription factors (Gao, Robe, Gaymard, Izquierdo, & Dubos, 2019). *BHLH039* induction serves as one of the robust Fe deficiency markers (Gratz, Manishankar, et al., 2019; Ivanov, Brumbarova, & Bauer, 2012; Khan et al., 2019). Each of the four members can interact with FIT, resulting in an active protein complex for upregulation of Fe uptake genes, with *BHLH039* playing the most prominent role among them (Wang et al., 2013; Yuan et al., 2008).

The nucleocytoplasmic partitioning of proteins is an important regulatory aspect affecting their function, and, therefore, the signaling cascades in which they are involved (Meier & Somers, 2011). During Fe deficiency, the function of the plasma membrane-localized FRO2 and IRT1 has to be synchronized with the transcriptional regulation of the Fe deficiency response in the nucleus, controlled by FIT and its activator interaction partner *bHLH039*. FIT undergoes strict posttranslational control and exists in two forms, active and inactive (Meiser, Lingam, & Bauer, 2011; Sivitz, Grinvalds, Barberon, Curie, & Vert, 2011), distinguishable based on the phosphorylation status (Gratz, Manishankar, et al., 2019). FIT is localized in the cytoplasm and nucleus, whereby active FIT shows greater accumulation in the nucleus versus the cytoplasm than inactive FIT (Gratz, Manishankar, et al., 2019). The FIT-*bHLH039* interaction is enhanced when FIT is activated by phosphorylation at Ser272 (Gratz, Manishankar, et al., 2019).

So far, studies on *bHLH039*, as representative of a subgroup Ib bHLH transcription factor, have remained focused on its transcriptional regulation and protein interaction with FIT. Therefore, this study was motivated by two significant gaps in understanding Fe acquisition regulation. First, the lack of information on the subcellular localization of *bHLH039* and second, the lack of understanding whether post-transcriptional events play a role in *bHLH039* regulation. We report here a surprising pattern of *bHLH039* localization that is not predominantly nuclear, as for the majority of studied transcription factors, and changes depending on the presence of another transcription factor in the cell, namely FIT. We analyze the localization of *bHLH039* in two different biological systems, including Arabidopsis. Through a combination of standard and advanced imaging approaches together with biochemical analysis, we quantitatively assign the localization and subcellular dynamics of *bHLH039* to the presence of FIT.

2 | MATERIALS AND METHODS

2.1 | Plant material and growth conditions

Tobacco (*Nicotiana benthamiana*) plants were grown on soil for 3–4 weeks in a greenhouse facility under long day conditions (16-hr light/8-hr dark). The Arabidopsis (*Arabidopsis thaliana*) ecotype

Col-0 was used as wild type (WT). *FIT* loss-of-function mutant plants, *fit-3* (GABI_108C10), were described previously (Jakoby et al., 2004). HA₃-*bHLH039* transgenic plants overexpressing *BHLH039*, N-terminally fused with a triple hemagglutinin tag, in WT (39/WT) or *fit-3* mutant background (39/*fit*) were described in Naranjo-Arcos et al. (2017). For protoplast isolation, WT and *fit-3* plants were grown for three weeks upright on half-strength Hoagland agar medium with sufficient (50 mM FeNaEDTA, +Fe) Fe supply before harvesting their shoots. For fractionation experiments, WT, 39/WT and 39/*fit* plants were grown for two weeks upright on half-strength Hoagland agar medium with sufficient (50 mM FeNaEDTA, +Fe) Fe supply and then transferred to new plates with either sufficient or deficient (0 mM FeNaEDTA, -Fe) Fe supply for 3 days before harvesting, as described previously (2-week system; Gratz, Manishankar, et al., 2019).

2.2 | Generation of fluorescent protein fusions

The pABind vector system with XVE-driven β -estradiol inducible promoter (Bleckmann, Weidtkamp-Peters, Seidel, & Simon, 2010) was used for expression of fluorescently tagged FIT and *bHLH039* proteins in tobacco leaf epidermis cells. The generation of pABind-GFP:FIT, pABind-mCherry:FIT, and pABind-GFP:*bHLH039* was previously described (Gratz, Manishankar, et al., 2019). Similarly, pDONR207:*bHLH039* (Gratz, Manishankar, et al., 2019) was used to generate pABind-mCherry:*bHLH039*. Free GFP was expressed using pMDC7:GFP (Khan et al., 2019), also under the control of the XVE-driven β -estradiol inducible promoter. For transient expression in Arabidopsis protoplasts, FIT-GFP was expressed using pMDC83:FIT (Gratz, Manishankar, et al., 2019), under the control of the 35S promoter. For *bHLH039*-mCherry, the *BHLH039* coding sequence was introduced in pDONR207 using primers 39 B1 (GGGGACAAGTTTGTACAAAAAAGCAGGCTTAATGTGTGCA TTAGTACCTCC) and 39ns B2 (GGGGACCACTTTGTACAAGAAAGCT GGGTTTATATAGAGTTTCCACATTC). Subsequently, the *BHLH039*-containing cassette was recombined into the Gateway-compatible vector pJNC1 under the control of the 35S promoter (Ivanov et al., 2014) to create pJNC1:*bHLH039*.

2.3 | Transient transformation of tobacco leaf epidermis cells

The Agrobacterium (*Rhizobium radiobacter*) strain C58 (GV3101) carrying pABind constructs with GFP- or mCherry-tagged *FIT* or *BHLH039*, or pMDC7:GFP were used for transient transformation of tobacco leaves. Agrobacterium cultures were grown to an OD₆₀₀ = 0.4, centrifuged and resuspended in a solution containing 250 μ M acetosyringone, 0.1% (w/v) glucose, 0.01% (v/v) Silwet, and 5% (w/v) sucrose. After one hour incubation on ice, the suspension was infiltrated into the abaxial side of tobacco leaves. p19 vector was co-infiltrated to enhance gene expression. Expression was induced

by application of a β -estradiol solution (20 μ M β -estradiol, 0.1% Tween 20) 16 hr before imaging.

2.4 | Confocal microscopy and cytoplasm-to-nucleus ratio determination

For cytoplasm-to-nucleus ratio determination, FIT-GFP, FIT-mCherry, bHLH039-GFP, bHLH039-mCherry, or free GFP proteins were transiently expressed in tobacco cells as described above. Full Z-stacks of epidermal cells were recorded on LSM780 confocal microscope (Zeiss). GFP was imaged with an excitation wavelength of 488 nm and emission detection at 500–530 nm. mCherry and FM4-64 membrane dye were imaged with an excitation of 561 nm with emission detection at 570–615 nm. C-Apochromat 40 \times /1.20 W Korr M27 water immersion objective was used. Pinhole was set to 1 Airy unit, equivalent to optical slices of 0.8 μ m, with a frame size of 1,024 \times 1,024 pixels and a pixel dwell time of 0.79 μ s. Full projections of Z-stack images were generated in ZEN 2012 Blue Edition software (Zeiss), and densitometry on the resulting uncompressed images was performed in the Fiji distribution of ImageJ (fiji.sc) to calculate the cytoplasm-to-nucleus ratio of protein localization (Gratz, Manishankar, et al., 2019). Total intensities of the nucleus and the cytoplasm fluorescence were measured separately. The ratio was calculated for each individual cell. Fifteen to 20 cells were processed per fluorescent reporter under each condition.

2.5 | Arabidopsis protoplast isolation, transformation, and imaging

Plant material was prepared as described in Dovzhenko, Bosco, Meurer, and Koop (2003). In short, shoots from 160 to 200 three-week-old Arabidopsis plants were chopped to fine pieces with a sterile scalpel in 5 ml of MMC medium (10 mM MES, 40 mM CaCl₂, mannitol to 550 mOsm, pH 5.8), followed by an overnight enzymatic digestion in MMC medium supplemented with macerozyme R10 and cellulase Onozuka R10 (0.5% each, Duchefa Biochemie). The homogenized leaf material was filtered through a 70 μ m mesh and centrifuged at 100 g for 20 min. The obtained pellet was resuspended in 10 ml MSC medium (10 mM MES, 20 mM MgCl₂, mannitol to 550 mOsm, sucrose to 550 mOsm, pH 5.8) and overlaid with 3 ml MMM solution (5 mM MES, 15 mM MgCl₂, mannitol to 600 mOsm, pH 5.8). After flotation for 10 min at 80 g, protoplasts were collected from the interphase and transferred to tubes containing W5 solution (2 mM MES, 154 mM NaCl, 125 mM CaCl₂, 5 mM KCl, 5 mM glucose, pH 5.8), adjusting the total volume to 10 ml. Protoplasts were counted, pelleted, and resuspended in MMM solution to a concentration of 500,000 protoplasts/ml. PEG-mediated protoplast transformation was performed as follows: 15 μ g of plasmid DNA in 20 μ l of MMM solution were mixed with 100 μ l protoplast suspension in 6-well plates (Greiner Bio-One, Germany). After 5 min, 120 μ l of PEG₄₀₀₀ solution (62% w/v PEG₄₀₀₀, 0.3 M mannitol, 0.15 M CaCl₂, prewarmed at 37°C)

was carefully added to the transformation mixture and incubated for 8 min. Afterwards, 120 μ l MMM solution and PCA regeneration medium (0.3% w/v B5 salts, 0.05% w/v MgSO₄, 0.05% w/v CaCl₂, 0.1% w/v MES, 2% w/v sucrose, 8% w/v glucose, 0.0002% w/v Capanthotenate, 0.1% v/v Gamborg B5 Vitamin Mix, 0.02 ng/ml biotin, pH 5.8) were added to a final volume of 1.6 ml; the plate was sealed and incubated overnight at 21°C. The protoplasts were imaged using an AxioImager.M2 fluorescent microscope (Zeiss). Images were taken with a Plan-Apochromat 40 \times /1.4 oil objective and recorded by an AxioCam 503 monochromatic camera. For GFP imaging, Filter set 38 HE eGFP shift free (E) (EX BP 470/40, BS FT 495, EM BP 525/50) was used. For mRFP/mCherry imaging, Filter set 43 HE Cy 3 shift free (E) (EX BP 550/25, BS FT 570, EM BP 605/70) was used.

2.6 | Preparation of nuclear and cytoplasmic protein fractions

Cellular fractionation was performed as described in Li et al. (2019). Leaves and roots were collected separately from Arabidopsis plants grown in the 2-weeks system described above. The plant material was ground in the presence of liquid nitrogen and resuspended in three volumes of buffer containing 20 mM Tris-HCl (pH 7.4), 25% glycerol, 20 mM KCl, 2 mM EDTA, 2.5 mM MgCl₂, 250 mM sucrose, and 1x protease inhibitor cocktail (Roche). The samples were then sequentially filtered through 70 μ m and 22–25 μ m nylon mesh before being centrifuged at 1,500 \times g at 4°C for 20 min to pellet the nuclei. The pellet was resuspended in a buffer containing 20 mM Tris-HCl (pH 7.4), 25% glycerol, 2.5 mM MgCl₂, 0.2% NP40, and 0.1% Triton X-100, and the cycle was repeated twice, after which the last pellet was resuspended in 1x protein loading buffer (62 mM Tris-HCl pH 6.8, 2.5% SDS, 2% 1,4-dithiothreitol, 10% glycerol), producing the nuclear fraction. The first supernatant (after the first centrifugation) was centrifuged at 18,800 \times g at 4°C for 20 min two times. This supernatant was mixed 1:1 (v/v) with 2x protein loading buffer, producing the cytosolic fraction.

2.7 | SDS-PAGE and protein detection by immunoblot

Protein samples were separated on a 4%–20% gradient polyacrylamide gel (Bio-Rad) and transferred to a nitrocellulose membrane following the protocol described in Gratz, Manishankar, et al. (2019). The presence of target proteins on the membrane was verified using immunodetection and chemiluminescence. Images of signals on the membranes were digitally recorded in the dynamic range using FluorChem Q machine (Biozym). Band signal intensities were quantified in Fiji distribution of ImageJ (fiji.sc) and used to calculate cytoplasm-to-nucleus ratios.

The following antibodies were used for immunodetection: Rat monoclonal anti-HA horseradish peroxidase conjugated (3F10; Roche) 1:5,000 was used to detect HA-bHLH039; Rabbit

anti-UGPase (AS05 086; Agrisera) 1:1,000 together with goat anti-rabbit IgG horseradish peroxidase (AS09 602; Agrisera) 1:5,000 were used to detect the cytoplasmic fraction marker protein UDP-glucose pyrophosphorylase (UGPase); Rabbit anti-histone H3 horseradish peroxidase (AS10710-HRP; Agrisera) was used to detect the nuclear fraction marker protein Histone H3.

2.8 | Fluorescence recovery after photobleaching (FRAP) analysis

Transient expression of pABind:bHLH039-GFP, pABind:FIT-GFP, pABind:FIT-mCherry, and pMDC7:GFP was performed as described above. FRAP measurements in nucleus and at the cell periphery were taken with a frame size of 256×256 and pixel dwell time of 1.0 μ s. A series of five images was taken before and 40 images after 50 iterations of photobleaching with full laser power of the argon laser at 488 nm. A non-bleached region of interest with the same size as the bleached region was used to correct for acquisition bleaching. The fluorescence intensity values before the photobleach (pre-bleach, F_{pre}) were averaged, and together with the first value after the bleach (post-bleach, F_{post}) and the intensity after recovery (recovery, F_{end}) were used to calculate the mobile fraction (M_f) according to the following equation: $M_f = [(F_{end} - F_{post}) / (F_{pre} - F_{post})] * 100$ (Bancaud, Huet, Rabut, & Ellenberg, 2010). For calculating F_{end} , the average of the five last scans was used and was adjusted for the intensity loss due to the acquisition based on the intensity measured in the non-bleached region. Ten to 15 cells were analyzed for each construct or combination.

2.9 | Statistical analysis

Experimental data was processed using analysis of variance (ANOVA) and Fisher's least significant difference post hoc test. For signal colocalization, Pearson's correlation coefficient (PCC) was calculated using the JACoP plugin of ImageJ (Bolte & Cordelières, 2006).

2.10 | Accession numbers

Sequence data from this article can be found in the TAIR and GenBank data libraries under accession numbers: *BHLH039* (TAIR: AT3G56980), *FIT* (TAIR: AT2G28160).

3 | RESULTS

3.1 | FIT is required for the nuclear localization of bHLH039

Partitioning of regulatory proteins between intracellular compartments represents a mean of controlling their activity. Since no information on the subcellular localization of bHLH039 was

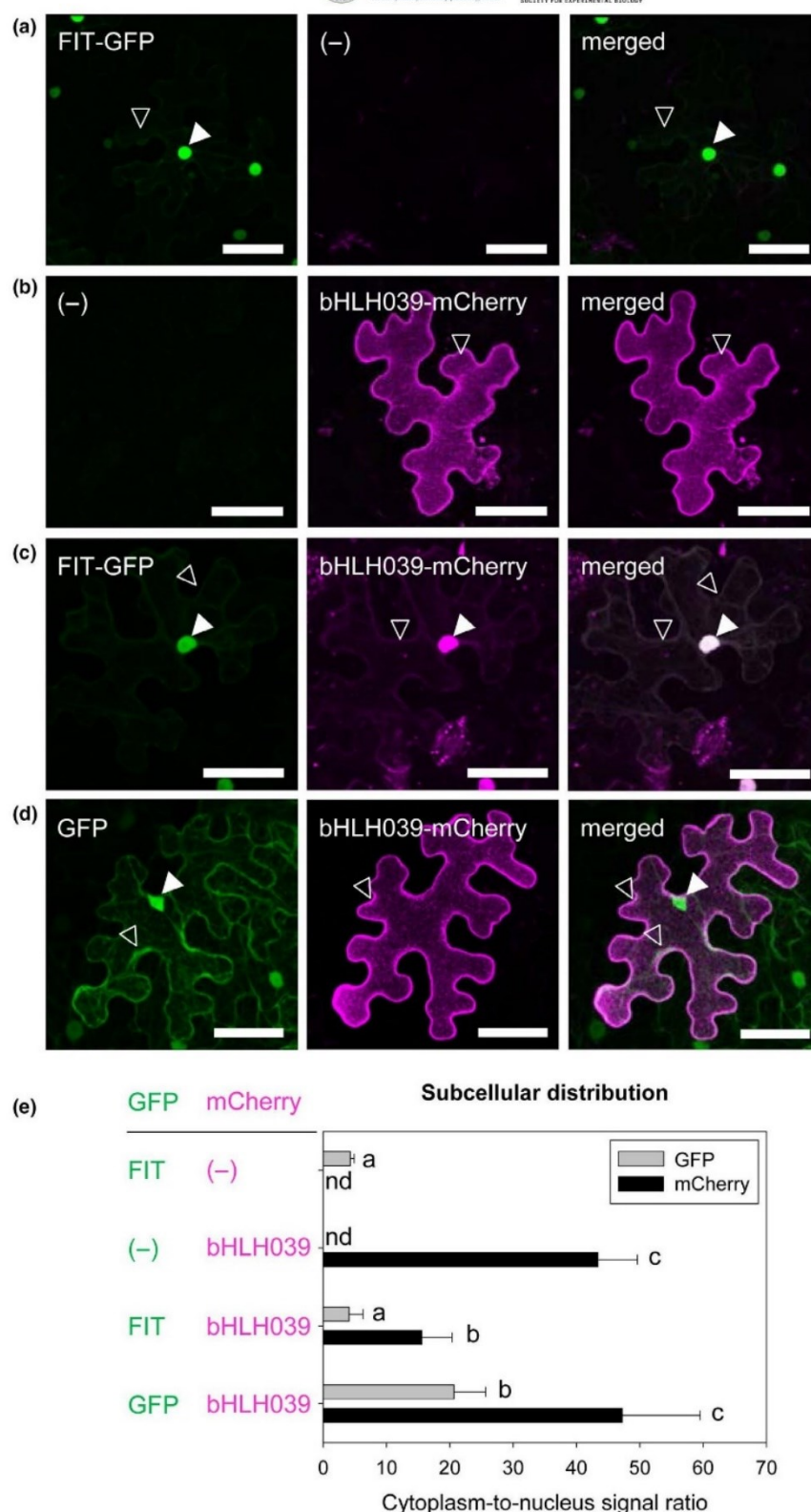
available, we determined the localization of this transcription factor, to assess whether partitioning between cytoplasm and nucleus is a potential target for its regulation, as is the case for FIT. Expressing FIT-GFP in tobacco leaf epidermis cells showed the reported (Gratz, Manishankar, et al., 2019) dual localization in the cytoplasm and the nucleus (Figure 1a). bHLH039-mCherry fusion, expressed in the same system, surprisingly showed strong signals at the cell periphery and only a rather weak presence in the nucleus (Figure 1b and Figure S1). However, coexpression of FIT and bHLH039 in the same cells led to a clear dual localization in nucleus and cytoplasm of bHLH039-mCherry and a strong colocalization with FIT-GFP in the nucleus (Figure 1c). When coexpressed with free GFP, bHLH039-mCherry had strong cell periphery localization (Figure 1d), similar to bHLH039-mCherry alone. We quantified the cytoplasm-to-nucleus ratio of the tested fluorescent proteins and found that indeed, only in the presence of FIT-GFP, bHLH039-mCherry showed a significant shift toward nuclear localization (Figure 1e), suggesting that the presence of FIT is important for the nuclear localization of bHLH039. At the same time, the localization ratio of FIT-GFP remained unchanged by the presence of bHLH039, suggesting that bHLH039 does not influence the localization of FIT. As a control, we performed the reverse experiment, where the fluorescent tags of bHLH039 and FIT were swapped (Figure S2). The experiment yielded the same result, showing that the observed effect was independent of the fluorescent tag.

FIT is weakly expressed in leaves (Bauer et al., 2004; Colangelo & Gueriot, 2004; Jakoby et al., 2004), which offers the possibility to test the effect of low FIT levels on bHLH039 subcellular localization. Indeed, bHLH039 showed a dual, nuclear and cytoplasmic, localization in a wild-type Arabidopsis leaf protoplast expression system (Figure 2a), similar to the subcellular localization of bHLH039-mCherry in WT protoplasts cotransformed with FIT-GFP (Figure 2b). In support of our previous observation in tobacco leaf cells, bHLH039 expressed alone in *fit-3* mutant protoplasts was mainly detectable at the cell periphery (Figure 2c), whereas cotransformation with FIT-GFP restored bHLH039 nuclear accumulation (Figure 2d). Thus, colocalization experiments in both tobacco and Arabidopsis protoplast cells demonstrate the importance of FIT for full-scale nuclear bHLH039 accumulation.

3.2 | bHLH039 presence in the nucleus is FIT-dependent in Arabidopsis

Since FIT presence aids bHLH039 nuclear accumulation in our test systems, we asked whether this is also the case in leaves and roots of Arabidopsis plants grown under different Fe supply conditions. Under Fe deficiency, FIT has a strong expression in the root and much weaker in the leaves (Bauer et al., 2004; Colangelo & Gueriot, 2004; Jakoby et al., 2004), raising the question whether the subcellular distribution of bHLH039 would be differentially regulated between the two organs. To address this, we quantified bHLH039

FIGURE 1 Subcellular localization of bHLH039 depends on FIT presence in tobacco leaf epidermis cells. (a-d) Localization of FIT-GFP, bHLH039-mCherry, and free GFP, alone or in combinations. Representative full projections of laser-scanning confocal images show GFP and mCherry fluorescence of FIT-GFP alone (a), bHLH039-mCherry alone (b), FIT-GFP and bHLH039-mCherry (c), and free GFP and bHLH039-mCherry (d), following β -estradiol induction of transiently transformed tobacco leaf epidermis cells. Nuclear and cytoplasmic fluorescence signals are indicated by arrowheads (filled and empty, respectively). Bars: 50 μ m. (e) Quantification of subcellular distribution of the fluorescently tagged protein combinations shown in (a-d). Cytoplasm-to-nucleus signal ratio was calculated for the GFP (gray bars), and mCherry (black bars) signals obtained for each combination ($n = 15-20$). Data are represented as mean \pm SD. Different letters indicate statistically significant differences ($p < .05$)



protein amounts in cytoplasmic and nuclear fractions from leaves (Figure 3a-c and Figure S3a-c) and roots (Figure 3d-f and Figure S3d-f) of transgenic *Arabidopsis* plants constitutively expressing triple hemagglutinin-tagged (HA_3)-bHLH039 in either wild-type (39/WT)

or *fit-3* loss-of-function (39/*fit*) background, grown under sufficient or deficient Fe supply. bHLH039 protein is active in enhancing Fe uptake in roots and leaves of 39/WT but not in 39/*fit* (Naranjo-Arcos et al., 2017). HA_3 -bHLH039 was found in both leaf and root

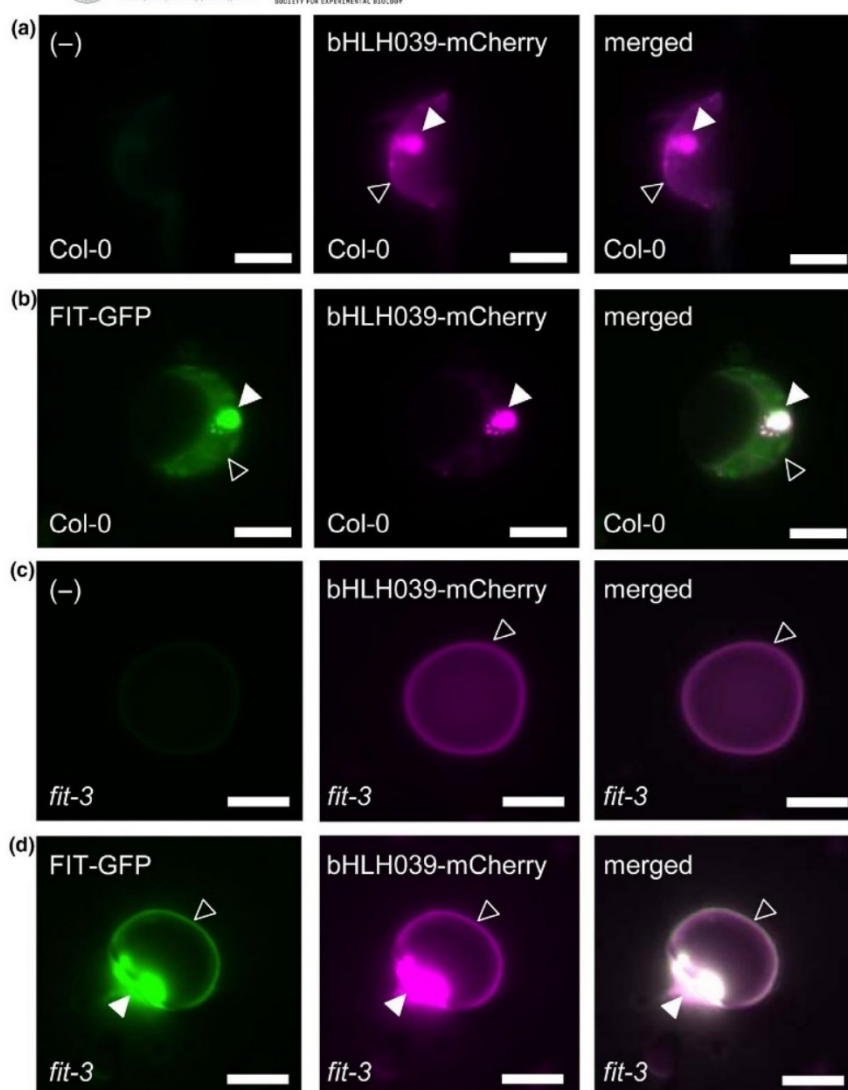


FIGURE 2 FIT-dependent subcellular localization of bHLH039 in Arabidopsis protoplasts. Arabidopsis protoplasts from wild-type Col-0 (a,b) and *fit-3* mutant (c,d) plants were transformed with bHLH039-mCherry alone (a,c) or FIT-GFP together with bHLH039-mCherry (b,d). Left panels, GFP channel; middle panels, mCherry channel; right panels, merged images. Nuclear and cytoplasmic fluorescence signals are indicated by arrowheads (filled and empty, respectively). Bars: 5 μ m

fractions of 39/WT and 39/*fit* (Figure 3a,b,d,e and Figure S3a,b,d,e). Remarkably, in the absence of FIT, a clear increase of 1.7 to 3-fold in cytoplasmic HA₃-bHLH039 (higher cytoplasm-to-nucleus signal ratio) is seen in both Fe supply conditions and both organs in 39/*fit* versus 39/WT (Figure 3c,f and Figure S3c,f). This shows that although a certain portion of bHLH039 can still accumulate in the nucleus in a FIT-independent manner, the presence of FIT strongly promotes bHLH039 nuclear localization in Arabidopsis. Comparing leaves and roots, we observed a marked difference, depending on Fe supply. In leaves, the nuclear localization of HA₃-bHLH039 increased under Fe deficiency compared with sufficient Fe supply in both plant lines (lower cytoplasm-to-nucleus signal ratio at -Fe vs. +Fe, Figure 3c and Figure S3c), whereas in roots the cytoplasm-to-nucleus signal ratio was higher under Fe deficiency compared with Fe sufficiency, indicative of decreased nuclear localization of bHLH039 under Fe deficiency, despite the presence of active FIT (Figure 3f and Figure S3f). Taken together, bHLH039 nuclear accumulation is organ-specific and Fe-dependent, and, to a large extent, dependent on FIT.

3.3 | In the presence of FIT, bHLH039 protein has increased mobility in the cytoplasm

Aiming to better understand the mechanism of bHLH039 localization and its FIT dependence, we measured the relative mobility of FIT and bHLH039 fluorescent protein fusions in the nucleus and the periphery of transformed tobacco cells. We applied fluorescence recovery after photobleaching (FRAP) to bHLH039-GFP, FIT-GFP, and free GFP as a control (Figure 4). In the absence of FIT, the bleached bHLH039-GFP area in the nucleus showed fluorescence recovery, suggesting that in this region, apart from being very weakly present (Figure 4a and Figure S4), the bHLH039-GFP protein is relatively mobile (Figure 4i). Outside the nucleus, however, the bleached area at the cell periphery remained almost completely devoid of signal, showing that bHLH039-GFP was kept in an immobile state (Figure 4b,i). A closer inspection of these images revealed that the signal at the cell periphery was not uniformly distributed but rather concentrated in immobile punctate structures (foci) (Figure 4b). In the presence of FIT-mCherry, bHLH039-GFP remained mobile in the nucleus (Figure 4c,i). The cytoplasmic bHLH039-GFP

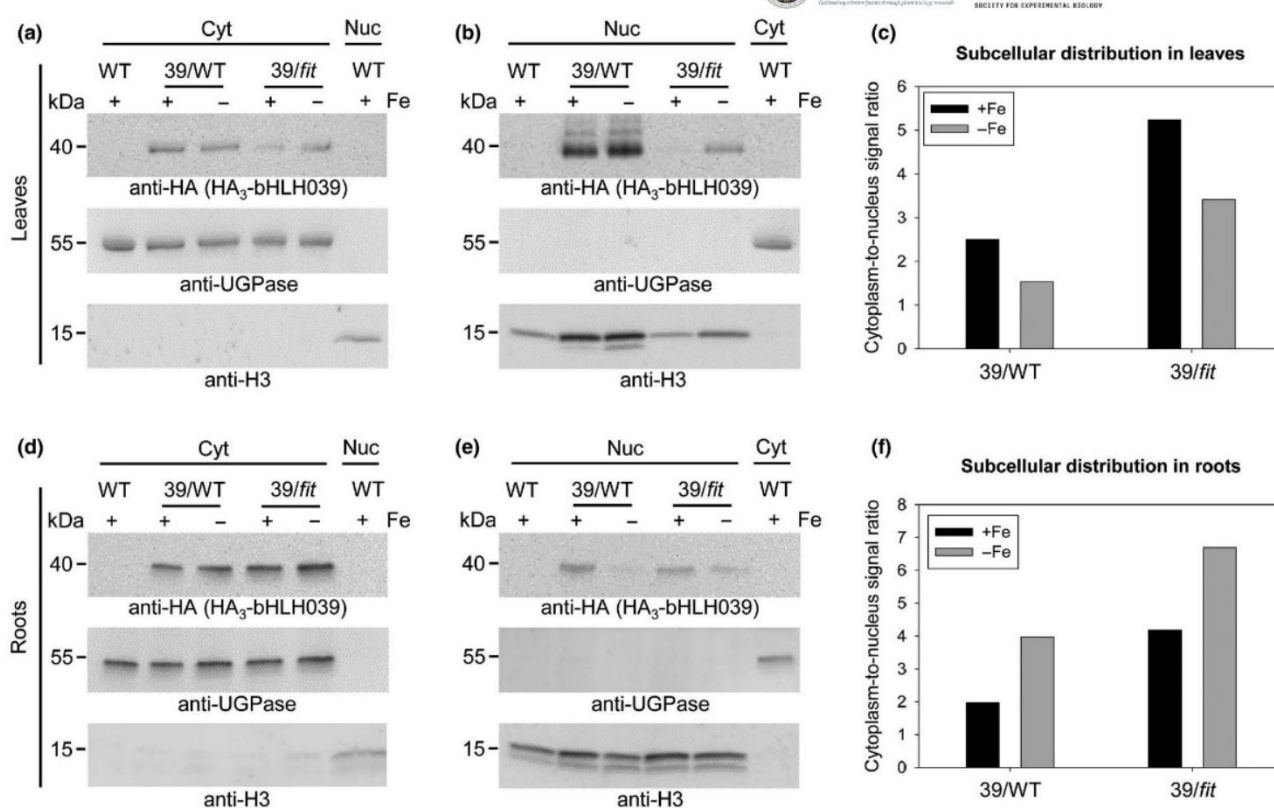


FIGURE 3 Nuclear accumulation of bHLH039 depends on FIT presence and Fe supply in Arabidopsis leaves and roots. Immunoblot analysis of HA₃-bHLH039 protein distribution in cytosolic (Cyt) (a,d) and nuclear (Nuc) (b,e) fractions of leaves (a,b) and roots (d,e) from plants overexpressing HA₃-bHLH039 in wild-type (39/WT) and *fit-3* mutant background (39/*fit*). WT plants were used as a control. Fractionation was performed on 2-week-old plants transferred for 3 days on sufficient (+Fe) or deficient (-Fe) Fe supply. HA₃-bHLH039 was detected with anti-HA-HRP antibody. Anti-UGPase and anti-H3 antibodies were used as markers for the cytosolic and nuclear fractions, respectively. Arrows indicate the detection of the respective full-length protein. Protein molecular weight (in kDa) is indicated. The intensity of each HA₃-bHLH039 protein band was normalized to the corresponding marker protein for the respective fraction. The obtained normalized values were used to calculate a cytoplasm-to-nucleus signal ratio representing the subcellular distribution of HA₃-bHLH039 in leaves (c) and in roots (f) of plants grown under sufficient (+Fe, black bars) and deficient (-Fe, gray bars) Fe supply. The assay was performed twice yielding comparable results (see also Figure S3)

foci, however, were almost completely absent and were replaced by diffuse cytoplasmic signal that recovered quickly after photobleaching (Figure 4d,i). In comparison, FIT-GFP (Figure 4e,f) and free GFP (Figure 4g,h) signals showed high mobility both in the nucleus and the cytoplasm (Figure 4i). Thus, in the presence of FIT, bHLH039 is kept in a mobile form, while without FIT, it is sequestered in immobile foci at the cell periphery, potentially preventing its entry in the nucleus.

The intriguing localization of bHLH039-GFP in static foci at the cell periphery in the absence of FIT raises the question on the nature of these structures and their relation to the plasma membrane. Using the lipophilic fluorescent dye FM4-64 to label the plasma membrane, we investigated the degree of colocalization between bHLH039-GFP and the marker staining. The bHLH039-GFP and FM4-64 signals were both located at the cell periphery, however, despite their proximity they were distinct from each other. In addition, FM4-64 fluorescence was uniform across the membrane and not in foci (Figure 4j,k). Consistently, quantitative analysis showed relatively poor colocalization between the two signals, with an average Pearson's correlation

coefficient (PCC) of .286 (while well-colocalizing signals have a PCC of above .5) (Figure 4k). Therefore, the bHLH039-GFP signals are in proximity to but not at the plasma membrane.

4 | DISCUSSION

4.1 | Nucleocytoplasmic partitioning of bHLH039 is FIT-dependent

We report here a pattern of bHLH039 localization that changes depending on the presence of FIT in the cell. It is known that the effects of bHLH039 on the Fe deficiency response in Arabidopsis are FIT-dependent and due to the dimerization of the two proteins (Naranjo-Arcos et al., 2017; Wang et al., 2013). Our data adds a new level of complexity to the FIT-bHLH039 regulation. bHLH039 accumulates to a low level in the nucleus in the absence of FIT, suggesting that additional factor(s), potentially other related

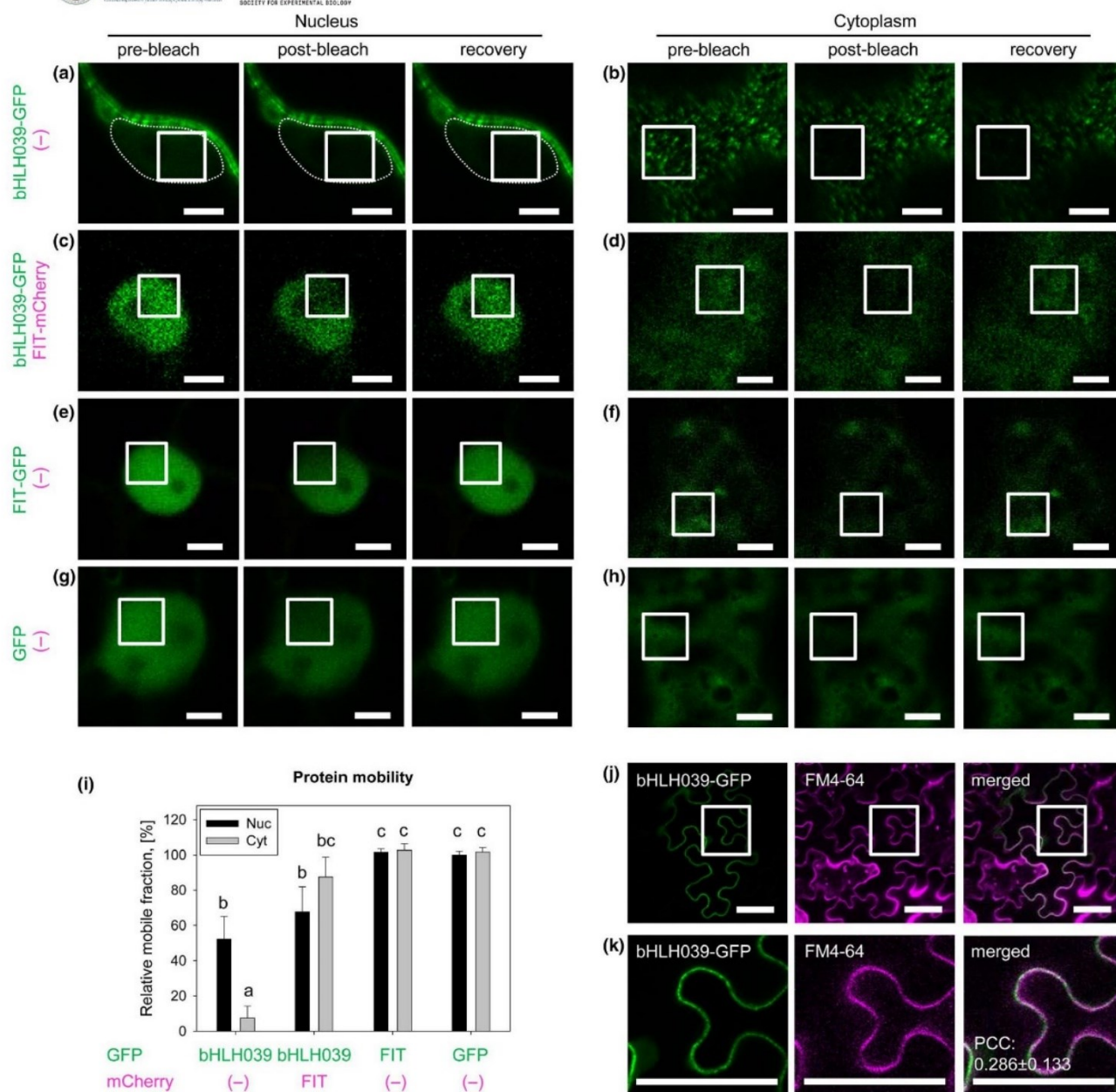


FIGURE 4 The intracellular mobility of bHLH039 depends on FIT. (a–i) Fluorescence recovery after photobleaching (FRAP) analysis of the protein mobility of GFP-tagged FIT and bHLH039. White rectangles in the laser-scanning confocal images of transiently transformed tobacco leaf epidermis cells indicate the bleached areas in the nucleus (a,c,e,g; optical cross-sections through the nucleus) and at the cell periphery (b,d,f,h; frontal images of the periphery of the cells). The protein mobility was assayed for bHLH039-GFP alone (a,b), bHLH039-GFP coexpressed with FIT-mCherry (c,d), FIT-GFP alone (e,f), and free GFP alone as a control (g,h). For each sample, representative pre-bleach, post-bleach and recovery images are shown. Due to the low intensity of the nuclear bHLH039-GFP signal in (a), the nucleus contour is traced with a punctate line. For an enhanced intensity image of nuclear bHLH039-GFP, see Figure S4. Bars: 5 μ m. (i) Protein mobility quantification for the samples shown in (a–h). The percentage of the mobile protein fraction for each protein is presented relative to the mobile fraction of nuclear free GFP alone ($n = 10–15$). Data are represented as mean \pm SD. Different letters indicate statistically significant differences ($p < .05$). (j–k) Colocalization analysis of GFP-tagged bHLH039 and the plasma membrane labeled with FM4-64. (k) Enlarged images of the areas in (j) indicated with white rectangles. bHLH039-GFP signals are detectable in close proximity to the plasma membrane; however, statistical analysis indicates lack of significant colocalization. Pearson's correlation coefficient (PCC) = $.286 \pm .133$ ($n = 7$). Bars: 50 μ m

transcription factors (Gao et al., 2019), may also influence this process. Still, FIT is essential for full-scale bHLH039 nuclear accumulation. In the absence of FIT, bHLH039 is retained in immobile

foci in close proximity to the plasma membrane. In the presence of FIT, bHLH039 is mobile and readily accumulates in the nucleus (Figure 5).

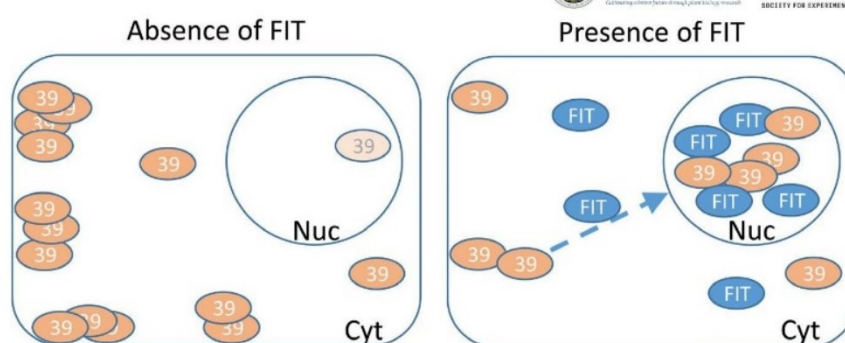


FIGURE 5 Different FIT-dependent subcellular localization patterns of bHLH039. Model summarizing the need of FIT presence for full-scale bHLH039 nuclear accumulation. Left, in the absence of FIT, bHLH039 is predominantly localized outside of the nucleus, concentrated in stable cytoplasmic foci in close proximity to the plasma membrane. Only a small portion of bHLH039 localizes to the nucleus. Right, in Fe-deficient wild-type root cells and/or in the presence of FIT, FIT aids the nuclear accumulation of bHLH039 preventing its sequestration in cytoplasmic foci. In the nucleus, the FIT-bHLH039 protein complex triggers the expression of Fe response genes

4.2 | Potential mechanisms of bHLH039 nuclear accumulation

The accumulation of bHLH039 in the nucleus in the presence of FIT may be achieved by different mechanisms. One possibility is that FIT helps maintain bHLH039 in a mobile form and/or shuttle together with it into the nucleus. Alternatively, FIT may prevent the nuclear export of bHLH039 and its sequestration in cytoplasmic foci. The physical exclusion of transcriptional regulators from the nucleus by sequestration in the cytoplasm is one strategy for regulating their activity. In animals, Bach1, STRA8, and the STAT family proteins are prominent examples of transcription factors translocating from the cytoplasm to the nucleus in response to different stimuli (Meyer & Vinkemeier, 2004; Tedesco, Sala, Barbagallo, Felici, & Farini, 2009; Yamasaki, Tashiro, Nishito, Sueda, & Igarashi, 2005). There are also several examples in plants, such as the transcription factors BES1 and BZR1 in response to brassinosteroid signaling (Yin et al., 2002), the PHR1 transcription factor in a phosphate status-dependent manner (Osorio et al., 2019), and the chromatin remodeling factor ET2 during cell differentiation (Ivanov et al., 2008). Interestingly, when retained in the cytoplasm, ET2 also accumulates in punctate structures (Ivanov et al., 2008), which may thus represent a common mechanism for the sequestration of proteins not immediately required by the cell. The *BHLH039* gene is strongly upregulated under Fe deficiency, suggesting that only minor levels of the protein are required at sufficient Fe supply, requiring a mechanism that keeps excess protein excluded from action. This notion is supported by the fact that overexpression of bHLH039 at +Fe probably overloads the Fe sequestration system and has drastic effects on Fe accumulation, since enough FIT is present to keep bHLH039 mobile and/or shuttle it to the nucleus (Naranjo-Arcos et al., 2017). Further research will be needed to uncover the exact nature of the cytoplasmic foci, where bHLH039 accumulates in the absence of FIT, and the participating proteins that potentially anchor bHLH039.

Another aspect to consider is whether active FIT is needed for bHLH039 nuclear accumulation. We could recently show that

FIT phosphorylation by CIPK11 at Ser272 is a major FIT-activating process, whereby both Ser272-phosphorylated and non-phosphorylated FIT forms can interact with bHLH039, with the non-phosphorylated S272AA FIT form showing a weaker interaction with bHLH039 (Gratz, Manishankar, et al., 2019). Additionally, phosphorylation events at Ser221, Tyr238, and Tyr278 also affect FIT activity (Gratz, Brumbarova, et al., 2019). Therefore, it is possible that differential FIT phosphorylation may modulate FIT activity levels and, in turn, the effect of FIT on bHLH039 nuclear accumulation. In the future, it will be crucial to understand the mechanism by which FIT influences bHLH039 cellular mobility, its nuclear accumulation, and the role of their direct interaction in this process.

4.3 | Biological significance of FIT-dependent bHLH039 nuclear accumulation

Our finding has interesting implications regarding the Fe deficiency-induced signaling cascade. It is tempting to speculate that the cytoplasmic retention of bHLH039 could be linked to direct crosstalk at protein level with other Fe deficiency-related proteins that are localized at the plasma membrane, such as the effectors FRO2 and IRT1, and/or the Fe response modulators CBL1/9 (Gratz, Manishankar, et al., 2019) and EHB1 (Khan et al., 2019). Posttranslational control plays a prominent role in the functioning of bHLH039 and potentially the other three group Ib bHLH proteins involved in Fe acquisition and homeostasis. It is possible that *fit* mutant plants are functional knock-out mutants of the four Ib bHLH proteins due to their reduced nuclear accumulation in the absence of FIT, which may explain the very strong Fe deficiency phenotype of the *fit* mutant.

The differences in subcellular partitioning of bHLH039 between leaves and roots at different Fe supply may reflect different organ-specific functions of this transcription factor (Andriankaja et al., 2014). Proteasomal degradation, similar to the stability control shown for FIT (Lingam et al., 2011; Meiser et al., 2011; Sivitz et al.,

2011), and/or other factor(s) that negatively regulate(s) bHLH039 nuclear accumulation, may account for the observed differential subcellular partitioning.

An important aspect of the phenomenon that we describe here is its potential conservation across the plant kingdom. A recent study in rice identified OsbHLH156 as a rice ortholog of FIT, albeit with low sequence similarity and controlling Strategy II, instead of Strategy I, Fe uptake. Interestingly, this transcription factor was found necessary for the nuclear localization of OsIRO2, the rice ortholog of bHLH039 (Wang et al., 2019). This underlines the importance of the here described phenomenon in Arabidopsis as an integral part of the plant Fe deficiency response.

ACKNOWLEDGMENTS

R.I., I.M., and P.B. are members of CRC 1208; I.M. is member of the MB Train graduate school, integrated in CRC 1208. This study was supported by the Deutsche Forschungsgemeinschaft (DFG, German Research Foundation)—Projektnummer 267205415—SFB 1208, project B05 to P.B. This work received funding from Germany's Excellence Strategy, EXC 2048/1, Project ID: 390686111.

CONFLICT OF INTEREST

The authors declare no conflicts of interest.

AUTHOR CONTRIBUTIONS

K.T., R.I., P.B., and T.B. designed the research. K.T., R.I., and T.B. designed experiments. K.T., R.I., M.E., B.A., I.M., and T.B. performed research. K.T., R.I., and T.B. analyzed data. R.I. and T.B. wrote the manuscript. K.T., R.I., I.M., P.B., and T.B. revised the manuscript. P.B. acquired funding. All authors participated in discussion of the manuscript.

REFERENCES

- Andriankaja, M. E., Danisman, S., Mignolet-Spruyt, L. F., Claeys, H., Kochanek, I., Vermeersch, M., ... Inzé, D. (2014). Transcriptional coordination between leaf cell differentiation and chloroplast development established by TCP20 and the subgroup Ib bHLH transcription factors. *Plant Molecular Biology*, *85*, 233–245.
- Bancaud, A., Huet, S., Rabut, G., & Ellenberg, J. (2010). Fluorescence perturbation techniques to study mobility and molecular dynamics of proteins in live cells: FRAP, photoactivation, photoconversion, and FLIP. *Cold Spring Harbor Protocols*, *2010*(12), pdb top90.
- Bauer, P., Thiel, T., Klatte, M., Bereczky, Z., Brumbarova, T., Hell, R., & Grosse, I. (2004). Analysis of sequence, map position, and gene expression reveals conserved essential genes for iron uptake in Arabidopsis and tomato. *Plant Physiology*, *136*, 4169–4183.
- Bleckmann, A., Weidtkamp-Peters, S., Seidel, C. A., & Simon, R. (2010). Stem cell signaling in Arabidopsis requires CRN to localize CLV2 to the plasma membrane. *Plant Physiology*, *152*, 166–176.
- Bolte, S., & Cordelières, F. P. (2006). A guided tour into subcellular colocalization analysis in light microscopy. *Journal of Microscopy*, *224*, 213–232.
- Brumbarova, T., Bauer, P., & Ivanov, R. (2015). Molecular mechanisms governing Arabidopsis iron uptake. *Trends in Plant Science*, *20*, 124–133.
- Colangelo, E. P., & Guerinot, M. L. (2004). The essential basic helix-loop-helix protein FIT1 is required for the iron deficiency response. *The Plant Cell*, *16*, 3400–3412.
- Dovzhenko, A., Dal Bosco, C., Meurer, J., & Koop, H. U. (2003). Efficient regeneration from cotyledon protoplasts in Arabidopsis thaliana. *Protoplasma*, *222*, 107–111.
- Gao, F., Robe, K., Gaymard, F., Izquierdo, E., & Dubos, C. (2019). The transcriptional control of iron homeostasis in plants: A tale of bHLH transcription factors? *Frontiers in Plant Science*, *10*, 6. <https://doi.org/10.3389/fpls.2019.00006>
- Gratz, R., Brumbarova, T., Ivanov, R., Trofimov, K., Tunnermann, L., Ochoa-Fernandez, R., ... Bauer, P. (2019). Phospho-mutant activity assays provide evidence for alternative phospho-regulation pathways of the transcription factor FER-LIKE IRON DEFICIENCY-INDUCED TRANSCRIPTION FACTOR. *New Phytologist*. <https://doi.org/10.1111/nph.16168>
- Gratz, R., Manishankar, P., Ivanov, R., Köster, P., Mohr, I., Trofimov, K., ... Brumbarova, T. (2019). CIPK11-dependent phosphorylation modulates FIT activity to promote Arabidopsis iron acquisition in response to calcium signaling. *Developmental Cell*, *48*(5), 726–740. <https://doi.org/10.1016/j.devcel.2019.01.006>
- Heim, M. A., Jakoby, M., Werber, M., Martin, C., Weisshaar, B., & Bailey, P. C. (2003). The basic helix-loop-helix transcription factor family in plants: A genome-wide study of protein structure and functional diversity. *Molecular Biology and Evolution*, *20*, 735–747.
- Ivanov, R., Brumbarova, T., & Bauer, P. (2012). Fitting into the harsh reality: Regulation of iron deficiency responses in dicotyledonous plants. *Molecular Plant*, *5*, 27–42. <https://doi.org/10.1093/mp/ssr065>
- Ivanov, R., Brumbarova, T., Blum, A., Jantke, A. M., Fink-Straube, C., & Bauer, P. (2014). SORTING NEXIN1 is required for modulating the trafficking and stability of the Arabidopsis IRON-REGULATED TRANSPORTER1. *The Plant Cell*, *26*, 1294–1307.
- Ivanov, R., Tiedemann, J., Czihal, A., Schallau, A., le Diep, H., Mock, H. P., ... Baumlein, H. (2008). EFFECTOR OF TRANSCRIPTION2 is involved in xylem differentiation and includes a functional DNA single strand cutting domain. *Developmental Biology*, *313*, 93–106.
- Jakoby, M., Wang, H. Y., Reidt, W., Weisshaar, B., & Bauer, P. (2004). FRU (BHLH029) is required for induction of iron mobilization genes in Arabidopsis thaliana. *FEBS Letters*, *577*, 528–534.
- Jeong, J., Merkovich, A., Clyne, M., & Connolly, E. L. (2017). Directing iron transport in dicots: Regulation of iron acquisition and translocation. *Current Opinion in Plant Biology*, *39*, 106–113.
- Khan, I., Gratz, R., Denezhkin, P., Schott-Verdugo, S. N., Angrand, K., Genders, L., ... Ivanov, R. (2019). Calcium-promoted interaction between the C2-domain protein EHB1 and metal transporter IRT1 inhibits Arabidopsis iron acquisition. *Plant Physiology*, *180*, 1564–1581.
- Li, H., Li, Y., Zhao, Q., Li, T., Wei, J., Li, B., ... Gao, C. (2019). The plant ESCRT component FREE1 shuttles to the nucleus to attenuate abscisic acid signalling. *Nature Plants*, *5*, 512–524.
- Lingam, S., Mohrbacher, J., Brumbarova, T., Potuschak, T., Fink-Straube, C., Blondet, E., ... Bauer, P. (2011). Interaction between the bHLH transcription factor FIT and ETHYLENE INSENSITIVE3/ETHYLENE INSENSITIVE3-LIKE1 reveals molecular linkage between the regulation of iron acquisition and ethylene signaling in Arabidopsis. *The Plant Cell*, *23*, 1815–1829. <https://doi.org/10.1105/tpc.111.084715>
- Meier, I., & Somers, D. E. (2011). Regulation of nucleocytoplasmic trafficking in plants. *Current Opinion in Plant Biology*, *14*, 538–546.
- Meiser, J., Lingam, S., & Bauer, P. (2011). Posttranslational regulation of the iron deficiency basic helix-loop-helix transcription factor FIT is affected by iron and nitric oxide. *Plant Physiology*, *157*, 2154–2166.
- Meyer, T., & Vinkemeier, U. (2004). Nucleocytoplasmic shuttling of STAT transcription factors. *European Journal of Biochemistry*, *271*, 4606–4612.
- Naranjo-Arcos, M. A., Maurer, F., Meiser, J., Pateyron, S., Fink-Straube, C., & Bauer, P. (2017). Dissection of iron signaling and iron accumulation by overexpression of subgroup Ib bHLH039 protein. *Scientific Reports*, *7*(1), 10911. <https://doi.org/10.1038/s41598-017-11171-7>



- Osorio, M. B., Ng, S., Berkowitz, O., De Clercq, I., Mao, C., Shou, H., ... Jost, R. (2019). SPX4 acts on PHR1-dependent and -independent regulation of shoot phosphorus status in *Arabidopsis*. *Plant Physiology*, *181*(1), 332–352. <https://doi.org/10.1104/pp.18.00594>
- Sivitz, A., Grinvalds, C., Barberon, M., Curie, C., & Vert, G. (2011). Proteasome-mediated turnover of the transcriptional activator FIT is required for plant iron-deficiency responses. *The Plant Journal*, *66*(6), 1044–1052. <https://doi.org/10.1111/j.1365-313X.2011.04565.x>
- Tedesco, M., La Sala, G., Barbagallo, F., De Felici, M., & Farini, D. (2009). STRA8 shuttles between nucleus and cytoplasm and displays transcriptional activity. *Journal of Biological Chemistry*, *284*, 35781–35793.
- Vorwieger, A., Gryczka, C., Czihal, A., Douchkov, D., Tiedemann, J., Mock, H. P., ... Baumlein, H. (2007). Iron assimilation and transcription factor controlled synthesis of riboflavin in plants. *Planta*, *226*, 147–158.
- Wang, H. Y., Klatte, M., Jakoby, M., Baumlein, H., Weisshaar, B., & Bauer, P. (2007). Iron deficiency-mediated stress regulation of four subgroup Ib BHLH genes in *Arabidopsis thaliana*. *Planta*, *226*, 897–908.
- Wang, N., Cui, Y., Liu, Y., Fan, H., Du, J., Huang, Z., ... Ling, H. Q. (2013). Requirement and functional redundancy of Ib subgroup bHLH proteins for iron deficiency responses and uptake in *Arabidopsis thaliana*. *Molecular Plant*, *6*, 503–513.
- Wang, S., Li, L., Ying, Y., Wang, J., Shao, J. F., Yamaji, N., ... Shou, H. (2019). A transcription factor OsbHLH156 regulates Strategy II iron acquisition through localizing IRO2 to the nucleus in rice. *New Phytologist*. <https://doi.org/10.1111/nph.16232>
- Yamasaki, C., Tashiro, S., Nishito, Y., Sueda, T., & Igarashi, K. (2005). Dynamic cytoplasmic anchoring of the transcription factor Bach1 by intracellular hyaluronic acid binding protein IHABP. *Journal of Biochemistry*, *137*, 287–296.
- Yin, Y., Wang, Z. Y., Mora-Garcia, S., Li, J., Yoshida, S., Asami, T., & Chory, J. (2002). BES1 accumulates in the nucleus in response to brassinosteroids to regulate gene expression and promote stem elongation. *Cell*, *109*, 181–191.
- Yuan, Y., Wu, H., Wang, N., Li, J., Zhao, W., Du, J., ... Ling, H. Q. (2008). FIT interacts with AtbHLH38 and AtbHLH39 in regulating iron uptake gene expression for iron homeostasis in *Arabidopsis*. *Cell Research*, *18*, 385–397.

SUPPORTING INFORMATION

Additional supporting information may be found online in the Supporting Information section.

How to cite this article: Trofimov K, Ivanov R, Eutebach M, et al. Mobility and localization of the iron deficiency-induced transcription factor bHLH039 change in the presence of FIT. *Plant Direct*. 2019;3:1–11. <https://doi.org/10.1002/pld3.190>

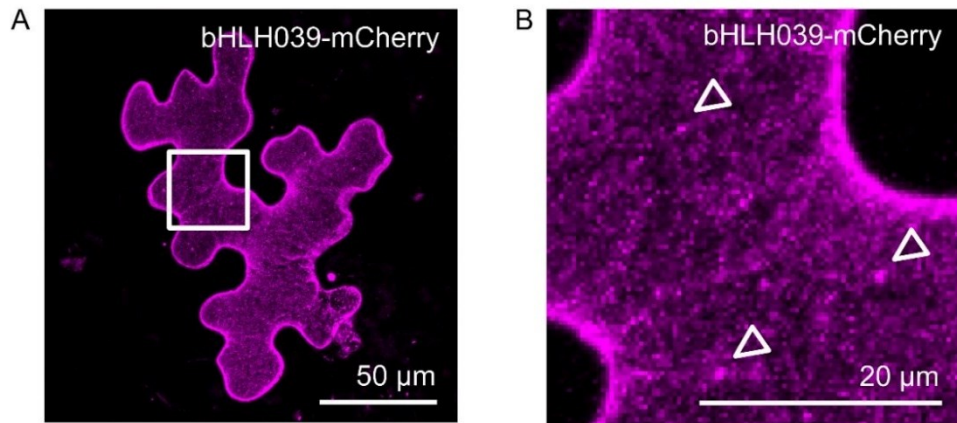
SUPPLEMENTAL DATA

Mobility and localization of the iron deficiency-induced transcription factor bHLH039 change in the presence of FIT

Ksenia Trofimov¹, Rumen Ivanov¹, Monique Eutebach¹, BÜsra Acaroglu¹, Inga Mohr¹, Petra Bauer^{1,2}, Tzvetina Brumbarova¹

¹ Institute of Botany, Heinrich Heine University, 40225 Düsseldorf, Germany

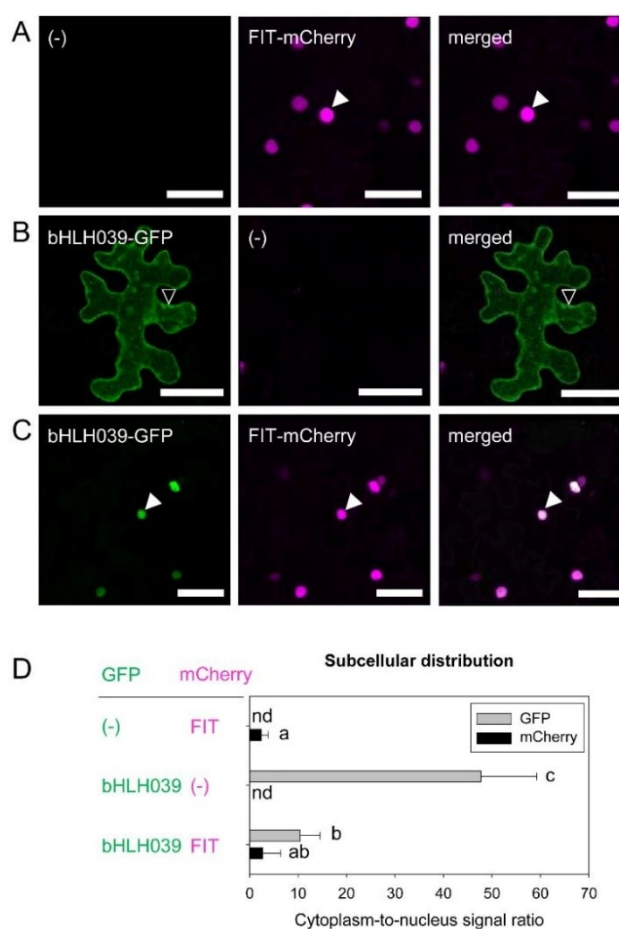
² Cluster of Excellence on Plant Sciences, Heinrich Heine University, 40225 Düsseldorf, Germany



Supplemental Figure 1. Presence of bHLH039-mCherry in cytoplasmic foci at the cell periphery of tobacco leaf epidermis cells.

(A) Image of bHLH039-mCherry localization in tobacco leaf epidermis from [Figure 1B](#). A white rectangle denotes the area of the cell presented in (B).

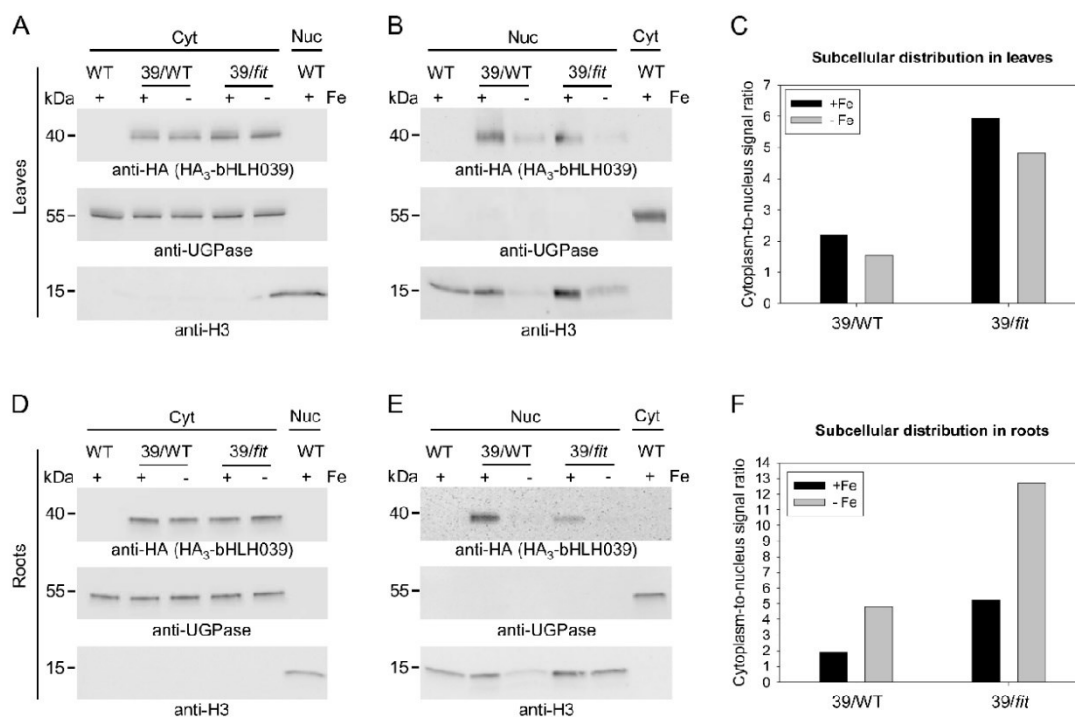
(B) Enlarged image of the area in (A) indicated with a white rectangle, showing bHLH039-mCherry-containing cytoplasmic foci at the periphery of the cell (empty arrowheads).



Supplemental Figure 2. FIT dependence of bHLH039 subcellular localization in tobacco leaf epidermis cells is not affected by the fluorescent tag.

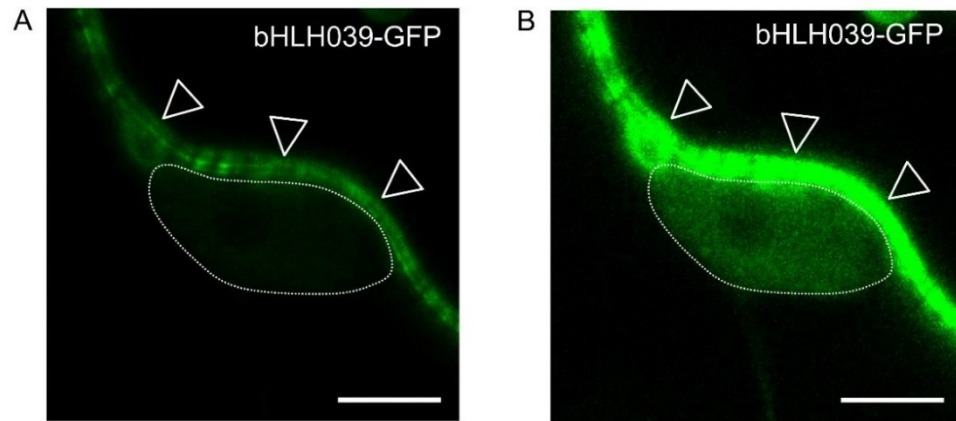
(A-C) Localization of FIT-mCherry and bHLH039-GFP, alone or in combinations. Representative full projections of laser-scanning confocal images show GFP and mCherry fluorescence of FIT-mCherry alone (A), bHLH039-GFP alone (B), and bHLH039-GFP and FIT-mCherry (C) in tobacco leaf epidermis cells. Nuclear and cytoplasmic fluorescence signals are indicated by arrowheads (filled and empty, respectively). Bars: 50 μ m.

(D) Quantification of subcellular distribution of the fluorescently tagged protein combinations shown in (A-C). Cytoplasm-to-nucleus signal ratio was calculated for the GFP (gray bars) and mCherry (black bars) signals obtained for each combination ($n = 15-20$). Data are represented as mean \pm SD. Different letters indicate statistically significant differences ($P < 0.05$).



Supplemental Figure 3. Analysis of bHLH039 nuclear accumulation by subcellular fractionation.

This figure shows the result from an independent fractionation repetition of the experiment presented in Figure 3. Immunoblot analysis of HA₃-bHLH039 protein distribution in cytosolic (Cyt) (A, D) and nuclear (Nuc) (B, E) fractions of leaves (A, B) and roots (D, E) from plants overexpressing HA₃-bHLH039 in wild-type (39/WT) and *fit-3* mutant background (39/*fit*). WT plants were used as a control. Fractionation was performed on 2 week-old plants transferred for 3 days on sufficient (+Fe) or deficient (-Fe) Fe supply. HA₃-bHLH039 was detected with anti-HA-HRP antibody. Anti-UGPase and anti-H3 antibodies were used as markers for the cytosolic and nuclear fractions, respectively. Arrows indicate the detection of the respective full-length protein. Protein molecular weight (in kDa) is indicated. The intensity of each HA₃-bHLH039 protein band was normalized to the corresponding marker protein for the respective fraction. The obtained normalized values were used to calculate a cytoplasm-to-nucleus signal ratio representing the subcellular distribution of HA₃-bHLH039 in leaves (C) and in roots (F) of plants grown under sufficient (+Fe, black bars) and deficient (-Fe, gray bars) Fe supply.



Supplemental Figure 4. Presence of bHLH039-GFP in the nucleus.

(A) Image of bHLH039-GFP from [Figure 4A](#). In the absence of FIT, bHLH039-GFP is strongly localized to the cell periphery (bright green signal, open arrowheads). Certain amount of bHLH039-GFP can be found in the nucleus (surrounded by white punctate line), judged by the presence of comparatively weak GFP signal intensity. (B) Enhanced intensity of image (A) reveals bHLH039-GFP fluorescent signal in the nucleus. Bars: 5 μm .

Author contributions to Paper IIIKsenia Trofimov

Conceptualization of study. Supervised the study. Performed initial experiments. Designed, performed, and analyzed following experiments: confocal imaging (2A, 2B, 2C, 2D), WB (Figure 3A, 3B, 3D, 3E, S3A, S3B, S3D, S3E). Contributed to the writing of the methods section. Reviewed/edited the manuscript.

Rumen Ivanov

Conceptualization of study. Supervised the study. Designed, performed, and analyzed following experiments: confocal imaging, cytoplasm-to-nucleus signal ratio quantification, FRAP, colocalization coefficient. Contributed to the writing of the manuscript, reviewed/edited the manuscript.

Monique Eutebach, Büsra Acaroglu

Assisted in plant growth, protoplast generation, and WB.

Inga Mohr

Contributed key material. Reviewed/edited the manuscript.

Petra Bauer

Supervised the study, provided funding, and reviewed/edited the manuscript.

Tzvetina Brumbarova

Conceptualization of study. Supervised the study. Designed, performed, and analyzed following experiments: cytoplasm-to-nucleus signal ratio, assisted in WB. Designed the outline of the manuscript. Wrote the manuscript, prepared final figures, and reviewed/edited the manuscript.

9 Manuscript I

FER-LIKE IRON DEFICIENCY-INDUCED TRANSCRIPTION FACTOR (FIT) accumulates in homo- and heterodimeric complexes in dynamic and inducible nuclear condensates associated with speckle components

FER-LIKE IRON DEFICIENCY-INDUCED TRANSCRIPTION FACTOR (FIT) accumulates in homo- and heterodimeric complexes in dynamic and inducible nuclear condensates associated with speckle components

Short title: FIT localizes in condensates

Ksenia Trofimov¹, Regina Gratz^{1,†}, Rumen Ivanov¹, Yvonne Stahl^{2,3}, Petra Bauer^{1,3,*}, Tzvetina Brumbarova^{1,*}

¹ Institute of Botany, Heinrich-Heine-University, 40225 Düsseldorf, Germany

² Institute for Developmental Genetics, Heinrich-Heine-University, 40225 Düsseldorf, Germany

³ Cluster of Excellence on Plant Science (CEPLAS), Heinrich-Heine-University, 40225 Düsseldorf, Germany

* Shared corresponding authors: Tzvetina Brumbarova (Tzvetina.Brumbarova@hhu.de), Petra Bauer (Petra.Bauer@hhu.de)

† Present address: Department of Forest Genetics and Plant Physiology, Swedish University of Agricultural Sciences, 90183 Umeå, Sweden

Author contributions

K.T., R.I., Y.S., P.B. and T.B. designed the research; K.T. performed research; K.T., R.I., Y.S., and T.B. analyzed data; R.G. contributed key materials; K.T. wrote the paper; P.B. acquired funding; all authors reviewed and edited the article.

Highlights

- FIT undergoes light-induced condensation and localizes to NBs, likely via LLPS
- Functionally relevant Ser271/272 defines an intrinsically disordered region and influences NB formation dynamics
- NBs are preferential sites for FIT dimerization with FIT and bHLH039, dependent on Ser271/272
- FIT NBs colocalize with NB markers related to splicing and light signaling

Keywords

anisotropy, bHLH039, condensates, FIT, FRAP, FRET-FLIM, IDR, LLPS, nuclear body, photobody, speckle, SR45

Abbreviations

bHLH	basic helix-loop-helix
bHLH039	BASIC HELIX-LOOP-HELIX039
C	mCherry
FIT	FER-LIKE IRON DEFICIENCY-INDUCED TRANSCRIPTION FACTOR
FLIM	fluorescence lifetime imaging microscopy
FRAP	fluorescence recovery after photobleaching
FRET	fluorescence resonance energy transfer
G	GFP
GFP	GREEN FLUORESCENT PROTEIN
IDR	intrinsically disordered region
LLPS	liquid-liquid phase separation
mCherry	monomeric Cherry
mRFP	monomeric RED FLUORESCENT PROTEIN
NB	nuclear body
NP	nucleoplasm
PB	photobody
R	mRFP
TF	transcription factor

Abstract

Several nuclear proteins undergo condensation. The question remains often whether this property is coupled to a functional aspect of the protein in the nucleus. The basic helix-loop-helix (bHLH) FER-LIKE IRON DEFICIENCY-INDUCED TRANSCRIPTION FACTOR (FIT) integrates internal and external signals to control the amount of iron that is acquired in accordance with growth. The previously described C-terminal Ser271/272 allows FIT to form active complexes with subgroup 1b bHLH factors such as bHLH039. FIT has lower nuclear mobility than mutant FITmSS271AA, but this behavior has remained mechanistically and functionally obscure. Here, we show that FIT undergoes a light-inducible subnuclear partitioning into nuclear condensates that we termed FIT nuclear bodies (NBs). The characteristics of FIT NBs could be examined using a standardized FIT NB analysis procedure coupled with different types of quantitative and qualitative microscopy-based approaches. We found that FIT condensates were likely formed by liquid-liquid phase separation. FIT accumulated preferentially in FIT NBs versus nucleoplasm when engaged in protein complexes with itself and with bHLH039. FITmSS271AA, instead, localized to NBs with different dynamics. FIT colocalized with splicing and light signaling NB markers. Hence, the inducible highly dynamic FIT condensates link active transcription factor complexes with post-transcriptional regulation processes.

Introduction

As sessile organisms, plants must adjust to an ever-changing environment. Read-out of environmental cues and rapid acclimation are necessary to ensure the plant's vitality. Accordingly, plants control micronutrient uptake. Overaccumulation causes toxicity but lack of a micronutrient leads to deficiency symptoms. Even though iron is one of the most abundant elements in the soil, its bioavailability as micronutrient is limited in most soils, rendering iron uptake a challenge for plants (Römheld and Marschner, 1986; Wedepohl, 1995).

An essential regulatory protein needed for iron acquisition is the basic helix-loop-helix (bHLH) transcription factor (TF) FER-LIKE IRON DEFICIENCY-INDUCED TRANSCRIPTION FACTOR (FIT; Colangelo and Guerinot, 2004; Jakoby et al., 2004; Yuan et al., 2005; Bauer et al., 2007). FIT is activated upon iron deficiency downstream of a cascade of bHLH TFs (Zhang et al., 2015; Li et al., 2016; Liang et al., 2017; Kim et al., 2019; Gao et al., 2020) and of a calcium-sensing protein kinase able to target phosphorylation site Ser271/272 of FIT (Gratz et al., 2019). FIT alone is not sufficient to upregulate iron acquisition, while it is active in a heterodimeric complex together with a member of the bHLH subgroup Ib such as bHLH039 (Yuan et al., 2008; Wang et al., 2013). Furthermore, FIT action is regulated through protein-protein contacts with multiple key players of hormonal and abiotic stress signaling pathways (Lingam et al., 2011; Le et al., 2016; Wild et al., 2016; Cui et al., 2018; Gratz et al., 2019, 2020). Thus, FIT behaves as a regulatory hub in root cells that perceives external and internal cues to adjust iron acquisition with growth (Schwarz and Bauer, 2020; Kanwar et al., 2021).

The subcellular localization of the FIT-bHLH039 module is remarkable. bHLH039 alone is inactive and present mainly close to the plasma membrane in cytoplasmic foci, while bHLH039 together with FIT localizes in the nucleus (Trofimov et al., 2019). FIT is predominately localized in the nucleus but not as mobile compared to mutant FITmSS271AA, that is a more inactive mutant form of FIT (Gratz et al., 2019). Subcellular partitioning of proteins involved in nutrient uptake has until now not been enough in the focus of research to understand the significance of the differing subcellular localization patterns.

One prominent type of subnuclear partitioning is conferred by biomolecular condensates, or nuclear bodies (NBs). NBs are membraneless, nuclear subcompartments, which can be of stable or dynamic nature. To form condensates, proteins need to have particular features that enable protein interactions and compaction in three-dimensional space. IDRs are flexible protein regions that allow conformational changes, and thus various interactions, leading to the required multivalency of a protein for condensate formation (Tarczewska and Greb-Markiewicz, 2019; Emenecker et al., 2020). As *Arabidopsis thaliana* (Arabidopsis) TFs are enriched in IDRs (Strader et al., 2022) it is not unlikely that the resulting multivalency in TFs drives condensation and results in microenvironments for interaction, probably more often than so far studied. IDRs are particularly characteristic in bHLH TFs in vertebrates and invertebrates (Tarczewska and Greb-Markiewicz, 2019), suggesting that this

feature may also be relevant for the bHLH TFs of plants. One possibility for condensates to form is to undergo liquid-liquid phase separation (LLPS). In this process, a solution is demixed into two or more phases (Emenecker et al., 2020). This mechanism has been examined in simplified *in vitro* systems, but the involvement of different cell components renders the mechanism more complex *in vivo* (Fang et al., 2019; Riback et al., 2020; Zhu et al., 2021).

NBs comprise an immense variety of types, and plants and animals share several of them, e.g., the nucleolus, Cajal bodies, and speckles. The nucleolus is involved in transcription of ribosomal DNA, processing of ribosomal RNA, and ribosome biogenesis (Kalinina et al., 2018; Lafontaine et al., 2021). Nucleoli share components and function with Cajal bodies, which are e.g., ribonucleoproteins and RNA processing (Love et al., 2017; Trinkle-Mulcahy and Sleeman, 2017). Speckles are known spliceosomal sites (Reddy et al., 2012; Galganski et al., 2017). Plant-specific NBs are photobodies (PBs), which are triggered by light, temperature, and circadian clock (Pardi and Nusinow, 2021). PBs harbor regulatory complexes of the photomorphogenic responses, including photoreceptors like phytochromes (phy) and bHLH TFs belonging to the PHYTOCHROME INTERACTING FACTORS (PIFs; Pardi and Nusinow, 2021). Another trigger for inducible condensate formation is temperature (Jung et al., 2020; Zhu et al., 2021).

NBs may act as hubs integrating environmental signals (Emenecker et al., 2020; Meyer, 2020). Especially PBs may combine external cues, such as light, as an input signal to steer developmental processes (Kaiserli et al., 2015; Meyer, 2020; Pardi and Nusinow, 2021). It is proposed that the formation of NBs could be an ancient mechanism for spatial organization within the nucleus (Emenecker et al., 2020). As more evidence on condensation in plants arises, this topic remains barely examined in the scope of plant nutrition.

The motivation for our study was to elucidate the mechanism behind subcellular distribution and nuclear mobility of FIT. We had found an interesting hint that FIT may undergo light-inducible nuclear condensation, when we detected FIT nuclear bodies (NBs). We developed a standardized FIT NB analysis procedure and applied it to characterize quantitative and qualitative aspects of the dynamic NB formation using different microscopy-based techniques. Thereby, we were able to link FIT NB formation with the activity status of FIT to form functional protein complexes. We found that splicing and light signaling were also associated with FIT NBs. Thus, this study lays ground for FIT NBs being regulatory hubs steering nutritional signaling and associating functional significance to FIT protein condensate formation.

Results

FIT localizes to NBs in light-inducible and dynamic manner likely as a result of LLPS

The TF FIT has a dynamic mobility and capacity to form TF complexes inside plant cells (Gratz et al., 2019; Trofimov et al., 2019). To explore possible mechanisms for dynamic FIT subcellular localization, we performed a microscopic study on FIT-GFP protein localization

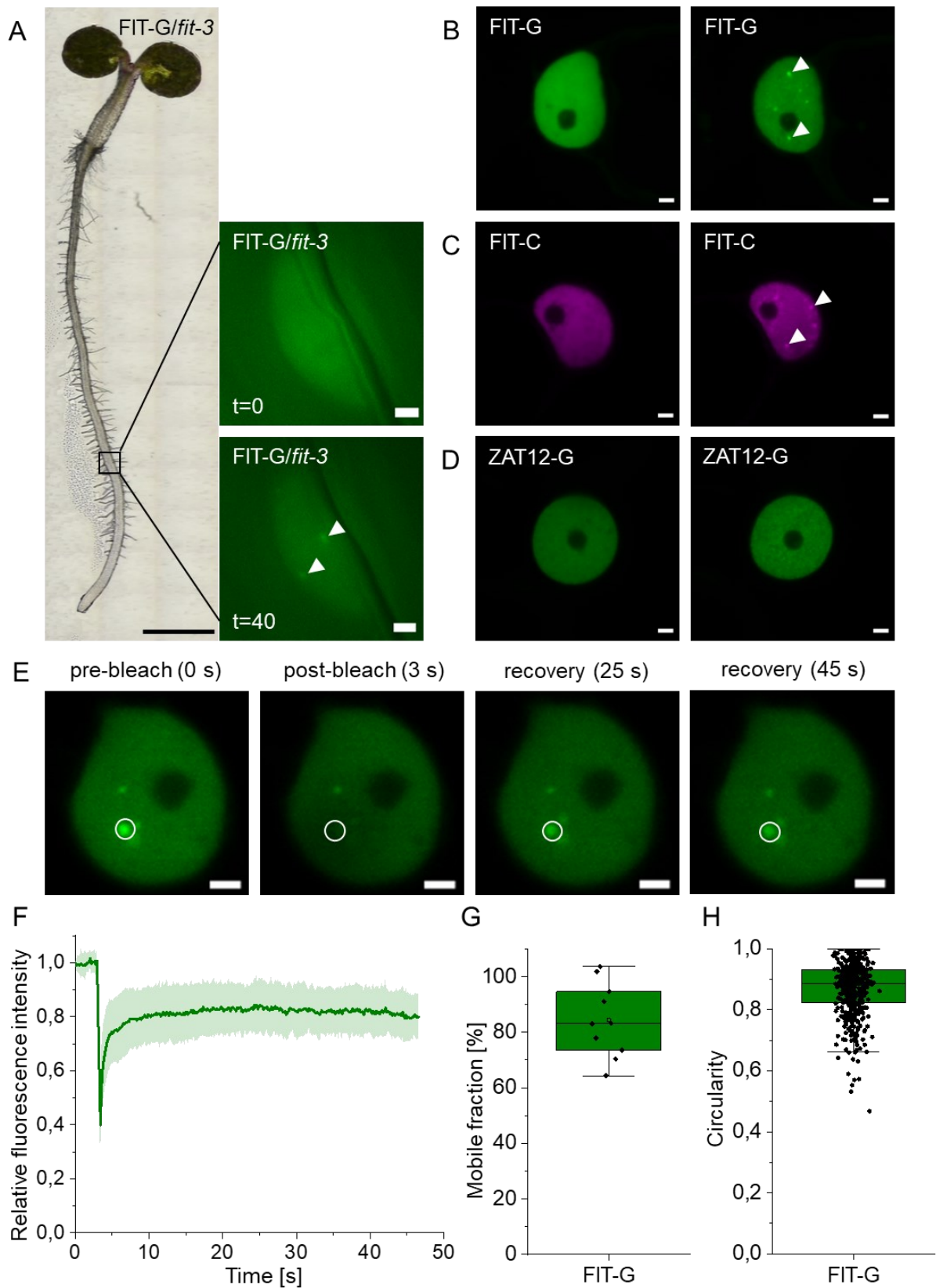


Figure 1. FIT accumulated in nuclear condensates, termed FIT nuclear bodies (NBs) in a light-inducible manner, most likely following liquid-liquid phase separation (LLPS).

A, Induction of FIT NBs in Arabidopsis root epidermis cells of the root differentiation zone. Left, light microscopy overview image of a 5-d-old Arabidopsis seedling (FIT-GFP/*fit-3*) grown in iron deficiency. Right, nuclear localization of FIT-GFP in the root epidermis cells as indicated in the overview image, at t=0 and t=40 min. FIT-GFP signals were evenly distributed in the nucleus at t=0 min, and after induction by excitation with 488 nm laser NB

formation accumulated in NBs at t=40 min. Note that root epidermis cells developed few NBs with weak FIT-GFP signals. B-H, Fluorescence protein analysis in transiently transformed *N. benthamiana* leaf epidermis cells. B-D, Confocal images of B, FIT-GFP, C, FIT-mCherry, and D, ZAT12-GFP at t=0 and t=5 min. At t=0 min, FIT-GFP and FIT-mCherry showed an even distribution within the nucleus. Following a 488 nm laser excitation, numerous NBs were clearly visible in all examined transformed cells at t=5 min. These NBs were termed FIT NBs. Under the same imaging conditions, ZAT12-GFP did not show NB formation. According to these results, a standardized FIT NB analysis procedure was set up (**Supplemental Figure S1**). See also **Supplemental Movie S1A-C**. E-G, FRAP measurements to test for liquid-like behaviour of FIT NBs, using the standardized FIT NB analysis procedure in transiently transformed *N. benthamiana* leaf epidermis cells. E, Images of the fluorescent signal during the FRAP experiment, taken before bleaching (0 s) and recovery of fluorescence at three time points after bleaching from 3 s to 45 s within the circled region of a NB. F, Diagram representing the relative fluorescence during the measurement, showing a high fluorescence recovery rate of FIT-GFP within NBs. G, Diagram representing the mobile fraction of FIT-GFP calculated based on the relative fluorescence recovery. The diagram indicates high mobility of FIT. H, Quantification of the FIT NB shape with the software ImageJ (National Institutes of Health), indicating that FIT NBs have circular shape. Mobility and circularity characteristics indicate that FIT NBs are most likely liquid condensates that are the result of LLPS.

Line diagram represents the mean and standard deviation. Box plots show 25-75 percentile with min-max whiskers, mean as small square and median as line. Scale bars of nuclei images, 2 μ m; scale bar full seedling, 1 mm. Arrowheads indicate NBs. G = GFP; C = mCherry.

in the root epidermis of the root differentiation zone of 5-d-old iron-deficient seedlings of *Arabidopsis thaliana* (*Arabidopsis*), where FIT is active and iron acquisition occurs (35S_{pro}:FIT-GFP complemented *fit-3*; Jakoby et al., 2004; Gratz et al., 2019). At first microscopic inspection, FIT-GFP was evenly distributed within the nucleus. After a lag time, FIT-GFP became re-localized at the subnuclear level (**Figure 1A**). Discrete FIT-GFP nuclear spots were visible after 40 min earliest, sometimes taking up to 2 h to appear. One to four spots were observed per nucleus. Nuclear FIT-GFP spots were triggered either by exposure of whole seedlings to 488 nm laser for several minutes or by shifting seedlings grown in white light into blue light for a total time of 2 h with subsequent immediate imaging. The observation of FIT nuclear spots in the root epidermis of the root differentiation zone was very interesting, suggesting that these might perhaps be NBs containing FIT. However, further inspection of the nuclear spots in root cells in this differentiating root zone was hampered by several difficulties, namely the small size and low accessibility of the nucleus, comparably low level of expression of FIT in roots (see also Lingam et al., 2011; Meiser et al., 2011), and especially considering the long lag time for detecting the nuclear spots. These factors made it impossible for us to apply quantitative fluorescence microscopy techniques to draw validated conclusions on the nature, dynamics, and functional significance of nuclear spots in root epidermis cells of the root differentiation zone of iron-deficient seedlings.

FIT-GFP that was transiently expressed in *Nicotiana benthamiana* (*N. benthamiana*) leaf epidermis cells under a β -estradiol-inducible promoter to control protein expression showed a very similar re-localization of FIT-GFP into nuclear spots as observed in the *Arabidopsis* root epidermis, again triggered by treatment with a 488 nm laser light stimulus.

Differences were, however, the duration of the lag time needed to observe this phenomenon, and the number of nuclear spots. As in Arabidopsis, FIT-GFP localized initially in uniform manner to the entire nucleus ($t=0$) of *N. benthamiana* leaf epidermis cells. A short duration of 1 min 488 nm laser light excitation induced the formation of FIT-GFP signals in discrete spots inside the nucleus after a lag time of only five minutes ($t=5$; **Figure 1B and Supplemental Movie S1A**). The nuclear FIT spots were systematically initiated, and nearly all nuclei in the imaged leaf disk showed numerous spots. A similar laser light excitation procedure was previously found to elicit PB formation of cryptochrome2 (CRY2) in Arabidopsis protoplasts and HEK293T cells (Wang et al., 2021). We deduced that the spots of FIT-GFP signal were NBs. FIT NB formation was not dependent on the fluorescent tag, as it was similar for FIT-mCherry when co-excited with 488 nm laser light (**Figure 1C**). Another TF and interactor of FIT, ZINC FINGER OF ARABIDOPSIS THALIANA12-GFP (ZAT12-GFP; Le et al., 2016), did not localize to NBs under the same imaging conditions (**Figure 1D and Supplemental Movie S1B**). Therefore, we concluded that FIT localization to NBs was a specificity of FIT and that formation of FIT NBs was not artificially caused by fluorescent tags or the imaging setup. Importantly, the *N. benthamiana* epidermis expression system was suited to control the parameters for light-induced triggering of FIT NBs and their quantitative analysis by fluorescence microscopy. We then developed a standardized experimental procedure for qualitative and quantitative FIT NB analysis in *N. benthamiana* (hereafter named 'standardized FIT NB analysis procedure'; **Supplemental Figure S1**).

LLPS is a possible way for condensate formation, and liquid-like features are quantifiable by mobility and shape analysis within condensates (Shin et al., 2017; Wang et al., 2021). We used the standardized FIT NB analysis procedure to examine whether this could also be a mechanism underlying the FIT NB formation. Mobility of FIT NBs was tested with the fluorescence recovery after photobleaching (FRAP) approach (Bancaud et al., 2010; Trofimov et al., 2019) by recording the recovery of the fluorescence intensity over time in a bleached NB (**Figure 1E-G**). According to relative fluorescence intensity the fluorescence signal recovered to a high extent with FIT NBs (**Figure 1F**), and the calculated mobile fraction of the NB protein was on average 80% (**Figure 1G**). Shape analysis of FIT NBs showed that the NBs reached a high circularity score (**Figure 1H**). According to Wang et al. (2021), fluorescence recovery and circularity scores as the ones measured for FIT NBs reflect high mobility and circular shape. Thus, FIT NBs behave in a liquid-like manner suggesting that LLPS might be the mechanism leading to FIT NB formation.

In summary, the developed standardized FIT NB analysis procedure was well suited for investigating dynamic properties of light-induced FIT NBs and characterizing them as the likely result of LLPS. Because of these properties, it is justified to term them 'FIT NBs'. We hypothesized that NB formation is a feature of the FIT protein that provides regulatory

specificity, and we subsequently investigated this hypothesis using the developed standardized FIT NB analysis procedure in all subsequent assays below.

FIT forms homodimeric complexes preferentially in NBs, dependent on Ser271/272

Next, we asked which properties of the FIT protein enable NB formation. Residue Ser271/272 is important for the homo- and heterodimerization capacity of FIT (Gratz et al., 2019). We therefore asked whether this site has an influence on FIT NB formation, and we compared the ability for NB formation of mutant FITmSS271AA-GFP with that of wild-type FIT-GFP protein. FITmSS271AA-GFP also localized to NBs, however with different dynamics.

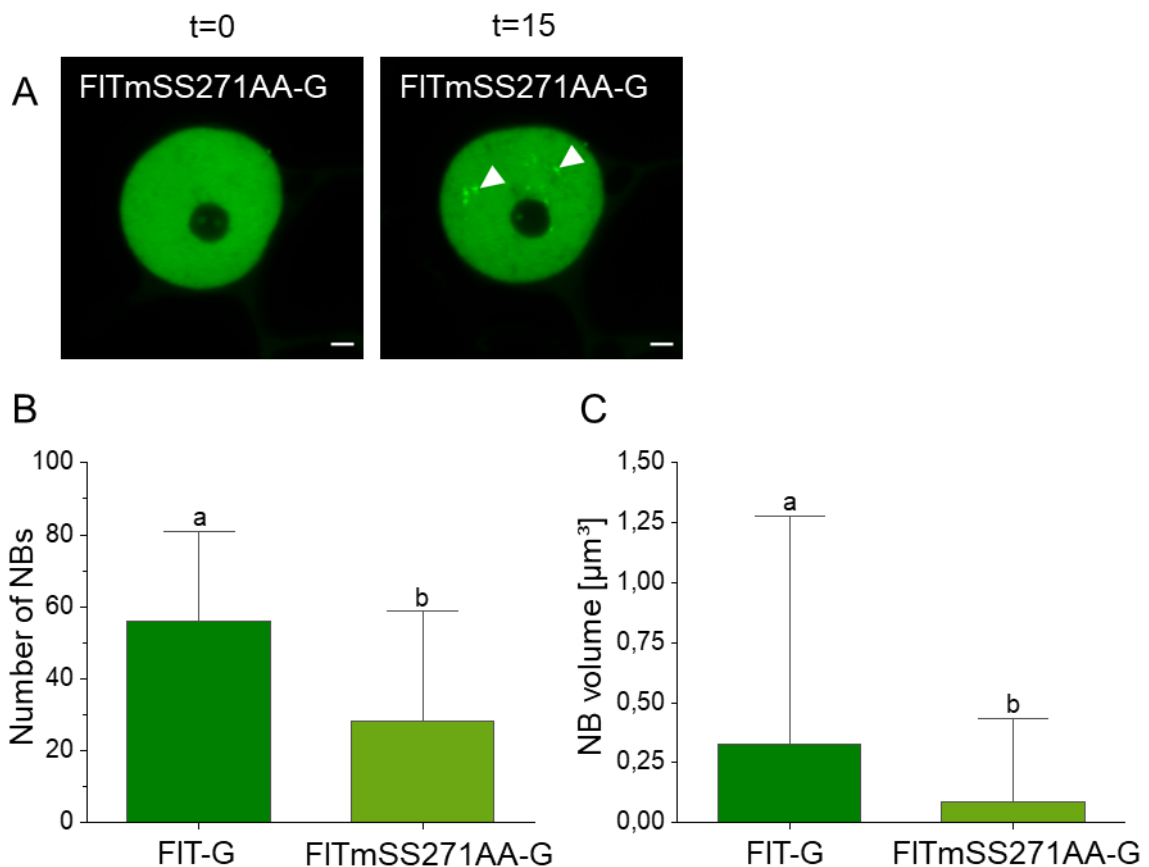


Figure 2. The FIT C-terminal Ser271/272 site was important for the capacity of FIT to localize to NBs.

A, Confocal images of nuclear localization of FITmSS271AA-GFP at t=0 and t=15 min. FITmSS271AA-GFP accumulated in NBs, but NB formation required a longer time compared to FIT-GFP. See also **Supplemental Movie S1, A and C**. B, Number of NBs, and C, size of NBs, of FIT-GFP and FITmSS271AA-GFP at t=5/15 min. NB number and size were determined with the software ImageJ (National Institutes of Health). FIT-GFP accumulated in more and larger NBs than FITmSS271AA-GFP. See **Supplemental Movie S1, A and C**. FITmSS271AA-GFP lacks IDR^{Ser271/272}. This IDR may be relevant for FIT NB formation (**Supplemental Figure S2**).

Bar diagrams represent the mean and standard deviation. Statistical analysis was performed with the Mann-Whitney test. Different letters indicate statistically significant differences ($P < 0.05$). Scale bar: 2 μm . Arrowheads indicate NBs. G = GFP. Analysis was conducted in transiently transformed *N. benthamiana* leaf epidermis cells, following the standardized FIT NB analysis procedure.

The formation of FITmSS271AA NBs was delayed in time (**Figure 2A**; $t=15$ instead of $t=5$). While FIT-GFP NB formation started in the first minutes after excitation (**Supplemental Movie S1A**), FITmSS271AA-GFP NB formation occurred earliest 10 min after excitation (**Supplemental Movie S1C**). In addition, NB number and size of FITmSS271AA-GFP were decreased in comparison to the ones from wild-type FIT-GFP (**Figure 2, B and C**). Hence, the dynamics of NB formation were dependent on Ser271/272.

The process of condensation is facilitated when proteins possess IDRs, since, importantly, IDRs may engage in numerous interactions in space due to rapid conformational changes (Tarczewska and Greb-Markiewicz, 2019; Emenecker et al., 2020). The three-dimensional conformation of wild-type FIT had predicted stretches of intrinsic disorganization, peaking before and at the basic region of the bHLH domain, and two in the C-terminal part, one of them around the Ser271/272 site (termed IDR^{Ser271/272}; **Supplemental Figure S2A**). In contrast, in the FITmSS271AA mutant this C-terminal region was no longer classified as IDR (**Supplemental Figure S2B**). This underlined the significance of the Ser271/272 site, not only for interaction but also for FIT NB formation.

We then tested whether FIT homodimerization was preferentially associated with NB formation. For that, we investigated whether FIT-GFP shows a differentiated homodimerization strength, first, inside the NBs versus the nucleoplasm (NP), and second, as wild-type FIT versus the mutant FITmSS271AA-GFP protein by performing anisotropy (or homo-FRET) measurements. Energy transfer between the same kind of fluorescently tagged proteins leads to depolarization of the emitted light (Stahl et al., 2013; Weidtkamp-Peters et al., 2022). Fluorescence anisotropy (FA) describes this depolarization and gives hints on the dimerization and oligomerization status of a protein as the FA value decreases (**Figure 3A**). We measured FA before ($t=0$) and after NB formation ($t=5$ for FIT and $t=15$ for FITmSS271AA), and analyzed the homodimerization strength for the whole nucleus, the NBs, and the residual NP (**Figure 3B-D**). Free GFP and GFP-GFP constructs were used as references for monomers and dimers (**Figure 3C and D**).

Whole nucleus FA values were lower at $t=5$ than at $t=0$ for FIT-GFP. Additionally, FA values were lower within the NBs compared to the NP (**Figure 3C**). Compared to wild-type FIT-GFP, FA values were not reduced for mutant FITmSS271AA-GFP at $t=15$ compared to $t=0$. Also, the FA values did not differ between NBs and NP for the mutant protein (**Figure 3D**). This indicated the presence of homodimeric FIT complexes in NBs.

In summary, wild-type FIT had better capacities to localize to NBs than mutant FITmSS271AA, presumably due its IDR^{Ser271/272} at the C-terminus. NBs were nuclear sites in which FIT formed preferentially homodimeric protein complexes.

FIT-bHLH039 interaction complexes preferentially accumulate in FIT NBs

FIT engages in protein-protein interactions with bHLH039 to steer iron uptake target gene induction in the nucleus, while mutant FITmSS271AA protein is less active in interacting

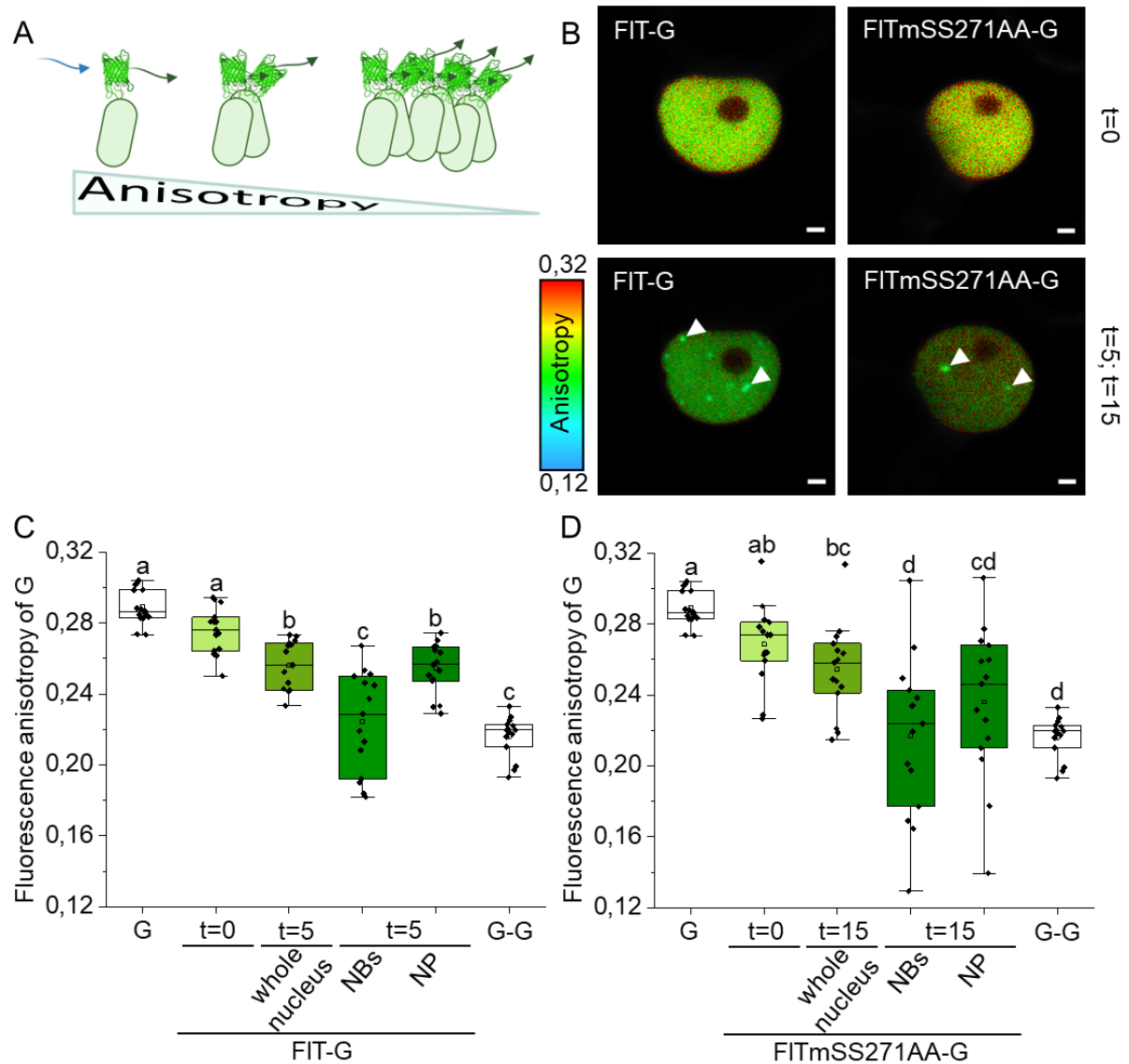


Figure 3. FIT was present in homodimeric protein complexes in NBs, dependent on Ser271/272 site.

Anisotropy (or homo-FRET) measurements of FIT-GFP and FITmSS271AA-GFP to determine homodimerization strength. A, Schematic illustration of the anisotropy principle. Energy transfer between the same kind of fluorescently tagged proteins leads to depolarization of the emitted light. Extent of the depolarization gives a hint on dimerization and oligomerization of a protein as the fluorescence anisotropy (FA) value decreases. B, Images showing colour-coded FA values of FIT-GFP and FITmSS271AA at t=0 and t=5/15 min. C-D, Quantification of FA values. FA was measured at t=0 within the whole nucleus and at t=5/15 min within the whole nucleus, in NBs and in residual NP. Free GFP and GFP-GFP served as references for mono- and dimerization. FA values for C, FIT-GFP, and D, FITmSS271AA-GFP. FA values decreased for FIT-GFP, but not FITmSS271AA-GFP, in the whole nucleus (compare t=0 with t=5/15 min). FA values were also lowered in NBs versus NP in the case of FIT-GFP but not FITmSS271AA-GFP (compare t=5/15 min of NBs and NP). This indicates stronger homodimerization of FIT than FITmSS271AA-GFP in the whole nucleus and in NBs. IDR^{Ser271/272} may therefore be relevant for FIT NB formation and FIT homodimerization (**Supplemental Figure S2**).

Box plots show 25-75 percentile with min-max whiskers, mean as small square and median as line. Statistical analysis was performed with one-way ANOVA and Tukey post-hoc test. Different letters indicate statistically significant differences ($P < 0.05$). Scale bar: 2 μm . Arrowheads indicate NBs. C and D show the same free GFP and GFP-GFP references because both measurements were performed on the same day. G = GFP. Fluorescence protein analysis was conducted in transiently transformed *N. benthamiana* leaf epidermis cells, following the standardized FIT NB analysis procedure.

with bHLH039 (Gratz et al., 2019). Hence, we tested whether FIT also interacts with bHLH039 preferentially inside NBs and whether mutant FITmSS271AA differs in this ability from wild-type FIT protein. bHLH039 alone does not localize inside the nucleus but requires FIT for nuclear localization (Trofimov et al., 2019), so that bHLH039 was not used alone to test its subnuclear localization.

Upon co-expression, FIT-GFP and bHLH039-mCherry colocalized fully in NBs that resembled the previously described FIT NBs. In the beginning, both proteins were uniformly distributed within the nucleus ($t=0$), and later became localized in NBs ($t=5$; **Figure 4A**).

We then examined the heterodimerization strength of FIT-GFP and bHLH039-mCherry, and FITmSS271AA-GFP and bHLH039-mCherry by FRET-fluorescence lifetime imaging microscopy (FRET-FLIM) measurements. In case of protein interaction (close proximity, ≤ 10 nm), energy transfer between a fluorescently tagged donor and a fluorescently tagged acceptor decreases the fluorescence lifetime of the donor (**Figure 4B**; Borst and Visser, 2010; Weidtkamp-Peters and Stahl, 2017). We quantified the fluorescence lifetime of FIT-GFP and FITmSS271AA-GFP respective of heterodimerization before ($t=0$) and after NB formation ($t=5$ for FIT and $t=15$ for FITmSS271AA) in the whole nucleus, in NBs, and in the NP (**Figure 4C-E**). FIT-GFP and FITmSS271AA-GFP (donor only) served as negative controls.

Fluorescence lifetime was decreased for the pair FIT-GFP and bHLH039-mCherry at $t=5$ within NBs compared to all other measured areas (**Figure 4D**). In contrast to that, the fluorescence lifetime decrease for the pair FITmSS271AA-GFP and bHLH039-mCherry at $t=15$ was not different between NBs and NP (**Figure 4E**). This indicated that heterodimeric complexes accumulated preferentially in FIT NBs.

In summary, heterodimerization of FIT with bHLH039 was spatially concentrated in NBs versus the remaining nuclear space and was less prominent for FITmSS271AA. Hence, the capacity of FIT to form an active TF complex was coupled with its presence in NBs. The occurrence of FIT homo- and heterodimerization preferentially in NBs suggests that FIT protein interaction may drive condensation. We therefore concluded that FIT NBs may be sites with active TF complexes for iron deficiency response regulation.

FIT NBs colocalize with speckle components

Numerous NB types are known, and they are associated with particular proteins that are indicative of the NB type. To further understand the identity, dynamics, and function of FIT NBs, we co-expressed FIT-GFP with seven different NB markers from The Plant Nuclear Marker collection (NASC) and observed NB formation and protein colocalization before ($t=0$) and after FIT NB formation ($t=5$). In cases where we detected a colocalization with FIT-GFP, we analyzed the localization of NB markers also in the single expression at $t=0$ and at $t=5$ after the 488 nm excitation, to detect potentially different patterns in single and co-expression.

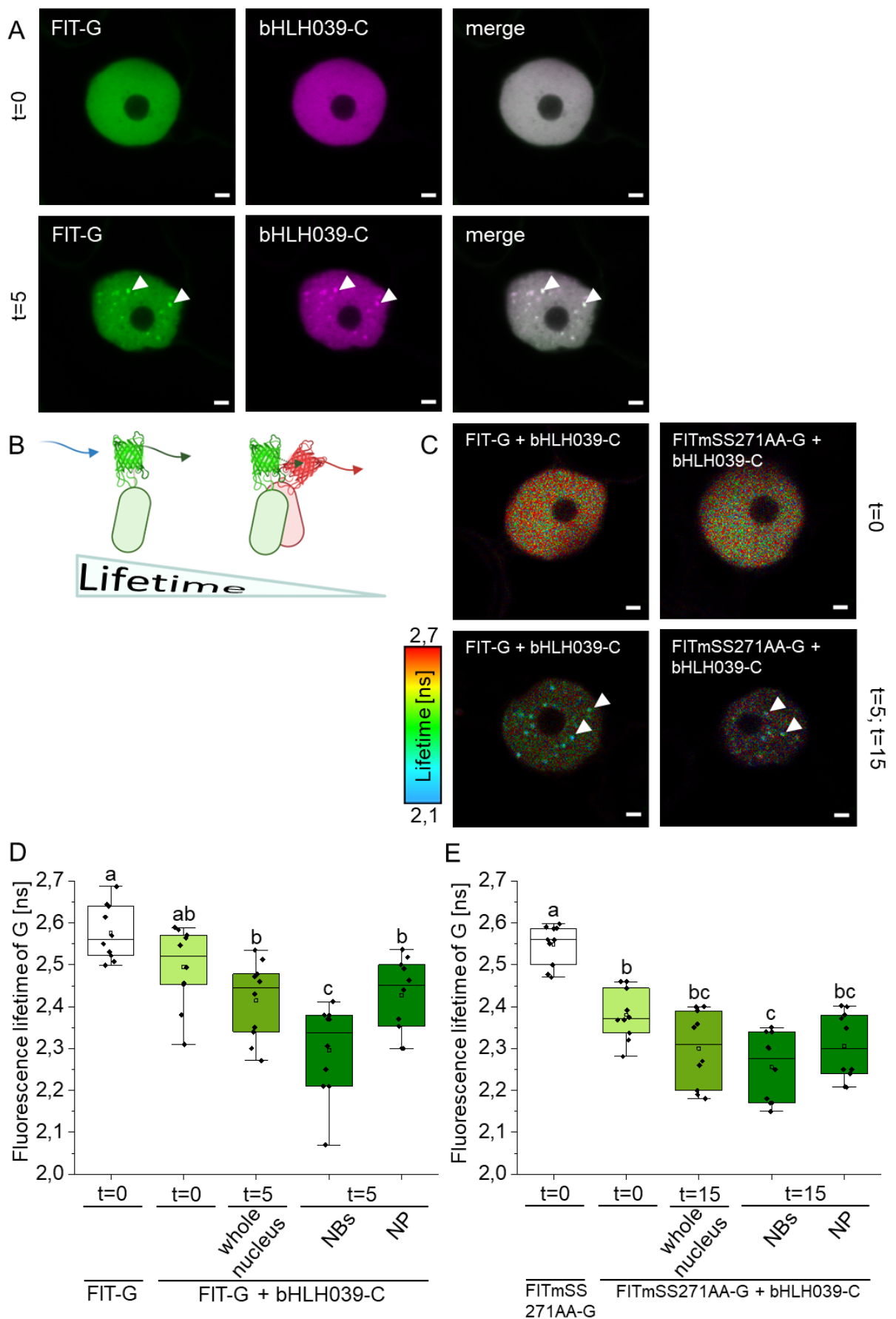


Figure 4. FIT was present in heterodimeric protein complexes with bHLH039 in NBs, dependent on Ser271/272 site.

A, Confocal images with colocalization of FIT-GFP and bHLH039-mCherry in the nucleus. Both proteins were evenly distributed within the nucleus at t=0 and colocalized fully in FIT NBs at t=5 min. B-E, FRET-FLIM measurements to determine heterodimerization strength of FIT and FITmSS271AA with bHLH039, respectively. FIT-GFP and FITmSS271AA-GFP (donor only) served as negative controls. B, Schematic illustration of the FRET-FLIM principle. Energy transfer occurs between two different fluorophores. One fluorophore acts as the donor and the other as the acceptor of the energy. In case of interaction (close proximity, ≤ 10 nm) the fluorescence lifetime of the donor decreases. C, Images showing colour-coded fluorescence lifetime values of FIT-GFP and FITmSS271AA-GFP co-expressed with bHLH039-mCherry at t=0 and t=5/15 min. D-E, FRET-FLIM measurements at t=0 within the whole nucleus and at t=5/15 min within the whole nucleus, inside NBs and in residual NP. Fluorescence lifetime was reduced for the pair of FIT-GFP and bHLH039-mCherry in NBs versus NP at t=5 min, indicating protein interaction preferentially inside NBs. Fluorescence lifetime values were not significantly different for the pair FITmSS271AA-GFP and bHLH039-mCherry in this same comparison at t=15 min, indicating that this pair did not preferentially interact in NBs. IDR^{Ser271/272} may therefore be relevant for FIT NB formation, and FIT homo- and heterodimerization (**Supplemental Figure S2**).

Box plots show 25-75 percentile with min-max whiskers, mean as small square and median as line. Statistical analysis was performed with one-way ANOVA and Tukey post-hoc test. Different letters indicate statistically significant differences ($P < 0.05$). Scale bar: 2 μ m. Arrowheads indicate NBs. G = GFP; C = mCherry. Fluorescence protein analysis was conducted in transiently transformed *N. benthamiana* leaf epidermis cells, following the standardized FIT NB analysis procedure.

All seven NB markers were expressed together with FIT-GFP, and according to the resulting extent of colocalization we subdivided them into three different types. The first type (type I) did colocalize with FIT-GFP neither at t=0 nor at t=5. This was the case for the Cajal body markers coilin-mRFP and U2 snRNP-specific protein U2B^{''}-mRFP (**Supplemental Figure S3**; Lorković et al., 2004; Collier et al., 2006). Coilin-mRFP localized into a NB within and around the nucleolus and with barely any protein in the residual NP, which did not colocalize with FIT NBs (**Supplemental Figure S3A**). The NBs of U2B^{''}-mRFP close to the nucleolus also did not colocalize with FIT NBs (**Supplemental Figure S3B**). Hence, FIT-GFP was not associated with Cajal bodies.

The second type (type II) of NB markers were partially colocalized with FIT-GFP. This included the speckle components ARGININE/SERINE-RICH45-mRFP (SR45) and the serine/arginine-rich matrix protein SRm102-mRFP. SR45 is involved in splicing and alternative splicing and is part of the spliceosome in speckles (Ali et al., 2003), and was recently found to be involved in splicing of iron homeostasis genes (Fanara et al., 2022). SRm102 is a speckle component (Kim et al., 2016). SR45-mRFP localized barely in the NP but inside few and very large NBs that remained constant at t=0 and t=5. FIT-GFP did not colocalize in those NBs at t=0, however, it colocalized with the large SR45-mRFP NBs at t=5 (**Figure 5A**). FIT-GFP also localized in typical FIT NBs in the residual NP at t=5 (**Figure 5A**). SRm102-mRFP showed low expression in the NP and stronger expression in a few NBs that also remained constant at t=0 and t=5. FIT-GFP colocalized with SRm102-mRFP in only few instances at t=5, but not t=0, while most FIT NBs did not colocalize with SRm102-mRFP NBs (**Figure 5B**). Both SR45-mRFP and SRm102-mRFP had the same localization pattern at t=0 and t=5, irrespective of

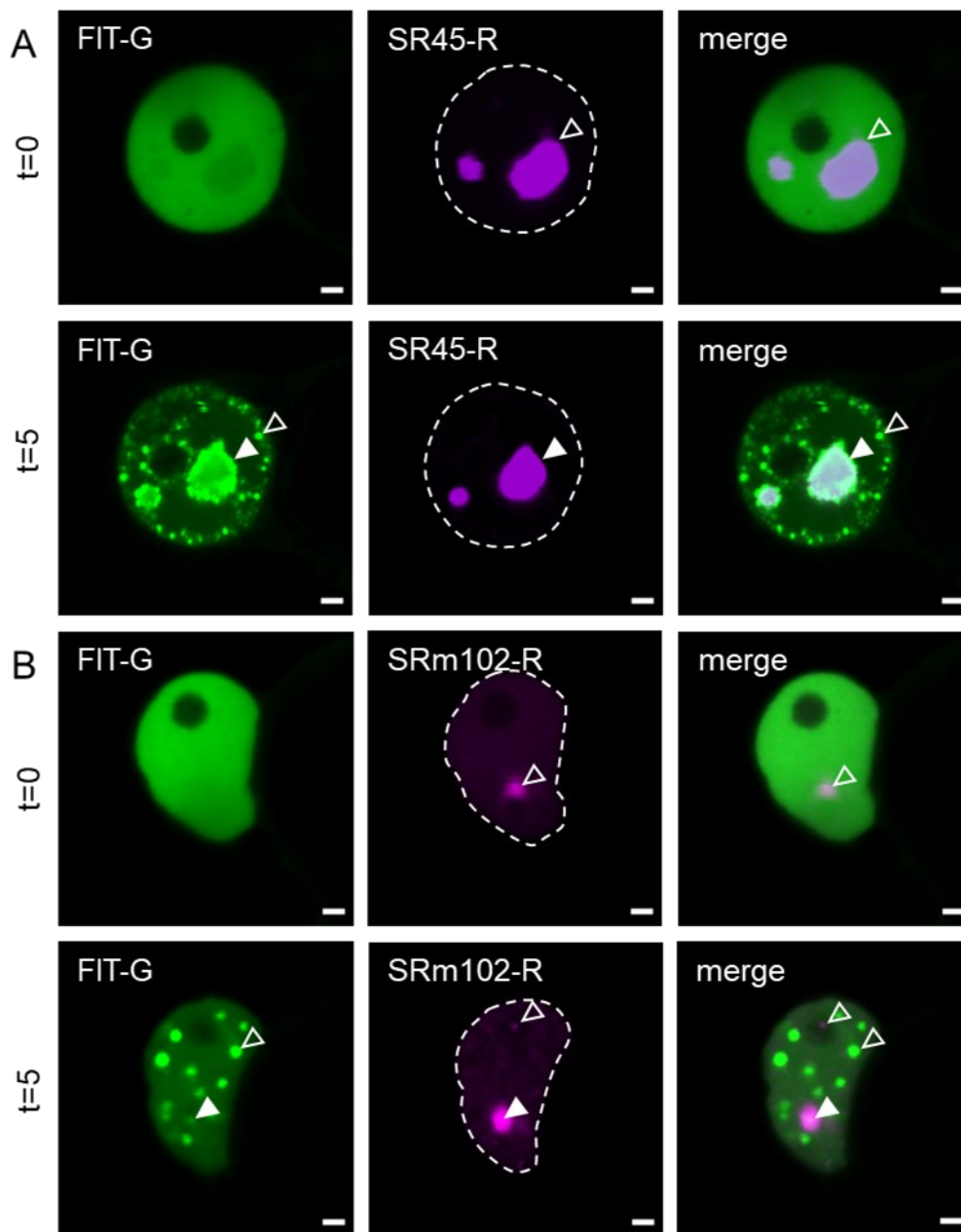


Figure 5. Two NB markers and splicing components were present in NBs in which FIT accumulated after the light trigger, whereas they were not part of FIT NBs (designated type II).

Confocal images showing localization of FIT-GFP and NB markers (type II) upon co-expression in the nucleus at t=0 and t=5 min. Co-expression of FIT-GFP with A, SR45-mRFP, and B, SRm102-mRFP. Type II NB markers localized inside NBs at t=0 and t=5 min. Similar localization patterns were observed upon single expression, showing that SR45 and SRm102 are present in distinct NB types (compare with **Supplemental Figure S4, A and B**). FIT-GFP colocalized with type II markers in their distinct NBs at t=5 min, but not t=0. FIT-GFP additionally localized in FIT NBs at t=5 min. Type II markers were not present in FIT NBs, while FIT-GFP became recruited into the distinct type II NBs upon the light trigger. Hence, FIT NBs could be associated with speckle components.

Scale bar: 2 μ m. Filled arrowheads indicate colocalization in NBs, empty arrowheads indicate no colocalization in NBs. G = GFP; R = mRFP. Fluorescence protein analysis was conducted in transiently transformed *N. benthamiana* leaf epidermis cells, following the standardized FIT NB analysis procedure. For data with type I markers (no colocalization) and type III markers (full colocalization) see **Supplemental Figure S3** and **Figure 6**.

FIT-GFP co-expression or 488 nm excitation (**Supplemental Figure S4**). These type II NB markers seemed to recruit FIT-GFP into NBs after 488 nm excitation that were present (pre-existing) before FIT-GFP NB formation, while FIT-GFP localized additionally in separate FIT NBs. Hence, FIT became associated with splicing components and speckles upon the light trigger.

A third type (type III) of three NBs markers, namely UAP56H2-mRFP, P15H1-mRFP, and PININ-mRFP, were fully colocalized with FIT-GFP. Until now, these NB marker proteins are not well described in plants. UAP56H2 is a RNA helicase, which is involved in mRNA export (Kammel et al., 2013). P15H1 was found as a putative Arabidopsis orthologue of an exon junction complex component in humans (Pendle et al., 2005), while PININ has a redundant role to its paralogue apoptotic chromatin condensation inducer in the nucleus (ACINUS) in alternative splicing (Bi et al., 2021).

UAP56H2-mRFP and P15H1-mRFP did not localize in NBs and were not responsive to the 488 nm excitation when expressed alone or together with FIT-GFP at t=0 (**Figure 6, A and B and Supplemental Figure S4, C and D**). When co-expressed with FIT-GFP and following the 488 nm excitation, at t=5, the two NB markers adopted the FIT NB pattern and colocalized with FIT-GFP in FIT NBs (**Figure 6, A and B**). PININ-mRFP was also uniformly distributed in the nucleus at t=0 like FIT-GFP and fully colocalized with FIT NBs at t=5 (**Figure 6C**). But curiously, PININ-mRFP showed a very different localization in the single expression. Predominately, it localized to a very large NB besides several small NBs with no expression in the NP at t=0 and at t=5 (**Supplemental Figure S4E**). Thus, FIT-GFP recruited these type III NB marker and speckle proteins fully into FIT NBs. Since type III NB markers are also potentially involved in splicing and mRNA export from the nucleus, these same functions may be relevant in FIT NBs.

Taken together, the colocalization studies underlined the dynamic behavior of inducible FIT NB formation. FIT NBs had a speckle function, in which on the one hand FIT was recruited itself into pre-existing splicing-related NBs (SR45-mRFP and SRm102-mRFP, type II), while on the other hand it also recruited speckle-localized proteins into FIT NBs (UAP56H2-mRFP, P15H1-mRFP, and PININ-mRFP, type III).

PB components influence FIT NB localization and formation

PBs are plant-specific condensates which harbor various light signaling components (Kircher et al., 2002; Bauer et al., 2004). Among them are the bHLH TFs of the PIF family. As key regulators of photomorphogenesis, they integrate light signals in various developmental and physiological response pathways (Leivar and Monte, 2014; Pham et al., 2018). Indeed, PIF4 may control iron responses in Arabidopsis based on computational analysis of iron deficiency response gene expression networks (Brumbarova and Ivanov, 2019). We tested in the same manner as described above for NB markers, whether FIT NBs coincide with two of

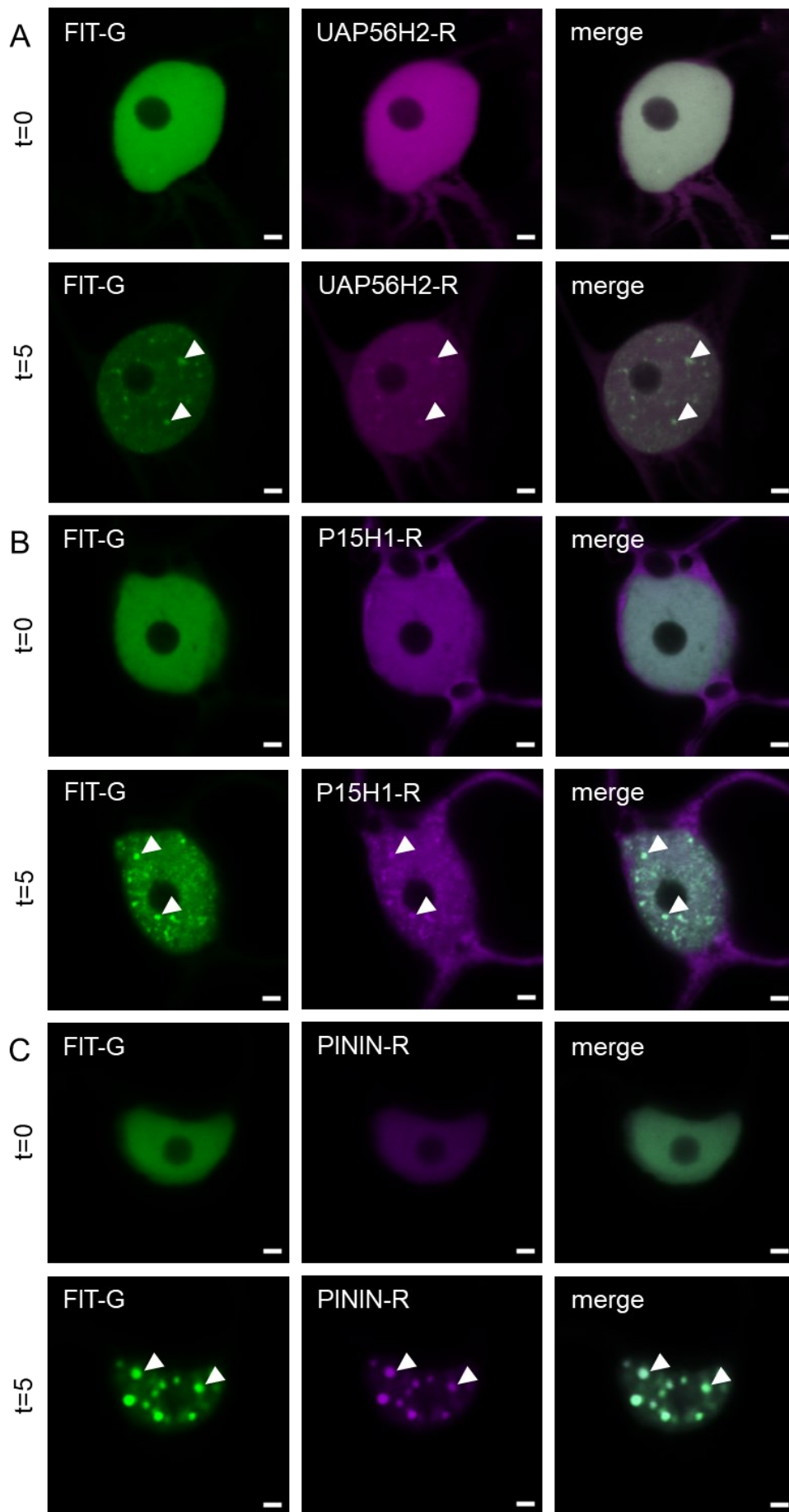


Figure 6. Three NB markers and speckle components became localized in FIT NBs and colocalized fully with FIT (designated type III), suggesting that FIT NBs have speckle function.

Confocal images showing localization of FIT-GFP and NB markers (type III) upon co-expression in the nucleus at t=0 and t=5 min. Co-expression of FIT-GFP with A, UAP56H2-mRFP, B, P15H1-mRFP, and C, PININ-mRFP. All three type III NB markers were homogeneously distributed and colocalized with FIT-GFP in the nucleus at t=0, while they colocalized with FIT-GFP in FIT NBs at t=5 min. UAP56H2-mRFP and P15H1-mRFP showed homogeneous localization in the single expression at both t=0 and t=5 min (compare with **Supplemental Figure S4, C and D**), while PININ-mRFP localized mainly in one large and several small NBs upon single expression at t=0 and t=5 min (compare with **Supplemental Figure S4E**). Hence, these three markers adopted the localization of FIT-GFP upon co-expression and suggest that FIT NBs have a speckle function.

Scale bar: 2 μ m. Arrowheads indicate colocalization within NBs. G = GFP; R = mRFP. Fluorescence protein analysis was conducted in transiently transformed *N. benthamiana* leaf epidermis cells, following the standardized FIT NB analysis procedure. For data with type I markers (no colocalization) and type II markers (partial colocalization) see **Supplemental Figure S3** and **Figure 5**.

the described PB markers, PIF3-mCherry and PIF4-mCherry (Van Buskirk et al., 2014; Qiu et al., 2019, 2021).

We detected distinct localization patterns for PIF3-mCherry and PIF4-mCherry. At t=0, PIF3-mCherry was predominantly localized in a single large PB (**Figure 7A**). In general, localization of single expressed PIF3-mCherry remained unchanged at t=0 and t=15 (**Supplemental Figure S5A**). Upon co-expression, FIT-GFP was initially not present in PIF3-mCherry PB at t=0. After 488 nm excitation and at t=5, FIT NBs were still not visible. Instead, FIT-GFP accumulated and finally colocalized with the large PIF3-mCherry PB at t=15, while the typical FIT NBs did not appear (**Figure 7A**).

PIF4-mCherry localized in two different patterns, and both differed substantially from that of PIF3-mCherry. In the one pattern at t=0, PIF4-mCherry was not localized to any PBs, but instead was uniformly distributed in the NP as was the case for FIT-GFP. Such a pattern was also seen at t=15, and then neither PIF4-mCherry nor FIT-GFP were localized in any PBs/NBs (**Figure 7B**). In the other pattern, PIF4-mCherry and FIT-GFP localized in multiple PBs at t=0 and t=15, whereas none of them corresponded morphologically to the typical FIT NBs (**Figure 7C**). The same two localization patterns were also found for PIF4-mCherry in the single expression, whereby 488 nm excitation did not alter PIF4-mCherry localization (**Supplemental Figure S5, B and C**).

Hence, FIT was able to localize to PBs when co-expressed with PIF3 and PIF4, underlining the ability of FIT as a key regulator to cross-connect iron acquisition regulation to other signaling pathways.

Discussion

In this study, we uncovered a previously unknown phenomenon, the light-induced accumulation of FIT condensates in FIT NBs. LLPS was most likely the underlying mechanism for this highly dynamic process. FIT NBs were enriched in active FIT TF complexes for iron deficiency gene regulation. FIT associated with speckles and PBs in a highly dynamic fashion. Based on these data, FIT NBs are dynamic microenvironments with active FIT TF complexes

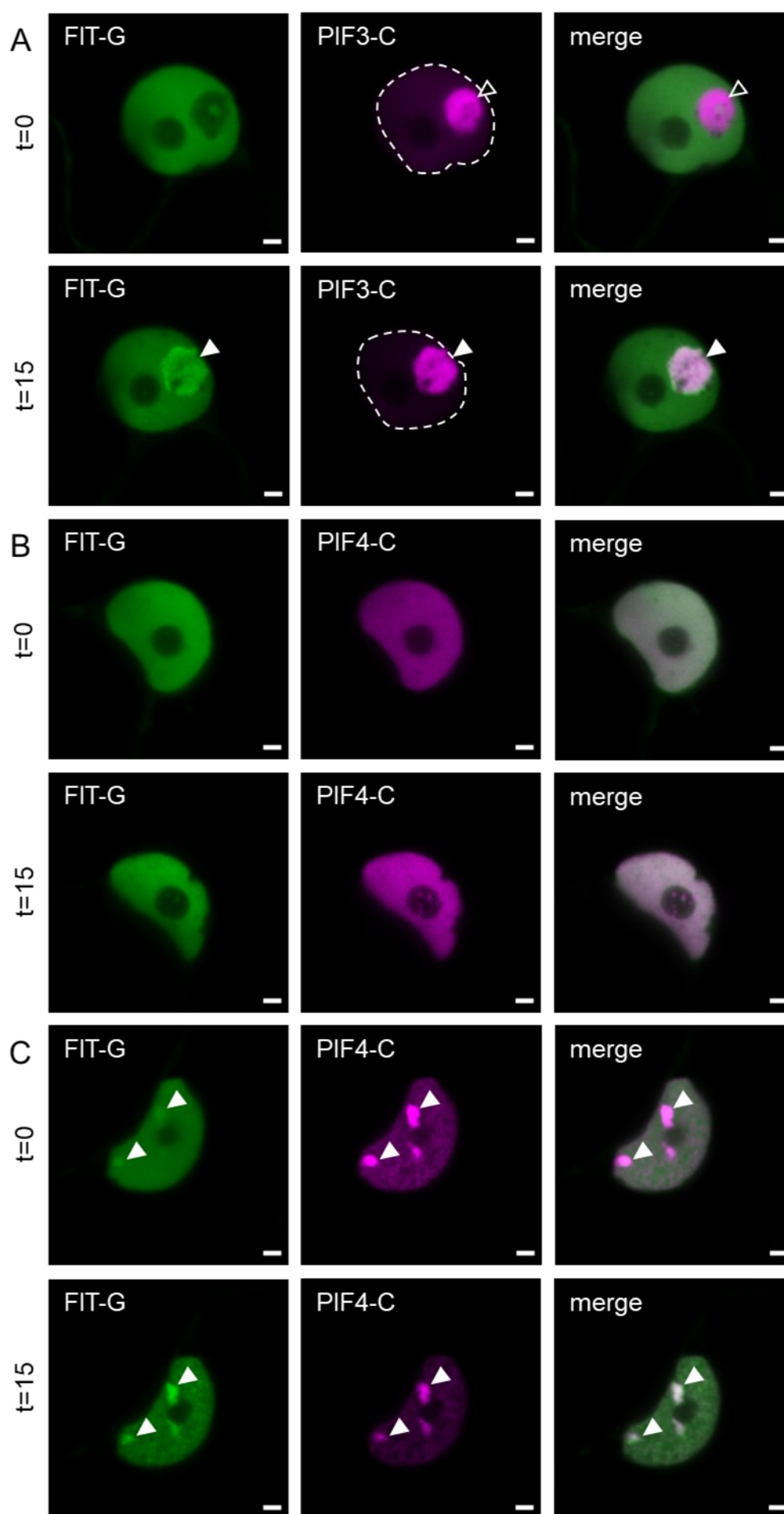


Figure 7. FIT colocalized with photobody (PB) markers in distinct PBs.

Confocal images showing localization of FIT-GFP and PB markers upon co-expression in the nucleus at $t=0$ and $t=15$ min. Co-expression of FIT-GFP with A, PIF3-mCherry, and B and C, PIF4-mCherry, in B, showing a typical pattern with absence of NBs (ca. 50% of nuclei), in C, showing a typical pattern with presence of NBs (ca. 50% of cells). When FIT-GFP was co-expressed with PB markers, FIT NBs did not appear at $t=5$ min, but instead, FIT-GFP colocalized with PB markers in PBs at $t=15$ min. A, PIF3-mCherry localized predominantly to a single large PB at $t=0$ and $t=15$ min. FIT-GFP colocalized with PIF3-mCherry in this single large PB at $t=15$ min. B, PIF4-mCherry and FIT-GFP were both homogeneously distributed in the nucleoplasm at $t=0$ and $t=15$ min. In C, FIT-GFP colocalized with PIF4-mCherry in PBs at $t=0$ and $t=15$ min. The same localization patterns were found for PIF3-mCherry and PIF4-mCherry upon single expression (compare with **Supplemental Figure S5**). Hence, FIT-GFP was recruited to the two distinct types of PIF3 and PIF4 PBs, whereas PIF3 and PIF4 were not recruited to FIT NBs. This suggests that FIT NBs are affected by the presence of PIF3- and PIF4-containing PBs and a connection to light signalling exists.

Scale bar: 2 μ m. Arrowheads indicate colocalization in PBs. G = GFP; C = mCherry. Fluorescence protein analysis was conducted in transiently transformed *N. benthamiana* leaf epidermis cells, following the standardized FIT NB analysis procedure.

that possibly are hubs to cross connect transcriptional iron deficiency gene expression with post-transcriptional regulation and light signaling.

A standardized procedure for FIT NB induction was crucial to delineate the characteristics of FIT NBs in reliable manner

A major aim of this study was to characterize the nature and potential function of light-induced FIT NBs. To be able to apply the quantitative microscopy-based techniques, we needed to control the appearance of NBs in reliable manner and FIT-GFP fluorescence needed to be sufficiently strong. This was clearly a limitation for inspection of root epidermis cells of the root differentiation zone in iron-deficient plants in which FIT-controlled iron uptake takes place. Not every root epidermis cell showed NBs and only few FIT NBs were detectable after a delay of 40 min to 2 h. Since condensation depleted FIT protein in the nucleoplasm, the remaining low FIT protein concentration can be the reason why FIT NBs remained few in number in the *Arabidopsis* root cells. The *N. benthamiana* protein expression system did not present these limitations and high-quality measurement data were obtained for all experimental series. Furthermore, this expression system is a well-established and widely utilized system in plant biology (Martin et al., 2009; Bleckmann et al., 2010; Leonelli et al., 2016; Burkart et al., 2022). The developed standardized assay generated reliable and accurate data for statistical analysis and quantification to conclude about FIT NB characteristics.

This way, we linked the dynamic process of FIT NB formation with LLPS, which was most likely the mechanism of FIT NB formation. First of all, according to FRAP data, FIT NBs maintained a dynamic exchange of FIT protein with the surrounding NP. Despite of that, the initiation of condensation may overall reduce the mobility of FIT-GFP versus FITmSS271AA-GFP in the whole nucleus in the absence of visible FIT NBs that we observed in a previous study (Gratz et al., 2019). bHLH039 accumulates in cytoplasmic foci at the cell periphery (Trofimov et al., 2019). In these foci, bHLH039 is immobile. Probably, bHLH039 was retained

in these cytoplasmic foci in a non-functional state, as it was only seen in the absence of FIT. This underlines the understanding that liquid condensates such as FIT NBs are dynamic microenvironments, whereas immobile condensates point rather towards a solid and pathological state (Shin et al., 2017).

Second, FIT NBs were mostly of circular shape. Circular condensates appear as droplets, in contrast to solid-like condensates that are irregularly shaped (Shin et al., 2017). This is speaking in favor of liquid-like features, suggesting that LLPS underlies FIT NB formation. A similar situation was described for CRY2 PBs, which were also of circular shape with mobile protein inside PBs (Wang et al., 2021). In conclusion, the properties of liquid condensation along with the findings that it occurred irrespective of the fluorescence protein tag preferentially with wild-type FIT, but with different dynamics for the mutant FITmSS271AA and not at all for ZAT12, allowed us to coin the term of 'FIT NBs'.

IDR^{Ser271/272} was crucial for interaction and NB formation of FIT

FIT NBs were hotspots for FIT interaction, allowing to assume that they are integrated in the iron deficiency response as interaction hubs. FIT formed homodimers and heterodimers with bHLH039 preferentially in NBs compared with the NP. These abilities distinguished wild-type FIT and mutant FITmSS271AA. According to these findings FITmSS271AA was less successful in interacting within NBs, indicating that wild-type FIT is a multivalent protein and IDR^{Ser271/272} is important for that. bHLH proteins interact with other proteins via the helix-loop-helix interface, which may certainly also be the case for FIT. Our study supports previous reports that FIT protein interaction via its C-terminus is relevant (Lingam et al., 2011; Le et al., 2016; Gratz et al., 2019). The property of being able to interact via the HLH and via the C-terminal domain allows FIT to be multivalent. It could not be distinguished whether FIT homodimers were a prerequisite for the localization of bHLH039 in NBs or whether FIT-bHLH039 complexes also initiated NBs on their own.

The predicted and disrupted C-terminal FIT IDR^{Ser271/272} in the FITmSS271AA mutant was relevant for NB formation capacity. IDRs are often required for protein interactions of hub proteins since the flexible IDRs adapt to interactions with multiple protein partners and are therefore crucial for multivalency (Tarczewska and Greb-Markiewicz, 2019; Emenecker et al., 2020; Salladini et al., 2020). Besides, evidence exists that the amino acid composition of IDRs is crucial for condensation (Powers et al., 2019; Emenecker et al., 2021; Huang et al., 2022). Very interestingly, post-translational modification in form of phosphorylation within IDRs is suggested to be a mechanism to regulate condensate formation (Owen and Shewmaker, 2019). Ser271/272 is targeted by a FIT-interacting protein kinase that was shown to affect FIT activity *in vivo* and FIT phosphorylation *in vitro* (Gratz et al., 2019). Hence, phosphorylation of Ser271/272 might perhaps be a trigger for NB formation *in vivo*.

Formation of FIT NB could happen *de novo* but also associate with pre-existing condensates in the nucleus

FIT may have formed FIT NBs as entirely newly formed structures upon the light trigger. But it is also possible that FIT joined pre-existing NBs, which then became the structures we termed FIT NBs. Partial or full colocalization of FIT-GFP with NB and PB markers revealed the remarkably high and intriguing dynamic nature of FIT NBs and suggests that both possibilities are plausible. Speaking in favor of pre-existing NBs is on the one hand that FIT NBs are seen upon a light trigger. Since FIT does not possess light-responsive domains, it is most likely that a light-responsive protein must be inducing FIT NB formation. The basic leucine zipper TF ELONGATED HYPOCOTYL5 (HY5) could be a good candidate, since HY5 is a mobile protein involved in iron acquisition in tomato (Gao et al., 2021; Guo et al., 2021). Possibly activation and condensation involve not only the studied NB and PB markers but also potentially signaling proteins or further scaffold proteins that are part of the multivalent protein complexes in FIT NBs. On the other hand, FIT-GFP accumulated not only in FIT NBs but also in the pre-existing NBs with type II NB markers (SR45 and SRm102) after the FIT NB induction procedure. In this respect, type II markers were similar to PIF3 and PIF4. FIT-GFP was recruited to pre-existing PBs and again only after the light trigger. Interestingly, typical FIT NB formation did not occur in the presence of PB markers, indicating that they must have had a strong effect on recruiting FIT. Overall, the dynamics of FIT colocalization with type II NB and PB markers suggest that these condensates dictated FIT condensation in their own pre-existing NBs/PBs. This recruiting process could be navigated via protein-protein interaction since this is the driving force of condensation (Kaiserli et al., 2015; Emenecker et al., 2020).

Speaking in favor of a *de novo* FIT NB formation is the localization with type III NB markers. The three fully colocalizing type III NB markers (UAP56H2, P15H1 and PININ) accumulated only in FIT NBs upon co-expression with FIT and mostly not on their own. The same was true for bHLH039, that joins FIT in FIT NBs, showing that FIT not only facilitated bHLH039 nuclear localization (Trofimov et al., 2019) but also condensation. Interestingly, FIT was able to change PININ nuclear localization. In single expression, PININ was localized to a major large NB, but in colocalization with FIT it joined the typical FIT NBs. This suggests that FIT dictates bHLH039 and type III NB markers and highlights that FIT is also able to set the tone for NB formation. Hence, FIT can recruit other proteins into NBs, and it is possible that FIT forms its own NBs. Protein-protein interaction could underly this recruitment, as evident for bHLH039 (Kaiserli et al., 2015; Emenecker et al., 2020). Ultimately, as a high diversification of condensates exists, a combination of newly formed NBs and localization to pre-existing NBs cannot be ruled out. Given the variety of proteins localizing in condensates, effort in isolating FIT NBs and identification of proteins within FIT NBs is necessary to further uncover the driving forces of FIT NB formation.

FIT NBs might have a transcriptional and post-transcriptional function

Since the type II and III markers are splicing components, the colocalization studies suggest that FIT NBs are speckles. On the one hand, the speckle nature coincides well with the dynamic nature of FIT NBs. Like FIT NBs, speckles are highly dynamic. They are forming around transcriptionally active sites in the interchromatin regions recruiting several protein functions like mRNA synthesis, maturation, splicing and export (Reddy et al., 2012; Galganski et al., 2017). The type II speckle component SR45, for instance, was shown to be a highly mobile protein in speckles and required phosphorylation for proper speckle localization (Ali et al., 2003; Reddy et al., 2012). These processes fit well to the described FIT NB attributes. On the other hand, speckle components are also linked with epigenetic mechanisms (Mikulski et al., 2022). The characterization of FIT NBs as speckles is interesting because regulation of splicing and epigenetic regulation is associated with iron deficiency gene expression. Genes were spliced incorrectly in a *sr45-1* null mutant Arabidopsis line, and gene expression of *FIT* and FIT target genes was increased in *sr45-1* seedlings, showing that an interplay between SR45 and the iron uptake machinery exists (Fanara et al., 2022). Alternative splicing was detected for FIT targets and the *BHLH* subgroup Ib genes in iron-deficient versus iron-sufficient conditions (Li et al., 2013). Hence, FIT NBs may regulate iron uptake gene expression at post-transcriptional level. Notably, PININ (type III), together with ACINUS, were shown to stabilize SR45 (type II) in plants (Bi et al., 2021). Further, UAP56H2, P15H1, and PININ (type III) are connected to SR45 and SRm102 (type II) in mammalian cells as all being part of the exon junction complex and interacting with each other (Lin et al., 2004; Pendle et al., 2005). This is an interesting parallel, as it suggests that type II and type III marker localization is conserved across kingdoms, underlying the ancient nature of condensates. Indeed, SR45 and PININ located to a very large NB in non-induced cells. This opens the possibility that the two proteins might localize to the same speckle, as also might FIT. Taken together, the observations confirm the high diversification and complexity of FIT NBs and speckles (Lorković et al., 2008) and it is tempting to speculate that FIT might regulate splicing and alternative splicing of its target genes by recruiting speckle components.

FIT is itself a direct target of FIT and the FIT-bHLH039 complex (Wang et al., 2007; Naranjo-Arcos et al., 2017), and perhaps FIT NB speckles appear at the *FIT* transcription site. Indeed, coupling of transcription with splicing or alternative splicing is an established idea in the mammalian field, and evidence for co-transcriptional splicing in plants is also recently rising (Nojima et al., 2015; Zhu et al., 2018; Chaudhary et al., 2019). Mediator complex condensation was shown to drive transcriptional control (Boija et al., 2018) and interestingly, FIT was also shown to interact with Mediator complexes, directly and indirectly (Yang et al., 2014; Zhang et al., 2014). Besides, other studies suggest TF condensation to be involved in transcriptional regulation (Kaiserli et al., 2015; Huang et al., 2022). Possibly, the basic region of FIT and

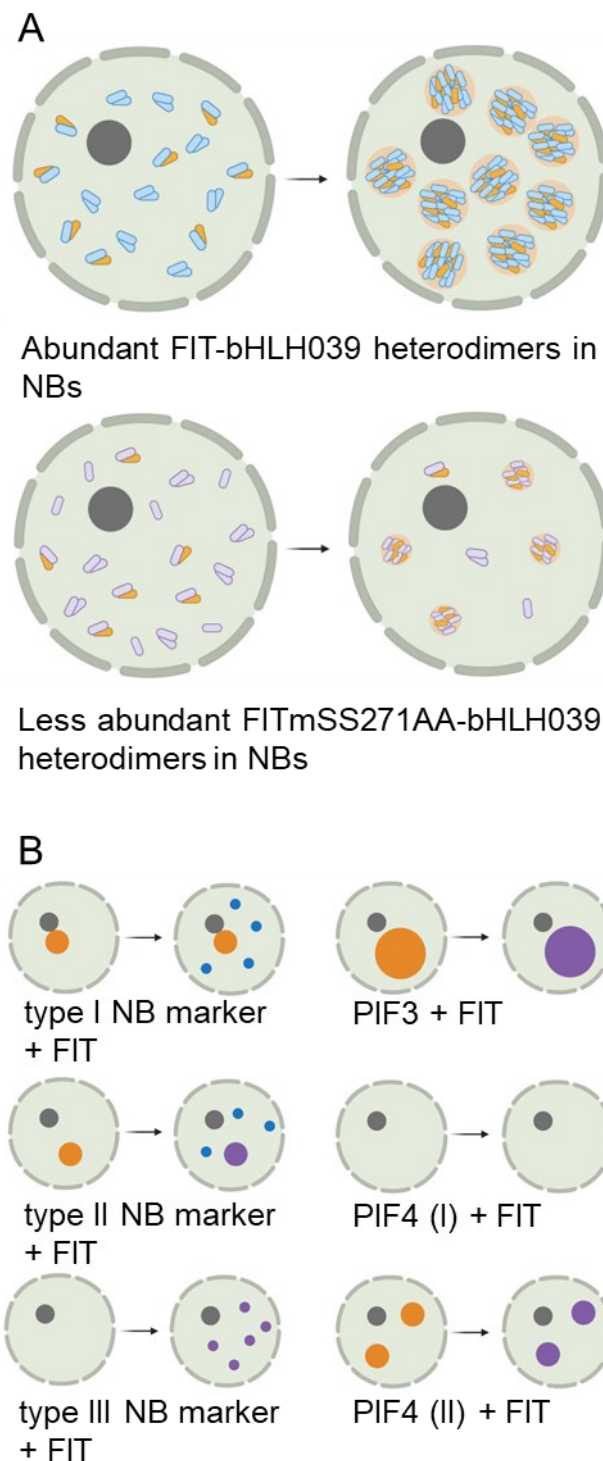


Figure 8. Schematic summary models illustrating the dynamics of FIT NB formation, suggesting that FIT NBs are related to transcriptional and post-transcriptional regulation in speckles.

A, Light-induced FIT NB formation in the presence of FIT (top) or FITmSS271AA (bottom) and bHLH039. FIT accumulates in FIT NBs, that are of circular shape and may undergo LLPS. FIT homodimers and FIT-bHLH039 heterodimers are present in the nucleus at $t=0$ and $t=5$ min. At $t=5$ min, homo- and heterodimers are preferentially present in FIT NBs versus NP. IDR^{Ser271/272} may be important for multivalency of FIT, as it is disrupted in FITmSS271AA. This mutant has low protein interaction ability (see also Gratz et al., 2019). Consequently, FITmSS271AA accumulates slowly in NBs (taking up to $t=15$ min). FIT-bHLH039 is an active TF complex for upregulating the expression of iron acquisition genes in roots in contrast to FITmSS271AA-bHLH039 (Gratz et al., 2019). Hence, FIT NBs are subnuclear sites related to transcriptional regulation and because of their colocalization

with speckle components, also to speckles. B, Dynamics of NBs revealed by co-expression. FIT did not colocalize with type I NB markers (Cajal body markers; *coilin*, *U2B''*). FIT colocalized with type III markers (speckle components; *UAP56H2*, *P15H1*, *PININ*) and these markers adopted the FIT pattern at $t=5$ min following the light trigger. Type II NB markers (speckle components; *SR45*, *SRm102*) and PB markers (*PIF3*, *PIF4*) localized to their own distinct NBs into which FIT became recruited in light-inducible manner. In case of type II NB markers, these markers did not localize in FIT NBs. Hence, there is a light-inducible effect acting upon FIT to become recruited by type II NBs and PBs or to recruit proteins into its own NBs. In summary, FIT NBs are light-inducible subnuclear sites linking transcriptional and post-transcriptional regulation in speckles.

A, Blue ovals = wild-type FIT; violet ovals = mutant FITmSS271AA; orange ovals = bHLH039. B, grey circles = nucleoli; orange circles = NB/PB marker NBs/PBs; blue circles = FIT NBs; lilac circles = colocalization of NB/PB marker NBs/PBs and FIT NBs.

bHLH039 might be accessible for DNA binding either within or outside of NBs to regulate target genes (Boija et al., 2018; Brodsky et al., 2020). In further studies, it will be interesting to analyze whether DNA and mRNA FIT targets are present inside FIT NBs and whether FIT may also interact directly with other speckle components.

The physiological integration and regulation of the induction of FIT NB formation can be subject of future studies. The rapid speed by which FIT NB appeared within 5 min in *N. benthamiana* leaf cells speaks in favor of protein rearrangement rather than protein synthesis. The long duration of FIT NB formation after blue light induction in *Arabidopsis* roots suggests that signal transduction was more complex and possibly involved intracellular or even cell-to-cell and long-distance leaf-to-root signaling. In how far a long-distance signal or a signaling cascade triggered by light is involved in FIT NB formation in roots remains to be investigated, but *CRY1/CRY2* and *HY5* are promising candidates for further studies (Gao et al., 2021; Guo et al., 2021). In order to undergo phase separation, a certain protein concentration must be reached (Bracha et al., 2018). Since FIT protein is subject of proteasomal turnover in roots, FIT NB formation may depend on FIT protein interaction partners in roots that need to be activated (Lingam et al., 2011; Meiser et al., 2011).

In summary, FIT engages in protein complexes inside dynamic NBs. FIT NBs contain active TF complexes for iron acquisition gene expression (**Figure 8A**). FIT NBs are speckles that link transcriptional with post-transcriptional regulation (**Figure 8B**). The appearance of FIT NBs is inducible by light, and light-regulated PB components are connected with FIT NBs and vice versa. It will be interesting in the future to test hormonal and environmental triggers that may stabilize FIT protein prior to examining the initiation of FIT NBs in root physiological situations and to investigate the effects on transcriptional and post-transcriptional regulation of FIT targets.

Materials and methods

Plant material and growth conditions

Arabidopsis thaliana 2x35S_{pro}:FIT-GFP/*fit-3* seedlings (Gratz et al., 2019) were used for localization studies. Seeds were sterilized and grown upright on Hoagland medium plates (macronutrients: 1.5 mM Ca(NO₃)₂ · 4H₂O, 0.5 mM KH₂PO₄, 1.25 mM KNO₃, 0.75 mM MgSO₄ · 7H₂O; micronutrients: 0.075 μM (NH₄)₆Mo₇O₂₄ · 4H₂O, 1.5 μM CuSO₄ · 5H₂O, 50 μM H₃BO₃, 50 μM KCl, 10 μM MnSO₄ · H₂O, 2 μM ZnSO₄ · 7H₂O; 1.4% (w/v) plant agar, 1% (w/v) sucrose, pH 5.8) with no iron supply for 5 d under long day conditions (16 h light/8 h dark) at 21°C in a plant chamber (CLF Plant Climatics) under white light (120 μmol m⁻² s⁻¹). *Nicotiana benthamiana* plants for transient protein expression were grown in the greenhouse facility for approx. 4 weeks under long day conditions (16 h light/8 h dark).

Microscopy of *Arabidopsis thaliana* seedlings

Protein localization studies in roots of 5-d-old seedlings of the *Arabidopsis thaliana* line 2x35S_{pro}:FIT-GFP/*fit-3* (Gratz et al., 2019) were performed with the widefield microscope ELYRA PS (Zeiss) equipped with a EMCCD camera. Whole seedlings were exposed to blue light, either for 2 h within a plant chamber (CLF Plant Climatics, 440-500 nm, 55 μmol m⁻² s⁻¹) or by exposure to 488 nm laser light for several minutes. GFP was excited with a 488 nm laser and detected with a BP 495-575 + LP 750 beam splitter. Images were acquired with the C-Apochromat 63x/1.2 W Korr M27 (Zeiss) objective, pixel dwell time of 1.6 μs and frame size of 512x512. Pictures were processed with the manufacturer's software ZEN lite (Zeiss).

Generation of fluorescent constructs

All constructs used in this study are listed in **Supplemental Table S1**. Generation of fluorescent translational C-terminal fusion of PIF3 and PIF4 with mCherry was performed with Gateway Cloning. CDS of *PIF3* was amplified with the PIF3 GW fw (5'-GGGGACAAGTTTGTACAAAAAAGCAGGCTATGCCTCTGTTTGAGCTT-3') and PIF3 GW rv (5'-GGGGACCACTTTGTACAAGAAAGCTGGGTCCGACGATCCACAAAAGT-3') primers, and CDS of *PIF4* was amplified with the PIF4 GW fw (5'-GGGGACAAGTTTGTACAAAAAAGCAGGCTATGGAACACCAAGGTTGG-3') and PIF4 GW rv (5'-GGGGACCACTTTGTACAAGAAAGCTGGGTTCGTGGTCCAAACGAGAACC-3') primers, and introduced into the entry vector pDONR207 via the BP reaction (Life Technologies) and subsequently into the inducible pABind 35S_{pro}:mCherry destination vector (Bleckmann et al., 2010) via the LR reaction (Life Technologies). Finally, *Rhizobium radiobacter* was transformed with the constructs for transient transformation of *Nicotiana benthamiana* leaf epidermal cells.

Transient transformation of *Nicotiana benthamiana* leaf epidermal cells

Transient protein expression was performed in *Nicotiana benthamiana* leaf epidermal cells according to Bleckmann et al. (2010). This was performed for localization studies, FRAP measurements, anisotropy (homo-FRET) measurements, FRET-FLIM measurements, and NB quantification. Cultures of *Rhizobium radiobacter* containing the construct of interest (**Supplemental Table S1**) were incubated overnight and cells were pelleted and dissolved in AS medium (250 μ M acetosyringone (in DMSO), 5% (w/v) sucrose, 0.01% (v/v) silwet, 0.01% (w/v) glucose). An OD_{600nm} of 0.4 was set for all constructs. A *Rhizobium radiobacter* strain containing the silencing repressor p19 vector (Shamloul et al., 2014) was used additionally for bHLH039-mCherry to enhance expression. After 1 h incubation on ice the suspension was infiltrated with a syringe into the abaxial side of the leaf. *Nicotiana benthamiana* plants were kept under long day conditions (16 h light/8 h dark) in the laboratory after infiltration. Imaging was performed 2-3 d after infiltration. Expression of constructs with an inducible 35S promoter was induced 16 h prior to imaging with β -estradiol (20 μ M β -estradiol (in DMSO), 0.1% (v/v) Tween 20).

Confocal microscopy

For localization studies a confocal laser scanning microscope LSM780 (Zeiss) was used. Imaging was controlled by the ZEN 2.3 SP1 FP3 (Black) (Zeiss) software. GFP was excited with a 488 nm laser and detected in the range of 491-553 nm. mCherry and mRFP were excited with a 561 nm laser and detected in the range of 562-626 nm. Fluorophore crosstalk was minimized by splitting of the excitation tracks and reduction of emission spectrum overlap. Images were acquired with the C-Apochromat 40x/1.20 W Korr M27 (Zeiss) objective, zoom factor of 8, pinhole set to 1,00 AU, pixel dwell time of 1.27 μ s and frame size of 1.024x1.024. Z-stacks for quantification were taken with the same settings, except with pixel dwell time of 0.79 μ s and frame size of 512x512. Pictures were processed with the manufacturer's software ZEN lite (Zeiss).

Standardized FIT NB analysis procedure

Following *Nicotiana benthamiana* leaf infiltration with *Rhizobium radiobacter*, FIT-GFP protein expression was induced after 2-3 d by β -estradiol, as described above. 16 h later, a leaf disc was excised and FIT-GFP fluorescence signals were recorded ($t=0$). The leaf disc was excited with 488 nm laser light for 1 min. 5 min later, FIT-GFP accumulation in FIT NBs was observed ($t=5$ min). See **Supplemental Figure S1**. This procedure was modified by using different time points for NB analysis and different constructs (**Supplemental Table S1**) and co-expression as indicated in the text. Imaging was performed at the respective wavelengths for detection of GFP and mRFP/mCherry, respectively.

FRAP measurements

FRAP measurements (Bancaud et al., 2010; Trofimov et al., 2019) were performed at the confocal laser scanning microscope LSM780 (Zeiss). Imaging was controlled by the ZEN 2.3 SP1 FP3 (Black) (Zeiss) software. GFP was excited with a 488 nm laser and detected in the range of 491-553 nm. Images were acquired with the C-Apochromat 40x/1.20 W Korr M27 (Zeiss) objective, zoom factor of 8, pinhole set to 2,43 AU, pixel dwell time of 1.0 μ s, frame size of 256x256, and 300 frames. After 20 frames, a NB was bleached with 50 iterations and 100% 488 nm laser power. Fluorescence intensity was recorded for the bleached NB (ROI), a non-bleached region equal in size to the NB (BG) as well as for the total image (Tot). Values were calculated and processed in Excel (Microsoft Corporation). Background subtraction and normalization to calculate the relative fluorescence intensity was performed as follows: $[(ROI(t)-BG(t)/Tot(T)-BG(t))*(Tot(t_0)-BG(t_0)/ROI(t_0)-BG(t_0))]$. The mobile fraction was calculated as follows: $[(F_{end}-F_{post})/(F_{pre}-F_{post})]*100$. F_{pre} marks the average of the 20 values before bleaching, F_{post} marks the value right after the bleaching, and F_{end} marks the average of the 280 values after the bleaching. Pictures were processed with the manufacturer's software ZEN lite (Zeiss). Total number of 10 measurements were performed in 3 independent experiments.

Anisotropy (homo-FRET) measurements

Anisotropy measurements (Stahl et al., 2013; Weidtkamp-Peters et al., 2022) were performed at the confocal laser scanning microscope LSM780 (Zeiss) equipped with a polarization beam splitter, bandpass filter (520/35), and a single-photon counting device HydraHarp (PicoQuant) with avalanche photo diodes (τ -SPADs). Emission was detected in parallel and perpendicular orientation. Rhodamine 110 was used to determine the G factor to correct for the differential parallel and perpendicular detector sensitivity. Calibration of the system was performed for every experiment and measurements were conducted in darkness. Free GFP and GFP-GFP were used as references for mono- and dimerization, respectively. GFP was excited with a linearly polarized pulsed (32 MHz) 485 nm laser and 0.05-1 μ W output power. Measurements were recorded with a C-Apochromat 40x/1.20 W Korr M27 (Zeiss) objective, zoom factor of 8, pixel dwell time of 12.5 μ s, objective frame size of 256x256, and 40 frames. Measurements were controlled with the manufacturer's ZEN 2.3 SP1 FP3 (Black) (Zeiss) software and SymPhoTime 64 (PicoQuant) software. SymPhoTime 64 (PicoQuant) software was used for analysis in the respective regions of interest (whole nucleus, NB, NP) and to generate color-coded FA value images. Minimal photon count was set to 200. Total number of 10-15 measurements per construct were performed in at least 2 independent experiments.

FRET-FLIM measurements

FRET-FLIM measurements (Borst and Visser, 2010; Weidtkamp-Peters and Stahl, 2017) were taken at the confocal laser scanning microscope FV3000 (Olympus) equipped with a multi-photon counting device MultiHarp 150 (PicoQuant) with avalanche photo diodes (τ -SPADs) and bandpass filter (520/35). Erythrosine B (quenched in saturated potassium iodide) was used to record the Instrument Response Function to correct for the time between laser pulse and detection. Calibration of the system was performed for every experiment and measurements were conducted in darkness. FIT-GFP and FITmSS271AA-GFP were used as negative controls (donor only), FIT-GFP or FITmSS271AA-GFP (donor) and bHLH039-mCherry (acceptor) as FRET pair. GFP was excited with a linearly polarized pulsed (32 MHz) 485 nm laser and 0.01-0.1 μ W output power. Measurements were recorded with a UPLSAPO 60XW (Olympus) objective, zoom factor of 8, pixel dwell time of 12.5 μ s, objective frame size of 256x256, and 60 frames. Measurements were controlled with the manufacturer's FV31S-SW (Olympus) software and SymPhoTime 64 (PicoQuant) software. SymPhoTime 64 (PicoQuant) software was used for analysis in the respective regions of interest (whole nucleus, NB, NP) and to generate color-coded fluorescence lifetime value images. Number of parameters for the fit depended on the region of interest. Total number of 10 measurements per construct were performed in at least 2 independent experiments.

Circularity quantification

Circularity quantification was performed with the software ImageJ (National Institutes of Health). Full intensity projection images were generated from Z-stacks in the ZEN lite (Zeiss) software and exported as TIFF (no compression, all dimensions). Images were duplicated in ImageJ and converted to RGB and 8-bit. Correct scale was set (in μ m) under 'Analyze' - 'Set Scale'. Threshold for the intensity limit (areas below that limit were not considered for quantification) was set under 'Image' - 'Adjust' - 'Threshold' and was set manually for every image. To separate the nuclear bodies better, 'Process' - 'Binary' - 'Watershed' was used. Parameters that should be quantified were selected under 'Analyze' - 'Set Measurements'. To perform the analysis, 'Analyze' - 'Analyze Particles' was selected. Calculated values were further processed in Excel (Microsoft Corporation). Total number of 15 images were quantified from 2 independent experiments.

Nuclear body quantification

Nuclear body quantification was performed with the software ImageJ (National Institutes of Health) and additional plugin '3D Object Counter'. Z-stacks were exported from the ZEN lite (Zeiss) software as TIFF (no compression, all dimensions) first. In ImageJ, Z-stacks were converted to RGB and 8-bit. Correct scale was set (in μ m) under 'Properties'. Parameters that should be quantified were selected under 'Plugins' - '3D Object Counter' - 'Set 3D Measurements'. To perform the analysis, 'Plugins' - '3D Object Counter' - '3D object

counter' was selected. Threshold for the intensity limit (areas below that limit were not considered for quantification) was set manually for every z-stack. Calculated values were further processed in Excel (Microsoft Corporation). Only size between 0,01-15 μm^3 was considered. Total number of 15 z-stacks per construct were quantified from 2 independent experiments.

Protein domain prediction

IDRs in FIT/FITmSS271AA were predicted with the tool PONDR-VLXT (www.pondr.com, Molecular Kinetics, Inc.). According to the sequence of the protein, a PONDR score was determined for each amino acid. A score above 0.5 indicates intrinsic disorder. The bHLH domain of FIT was predicted with InterPro (www.ebi.ac.uk/interpro, EMBL-EBI).

Statistical analysis

Line and bar diagrams represent the mean and standard deviation. Box plots show 25-75 percentile with min-max whiskers, mean as small square and median as line. Graphs and statistical analysis were created and performed with OriginPro (OriginLab Corporation). Data was tested for normal distribution with the Shapiro-Wilk test. Statistical significance of data with normal distribution was tested by one-way Anova with Tukey post-hoc test. Statistical significance of data with non-normal distribution was tested by Mann-Whitney test. Different letters indicate statistically significant differences ($P < 0.05$). Illustrations were created with BioRender.com.

Accession numbers

Sequence data from this article can be found in the EMBL/GenBank data libraries under accession numbers: *bHLH039* (AT3G56980), *COILIN* (AT1G13030), *FIT* (AT2G28160), *P15H1* (AT1G11570), *PIF3* (AT1G09530), *PIF4* (AT2G43010), *PININ* (AT1G15200), *SR45* (AT1G16610), *SRm102* (AT2G29210), *U2B"* (AT2G30260), *UAP56H2* (AT5G11170), and *ZAT12* (AT5G59820).

Supplemental Data

Supplemental Figure S1. A standardized FIT NB analysis procedure was developed to analyze the characteristics and dynamics of FIT NBs. (Supports Figure 1)

Supplemental Figure S2. An intrinsically disordered region, IDR^{Ser271/272}, is present in the FIT C-terminus and disrupted in the FITmSS271AA mutant. (Supports Figure 2, 3, and 4)

Supplemental Figure S3. FIT NBs did not colocalize with Cajal body components (designated type I). (Supports Figure 5 and 6)

Supplemental Figure S4. Type II and III NB markers are similarly localized upon single expression as upon co-expression with FIT, except PININ. (Supports Figure 5 and 6)

Supplemental Figure S5. PB markers are similarly localized upon single expression and upon co-expression with FIT. (Supports Figure 7)

Supplemental Table S1. List of vectors used in this study.

Supplemental Movie S1. Light induction triggers the formation of NBs with FIT and FITmSS271AA with different dynamics. (Supports Figure 1 and 2)

Acknowledgements

We thank Elke Wieneke and Monique Eutebach (Institute of Botany, Heinrich-Heine-University, Düsseldorf, Germany) for excellent technical assistance. We thank Rebecca C. Burkart (Institute of Developmental Genetics, Heinrich-Heine-University, Düsseldorf, Germany), Sebastian Hänsch and Stefanie Weidtkamp-Peters (Center for Advanced Imaging, Heinrich-Heine-University, Düsseldorf, Germany) for help and advice with microscopy and data analysis. K.T. is an associate member of the DFG-funded International Graduate School for Plant Science *iGRADplant* (IRTG 2466 "Network, exchange, and training program to understand plant resource allocation"), Düsseldorf, Germany.

Funding

This work was funded by Deutsche Forschungsgemeinschaft (DFG, German Research Foundation) under GRK F020512056 (NEXTplant), SFB 1208 project B05, and Germany's Excellence Strategy – EXC-2048/1 – project ID 390686111. Funding for instrumentation: Zeiss ELYRA PS: DFG- INST 208/613-1 FUGG; Zeiss LSM780 + 4-channel FLIM extension (Picoquant): DFG- INST 208/551-1 FUGG; Olympus FV3000 Confocal Laser Scanning Microscope with 4-channel FLIM extension (PicoQuant rapidFLIM): DFG- INST 1358/44-1 FUGB.

References

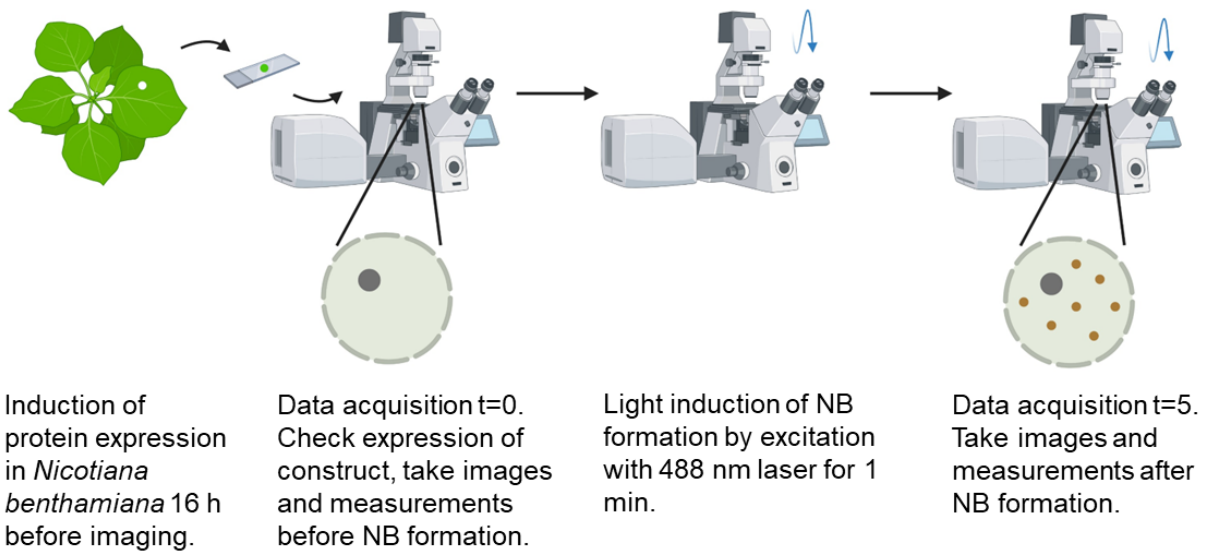
- Ali, G.S., Golovkin, M., and Reddy, A.S.N.** (2003). Nuclear localization and in vivo dynamics of a plant-specific serine/arginine-rich protein. *Plant J.* **36**: 883–893.
- Bancaud, A., Huet, S., Rabut, G., and Ellenberg, J.** (2010). Fluorescence Perturbation Techniques to Study Mobility and Molecular Dynamics of Proteins in Live Cells: FRAP, Photoactivation, Photoconversion, and FLIP. *Cold Spring Harb. Protoc.*: 1303–1325.
- Bauer, D., Viczian, A., Kircher, S., Nobis, T., Nitschke, R., Kunkel, T., Panigrahi, K.C.S., Ádám, É., Fejes, E., Schäfer, E., and Nagy, F.** (2004). Constitutive Photomorphogenesis 1 and Multiple Photoreceptors Control Degradation of Phytochrome Interacting Factor 3, a Transcription Factor Required for Light Signaling in Arabidopsis. *Plant Cell* **16**: 1433–1445.
- Bauer, P., Ling, H.Q., and Guerinot, M. Lou** (2007). FIT, the FER-LIKE IRON DEFICIENCY INDUCED TRANSCRIPTION FACTOR in Arabidopsis. *Plant Physiol. Biochem.* **45**: 260–261.
- Bi, Y. et al.** (2021). Arabidopsis ACINUS is O-glycosylated and regulates transcription and alternative splicing of regulators of reproductive transitions. *Nat. Commun.* **12**: 1–13.
- Bleckmann, A., Weidtkamp-Peters, S., Seidel, C.A.M., and Simon, R.** (2010). Stem Cell Signaling in Arabidopsis Requires CRN to Localize CLV2 to the Plasma Membrane. *Plant Physiol.* **152**: 166–176.
- Boija, A. et al.** (2018). Transcription Factors Activate Genes through the Phase-Separation Capacity of Their Activation Domains. *Cell* **175**: 1842–1855.
- Borst, J.W. and Visser, A.J.W.G.** (2010). Fluorescence lifetime imaging microscopy in life sciences. *Meas. Sci. Technol.* **21**: 1–21.
- Bracha, D., Walls, M.T., Wei, M.T., Zhu, L., Kurian, M., Avalos, J.L., Toettcher, J.E., and Brangwynne, C.P.** (2018). Mapping Local and Global Liquid Phase Behavior in Living Cells Using Photo-Oligomerizable Seeds. *Cell* **175**: 1467–1480.
- Brumbarova, T. and Ivanov, R.** (2019). The Nutrient Response Transcriptional Regulome of Arabidopsis. *iScience* **19**: 358–368.
- Burkart, R.C., Strotmann, V.I., Kirschner, G.K., Akinci, A., Czempik, L., Dolata, A., Maizel, A., Weidtkamp-Peters, S., and Stahl, Y.** (2022). PLETHORA-WOX5 interaction and subnuclear localization control Arabidopsis root stem cell maintenance. *EMBO Rep.* **23**: 1–18.
- Van Buskirk, E.K., Reddy, A.K., Nagatani, A., and Chen, M.** (2014). Photobody Localization of Phytochrome B Is Tightly Correlated with Prolonged and Light-Dependent Inhibition of Hypocotyl Elongation in the Dark. *Plant Physiol.* **165**: 595–607.
- Colangelo, E.P. and Guerinot, M. Lou** (2004). The Essential Basic Helix-Loop-Helix Protein FIT1 Is Required for the Iron Deficiency Response. *Plant Cell* **16**: 3400–3412.
- Collier, S., Pendle, A., Boudonck, K., van Rij, T., Dolan, L., and Shaw, P.** (2006). A Distant Coilin Homologue Is Required for the Formation of Cajal Bodies in Arabidopsis. *Mol. Biol. Cell* **17**: 2942–2951.
- Cui, Y., Chen, C.L., Cui, M., Zhou, W.J., Wu, H.L., and Ling, H.Q.** (2018). Four IVa bHLH Transcription Factors Are Novel Interactors of FIT and Mediate JA Inhibition of Iron Uptake in Arabidopsis. *Mol. Plant* **11**: 1166–1183.
- Emenecker, R.J., Holehouse, A.S., and Strader, L.C.** (2020). Emerging Roles for Phase Separation in Plants. *Dev. Cell* **55**: 69–83.
- Emenecker, R.J., Holehouse, A.S., and Strader, L.C.** (2021). Sequence determinants of in cell condensate morphology, dynamics, and oligomerization as measured by number and brightness analysis. *Cell Commun. Signal.* **19**: 1–15.
- Fanara, S., Schloesser, M., Hanikenne, M., and Motte, P.** (2022). Altered metal distribution in the sr45-1 Arabidopsis mutant causes developmental defects. *Plant J.* **110**: 1332–1352.
- Fang, X., Wang, L., Ishikawa, R., Li, Y., Fiedler, M., Liu, F., Calder, G., Rowan, B., Weigel, D., Li, P., and Dean, C.** (2019). Arabidopsis FLL2 promotes liquid–liquid phase separation of polyadenylation complexes. *Nature* **569**: 265–269.
- Galganski, L., Urbanek, M.O., and Krzyzosiak, W.J.** (2017). Nuclear speckles: Molecular organization, biological function and role in disease. *Nucleic Acids Res.* **45**: 10350–10368.
- Gao, F., Robe, K., Bettembourg, M., Navarro, N., Rofidal, V., Santoni, V., Gaymard, F., Vignols, F., Roschztardt, H., Izquierdo, E., and Dubos, C.** (2020). The Transcription Factor bHLH121 Interacts with bHLH105 (ILR3) and Its Closest Homologs to Regulate Iron Homeostasis in Arabidopsis. *Plant Cell* **32**: 508–524.
- Gao, Y.Q., Bu, L.H., Han, M.L., Wang, Y.L., Li, Z.Y., Liu, H.T., and Chao, D.Y.** (2021). Long-distance blue light signalling regulates phosphate deficiency-induced primary root growth inhibition. *Mol. Plant* **14**: 1539–1553.
- Gratz, R. et al.** (2019). CIPK11-Dependent Phosphorylation Modulates FIT Activity to Promote Arabidopsis Iron Acquisition in Response to Calcium Signaling. *Dev. Cell* **48**: 726–740.
- Gratz, R., Brumbarova, T., Ivanov, R., Trofimov, K., Tünnermann, L., Ochoa-Fernandez, R., Blomeier, T., Meiser, J., Weidtkamp-Peters, S., Zurbruggen, M., and Bauer, P.** (2020). Phospho-mutant activity assays

- provide evidence for alternative phospho-regulation pathways of the transcription factor FER-LIKE IRON DEFICIENCY-INDUCED TRANSCRIPTION FACTOR. *New Phytol.* **225**: 250–267.
- Guo, Z., Xu, J., Wang, Y., Hu, C., Shi, K., Zhou, J., Xia, X., Zhou, Y., Foyer, C.H., and Yu, J.** (2021). The phyB-dependent induction of HY5 promotes iron uptake by systemically activating FER expression. *EMBO Rep.* **22**: 1–15.
- Huang, X., Xiao, N., Zou, Y., Xie, Y., Tang, L., Zhang, Y., Yu, Y., Li, Y., and Xu, C.** (2022). Heterotypic transcriptional condensates formed by prion-like paralogous proteins canalize flowering transition in tomato. *Genome Biol.* **23**: 1–21.
- Jakoby, M., Wang, H.Y., Reidt, W., Weisshaar, B., and Bauer, P.** (2004). FRU (BHLH029) is required for induction of iron mobilization genes in *Arabidopsis thaliana*. *FEBS Lett.* **577**: 528–534.
- Jung, J.-H. et al.** (2020). A prion-like domain in ELF3 functions as a thermosensor in *Arabidopsis*. *Nature* **585**: 256–260.
- Kaiserli, E., Páldi, K., O'Donnell, L., Batalov, O., Pedmale, U. V., Nusinow, D.A., Kay, S.A., and Chory, J.** (2015). Integration of Light and Photoperiodic Signaling in Transcriptional Nuclear Foci. *Dev. Cell* **35**: 311–321.
- Kalinina, N.O., Makarova, S., Makhotenko, A., Love, A.J., and Taliansky, M.** (2018). The Multiple Functions of the Nucleolus in Plant Development, Disease and Stress Responses. *Front. Plant Sci.* **9**: 1–19.
- Kammel, C., Thomaier, M., Sørensen, B.B., Schubert, T., Längst, G., Grasser, M., and Grasser, K.D.** (2013). *Arabidopsis* DEAD-Box RNA Helicase UAP56 Interacts with Both RNA and DNA as well as with mRNA Export Factors. *PLoS One* **8**: 1–12.
- Kanwar, P., Baby, D., and Bauer, P.** (2021). Interconnection of iron and osmotic stress signalling in plants: is FIT a regulatory hub to cross-connect abscisic acid responses? *Plant Biol.* **23**: 31–38.
- Kim, D.W., Jeon, S.J., Hwang, S.M., Hong, J.C., and Bahk, J.D.** (2016). The C3H-type zinc finger protein GDS1/C3H42 is a nuclear-speckle-localized protein that is essential for normal growth and development in *Arabidopsis*. *Plant Sci.* **250**: 141–153.
- Kim, S.A., Lacroix, I.S., Gerber, S.A., and Guerinot, M. Lou** (2019). The iron deficiency response in *Arabidopsis thaliana* requires the phosphorylated transcription factor URI. *Proc. Natl. Acad. Sci.* **116**: 24933–24942.
- Kircher, S., Gil, P., Kozma-Bognár, L., Fejes, E., Speth, V., Husselstein-Muller, T., Bauer, D., Ádám, É., Schäfer, E., and Nagy, F.** (2002). Nucleocytoplasmic Partitioning of the Plant Photoreceptors Phytochrome A, B, C, D, and E Is Regulated Differentially by Light and Exhibits a Diurnal Rhythm. *Plant Cell* **14**: 1541–1555.
- Lafontaine, D.L.J., Riback, J.A., Bascetin, R., and Brangwynne, C.P.** (2021). The nucleolus as a multiphase liquid condensate. *Nat. Rev. Mol. Cell Biol.* **22**: 165–182.
- Le, C.T.T., Brumbarova, T., Ivanov, R., Stoof, C., Weber, E., Mohrbacher, J., Fink-Straube, C., and Bauer, P.** (2016). ZINC FINGER OF ARABIDOPSIS THALIANA12 (ZAT12) Interacts with FER-LIKE IRON DEFICIENCY-INDUCED TRANSCRIPTION FACTOR (FIT) Linking Iron Deficiency and Oxidative Stress Responses. *Plant Physiol.* **170**: 540–557.
- Leivar, P. and Monte, E.** (2014). PIFs: Systems Integrators in Plant Development. *Plant Cell* **26**: 56–78.
- Leonelli, L., Erickson, E., Lyska, D., and Niyogi, K.K.** (2016). Transient expression in *Nicotiana benthamiana* for rapid functional analysis of genes involved in non-photochemical quenching and carotenoid biosynthesis. *Plant J.* **88**: 375–386.
- Li, W., Lin, W.-D., Ray, P., Lan, P., and Schmidt, W.** (2013). Genome-Wide Detection of Condition-Sensitive Alternative Splicing in *Arabidopsis* Roots. *Plant Physiol.* **162**: 1750–1763.
- Li, X., Zhang, H., Ai, Q., Liang, G., and Yu, D.** (2016). Two bHLH Transcription Factors, bHLH34 and bHLH104, Regulate Iron Homeostasis in *Arabidopsis thaliana*. *Plant Physiol.* **170**: 2478–2493.
- Liang, G., Zhang, H., Li, X., Ai, Q., and Yu, D.** (2017). bHLH transcription factor bHLH115 regulates iron homeostasis in *Arabidopsis thaliana*. *J. Exp. Bot.* **68**: 1743–1755.
- Lin, C.L., Leu, S., Lu, M.C., and Ouyang, P.** (2004). Over-expression of SR-cyclophilin, an interaction partner of nuclear pinin, releases SR family splicing factors from nuclear speckles. *Biochem. Biophys. Res. Commun.* **321**: 638–647.
- Lingam, S., Mohrbacher, J., Brumbarova, T., Potuschak, T., Fink-Straube, C., Blondet, E., Genschik, P., and Bauer, P.** (2011). Interaction between the bHLH Transcription Factor FIT and ETHYLENE INSENSITIVE3/ETHYLENE INSENSITIVE3-LIKE1 Reveals Molecular Linkage between the Regulation of Iron Acquisition and Ethylene Signaling in *Arabidopsis*. *Plant Cell* **23**: 1815–1829.
- Lorković, Z.J., Hilscher, J., and Barta, A.** (2008). Co-localisation studies of *Arabidopsis* SR splicing factors reveal different types of speckles in plant cell nuclei. *Exp. Cell Res.* **314**: 3175–3186.
- Lorković, Z.J., Hilscher, J., and Barta, A.** (2004). Use of Fluorescent Protein Tags to Study Nuclear Organization of the Spliceosomal Machinery in Transiently Transformed Living Plant Cells. *Mol. Biol. Cell* **15**: 3233–3243.
- Love, A.J., Yu, C., Petukhova, N. V., Kalinina, N.O., Chen, J., and Taliansky, M.E.** (2017). Cajal bodies and their role in plant stress and disease responses. *RNA Biol.* **14**: 779–790.
- Martin, K., Kopperud, K., Chakrabarty, R., Banerjee, R., Brooks, R., and Goodin, M.M.** (2009). Transient

- expression in *Nicotiana benthamiana* fluorescent marker lines provides enhanced definition of protein localization, movement and interactions in planta. *Plant J.* **59**: 150–162.
- Meiser, J., Lingam, S., and Bauer, P.** (2011). Posttranslational Regulation of the Iron Deficiency Basic Helix-Loop-Helix Transcription Factor FIT Is Affected by Iron and Nitric Oxide. *Plant Physiol.* **157**: 2154–2166.
- Meyer, H.M.** (2020). In search of function : nuclear bodies and their possible roles as plant environmental sensors. *Curr. Opin. Plant Biol.* **58**: 33–40.
- Mikulski, P., Wolff, P., Lu, T., Nielsen, M., Echevarria, E.F., Zhu, D., Questa, J.I., Saalbach, G., Martins, C., and Dean, C.** (2022). VAL1 acts as an assembly platform co-ordinating co-transcriptional repression and chromatin regulation at Arabidopsis FLC. *Nat. Commun.* **13**: 1–12.
- Naranjo-Arcos, M.A., Maurer, F., Meiser, J., Pateyron, S., Fink-Straube, C., and Bauer, P.** (2017). Dissection of iron signaling and iron accumulation by overexpression of subgroup Ib bHLH039 protein. *Sci. Rep.* **7**: 1–12.
- Owen, I. and Shewmaker, F.** (2019). The Role of Post-Translational Modifications in the Phase Transitions of Intrinsically Disordered Proteins. *Int. J. Mol. Sci.* **20**: 1–14.
- Pardi, S.A. and Nusinow, D.A.** (2021). Out of the Dark and Into the Light: A New View of Phytochrome Photobodies. *Front. Plant Sci.* **12**: 1–15.
- Pendle, A.F., Cark, G.P., Boon, R., Lewandowska, D., Lam, Y.W., Andersen, J., Mann, M., Lamond, A.I., Brown, J.W.S., and Shaw, P.J.** (2005). Proteomic Analysis of the Arabidopsis Nucleolus Suggests Novel Nucleolar Functions. *Mol. Biol. Cell* **16**: 260–269.
- Pham, V.N., Kathare, P.K., and Huq, E.** (2018). Phytochromes and Phytochrome Interacting Factors. *Plant Physiol.* **176**: 1025–1038.
- Powers, S.K. et al.** (2019). Nucleo-cytoplasmic Partitioning of ARF Proteins Controls Auxin Responses in Arabidopsis thaliana. *Mol. Cell* **76**: 177–190.
- Qiu, Y., Li, M., Kim, R.J.A., Moore, C.M., and Chen, M.** (2019). Daytime temperature is sensed by phytochrome B in Arabidopsis through a transcriptional activator HEMERA. *Nat. Commun.* **10**: 1–13.
- Qiu, Y., Pasoreck, E.K., Yoo, C.Y., He, J., Wang, H., Bajracharya, A., Li, M., Larsen, H.D., Cheung, S., and Chen, M.** (2021). RCB initiates Arabidopsis thermomorphogenesis by stabilizing the thermoregulator PIF4 in the daytime. *Nat. Commun.* **12**: 1–13.
- Reddy, A.S.N., Day, I.S., Gohring, J., and Barta, A.** (2012). Localization and Dynamics of Nuclear Speckles in Plants. *Plant Physiol.* **158**: 67–77.
- Riback, J.A., Zhu, L., Ferrolino, M.C., Tolbert, M., Mitrea, D.M., Sanders, D.W., Wei, M.-T., Kriwacki, R.W., and Brangwynne, C.P.** (2020). Composition-dependent thermodynamics of intracellular phase separation. *Nature* **581**: 209–214.
- Römheld, V. and Marschner, H.** (1986). Mobilization of iron in the rhizosphere of different plant species. *Adv. Plant Nutr.* **2**: 155–204.
- Salladini, E., Jørgensen, M.L.M., Theisen, F.F., and Skriver, K.** (2020). Intrinsic Disorder in Plant Transcription Factor Systems: Functional Implications. *Int. J. Mol. Sci.* **21**: 1–35.
- Schwarz, B. and Bauer, P.** (2020). FIT, a regulatory hub for iron deficiency and stress signaling in roots, and FIT-dependent and -independent gene signatures. *J. Exp. Bot.* **71**: 1694–1705.
- Shamloul, M., Trusa, J., Mett, V., and Yusibov, V.** (2014). Optimization and Utilization of Agrobacterium-mediated Transient Protein Production in *Nicotiana*. *J. Vis. Exp.*: 1–13.
- Shin, Y., Berry, J., Pannucci, N., Haataja, M.P., Toettcher, J.E., and Brangwynne, C.P.** (2017). Spatiotemporal Control of Intracellular Phase Transitions Using Light-Activated optoDroplets. *Cell* **168**: 159–171.
- Stahl, Y. et al.** (2013). Moderation of Arabidopsis root Stemness by CLAVATA1 and ARABIDOPSIS CRINKLY4 Receptor Kinase Complexes. *Curr. Biol.* **23**: 362–371.
- Strader, L., Weijers, D., and Wagner, D.** (2022). Plant transcription factors — being in the right place with the right company. *Curr. Opin. Plant Biol.* **65**: 102136.
- Tarczewska, A. and Greb-Markiewicz, B.** (2019). The Significance of the Intrinsically Disordered Regions for the Functions of the bHLH Transcription Factors. *Int. J. Mol. Sci.* **20**: 1–20.
- Trinkle-Mulcahy, L. and Sleeman, J.E.** (2017). The Cajal body and the nucleolus: “In a relationship” or “It’s complicated”? *RNA Biol.* **14**: 739–751.
- Trofimov, K., Ivanov, R., Eutebach, M., Acaroglu, B., Mohr, I., Bauer, P., and Brumbarova, T.** (2019). Mobility and localization of the iron deficiency-induced transcription factor bHLH039 change in the presence of FIT. *Plant Direct* **3**: 1–11.
- Wang, H.Y., Klatte, M., Jakoby, M., Bäumllein, H., Weisshaar, B., and Bauer, P.** (2007). Iron deficiency-mediated stress regulation of four subgroup Ib BHLH genes in Arabidopsis thaliana. *Planta* **226**: 897–908.
- Wang, N., Cui, Y., Liu, Y., Fan, H., Du, J., Huang, Z., Yuan, Y., Wu, H., and Ling, H.Q.** (2013). Requirement and Functional Redundancy of Ib Subgroup bHLH Proteins for Iron Deficiency Responses and Uptake in Arabidopsis thaliana. *Mol. Plant* **6**: 503–513.
- Wang, X., Jiang, B., Gu, L., Chen, Y., Mora, M., Zhu, M., Noory, E., Wang, Q., and Lin, C.** (2021). A photoregulatory mechanism of the circadian clock in Arabidopsis. *Nat. Plants* **7**: 1397–1408.

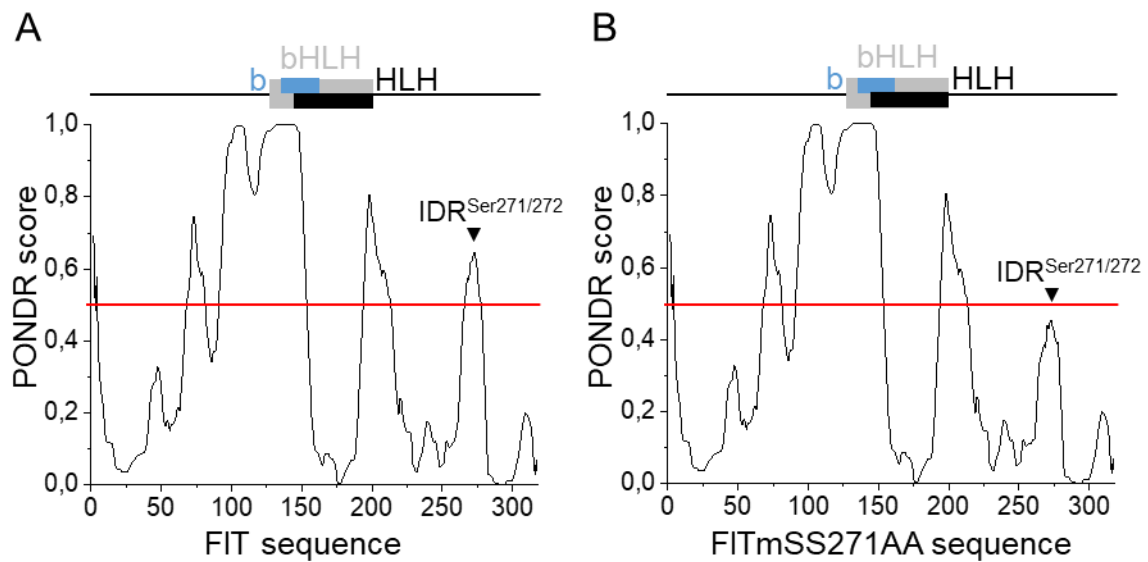
- Wedepohl, K.H.** (1995). The composition of the continental crust. *Geochim. Cosmochim. Acta* **59**: 1217–1232.
- Weidtkamp-Peters, S., Rehwald, S., and Stahl, Y.** (2022). Homo-FRET Imaging to Study Protein–Protein Interaction and Complex Formation in Plants. In *Plant Synthetic Biology: Methods and Protocols*, M.D. Zurbriggen, ed (Springer US: New York, NY), pp. 197–208.
- Weidtkamp-Peters, S. and Stahl, Y.** (2017). The Use of FRET/FLIM to Study Proteins Interacting with Plant Receptor Kinases. In *Plant Receptor Kinases: Methods and Protocols*, R.B. Aalen, ed (Springer New York: New York, NY), pp. 163–175.
- Wild, M., Davière, J.M., Regnault, T., Sakvarelidze-Achard, L., Carrera, E., Lopez Diaz, I., Cayrel, A., Dubeaux, G., Vert, G., and Achard, P.** (2016). Tissue-Specific Regulation of Gibberellin Signaling Fine-Tunes Arabidopsis Iron-Deficiency Responses. *Dev. Cell* **37**: 190–200.
- Yang, Y., Ou, B., Zhang, J., Si, W., Gu, H., Qin, G., and Qu, L.-J.** (2014). The Arabidopsis Mediator subunit MED16 regulates iron homeostasis by associating with EIN3/EIL1 through subunit MED25. *Plant J.* **77**: 838–851.
- Yuan, Y., Wu, H., Wang, N., Li, J., Zhao, W., Du, J., Wang, D., and Ling, H.Q.** (2008). FIT interacts with AtbHLH38 and AtbHLH39 in regulating iron uptake gene expression for iron homeostasis in Arabidopsis. *Cell Res.* **18**: 385–397.
- Yuan, Y.X., Zhang, J., Wang, D.W., and Ling, H.Q.** (2005). AtbHLH29 of Arabidopsis thaliana is a functional ortholog of tomato FER involved in controlling iron acquisition in strategy I plants. *Cell Res.* **15**: 613–621.
- Zhang, J., Liu, B., Li, M., Feng, D., Jin, H., Wang, P., Liu, J., Xiong, F., Wang, J., and Wang, H.** (2015). The bHLH Transcription Factor bHLH104 Interacts with IAA-LEUCINE RESISTANT3 and Modulates Iron Homeostasis in Arabidopsis. *Plant Cell* **27**: 787–805.
- Zhang, Y., Wu, H., Wang, N., Fan, H., Chen, C., Cui, Y., Liu, H., and Ling, H.Q.** (2014). Mediator subunit 16 functions in the regulation of iron uptake gene expression in Arabidopsis. *New Phytol.* **203**: 770–783.
- Zhu, P., Lister, C., and Dean, C.** (2021). Cold-induced Arabidopsis FRIGIDA nuclear condensates for FLC repression. *Nature* **599**: 657–661.

Supplemental figures, movies, tables and legends



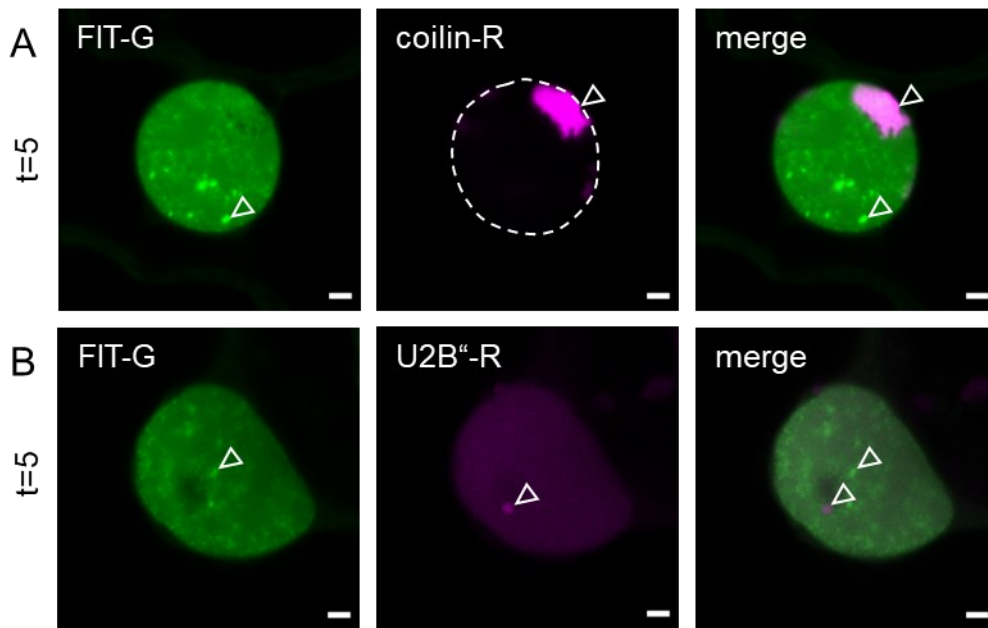
Supplemental Figure S1. A standardized FIT NB analysis procedure was developed to analyze the characteristics and dynamics of FIT NBs. (Supports Figure 1)

Experimental steps for FIT NB induction in transiently transformed *N. benthamiana* leaf epidermis cells. Fluorescence protein expression was induced by β -estradiol ('induction of protein expression') 16 h prior to imaging and measurements. Leaf discs were excised, and initial fluorescence images and measurements were taken ('data acquisition t=0'). Leaf discs were exposed to 488 nm laser light as a light trigger for 1 min ('light induction of NB formation'), and 5 min later, fluorescence images and measurements were taken again ('data acquisition t=5'). With this procedure, FIT NBs were visible, and their characteristics could be analyzed. In some cases, fluorescence images and measurements were taken at t=15 min, as indicated in the text. Imaging was performed at the respective wavelengths for detection of GFP and mRFP/mCherry, respectively.



Supplemental Figure S2. An intrinsically disordered region, IDR^{Ser271/272}, is present in the FIT C-terminus and disrupted in the FITmSS271AA mutant. (Supports Figure 2, 3, and 4)

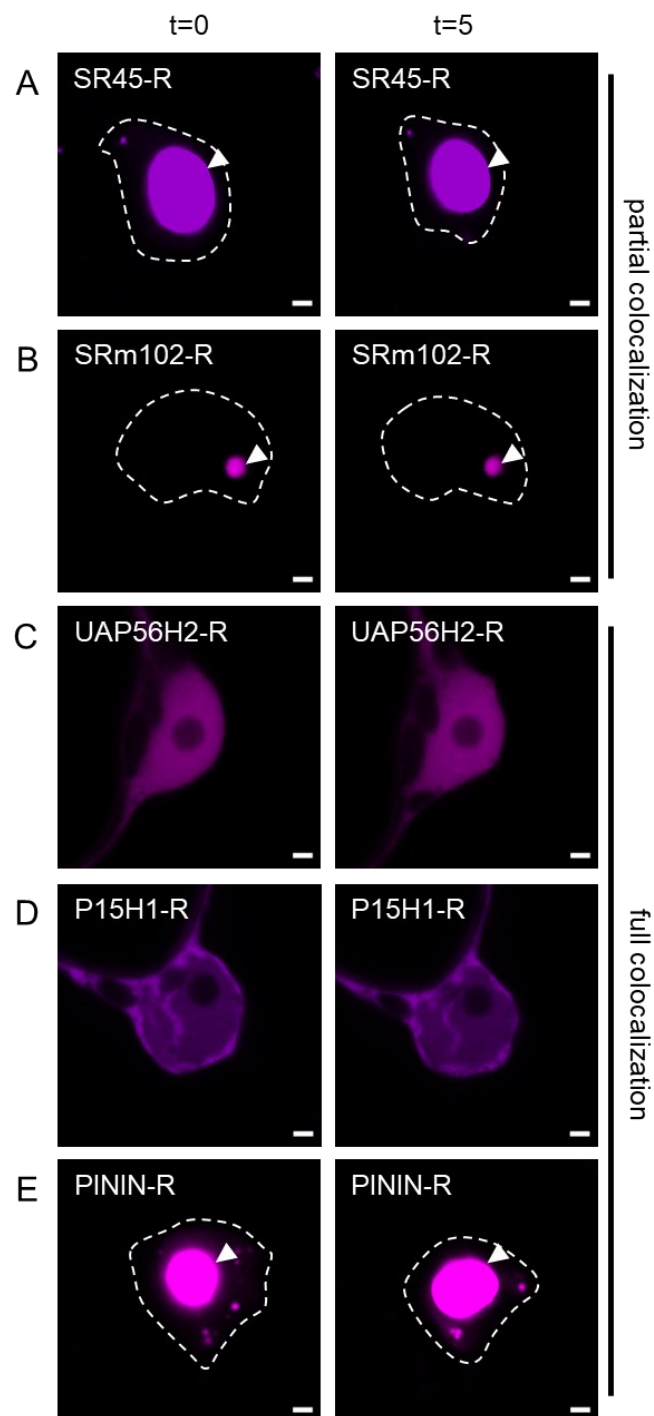
Diagrams representing the PONDNR scores for each amino acid position in A, FIT, and B, FITmSS271AA protein sequences. Analysis was performed via the tool PONDNR-VLXT (Molecular Kinetics, Inc.). A score >0.5 indicates intrinsic disorder. The 0.5 threshold is marked with a red line. Above the graph, schematic representation of FIT protein showing the position of the bHLH domain in grey (126-201 aa) and subdivided into the basic region in blue (DNA binding site, 132-162 aa) and the helix-loop-helix region in black (dimerization site, 142-201 aa). Domain prediction was performed with InterPro (EMBL-EBI). FIT has four regions with a score >0.5 that are predicted IDRs, two of them in the C-terminal part following the bHLH domain, with one out of them comprising the position SS271/272, indicated by an arrowhead, termed IDR^{Ser271/272}. In FITmSS271AA, the PONDNR score dropped for this region below the threshold.



Supplemental Figure S3. FIT NBs did not colocalize with Cajal body components (designated type I). (Supports Figure 5 and 6)

Confocal images showing localization of FIT-GFP and NB markers (type I) upon co-expression in the nucleus at t=5 min. Co-expression of FIT-GFP with A, coilin-mRFP, and B, U2B⁺-mRFP. FIT NBs were present at t=5 min and did not colocalize with NBs of the two markers.

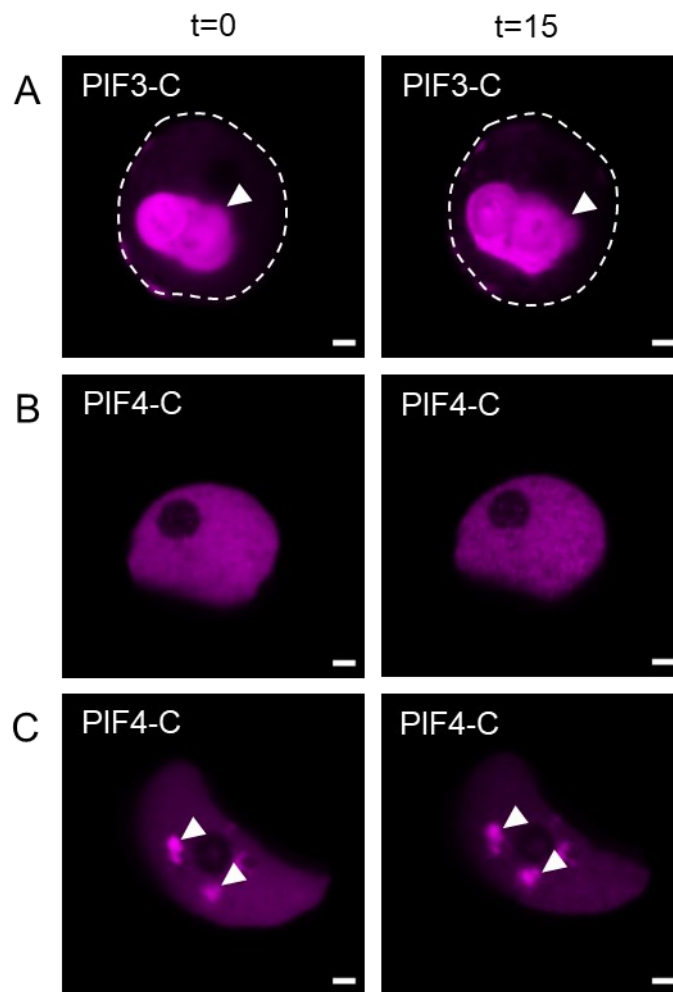
Scale bar: 2 μ m. Arrowheads indicate non colocalizing NBs. G = GFP; R = mRFP. Fluorescence protein analysis was conducted in transiently transformed *N. benthamiana* leaf epidermis cells, following the standardized FIT NB analysis procedure.



Supplemental Figure S4. Type II and III NB markers are similarly localized upon single expression as upon co-expression with FIT, except PININ. (Supports Figure 5 and 6)

Confocal images showing localization of NB markers (type II and III) upon their single expression in the nucleus at t=0 and t=5 min, in A, SR45-mRFP, B, SRm102-RFP, C, UAP56H2-mRFP, D, P15H1-mRFP, and E, PININ-mRFP. Single SR45-mRFP and SRm102-RFP localized in NBs similar to the colocalization with FIT at t=0 and t=5 min (compare with **Figure 5**). Single UAP56H2-mRFP and P15H1-mRFP did not localize in NBs and were uniformly distributed, similar to the colocalization with FIT at t=0 (compare with **Figure 6, A and B**). Only single PININ-mRFP showed a different localization pattern between its single expression versus co-expression with FIT-GFP. Upon single expression it localized in NBs at t=0 and t=5 min, while in co-expression with FIT-GFP it showed no NBs at t=0 but followed the FIT NB pattern at t=5 min (compare with **Figure 6C**).

Scale bar: 2 μ m. Arrowheads indicate NBs. R = mRFP. Fluorescence protein analysis was conducted in transiently transformed *N. benthamiana* leaf epidermis cells, following the standardized FIT NB analysis procedure.



Supplemental Figure S5. PB markers are similarly localized upon single expression and upon co-expression with FIT. (Supports Figure 7)

Confocal images showing localization of PB markers upon their single expression in the nucleus at t=0 and t=15 min, in A, PIF3-mCherry, and in B and C, PIF4-mCherry in two different patterns. Single PIF3-mCherry localized to a very large PB at t=0 and t=15 min. Single PIF4-mCherry localized either in a uniform manner in the nucleus as seen in B, or in several PBs as seen in C. Hence, PIF3-mCherry and PIF4-mCherry were similarly localized in single expression as upon co-expression with FIT-GFP (compare with **Figure 7**).

Scale bar: 2 μ m. Arrowheads indicate NBs. C = mCherry. Fluorescence protein analysis was conducted in transiently transformed *N. benthamiana* leaf epidermis cells, following the standardized FIT NB analysis procedure.

Supplemental Movie S1. Light induction triggers the formation of NBs with FIT and FITmSS271AA with different dynamics. (Supports Figure 1 and 2)

Time series showing representative localization of A, FIT-GFP, B, ZAT12-GFP, and C, FITmSS271AA-GFP, each of them from 0 to 20 min after the light trigger in the nucleus. Pictures were taken in 15-sec intervals. FIT-GFP accumulated in NBs within the first minutes after light excitation. ZAT12-GFP did not show NB formation and was a negative control to show that GFP did not cause the NB effect. FITmSS271AA-GFP accumulated late in NBs (starting at 10 min), which were also smaller in size, indicating that Ser271/272 is important.

Scale bar: 2 μm . G = GFP. Fluorescence protein analysis was conducted in transiently transformed *N. benthamiana* leaf epidermis cells, following the standardized FIT NB analysis procedure.

Supplemental Table S1. List of vectors used in this study.

Vector	Application	Source
ipABind:cFIT-GFP	Imaging, FRAP, anisotropy, FRET-FLIM	Gratz et al., 2019
ipABind:cFIT-mCherry	Imaging	
ipABind:cFITmSS271AA-GFP	Imaging, anisotropy, FRET-FLIM	
ipABind:cbHLH039-mCherry	Imaging, FRET-FLIM	Trofimov et al., 2019
pMDC83:ZAT12-GFP	Imaging	Le et al., 2016
pROK2:COILIN-mRFP	Imaging	The Plant Nuclear Marker collection (NASC)
pROK2:P15H1-mRFP	Imaging	
pROK2:PININ-mRFP	Imaging	
pROK2:SR45-mRFP	Imaging	
pROK2:SRm102-mRFP	Imaging	
pROK2:U2B ⁺ -mRFP	Imaging	
pROK2:UAP56H2-mRFP	Imaging	
ipABind:cPIF3-mCherry	Imaging	
ipABind:cPIF4-mCherry	Imaging	

Author contributions to Manuscript IKsenia Trofimov

Conceptualization of study. Supervised the study. Performed initial experiments. Designed, performed, and analyzed all experiments. Designed the outline of the manuscript. Wrote the manuscript, prepared final figures, and reviewed/edited the manuscript.

Regina Gratz

Contributed key material.

Rumen Ivanov

Conceptualization of study. Supervised the study. Helped designing, performing, and analyzing experiments. Reviewed/edited the manuscript.

Yvonne Stahl

Conceptualization of study. Supervised the study. Helped designing, performing, and analyzing anisotropy (homo-FRET) and FRET-FLIM experiments. Contributed key material. Reviewed/edited the manuscript.

Petra Bauer

Conceptualization of study. Supervised the study, provided funding, and reviewed/edited the manuscript.

Tzvetina Brumbarova

Conceptualization of study. Supervised the study. Helped designing, performing, and analyzing experiments. Reviewed/edited the manuscript.

10 Concluding remarks

This thesis elaborated two levels of iron uptake regulation. On the one hand, we showed that FIT undergoes post-translational modification in form of phosphorylation events which alter its interaction. On the other hand, we showed a dynamic subcellular organization of FIT and bHLH039, which most likely is another level of controlling iron uptake.

Unlike its target genes, *FIT* is transcribed predominately during the night, when no iron uptake usually takes place (Santi and Schmidt, 2009). This suggests that FIT protein is readily available when iron uptake is demanded during the day to act fast on target gene transcription and therefore adapting iron uptake in a rapid manner to environmental changes. Hence, a post-translational modification must be in place to regulate FIT protein activation and the iron uptake module FIT-bHLH039 to initiate the iron uptake machinery, but also deactivation to stop the uptake to avoid toxicity. It was suspected that FIT exist in two pools of active and inactive protein (Lingam et al., 2011; Meiser et al., 2011; Sivitz et al., 2011). The identification of possible serine and tyrosine phosphorylation sites enabled to assess their influence on FIT-bHLH039 interaction. bHLH TFs act in dimers (Heim et al., 2003) and a functional heterodimer of FIT and bHLH039 is essential for iron uptake regulation, as neither FIT nor bHLH039 can upregulate iron uptake alone (Yuan et al., 2008; Wang et al., 2013; Naranjo-Arcos et al., 2017). Phospho-dead FITmSS271AA was engaging less in interaction. Reduced capacity to interact with bHLH039 explains FITmSS271AA mutant inability to complement *fit* mutant plants. Hence, phosphorylation activates FIT protein, enabling a proper heterodimerization with bHLH039 to drive iron uptake.

Equally important to the activation is the deactivation of FIT that could be demonstrated by the phospho-mimicking FITmY278E form. FITmY278E showed reduced interaction capacity with bHLH039 and lower protein stability. Most likely, FIT is released from its interaction partner upon Tyr278 phosphorylation and subjected to degradation. By this, a previously active and 'used' FIT is removed to keep the iron uptake regulation modifiable.

We could show that bHLH039 is not localized in the nucleus without FIT and retained in the cytoplasm in cytoplasmic foci. Other proteins were previously shown to localize in cytoplasmic foci as well when not correctly localized in the nucleus (Rösler et al., 2007; Ivanov et al., 2008). A TF in the cytoplasm is associated with an inactive form (Allen and Strader, 2021). Since these foci are immobile, bHLH039 probably remains in an inactive state as the immobility is indicative of a pathological state. This is supported by the fact that bHLH039 requires functional FIT for action, which in turn positively regulates *FIT* transcription (Naranjo-Arcos et al., 2017). Therefore, nuclear localization of bHLH039 is favorable for the upregulation of the iron uptake machinery, but dependent on FIT presence. A possibility by how FIT is dictating bHLH039 localization could be interaction that either recruits bHLH039 into the nucleus or prevents bHLH039 from exiting the nucleus (possibility (ii) of nucleocytoplasmic partitioning elucidated in 4.2). Remarkably, an analogue nucleocytoplasmic partitioning was

observed in rice for bHLH039 orthologue OsIRO2 (Liang et al., 2020; Wang et al., 2020). This suggests that nucleocytoplasmic partitioning of bHLH039 could be a common and conserved feature within iron uptake regulation of Strategy I and II plants.

Contrarily, FIT localization did not depend on bHLH039, but it changed from a homogenous distribution within the nucleus to NBs. FIT NB formation goes along with the reduced FIT mobility and also the predominant localization in the nucleus. Compared to the phospho-dead FITmSS271AA, wild-type FIT had a stronger and faster NB formation, and stronger homodimerization within NBs. Since FIT homodimers are not sufficient for iron uptake (Yuan et al., 2008), the localization of FIT homodimers within NBs could be an initiating step for NB formation. FIT could possibly recruit bHLH039 into NBs by interaction, creating a hub for the iron uptake module. In favor of this speaks that FIT also heterodimerized stronger with bHLH039 in NBs compared to FITmSS271AA. As condensation mainly depends on interactions, wild-type FIT has the advantage of proper homo- and heterodimerization, while this is reduced in FITmSS271AA. Here, phosphorylation as well as the presence of IDR^{Ser271/272} is an important factor, as this keeps wild-type FIT in the nucleus, probably by interaction with other proteins, and in turn affecting its mobility due to the increasing size of the complex. Possibly, a combination of loss of phosphorylation as well as loss of IDR in the C-terminus could synergistically lead to a conformational change of FIT protein and influence FIT multivalency and condensation. When FIT localizes in condensates, it colocalizes there with bHLH039, but also proteins involved in splicing, thus this type of condensate could have a role in transcriptional or post-transcriptional regulation, possibly of FIT target genes.

Evidence exists that a light- or circadian clock-dependent iron uptake regulation takes place, showing that iron uptake is a process adjusting to the environmental conditions. We have seen FIT NB formation as a consequence of blue light excitation. Blue and red light are usually absorbed in the scope of photosynthesis and can therefore be signals for a photosynthetically active period (Smith et al., 2017). This could serve as a cue for the plant that iron sinks are active, and iron is needed. Subsequently, initiation of NB formation, which in turn spatially concentrates the iron uptake module, could be a way to meet the iron demand.

In summary, this work has provided a detailed insight into the regulation of FIT. FIT is underlying a dual regulation via phosphorylation which affects its interaction within the iron uptake module with bHLH039. The subcellular localization showed that bHLH039 localization is dependent on FIT and that their interaction is concentrated within condensates, suggesting an additional level of regulation within iron uptake.

Further research will be necessary to understand the exact signaling mechanism that connects FIT activation and FIT NB formation. Particularly, identifying factors that navigate FIT NB formation will help to fully understand FIT NB function and might provide a link to environmental cues.

References

- Heim, M.A., Jakoby, M., Werber, M., Martin, C., Weisshaar, B., and Bailey, P.C.** (2003). The Basic Helix-Loop-Helix Transcription Factor Family in Plants: A Genome-Wide Study of Protein Structure and Functional Diversity. *Mol. Biol. Evol.* **20**: 735–747.
- Ivanov, R., Tiedemann, J., Czihal, A., Schallau, A., Hong Diep, L., Mock, H.-P., Claus, B., Tewes, A., and Bäumlein, H.** (2008). EFFECTOR OF TRANSCRIPTION2 is involved in xylem differentiation and includes a functional DNA single strand cutting domain. *Dev. Biol.* **313**: 93–106.
- Liang, G., Zhang, H., Li, Y., Pu, M., Yang, Y., Li, C., Lu, C., Xu, P., and Yu, D.** (2020). *Oryza sativa* FER-LIKE FE DEFICIENCY-INDUCED TRANSCRIPTION FACTOR (OsFIT/OsbHLH156) interacts with OsIRO2 to regulate iron homeostasis. *J. Integr. Plant Biol.* **62**: 668–689.
- Lingam, S., Mohrbacher, J., Brumbarova, T., Potuschak, T., Fink-Straube, C., Blondet, E., Genschik, P., and Bauer, P.** (2011). Interaction between the bHLH Transcription Factor FIT and ETHYLENE INSENSITIVE3/ETHYLENE INSENSITIVE3-LIKE1 Reveals Molecular Linkage between the Regulation of Iron Acquisition and Ethylene Signaling in Arabidopsis. *Plant Cell* **23**: 1815–1829.
- Meiser, J., Lingam, S., and Bauer, P.** (2011). Posttranslational Regulation of the Iron Deficiency Basic Helix-Loop-Helix Transcription Factor FIT Is Affected by Iron and Nitric Oxide. *Plant Physiol.* **157**: 2154–2166.
- Naranjo-Arcos, M.A., Maurer, F., Meiser, J., Pateyron, S., Fink-Straube, C., and Bauer, P.** (2017). Dissection of iron signaling and iron accumulation by overexpression of subgroup Ib bHLH039 protein. *Sci. Rep.* **7**: 1–12.
- Rösler, J., Klein, I., and Zeidler, M.** (2007). Arabidopsis *fhl/fhy1* double mutant reveals a distinct cytoplasmic action of phytochrome A. *Proc. Natl. Acad. Sci. U. S. A.* **104**: 10737–10742.
- Santi, S. and Schmidt, W.** (2009). Dissecting iron deficiency-induced proton extrusion in Arabidopsis roots. *New Phytol.* **183**: 1072–1084.
- Sivitz, A., Grinvalds, C., Barberon, M., Curie, C., and Vert, G.** (2011). Proteasome-mediated turnover of the transcriptional activator FIT is required for plant iron-deficiency responses. *Plant J.* **66**: 1044–1052.
- Smith, H.L., McAusland, L., and Murchie, E.H.** (2017). Don't ignore the green light: exploring diverse roles in plant processes. *J. Exp. Bot.* **68**: 2099–2110.
- Wang, N., Cui, Y., Liu, Y., Fan, H., Du, J., Huang, Z., Yuan, Y., Wu, H., and Ling, H.Q.** (2013). Requirement and Functional Redundancy of Ib Subgroup bHLH Proteins for Iron Deficiency Responses and Uptake in Arabidopsis thaliana. *Mol. Plant* **6**: 503–513.
- Wang, S., Li, L., Ying, Y., Wang, J., Shao, J.F., Yamaji, N., Whelan, J., Ma, J.F., and Shou, H.** (2020). A transcription factor OsbHLH156 regulates Strategy II iron acquisition through localising IRO2 to the nucleus in rice. *New Phytol.* **225**: 1247–1260.
- Yuan, Y., Wu, H., Wang, N., Li, J., Zhao, W., Du, J., Wang, D., and Ling, H.Q.** (2008). FIT interacts with AtbHLH38 and AtbHLH39 in regulating iron uptake gene expression for iron homeostasis in Arabidopsis. *Cell Res.* **18**: 385–397.